Computational and Experimental Assessment of Supercritical Natural Circulation Loop: Steady-state Thermalhydraulics and Stability Aspects

A Thesis Submitted in Partial Fulfillment of
the Requirements for the Degree of

DOCTOR OF PHILOSOPHY

by

Milan Krishna Singha Sarkar

under the supervision of

Dr. Dipankar Narayan Basu

Department of Mechanical Engineering
Indian Institute of Technology Guwahati
Guwahati-781039, India
January 2019

Department of Mechanical Engineering
Indian Institute of Technology Guwahati
Guwahati-781039
Assam, India

Declaration

I do hereby declare that the information presented in this dissertation entitled **"Computational and Experimental Assessment of Supercritical Natural Circulation Loop: Steady-state Thermalhydraulics and Stability Aspects"** is entirely my own account of research performed in the Department of Mechanical Engineering, Indian Institute of Technology Guwahati, Assam, India under the guidance of **Dr. Dipankar Narayan Basu**. The results contained in this thesis have not been submitted in part or full to any other University or Institution for the award of any degree or diploma.

Dated: 25.01.2019

Milan Krishna Singha Sarkar
Research Scholar
Department of Mechanical Engineering
Indian Institute of Technology Guwahati
Guwahati-781039, Assam, India

Department of Mechanical Engineering
Indian Institute of Technology Guwahati
Guwahati-781039
Assam, India

Certificate

It is certified that the work contained in the thesis entitled **"Computational and Experimental Assessment of Supercritical Natural Circulation Loop: Steady-state Thermalhydraulics and Stability Aspects"** submitted by **Milan Krishna Singha Sarkar** (Reg. No. 126103023) to the Indian Institute of Technology Guwahati for the award of the degree of **Doctor of Philosophy** has been carried out under my supervision in the Department of Mechanical Engineering, Indian Institute of Technology Guwahati. This work has not been submitted elsewhere for the award of any other degree or diploma.

The thesis, in my opinion, has reached the standard fulfilling the requirements for the award of the degree of Doctor of Philosophy in accordance with the regulations of the institute.

Dated: 25.01.2019

Dr. Dipankar Narayan Basu
Assistant Professor
Department of Mechanical Engineering
Indian Institute of Technology Guwahati
Guwahati-781039, Assam, India

Dedicated

To

My Elder Brother

Jiban Krishna Singha Sarkar

(02.01.1981-28.07.2011)

Acknowledgment

I would like to express my deep gratitude to all of those who have helped me in various ways during the tenure of my PhD work at IIT Guwahati. I have been supported and accompanied by many people and each one has played an indispensable role during my work. I am grateful to all of them.

I am immensely indebted to my supervisor Dr. Dipankar Narayan Basu, for his valuable advices, expert guidance, patience and encouragement and for all the support he has given me from the day one to throughout my PhD program. He provided me the complete freedom in my research and allowed me to work in my own way. He always has listened my ideas with endurance and constantly motivated to accomplish my goal. I have immensely benefited from each and every moment of my association with him. I will forever remain indebted to him for his untiring effort and help extended to me that went even beyond academics. The extraordinary experience of working with him would be remembered in my life.

I must take this opportunity to express my gratitude to the Chairman of my doctoral committee Prof. Manmohan Pandey and other members Dr. Gavara Madhusudhana and Dr. Tapas K. Mandal for their valuable suggestions and encouragements during the period of my research study. I extend my sincere gratitude to Dr. Ganesh Natarajan and Dr. Subrata K. Majumder for their precious suggestions about critical issues related to my research work during the various presentations.

I sincerely appreciate Prof. Santosha K. Dwivedy, Prof. Pinakeswar Mahanta, and Prof. Anoop K. Dass, the present and former Heads of the department, for extending all necessary facilities of the department. I wish to express my sincere gratefulness to Dr. Amaresh Dalal for his valuable suggestions related to academic and nonacademic section throughout my study period. Thanks to all the faculty members of the department for not only their technical suggestions at times but also their friendly interactions that create an enjoyable working environment in the department.

I wish to express my sincere thanks to Scientific Officers and Technical staffs Mr. R. Saikia, Mr. P. Pal, Mr. N. Bora, Mr. M. Dowarah, Mr. S. Sharma, Mr. S. Ahmed and Mr. J. Baumatary for their assistant whenever needed during my study. I am very much thanks to staff of the workshop Mr. N.K. Das, Mr. D. Chetri, Mr. B.K. Choudhury and Mr. M.K. Baishya for their helping hand for the experimentation. I also thanks to former and present staff of the Department, Mr. N. Das, Mr. N. Dutta, Mr. and Mr. R. Talukdar.

I would like to cordially thank to my seniors, juniors and friends Dr. V. K. Mishra, Mr. Daya Shankar, Dr. S. Agarwal, Dr. S. Sarma, Dr. A. Barma, Dr. Chandan Kumar, Dr. A.K. Jha, Dr. S. Kotoky, Dr. Dr. G.S. Sinha, Dr. G. Bolar, Dr. J. Manik, Dr. B. Das, Dr. H. Niyas, Dr. G.N. Shelke, Dr. Azd Zayoud, Dr. Seikh M. Kamal, Dr. A. Ghatak, Dr. P. Mandal, Mr. S.P. Jaiswal, Mr. R.P. Soni, Mr. B.K. Naik, Mr. Satyendra Nath Baro, Mr. Srikant Prasad, Mr. Biplab Das, Mr. Ashif Iqbal, Mr. Debarshi Mallick, Mr. Rakesh Bhadra, Mr. Rasmi Ranjan Behera, Mr. Subhra Sankar Kalita, Mr. Biswajyoti Das, Mr. Kiran Saikia, Mrs. Urmimala Saikia, Mr. Achinta Sarkar, Mr. Debabrata Gayen, Mr. Shahnawaz Ahmed, Mr. Anupam Alok, Mr. Bhaskarjyoti Sarma, Mr. Nitesh Kumar, Mr. Sambit Majumder, Mr. Sunku Prasad, for their support and advice in different occasions of my PhD program.

I am deeply indebted to dearest friend Dr. Sanjib Barma, Dr. M.S. Manna, Mr. Prosenjit Mandal and many other individuals with whom I have come into contact during my stay in IIT Guwahati. Their friendships and hearty attachments have made my life colorful and precious.

The seeds of my research career was planted by my elder brother late Jiban Krishna Singha Sarkar. He was constantly motivated and pushed me to do PhD. I consider myself most unfortunate as I could not present this work to my brother who left for heaven abode. It is very much unfortunate that when I am doing research then he is not with me. His sudden expiry made my life greatly empty. I pray to God please keep my brother in peace.

I would like to convey my special thanks and love to my parents Mr. Tarun Kumar Singha Sarkar and Mrs. Jyotsna Singha Sarkar for their great encouragement, guidance, love, affection, motivation and warm blessings. It is not possible to express in words that the inspiration I have got from my wife Dipika, whose noble sacrifice, invaluable love and support have brought me to this position. I am also thankful to my little daughter Jiniya for her sacrifice

of love due to separation from me during these days. Most deeply, I thank my in-laws Mr. Bisweswar Sarkar and Mrs. Malati Sarkar for their support, patience, motivation and blessings for the completion of this work. I also like to thanks my elder brother Mr. Bharat Kumar Singha Sarkar and sister-in-law Mrs. Anita Singha Sarkar for their motivation and family support during the research. The mental support and refreshment I got from my sweet nephew Munmun and Bishal, and many cosine brothers and sisters, namely Nilambar, Tumpa, Gouri and many more.

I will always remain grateful to my beloved friend late Biblab Kar and my respected teacher late Haripada Basak who have shown me a path to move on in my life.

This list is obviously incomplete, but let me submit that the omissions are inadvertent and I once again record my deep felt gratitude to all those who have cooperated with me either directly or indirectly in this endeavor.

Last but not the least, I express my deepest gratitude to all my well-wishers.

Milan Krishna Singha Sarkar

Abstract

Despite the mathematical intricacy, the natural circulation loop (NCL) proposes a convenient route of energy and species transport from a high-temperature source to a low-temperature sink, without them in direct contact. The buoyancy force originating from the density gradient is the prime driving force of any natural circulation system. Operating regime of single-phase NCLs is limited by the constraints of saturation temperature and low flow rate, whereas the possibility of dry-out and appearance of different flow regimes with contrasting heat transfer behavior are of great concern in two-phase loops. Supercritical fluid offers a potent alternative due to its good heat transport capability and large volumetric expansion, thereby coupling the advantages of single- and two-phase versions. Accordingly the concept of supercritical natural circulation loop (SCNCL) has evolved in the present millennium as one of the most important initiatives under generation-IV nuclear reactors.

Both numerical and experimental appraisal of SCNCL is presented in the current thesis. Thorough numerical investigation have been performed to explore the steady-state, as well as transient, behaviour of SCNCL. The mode of heating is a critical factor on steady-state thermalhydraulics of SCNCL. Both Dirichlet and Neuman type modes are of equal importance, according to the design of system. Thus, several subsequent steady-state studies have been performed, where, heating is envisaged in both constant temperature and constant heat flux modes and cooling is always through a constant temperature sink. To find out a complete observation on the thermalhydraulic of SCNCL, influence of various operating parameters, like system pressure, source and sink temperature, working fluids, inclination angle, heating power, and various geometric dimensions have been studied meticulously. Steady-state analysis of SCNCL begins with the study of thermalhydraulic comparison of water, CO_2 and R134a as the working fluids under identical set of operating conditions. Effort is made to identify the best working fluid from heat transfer point of view.

An interesting observation was found for the variation in loop flow rate with power under steady-state. Mass flow rate was identified to increase with rise in heater power till a maxima, followed by a rapid deterioration in both flow rate and heat transfer coefficient, and a hike in the fluid temperature level. This phenomenon was identified as a natural circulation version of heat transfer deterioration (HTD), which is a well-explored topic for forced flow channels. For such systems, it is common to have tubes or annular channels with known wall heat flux, and the HTD is characterized by a rapid increase in the wall temperature, owing to the failure in the wall-to-fluid heat transfer mechanism. For SCNCL, however, the nature of the phenomenon is different, the similarity being in the deterioration of the heat transfer coefficient and occurrence around the pseudocritical point. To recognize this difference, and also the role of the reduction in flow rate in lowering the heat transfer coefficient, the terminology is modified as the flow-induced heat transfer deterioration (FiHTD). That leads to a drastic deterioration in heat transfer coefficient and hence can be identified as a practicable limit of operation. Power level corresponding to the appearance of

FiHTD can be increased by raising pressure and lowering sink temperature. A mechanism can also be devised to maneuver the sink temperature with heater power for delaying the appearance of such deterioration. Supercritical CO_2 based SCNCL can be a superior choice, as long as the power level can be limited to the FiHTD, owing to the higher flow rate and lower fluid temperature levels. However, if the expected power range of operation goes beyond the FiHTD constraint, single-phase water-based loops are a safer option, due to the consistent behavior. Asymmetric temperature and velocity profiles can be observed across flow sections, particularly with larger source-to-sink temperature differential, due to the local buoyancy effects.

It is apparent that the steady-state thermalhydraulics of an SCNCL is dominated by the geometric parameters. That necessitates a comprehensive study to understand the role of geometric variables on the thermalhydraulic characteristics of SCNCL in general and FiHTD in particular. Influence of several parameters, including loop diameter, height, width, inclination angle, heating and cooling length and their orientation, has been explored with the objective being the identification of a set of guidelines corresponding to a safer design.

SCNCLs being prone to system instabilities, systematic stability appraisal is mandatory to identify the condition for stable operating zone. In the present thesis, therefore, a comprehensive transient analysis and dynamic performance evaluation have been carried out to observe the stability performance of SCNCL. Consequently, a 2D computational model of rectangular NCL is developed and used to explore the transient nature of the same. The system exhibited both stable and unstable performance. Despite the absence of exclusive phase change, SCNCL can experience a huge density variation for a small temperature change around the pseudocritical point. This is the likeliest of reasons that may push the system towards instabilities quite similar to the two-phase versions. Influence of sink temperature on transient analysis of SCNCL is thoroughly investigated and a stability map is prepared accordingly. A Lorenze like chaotic flow is observed in the unstable zone of operation of SCNCL.

To enlarge the corresponding experimental database for SCNCL, experiments have been performed using R134a as the working fluid. R134a exhibits a low critical pressure, which makes it relatively easier to achieve supercritical condition with compared to water. The motivation of the present experimental study is to identify the thermalhydraulic characteristic and stability behaviour of SCNCL. Influence of sink temperature, operating pressure, tilt angle and input heating power are thoroughly investigated. Pressure and sink temperature are found to be the most influencing parameters for operation of SCNCL. Loop mass flow rate has been found to increase with the increase in power for all chosen conditions. Mass flow rate gradually changes with tilt angle, with the highest mass flow rate appearing for the vertical loop. There is no instability observed for the selected range of operating condition.

This dissertation reports, both numerical and experimental evaluation of the thermalhydraulic behavior and stability aspects of SCNCL. Several gaps from the literature have been identified and effort is made to address a few, with the identification of FiHTD being the most significant contribution. The goal of transient analysis is achieved by producing a detailed stability map for sink temperature. Both experimental observations and numerical predictions are found to be in consensus, with the maximum deviation being limited to 15%.

Contents

List of Figures

List of Tables

Nomenclature

A	Cross-sectional area (m^2)
C_p	Specific heat (J kg^{-1} K^{-1})
C_μ, $C_{1\varepsilon}$, $C_{2\varepsilon}$	Parameters in RNG model equations
$C_{3\varepsilon}$	Parameters in RNG model equations
D	Diameter (m)
Eu_m	Modified Euler number
f	Friction factor
g	Gravitational acceleration (m s^{-2})
G	Mass flux (kg m^{-2} s^{-1})
G_b	Turbulent kinetic energy due to buoyancy (kg $m^{-1}s^{-3}$)
G_k	Turbulent kinetic energy due to men velocity gradient (kg $m^{-1}s^{-3}$)
G_{pc}	Mass flux at pseudocritical point (kg m^{-2} s^{-1})
Gr_m	Modified Grashof number
h	Enthalpy (J kg^{-1})
H	Height (m)
h_f	Heat transfer coefficient (W $m^{-2}K^{-1}$)
k	Turbulent kinetic energy (m^2 s^{-2})
L	Length (m)
$\dot{m}$	Mass flow rate (kg s^{-1})
Nu	Nusselt number
p	Pressure (N m^{-2})
Pr	Prandtl number
q''	Heat flux (W m^{-2})
Q	Input Power (W)
$\dot{Q}$	Heat transfer rate (W)
Re	Reynolds number (= $4\,\dot{m}/\pi D\mu$)
Ri_m	Modified Richardson number
R_ε	Parameter in RNG model equation
S	Strain tensor

S_E	Energy source (W m^{-3})
St_m	Modified Stanton number
T	Temperature (K)
t	Time (s), Thickness (m)
u, v	Velocity (m s^{-1})
$\vec{V}_n$	Normal velocity (m s^{-1})
W	Width (m)
x, z	Space coordinate
y	Distance from the wall to the cell center

Greek symbols

α	Thermal diffusivity
α_k, α_ε	Parameters in RNG model equations
β	Volumetric expansion coefficient (K^{-1})
θ	Inclination angle (rad)
δ_{ij}	Kronecker delta
ε	Turbulent dissipation rate (m^2 s^{-3})
ρ	Density (kg m^{-3})
μ	Dynamic viscosity (kg m^{-1} s^1)
λ	Thermal conductivity (W m^{-1} K^{-1})
τ	Shear stress (N m^{-2})
Π_h	Heated perimeter (m)
ξ	Velocity (m s^{-1})
ϕ	Angle (degree)
η	Parameter in RNG model equation
ΔT	Temperature difference across the heater (K)

Subscripts and superscripts

b	Bounding
c	Cooler
Π_h	Critical
eff	Effective
h	Heater

hy	Hydraulic
i	x-direction, number of planes, inlet
in	Inlet
j	y-direction
o	Outlet
$m, '$	Modified
max	Maximum
pc	Pseudo-critical
t	Turbulent
tot	Total
$*$	Non-dimensional
e	Electric
th	Thermal
w	Wall

Acronyms

CL	Cooler left
CC	Cooler center
CCW	Counter clock wise
CR	Cooler right
CW	Clock wise
DAS	Data acquisition system
ECCS	Emergency core cooling system
FIASCO	Flow instability analysis under supercritical operating conditions
HC	Heater center
HHHC	Horizontal heater horizontal cooler
HHVC	Horizontal heater vertical cooler
HL	Heater left
HR	Heater right
HTD	Heat transfer deterioration
LOCA	Loss of coolant accident
LPM	Liter per minute
NAFA	Numerical analysis of fluid flow in axi-symmetric geometries

NCL	Natural circulation loop
NIST	National institute of standards and technology
NOLSTA	Nonlinear stability analysis code
N_{SUBPC}	Sub pseudocritical number
N_{TPC}	True trans pseudocritical number
PISO	Pressure-implicit with splitting of operators
PRESTO	Pressure staggering option
RELAP	Reactor excursion and leak analysis program
RNG	Re-normalization group
SCNCL	Supercritical natural circulation loop
sCO_2	Supercritical CO_2
SPORT	Special predictions of reactor transients and stability
SS	Steady-state, stainless steel
SST	Shear-stress transport
SUCLIN	Linear stability analysis code
UDF	User-defined function
V	Valve
VHHC	Vertical heater horizontal cooler
VHVC	Vertical heater vertical cooler

Chapter 1: Introduction

1.1. Basic Physics of Natural Circulation Loop

The cause of fluid flow from one point to another point is the effect of various driving forces. When this driving potential is generated by the use of external energy sources like, pump, compressor, then that type of flow is classified as forced flow. On the other hand when so called change engendered due to the gradient of fluid temperature/density, then it falls to the family of natural convection flow. If the initial and final position of fluid in a flow field is same then it is recognized as a circulation flow field and corresponding forced and natural flow fields are referred to forced and natural circulation respectively. The water cycle and human blood circulation (Figure 1-1) are the most common examples of natural and forced circulation systems respectively. The first cycle is purely completed by generation of density gradient of water, whereas, later one have a pumping system in the form of heart and that create sufficient pressure difference to build the flow field. Natural circulation refers to the ability of a fluid in a system to circulate continuously. The difference of density or precisely available buoyancy force is the prime driving force of any natural circulation system. A fluid system designed for natural circulation will have a heat source and a heat sink and it has to be ensured that the position of the heat sink is always at a higher elevation than the heat source. The heat source and heat sink are connected in such a way that it forms a continuous circulation path or loop of fluid motion and that type of configuration is categories as natural circulation loops (NCLs) (Figure 1-2).

The primary physics behind the NCL is like, most of the materials are expanded when they are heated and becomes less dense and opposite phenomenon occurs when they are cooled. Fluid get heated at the heat source section of NCL and becomes lighter than the surrounding fluid and then rises. While, at heat sink section fluid extract heat and becomes denser than nearby fluid and then it drawn downward by gravity. Together, these effects produces a flow field of fluid motion from the heat source to the heat sink and back again. The generated flow filed is purely buoyancy driven.

(a)

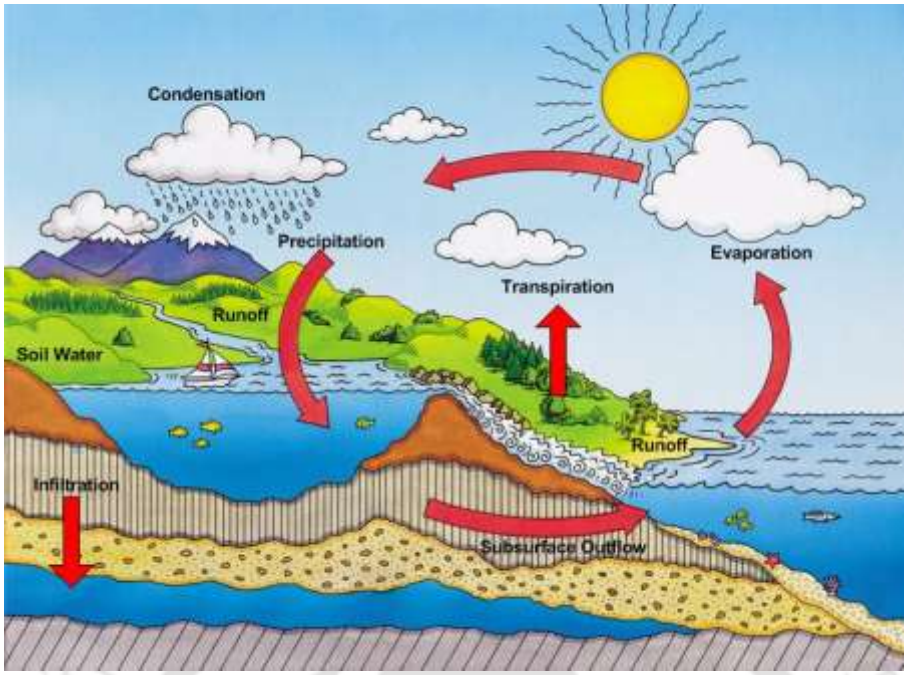

(b)

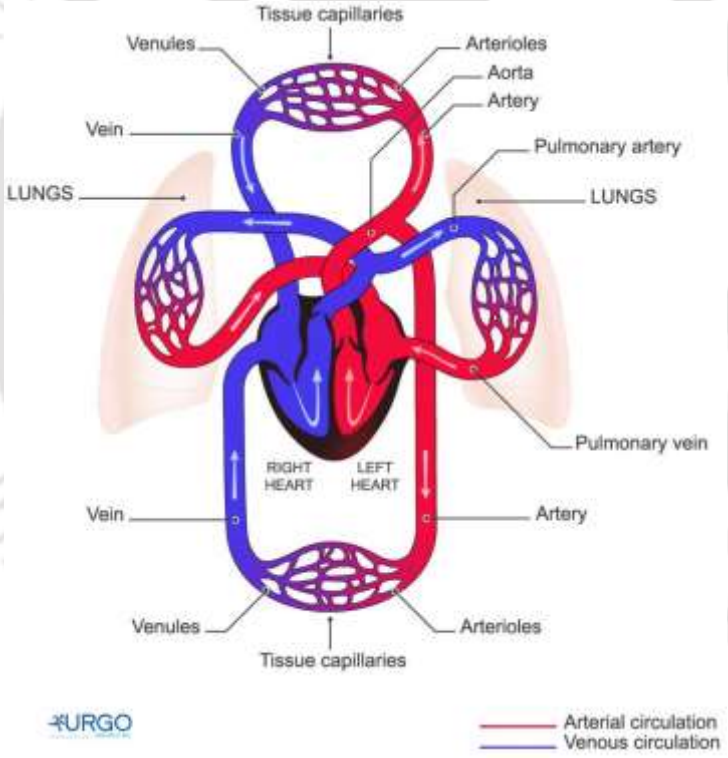

Figure 1-1. (a) Water cycle (natural circulation) (https://goo.gl/4suUqJ) and (b) human blood cycle (https://goo.gl/XTa1za).

NCLs, despite the mathematical intricacy, proposes a convenient route of energy and species transport. The density differential can be accomplished either by introducing a lighter phase into the primary fluid or by modulating fluid temperature through complementary energy interactions with the surrounding in different segments of the flow path. The later contrives a

proficient option of energy transport from a high-temperature source to a low-temperature sink, without them in direct contact. Warmer fluid from the source can rise to the sink owing to buoyancy, to dispense the accrued energy there, and return as a cooler medium, prepared to accumulate energy from the source again. Therefore it is obligatory to place the sink at a higher elevation than the source to establish the favorable buoyancy field, as is shown in Figure 1-2, and that is the only constraint for NCL configuration. Such simplicity in construction to suit any physical silhouette and enhanced reliability due to the absence of rotating machinery have stimulated innumerable engineering innovations, ranging from gigantic power cycles, nuclear plants and automobiles, through domestic refrigerators, chemical processes and solar heaters, to miniature chip cooling, with undisputed success.

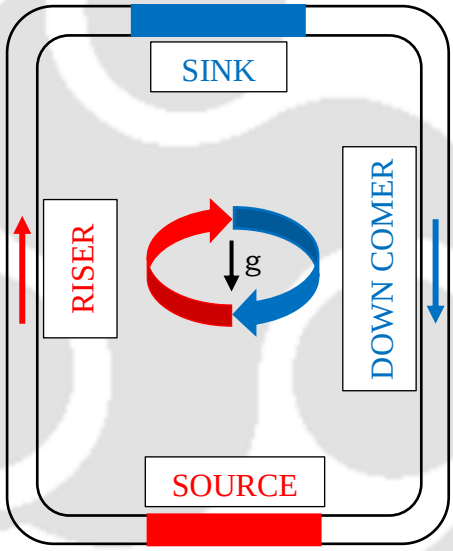

Figure 1-2. Schematic representation of a generalized natural circulation loop, with sink mounted at a higher elevation than the source.

It is improbable to converge on any initiation period for commercial utilization of NCLs as heat transport systems. One of the pioneering application can be identified in early-1950s for turbine rotor cooling. Several arrangements have historically been proposed and developed with varying nature of the working medium, shape and imposed body force. Zvirin, 1981 and Greif, 1988 are presented general reviews on NCLs which are the pioneer article on categorization of loops and basic understanding of the phenomena of NCLs. A complete list of classification is shown in Figure 1-6. While the other factors are typical to a situation, the selection of operating fluid is

generally governed by the operation convenience and range of parameters explored. Single-phase, mostly liquid-based, loops are favored in PWRs, solar heaters and electronic cooling applications; whereas two-phase systems, comprising distinct boiling and condensing sections, are prevalent in power cycles, refrigerators and heat pipes. Both are well-explored devices and under scrutiny since the very inception of the concept of NCL. The supercritical NCL, however, is a relatively new concept, with the pioneering research paper being publicized only in late 1990s. Significant count of theoretical and experimental studies have followed over next one and half-decades, only to propose several contradicting theories about the system performance, on both thermalhydraulic and stability aspects, leaving a reasonably thin knowledge base.

1.2. Application of NCL

Due to simplicity of design and inherent passive safety, NCLs are widely used in various engineering applications (Figure 1-3). Common applications of NCL are in solar water heater, nuclear reactors, geothermal power extraction plant, cooling of transformer, and rotating machineries etc. A recent application can be the cooling of electronic devices, like new-generation computer processor. Absence of any rotating machinery for driving the flow makes it geometrically simpler and economic, and also promises enhanced reliability and protection against power failures. Such advantageous features, aided by the flexibility of selecting from a wide range of fluids based on the desired conditions, often supersede the drawbacks of low driving head and stability-related apprehensions. Accordingly NCLs have encroached assorted application fields, encompassing solar heaters (Koffi et al., 2008; Zerrouki et al., 2002), geothermal power extraction (Atrens et al., 2010), high-temperature reactor cooling (Choi et al., 2011; IAEA, 2009), cryogenic refrigerators (Chang et al., 2003) and miniature electronic cooling (Haider et al., 2002), just to name a few.

The demand of energy is directly related with the total population of the world, which is escalating every day and hence the same is true for the demand of energy. The coal and natural gases are the conventional sources of energy all over the world, but unfortunately, none of them are renewable in nature and will relinquish in near future. Therefore the natural tendency is to focus on renewable sources, where the lack of complete understanding about

the concerned technology, location dependence and intermittent nature of power production, and high infrastructural cost act as major hindrances. Nuclear energy is one of the cleanest, safest and reliable option precisely in this context. Figure 1-4 shows the growing capacity of nuclear power generation in India upto 2016.

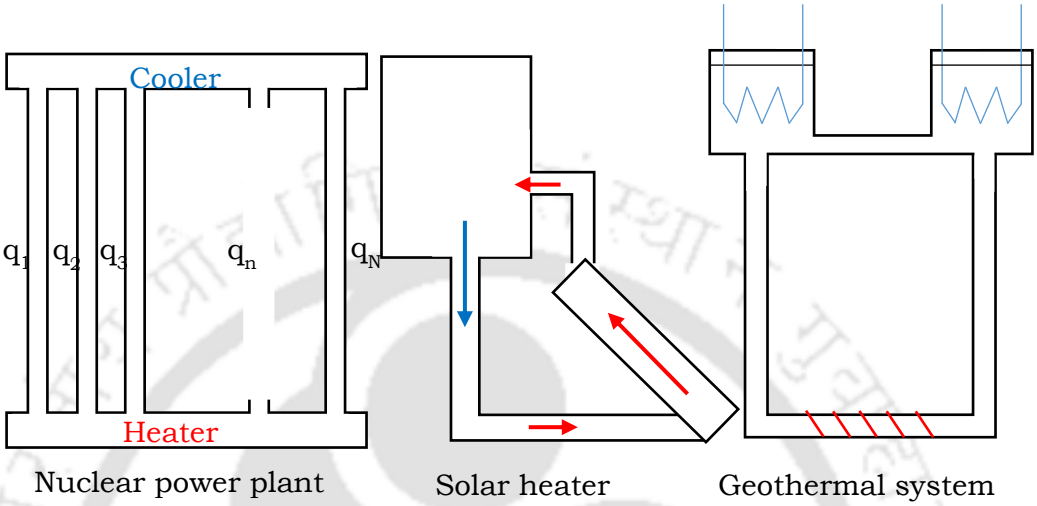

Figure 1-3. Applications of NCL

A significant amount of energy were produced from nuclear source of energy. Common people have several concern about the nuclear power plant, particularly about the safety of the system and radioactive waste disposal. Due to dealing with radioactive material, safety aspect of nuclear power plant is a most important issue. Any comparison of accidental effect of nuclear and conventional power plant is not satisfactory, because the amount of loss is huge for nuclear plant accident. The notable nuclear disasters are Three Mile Island accident in 1979, Chernobyl accident in 1986 and Fukushima Daiichi accident in 2011. All of the above said disasters are occurred due to the failing of the safety system of the plants, by intentionally or accidentally. Thus the researchers are worked extensively from some decades to make a modified system, which can able to operate naturally. In the context of that natural type cooling systems are comes in to the picture. According to basic principle of NCLs, there is no requirement of any moving element to generate the flow field in the system, which is the prime efficacy to use of NCL for nuclear reactor cooling.

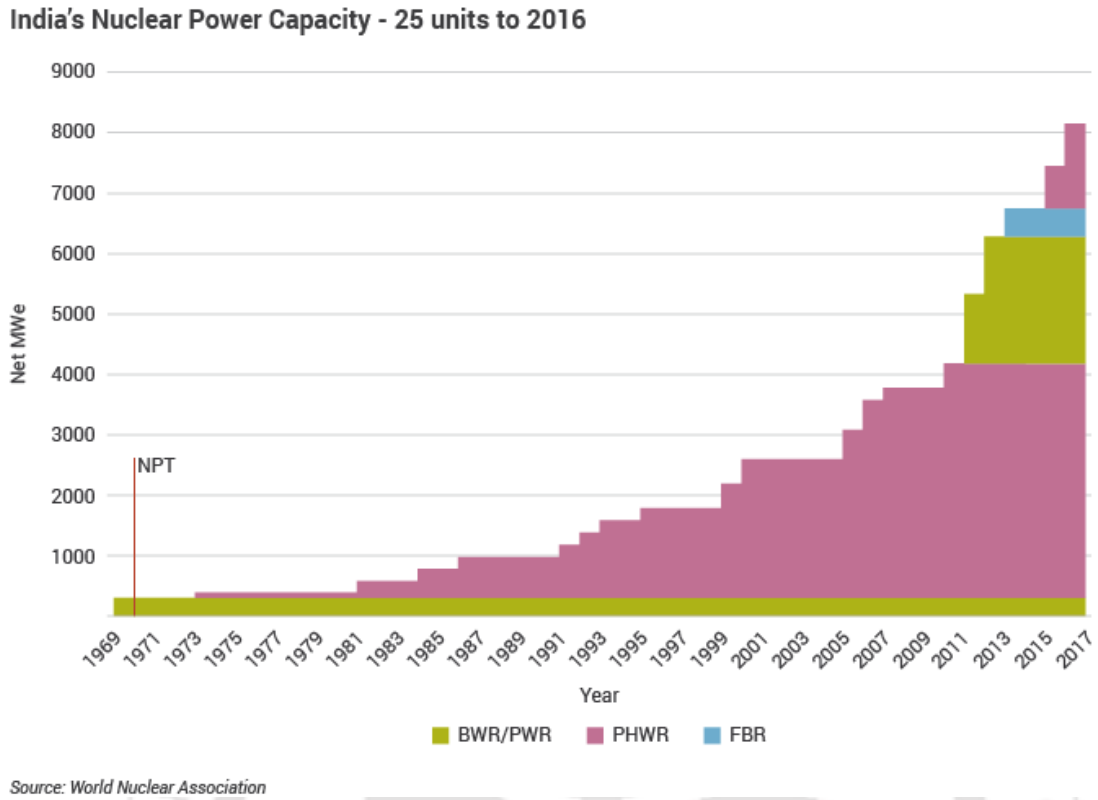

Figure 1-4. Nuclear power generation in india (https://goo.gl/gJT141)

1.3. Advantages of NCL

Various advantages of NCL are pointed out and discussed in the following section.

1.3.1. Simplicity

The primary advantage of NCL is, its simplicity in design and in operation. There is no requirement of any active prime mover and rotating machinery to construct an NCL, thereby greatly simplifying the construction, operation and maintenance of the system. As long as the sink is mounted at a higher elevation than the source, any geometric orientation is possible.

1.3.2. Safety aspects

Buoyancy is the driving force of any NCL, which is a natural consequence of change in fluid temperature. Therefore the circulation in NCL will continue even with the smallest possible heat interaction, consequently eliminating any possibility of LOCA-type accidents, like those happened in TMI-2 or Chernobyl. This feature of NCL has allowed its application in many systems, where safety is of utmost importance. In all modern designs of nuclear power reactors, particularly in Generation-IV concepts natural circulation is a backup for the removal of decay heat in the event of a pumping

power failure. Besides this, the requirement of driving force for natural circulation systems is rather low compared to forced circulation systems. As a result, the thermal response of NCL is slow, which gives more time to the operator for responding to the plant disorder.

1.3.3. Better flow distribution

The flow distribution in parallel channel cores is much more uniform in a natural circulation system compared to a force circulation one. Use of pumps restrict the uniform distribution of pressure in the headers, which may cause maldistribution of flow in the parallel channels.

1.3.4. Flow characteristics

Due to the absence of any prime mover, the two phase region of the loop need not be restricted to a specified zone in case of natural circulation system. In principle two phase flow may occur throughout the entire length of the loop.

1.4. Challenges of NCL

With numerous advantages, NCL have some challenges also, which are listed below.

1.4.1. Low driving force

One of the main constraint with NCL is the low driving force. The most effective ways of increasing the driving force is either to increase the loop height or to decrease the loop resistance, with both incurring additional construction cost. Moreover, use of tall risers can make NCL slender in structure and may raise seismic concerns.

1.4.2. Low mass flux

Generally, the generated mass flux through a NCL is low. Consequently, the allowable maximum channel power is low leading to a larger core volume with comparison to a forced circulation system of the same rating. In addition, handling of large volumes can result in zonal control problems and stability (Vijayan and Nayak, 2005).

1.4.3. Instability effects

Instability is common to both forced and natural circulation systems, with the latter being inherently less stable than former. This is pertinent to the nonlinear nature of the natural circulation phenomenon, where any

alteration in the driving force affects the flow, which in turn affects the driving force itself, often stimulating to a continued oscillatory behavior. In addition, due to the low driving force, the stabilizing effect is limited in NCL.

1.4.4. Specification of a start-up and operating procedure

The initial conditions to startup of any natural circulation systems are commonly stagnant low pressure and low temperature. During the pressure and power raising process, the system commonly passes through an unstable zone, which has to be avoided as instability can cause premature critical heat flux occurrence. Thus, it is essential to specify a start-up procedure that avoids the instability. Selection of the pressure at which to initiate boiling and appropriate procedures for raising pressure and power is central to the specification of a start-up procedure. Furthermore, it may become essential to control the inlet subcooling as a function of power (Vijayan and Nayak, 2005).

1.4.5. Low critical heat flux

The critical heat flux depends on the geometric and operating parameters of the system. The prime operating parameters of concern are the pressure, flow, exit quality, inlet subcooling and heat flux distribution. The low mass flux also has an impact on the critical heat flux of the system. Since flow in natural circulation reactors is low, hence tends to use the maximum allowable exit quality to minimize the size. In the process, critical heat flux value tends to be significantly lower than that of forced circulation systems (Vijayan and Nayak, 2005).

1.5. Classification of NCL

According to the requirement of user for study purpose and implementation in real life system, NCLs are classified by many different ways. Consistent with physical shape and size of heat source and sink the NCLs are categorized as Heat points, Toroidal and Rectangular (Figure 1-5). Furthermore, NCL can have various configurations based on the state of working fluids, interaction with the surroundings, inventory, number of channels and body force field. A detailed classification of NCL is shown in Figure 1-6.

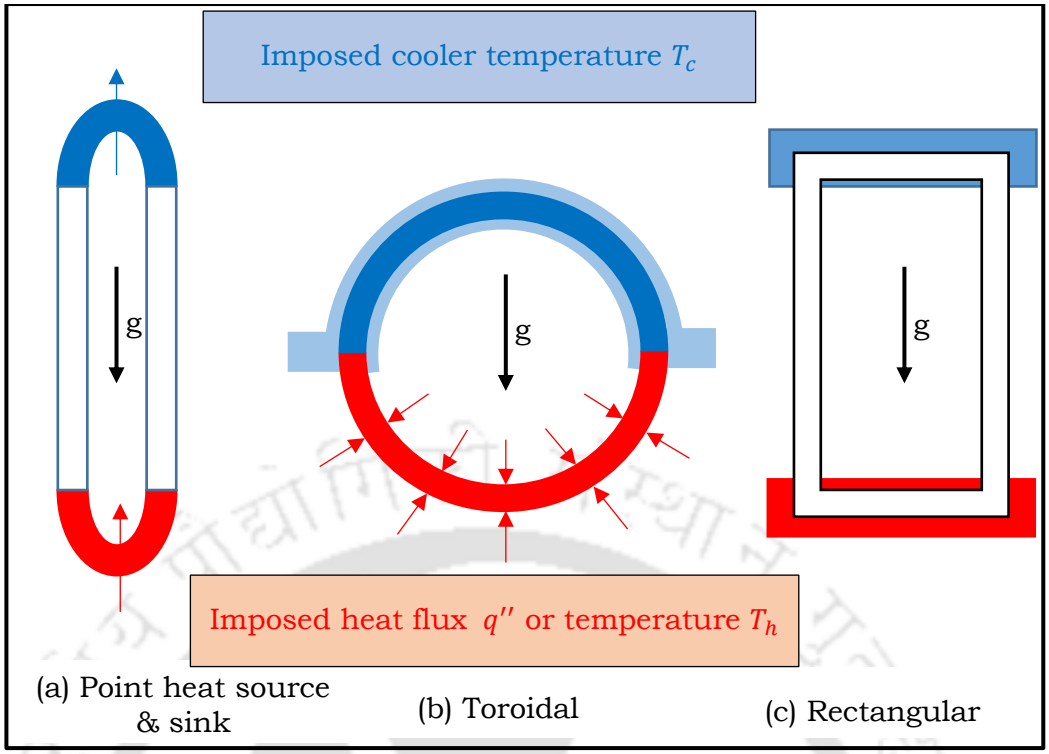

Figure 1-5. Different types of NCL

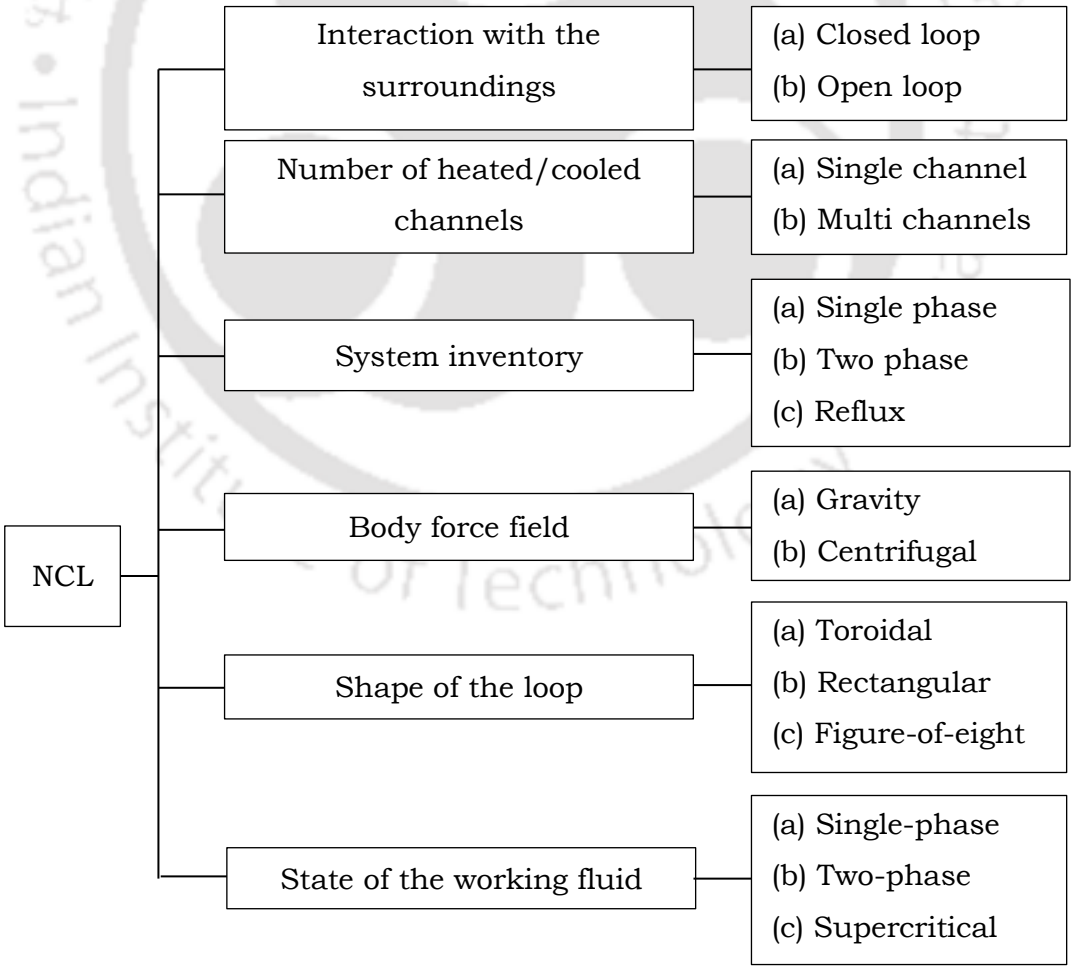

Figure 1-6. Detailed classification of NCL

1.6. Supercritical Natural Circulation Loop (SCNCL)

In order to exploit the enormous energy potential of nuclear fission, modern reactor designs are increasingly adopting higher temperature levels, to expand the thermal efficiency limit. While the single- and two-phase systems are constrained by the saturation temperature criterion, advances in material research allows sustained operation at high temperatures, approaching the borders of 800°C or even higher, and also at higher pressures. That encouraged the scientists to explore the supercritical state and led to the conceptual development of the supercritical water reactor (SCWR), which is an integral constituent of the generation-IV initiative of reactor design. While the US reference design of SCWR primarily adopts forced-flow channels, a few schemes have also recommended embracing NCL as the primary coolant circulation mode, such as the high-temperature CANDU reactor (Bushby et al., 2000) and B-500 SKDI design (Silin et al., 1993). Implementation of natural circulation for reactor core cooling during normal, as well as accidental, condition promises a significant gain in thermodynamic efficiency. The once-through design also eliminates bulky components like separating drum, dryer and recirculation channels, warranting a compact structure. The possibility of employing a variety of fluid to suit the requisite temperature range makes supercritical loop a lucrative technology.

Single-phase liquid is characterized by large thermal conductivity compared to vapor and quite regularized heat transfer behavior. A boiling loop, on the contrary, can exhibit substantial volumetric expansion, yielding considerably large flow rates. Supercritical fluid can integrate the advantages of both the mediums. While the change in density around the pseudocritical point is comparable to liquid-to-vapor phase change, Prandtl number exhibits a peak there, registering excellent heat transport characteristics as a consequence. Accordingly the SCNCLs are characterized by large flow rates and significant heat transfer coefficient, and are anticipated to demonstrate traits of both single- and two-phase NCLs. Vijayan et al., 2010 reported the steady-state behavior of SCNCL to be similar to the two-phase loops, while its stability characteristics followed the single-phase version. However the drastic variation in the thermophysical properties of any supercritical fluid is confined to a small region around the pseudocritical point (Figure 1-7), typically

covering a temperature span of about 30°C, with fairly monotonous representation away from the pseudocritical temperature (T_{pc}). Consequently the benefits of supercritical fluid in an NCL can be harnessed only by operating around that particular zone and hence the performance of SCNCL can deviate a lot depending on the regime of operation.

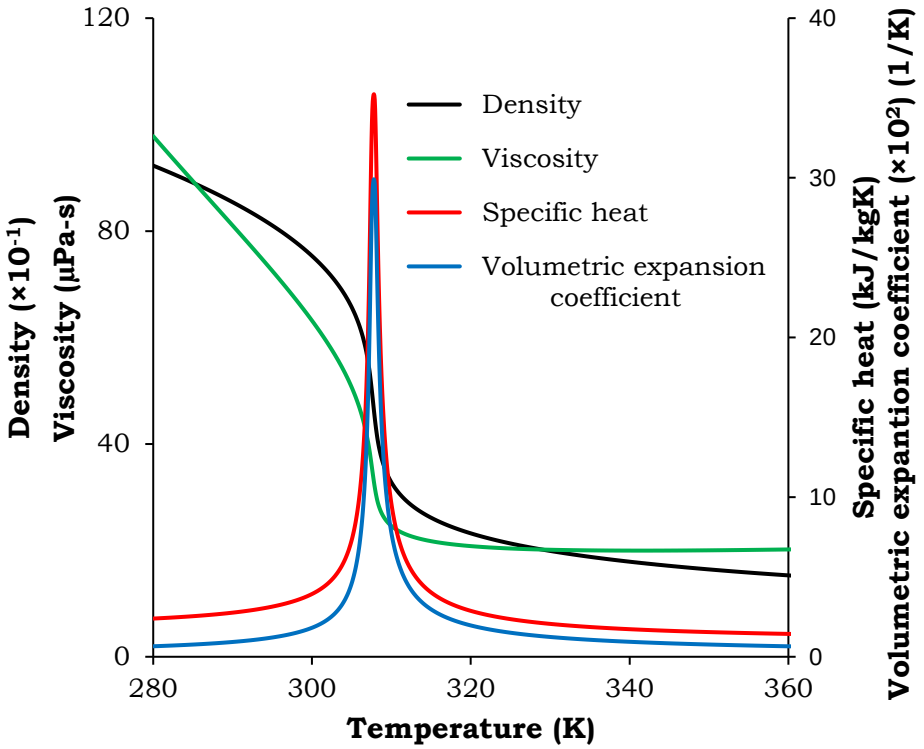

Figure 1-7. Variation in thermo-physical properties of CO_2 with temperature at 8 MPa (NIST, 2011).

Following the conceptual development of CANDU-X reactor (https://goo.gl/yNDUME) around 1998, which was proposed to operate with supercritical water at 25 MPa pressure level as coolant in both forced and natural circulation mode, Chatoorgoon, 2001 was the first to propose an analytical model of SCNCL to envisage the stability and thermalhydraulic characteristics. While most of the conclusions from their simplified approach has been found to veer from real-world, their study served as an excellent launching pad for research on SCNCL. Several semi-analytical and computational studies followed, with limited number of experimental efforts as well. While the initial efforts concentrated mostly on the overall performance, gross discrepancy between the theoretical and experimental results were observed. That shifted the focus towards the local behavior of supercritical fluid in different segments of the loop, which has consequently

been found to play a major role on the overall behavior. More on this issue will be elaborated in the subsequent discussion.

There are some concerns to be taken care of before the commercial implementation of SCNCL. Due to the high operating pressure and temperature the selection of material is a challenge for SCNCL. Stability of the system also needs to be ascertained from thermalhydraulic, neutronic, as well as, structural interaction point of view. Due to high operating parameters, laboratory experimentation equipment's are more expensive than single-phase or two-phase NCL experimentations.

1.7. Motivation behind the Present Work

The tremendous potential of supercritical fluid as a heat transport medium is the main inspiration of the present research work. Merely, by altering the operating condition, the single- and two-phase NCL becomes SCNCL and which can able to perform prominently than preceding versions. The term 'SCNCL' itself describing the operating condition of the system, nature of the flow field and physical geometry of the system. The prime motivation to take SCNCL as a research topic is originates from all of the above mentioned fields. The operating condition of the said system is supercritical, and it has been knowing to us that at near pseudocritical point the thermophysical properties of fluids are extremely sensitive with the temperature. The value of both volumetric expansion coefficient and specific heat are maximum at pseudocritical point. As a result, the system can able to produce an extremely large driving force and consequently much more heat transfer than conventional system. The geometry of the system is a closed loop and the generated flow field is natural circulation type. The driving force of the system is available buoyancy force in the system and hence there is no requirement of any moving elements. This elimination of rotating machineries enormously simplified the system and eradicates all safety issues related with the particular items. The system is also simplified due to the supercritical operating condition, because at this condition fluid is in supercritical single-phase state and hence there is no requirement of bulky components like, steam generator and steam separator. SCNCL is a compelling technology for cooling of modern nuclear reactors, which promises enhanced thermalhydraulic performance in a simple design. Due to simplicity of design, thermal efficiency of SCNCL is higher than the conventional system. From last

few years, significant amount of theoretical and experimental work is reported on the same. However the knowledge base is still far from complete and hence a thorough study over SCNCL have been documented in the present dissertation.

1.8. Outline of the Thesis

This thesis contains nine chapters: an introduction, state-of-art, conclusion and six technical chapters. Each chapter has its own introduction and conclusions, and more or less read independent from the other chapters.

Chapter 1 presents a brief introduction and historical background of NCL, classification, practical application, advantages and challenges of NCL and SCNCL.

Chapter 2 presents a comprehensive appraisal of the relevant literature. The available literatures are subdivided into different categories like, heat transfer aspect, steady state and transient, numerical and experimental study of SCNCL. Detail literature review help to find out or fixed the thesis objectives.

Chapter 3 presents the details of numerical modeling for SCNCL. The meticulous discussion over numerical scheme, grid generation, boundary conditions, validation of numerical models are included here.

Chapter 4 presents a computational investigation for thermalhydraulic comparison of water, CO_2 and R134a as working fluids in a temperature-coupled rectangular natural circulation loop. Influence of different working fluids, operating pressures and temperatures are studied.

Chapter 5 presents a steady state analysis of SCNCL with different working fluids. Heating is provided in constant heat flux mode, whereas cooling is through a constant temperature sink. Effect of different source power, sink temperature and operating pressures are examined.

Chapter 6 presents the effect of geometric parameters on thermalhydraulic characteristics of SCNCL. Accordingly a computational model of a rectangular loop is developed and employed to explore the influence of geometric variables, including diameter, height, width, inclination, corner bends, and heating and cooling lengths and their orientations.

Chapter 7 presents the design and development of experimental setup. Experimental studies have been executed to recognize the steady state and transient behavior of the SCNCL employing subcritical as well as supercritical R134a. Effect of source power, sink temperature, operating pressure and tilt angles in two different planes have been experimentally investigated. Experimental results compared with computational results for identical operating conditions.

Chapter 8 presents the detail transient analysis of supercritical CO_2 based SCNCL. Particularly, for this study a two dimensional computational model developed with identical dimensions of base model. To complete the transient analysis a thorough dynamic performance study have been documented here.

Chapter 9 presents the major conclusions and recommendations for future work. The dissertation accomplishes with important outcomes based on the present study.

Chapter 2: Review of Literature

2.1. Preamble

SCNCL is a compelling technology for cooling of modern nuclear reactors, which promises enhanced thermalhydraulic performance in a simple design. Use of supercritical fluids promises a simplified design, along with higher thermal efficiency for heat transport systems. Characteristics of such loops are markedly different from its single-phase and two-phase counterparts, while carrying quite a few similarities with both as well. Therefore significant number of research studies have been carried out on SCNCL in the present millennium. Present chapter attempts to present a state-of-the-art summary of all relevant observations. The review study begins with the categorization of available literatures of SCNCL. Most of the reported studies are theoretical in nature, with only a limited number of experimental works being reported. Therefore, at the beginning of study literatures are divided into two major groups, namely numerical and experimental. In both the approaches, the main objective of the study is steady-state and transient analysis of thermalhydraulic and stability aspect of SCNCL. The study of flow characteristic and heat transfer aspect are the most vital segments for steady-state analysis. In the stability analysis section, the time-domain and frequency-domain approach of stability analysis are discussed separately. Available experimental works are described, with exhaustive discussion on the novelty of the concerned facility and major observations. Finally a few topics are ear-marked as the possible guidelines for future research. Several gaps are identified from a meticulous review study and accordingly, finalized the objectives of the present thesis.

The concept of SCNCL is an important inclusion in Generation-IV nuclear reactors. Use of supercritical fluids promises a simplified design, along with higher thermal efficiency for heat transport systems. Characteristics of such loops are markedly different from its single-phase and two-phase counterparts, while carrying quite a few similarities with both as well. Low driving head and possibility of thermalhydraulic instabilities, however, are major concerns and hence lots of research studies have been

reported on such systems, particularly in relation with the working medium. The loop fluid continues to be in the same phase, commonly liquid, throughout the flow path for single-phase NCLs, which are used for heat removal in solar heaters (Close, 1962; Shitzer et al., 1979), PWRs (Delmastro, 2000) and electronic chip cooling (Kim et al., 2008), to name just a few of many possible applications. Higher rate of heat removal and larger circulation rates are associated with two-phase NCLs due to the presence of boiling and/or condensing sections, and hence found application mostly in power industries. Two recent examples can be Economic Simplified Boiling Water Reactor (Rohde et al., 2010) and Advanced Heavy Water Reactor (Sinha and Kakodkar, 2006).

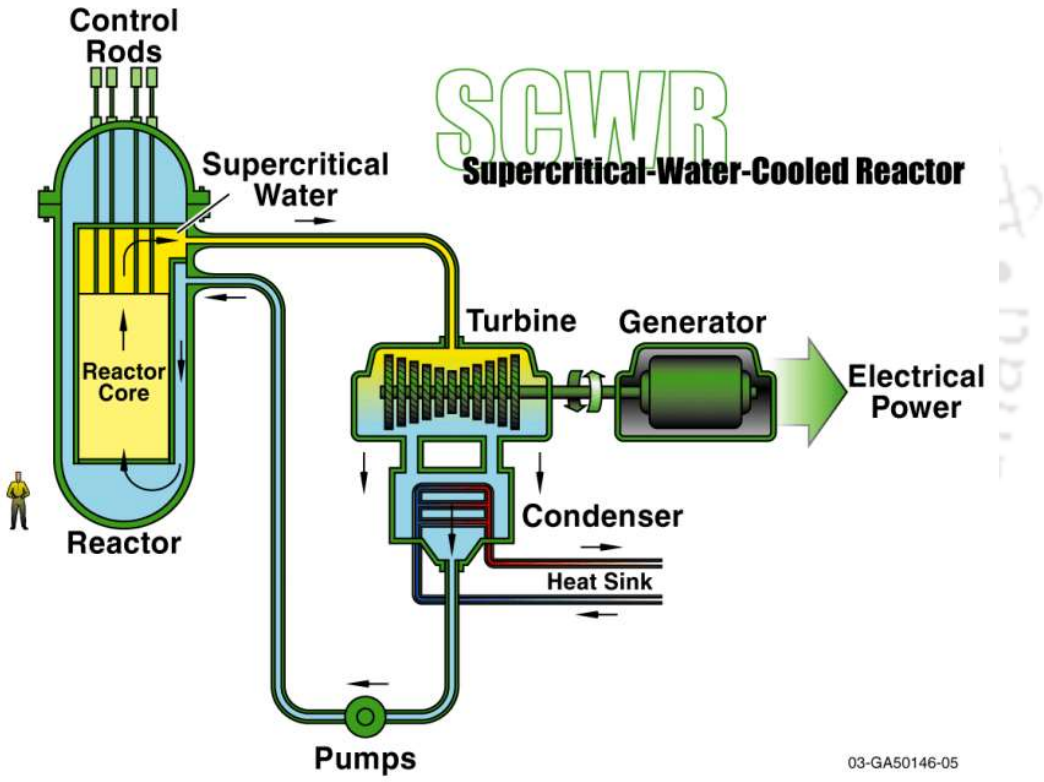

Figure 2-1. U.S. Supercritical water cooled reactor (Buongiorno and MacDonald, 2003).

Supercritical Water Reactor (SCWR) is one of most important concepts of generation-IV initiative of nuclear reactors (Buongiorno and MacDonald, 2003). The schematic of U.S. version of SCWR is shown in Figure 2-1 . SCWRs are basically light water reactors and operating at above the thermodynamic critical point of water (374 ℃, 22.1 MPa). The involvement of higher operating parameters of SCWR, enhances the thermal efficiency around 44% or more

(IAEA, 2005; Yamaji et al., 2005). Furthermore, the higher steam enthalpy allows to reduce the size of the turbine system and hence the capital costs of the conventional island reduced markedly. The notable examples of experimental facility of SCNCLs were developed by the group of 'Bhabha Atomic Research Centre' in India and the group of 'Nuclear Power Institute of China' and 'China Institute of Atomic Energy' in China (Chen et al., 2012b, 2012c, 2013e, Liu et al., 2015, 2016a, 2016b, 2017, Sharma et al., 2010a, 2012, 2013, 2014). The concept of SCNCL is relatively new, with lots of potential for application to nuclear industry in near future. Hence it is essential to summarize the research outcome till date to present a comprehensive picture of the state-of-the-art of SCNCL and current work focuses precisely on the same, providing a systematic development of SCNCL and ascertain the key topics for future investigations.

2.2. Steady-state Flow Characteristics

Steady-state implies a condition where the system parameters are invariant with time. Assessment of steady-state characteristics is important both for system design and performance comparison point of view and hence various theoretical models have been proposed Chatoorgoon, 2001 was probably the first one to develop an analytical model of single-channel SCNCL, as he presented numerical results using SPORTS (Special Predictions Of Reactor Transients and Stability) code (Chatoorgoon, 1986). He studied both distributed and point heat source and sink, with the point source being a simplified representation to eliminate nonlinear effects. Solving conservation equations for mass, momentum and energy, steady-state flow rate was found to increase with power supply till a maxima and decrease afterwards (Figure 2-2). He postulated that the stability threshold for such system can be determined through steady-state analysis using the following criterion.

$$\frac{\partial G}{\partial Q} = 0 \tag{2-1}$$

Therefore the location of maximum flow rate was identified as the threshold. The value of power corresponding to that maxima was termed as the bounding power. Integration of steady-state momentum equation around the loop also provided a closed-form expression of mass flux having the following form,

$$G^2 = \frac{2DgH(\rho_1 - \rho_1)}{\frac{f_1 L_1 + f_3 L_3}{\rho_1} + \frac{f_2 L_2}{\rho_2}} \quad (2\text{-}2)$$

Here 1 refers to the section between entrance and heat source, 2 is the hot leg between heat source and sink and 3 is the cold leg of the loop. f_i and ρ_i indicates the friction factor (inclusive of obstruction coefficient) and fluid density in the i^{th} section. A simple equation of state was considered with density being a sole function of enthalpy and no pressure dependence. Couple of non-dimensional parameters were introduced as,

$$Q_b^* = \frac{Q_b}{AG_{max}h_1} \qquad G_{max}^* = \frac{G_{max}}{\xi\rho_1} \quad (2\text{-}3)$$

Here G_{max} is the maximum steady-state mass flow rate, Q_b is the bounding power corresponding to maxima of mass flow rate and $\xi = \sqrt{2DgH/f_2L_2}$. L_t refers to the total length of the loop, whereas h_1 is the fluid enthalpy in the cold leg. These parameters were found useful for scaling analysis and experimental design, and were also used for stability analysis.

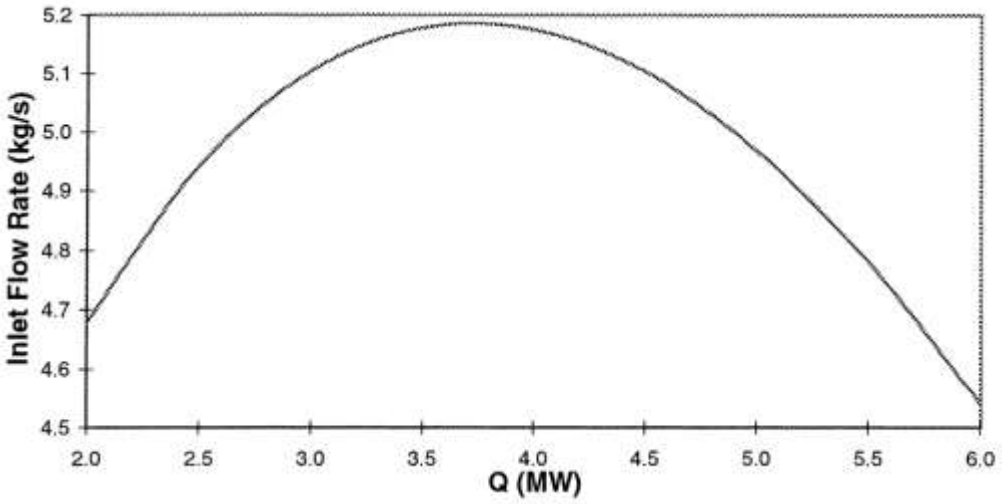

Figure 2-2. Effect of power on steady-state flow rate with distributed heat source and sink Chatoorgoon, 2001.

The same methodology was extended in the subsequent numerical studies of Chatoorgoon et al., 2005a, 2005b, as they analyzed the relative influence of various geometrical parameters (heater and cooler lengths, loop height, inlet and outlet restriction coefficients) on the stability behavior with different fluids like water, carbon dioxide and hydrogen. Steady-state profiles of flow rate for different fluids were found to be quite similar in nature, but with considerable magnitude difference. It was also observed that the flow rate corresponding to the stability threshold can be predicted using the peak

steady-state flow rate with about 95% accuracy. Another computational model named FIASCO based on implicit finite difference scheme was proposed by Jain and Rizwan-uddin, 2006 using constant pressure drop boundary condition, along with constant inlet conditions. Predicted steady-state profile of mass flow rate with heater power was found to be quite similar to the observations of Chatoorgoon et al., 2005b.

Vijayan et al., 2010, proposed a general 1-D theoretical model of a closed rectangular NCL of uniform diameter with horizontal-heater-horizontal-cooler (HHHC) configuration along with adiabatic connecting pipes to compare the steady-state and stability performances of geometrically-identical single-phase, two-phase and supercritical loops, all using water as the working fluid. Boussinesq approximation was used for single-phase loops, whereas equivalent expansion coefficients were defined for two-phase and supercritical loops. Finite difference discretization was followed for supercritical systems, with an equation of state defining density as a function of enthalpy and pressure. Single-phase flow rate monotonically increased with power, whereas two-phase loop exhibited a maxima after initial increase. Steady-state flow behavior of SCNCL was found to be similar to single-phase loops at lower power. But, with increase in power supply, profile behaved akin to the two-phase system. The reduction in flow rate corresponded to the pseudo-critical zone, as thermal expansion coefficient showed a rapid reduction. That approach was extended by Sharma et al., 2010c, 2010b on a similar model, but having different dimensions, to develop two contrasting computer codes, namely, SUCLIN and NOLSTA. The first one employed frequency-domain approach to perform linear stability analysis, whereas the second one followed time-domain non-linear. Both predicted nearly identical steady-state performances. Effects of various parameters like pipe diameter, system pressure, heater inlet temperature and loop height were investigated. Loop flow rate was found to increase rapidly with the increase in diameter and height (Figure 2-3) and moderately with system pressure, whereas it decreased significantly with higher heater inlet temperature. In subsequent studies (Sharma et al., 2013, 2010a), NOLSTA was applied to an open loop in HHHC orientation with 13.88 mm inner diameter and 2 m height. Steady-state results exhibited decent comparison with the experimental study of Lomperski et al., 2004 performed with CO_2 at 8 MPa and 297 K. Effect of loop orientation on mass flow rate was numerically evaluated. HHHC configuration

was found to have the maximum flow rate for any given power input, whereas the vertical-heater-vertical-cooler (VHVC) configuration experienced the least.

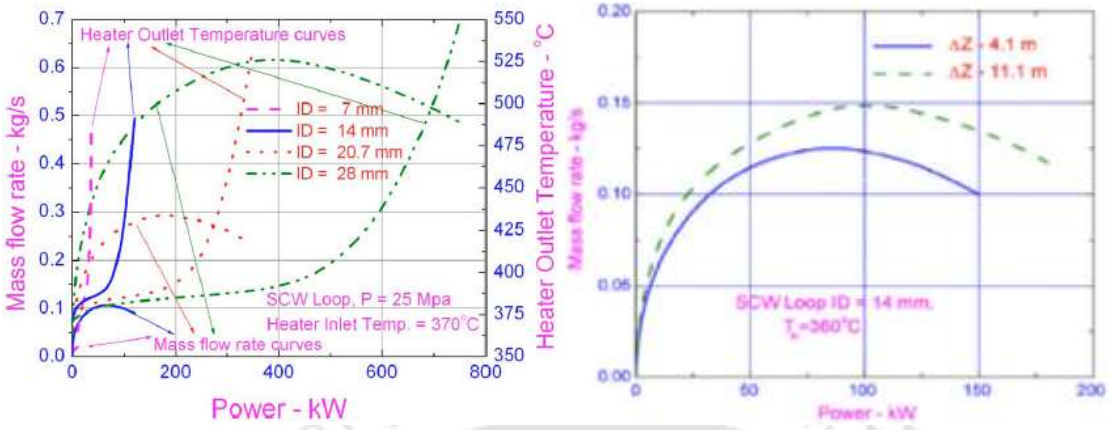

(a) Effect of loop diameter (b) Effect of loop height

Figure 2-3. Influence of (a) loop diameter and (b) height on steady-state mass flow rate (Sharma et al., 2010a).

A 3D computational model was developed by Yadav et al., 2012a using Fluent for steady-state simulation of a rectangular NCL with specified source and sink temperatures. Implicit finite volume algorithm was followed with second-order upwind discretization for convective terms and PRESTO for the pressure term. PISO scheme was used to solve the coupling model between velocity and pressure and RNG $\kappa - \varepsilon$ turbulence model was employed. Both water and CO_2 were considered as the working fluids at three different pressures and temperatures to compare their heat transfer and fluid flow aspects. Comparison of velocity contours with water at 1.013 bar and CO_2 at 100 bar at some selected locations of the loop are presented in Figure 2-4. The asymmetry in velocity profile at any cross-section is clearly evident, which originates due to local buoyancy effects, more on which is discussed later on. CO_2 continually exhibited greater velocity magnitude than water at any given power condition. Analyzing the simulated results, they also proposed correlations for estimating friction factor (f) and Reynolds number (Re) in terms of Grashof number (Gr) in the following form.

$$f = (0.7907\, ln(Re) - 1.868)^{-2}$$
$$Re = 2.066 \left(Gr_m \frac{D}{L_t}\right)^{1/2.77} \quad (2\text{-}4)$$

The proposed relations are applicable in the range of 27,000 $\leq Re \leq$ 180,000, with an R^2-value of 0.9387, thereby showing a good regressed fit. A maximum deviation of 6.5% was observed with all the simulated results.

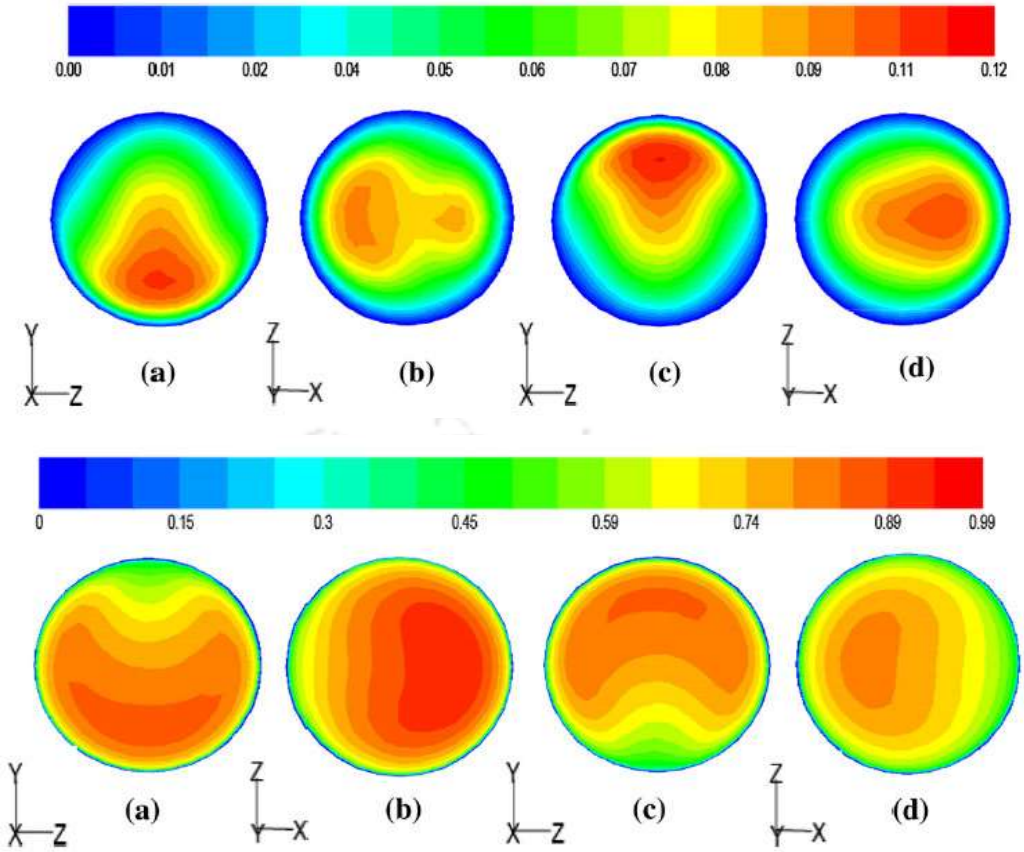

Figure 2-4. Velocity contour plot for water and CO_2 respectively at the centre of (a) source, (b) riser, (c) sink and (d) downcomer (Yadav et al., 2012b).

Swapnalee et al., 2012 used their experimental data to propose a general correlation to estimate the steady-state flow in SCNCL in terms of a relationship between dimensionless density and dimensionless enthalpy. The definitions proposed by Ambrosini and Sharabi, 2008 were used for the dimensionless quantities, as those can provide a unique profile of dimensionless density against dimensionless enthalpy for CO_2. The correlation was found to be applicable for CO_2, H_2O and a few other fluids. The relationship was proposed by a sigmoidal curve relationship in the following form.

$$\rho^* = A + \frac{B}{1 + exp(1.5181\, h^* + 0.5689)} \tag{2-5}$$

Here A = 0.15704 and B = 2.4785. The dimensionless quantities are defined as,

$$\rho^* = \frac{\rho}{\rho_{pc}} \qquad h^* = \frac{\beta_{pc}}{C_{p,pc}}\left(h - h_{pc}\right) \tag{2-6}$$

The proposed relationship is independent of system pressure and applicable for different supercritical fluids.

2.3. Heat Transfer Aspects of SCNCL

Present focus of SCNCL being in the nuclear field, it is important to ensure a high heat transfer rate, as any deterioration in heat transfer can be fatal for the plant operation. Very high rate of fission heat generation necessitates a high value of heat transfer coefficient throughout the heating channel and hence it is an active area of research to avoid such loss-of-coolant-accident (LOCA). Working fluid remains as liquid in single-phase NCL, which provides high thermal conductivity. But low fluid velocity results in low heat transfer coefficient. Two-phase NCL can provide much higher heat transfer coefficient, but the separation of phases can be difficult in natural circulation systems, as incorporation of any mechanical separators can introduce undesirable pressure losses. Supercritical loops can integrate the advantage of high conduction heat transport of single-phase loops and high flow rate of two-phase loops, without requiring the separation of phases. However supercritical fluids exhibit drastic changes in thermo-physical properties around the pseudo-critical point, as is shown in Figure 1-7 for CO_2 at 8 MPa, which may induce sharp deterioration of heat transfer coefficient. Hence a comprehensive knowledge about the heat transfer and flow aspects of SCNCL is important and number of recent research studies have focused on the system thermalhydraulics, mostly to characterize the relative influence of various geometric and operating parameters. Following sections present a systematic approach to summarize the observations from related studies.

2.3.1. Temperature differential between heat source and sink

The temperature difference between the thermal source and sink is probably the most influencing parameter in deciding the loop thermalhydraulics. The phenomenon of natural circulation is generally decided by an interplay between buoyancy and friction, with inertia having negligible effect. The buoyancy force in single-phase NCL linearly increases with increased temperature differential and hence induces near-linear increase in mass flow rate and heat transport capability. But properties of supercritical fluid being strongly temperature-dependent, development of buoyancy field depends on the temperature range involved. Density drops rapidly around the pseudo-critical point, resulting in a peak of the volumetric expansion coefficient. Hence, if the fluid temperature crosses the pseudo-

critical region during its passage through the heater, a high density differential is developed, providing a strong buoyancy field. Concerned increase in flow rate also enhances the frictional resistances. Fluid viscosity can also drop sharply, altering the frictional forces. The combination of these two opposing effects resolves the loop flow rate and associated rate of heat transfer.

When the cooler temperature is near the pseudo-critical temperature, viscous forces are dominated by buoyancy force and causes enhanced mass flow rate and heat transfer. The reverse condition occurs at very high loop temperatures, particularly for CO_2. Nusselt number decreases with high temperature differential between heater and cooler, because of increase in thermal conductivity (Cao and Zhang, 2012). Pseudo-critical temperature being dependent on system pressure, such drastic property variations occur at higher temperature levels for higher pressures, which causes enhanced flow rate and increased heat transfer rate (Yadav et al., 2012c, 2012b). For high temperature differential between heater and cooler, mass flow rate can decrease as well (Yadav et al., 2012a, 2012c), whereas similar effect can be found with increasing heater power (Chen et al., 2013b). Mass flow rate, on the other hand, can decrease with increasing coolant temperature near pseudo-critical zone, if the heater temperature or heating power is kept constant.

Heat transfer coefficient of supercritical CO_2 has been found to increase with increase in operating pressure and produce a maxima with increasing temperature (Yadav et al., 2012c). Due to stable temperature of cooler, concerned heat transfer coefficient is nearly unchanged with enhancement in bulk temperature. But heat transfer coefficient at heater is greatly affected due to rapid deterioration of thermal conductivity around pseudo-critical point (Chen et al., 2013c). Level of heat transfer coefficient can be found to be significantly higher than single-phase system and nearly comparable with boiling loops. Experimental study of Tokanai et al., 2010 on CO_2-based SCNCL also reported high heat transfer coefficient, as large as about 1.6 kW/m^2K.

Following the argument of Zhang et al., 2010, fluid near the wall of the heater is at a higher temperature and lower density, compared to the cooler bulk fluid near the centerline. This density difference locally generates a strong buoyancy force, leading to an upward radial flow velocity. The same

phenomenon occurs at the cooler also, but with downward radial velocity, due to cooler and denser fluid near the wall. As a result, fluid near the upper wall of the cooler and lower wall of the heater directly drives the heat and mass transfer into the main flow field, resulting in enhanced heat transfer. The reverse situation appears for lower wall of the cooler and upper wall of the heater, restricting the corresponding heat transfer. Figure 2-5 presents the variation of wall Nusselt number at four specific locations of a rectangular loop. Here wall 1 and 2 refers to the upper and lower wall of the cooler,

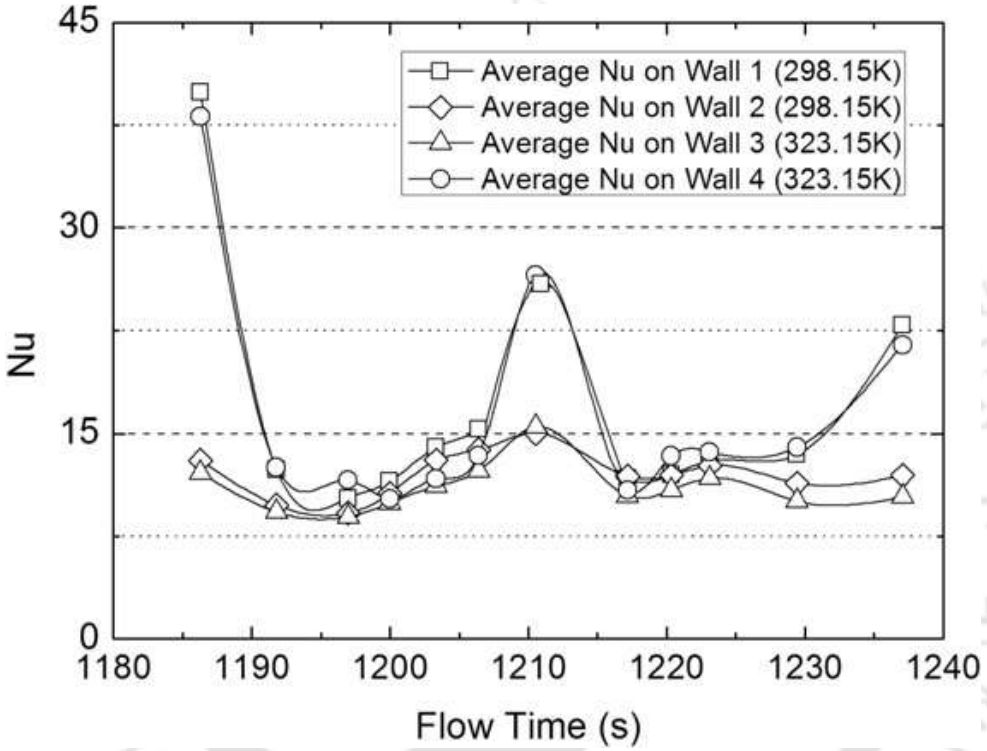

Figure 2-5. Evolution of average Nusselt number at four different sections of a rectangular loop in one typical cycle (Zhang et al., 2010).

whereas 3 and 4 indicates the upper and lower walls of the heater (Zhang et al., 2010). Throughout the cycle, heat transfer coefficients at wall 1 and 4 are significantly higher than the other two. That leads to asymmetric velocity and temperature distribution across a cross-section anywhere in the loop, as was reported by Yadav et al., 2012c. Similar to *Nu*, other flow parameters also exhibit periodic variation at any particular location of the loop and such periodic change in pressure difference across any flow section can cause flow reversal, along with other influencing factors like symmetric geometry, turbulence and higher heating wall temperature. Large change in density causes greater buoyancy force and reduction in fluid thermal conductivity does not allow sufficient cooling in the cooler section, which can reverse the

flow direction. Reynolds number increase with increase in heater temperature near T_{pc}, because of decrease in fluid viscosity and increase in fluid velocity (Chen et al., 2010; Yadav et al., 2012a). But when the heater temperature is far away from T_{pc}, *Re* decreases due to gradual increase of fluid viscosity, despite no drastic change in velocity. So it can be concluded that the profile of mass flow rate and Nu with changes in temperature differential between heater and cooler are quite similar qualitatively, as can be emphasized from Figure 2-6 for CO_2 at 9 MPa pressure and constant sink temperature of 310 K. Both of them increase rapidly when heater temperature is around T_{pc}, but decreases for larger temperature differential, whereas heat transfer coefficient continually increases with temperature differentials.

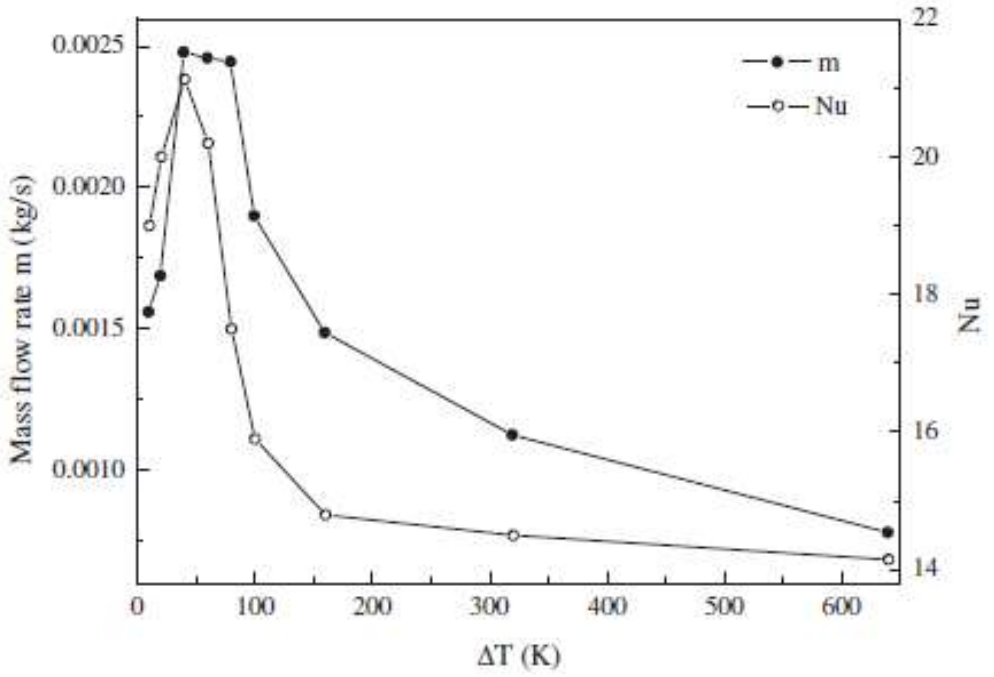

Figure 2-6. Variations of mass flow rate and average Nusselt number with the temperature difference between heater and cooler (ΔT) (Cao and Zhang, 2012).

2.3.2. Heater and Cooler orientation

Orientation of heat addition and removal do have significant influence on the loop characteristics, both from thermalhydraulic and stability point of view. With relocation of heating or cooling section, magnitude of buoyancy force gets altered, due to the change in effective rising height of the lower-

density fluid or falling height of the higher-density fluid. Buoyancy being the sole driving force, it distinctly modifies the loop flow rate and heat transfer aspect gets affected accordingly. Chen et al., 2014 considered four different orientations of heater, at middle and left of bottom horizontal arm and middle and down of left vertical arm. Cooler was considered to be fixed at the middle of top horizontal arm. Nusselt number was found to increase with heat flux. Either of the vertical configurations produced nearly the same value of *Nu* over the entire range of heat fluxes. For higher heat flux levels, however, both the horizontal configurations showed a phase-lag in Nu prediction with time and considerable deviation from each other at lower heat fluxes. Swapnalee et al., 2012 experimented with both heater and cooler in horizontal and vertical arms of a rectangular loop. It has been found that HHHC configuration can produce higher values of Re and Gr than other orientations. Flow reversal occurs more frequently in HHHC loop because of higher level of instability and symmetric geometrical orientation, whereas asymmetric configuration mostly results in flow in pre-defined direction (Chen et al., 2013a). It is clearly evident from the limited literature that the orientation of heater and cooler has more obvious influence on flow rate than heat transfer characteristic in SCNCL. However further studies are desired before drawing any final conclusion.

2.3.3. Effect of inclination angle

Inclined loop lowers the vertical distance between heat source and sink in comparison to an upright loop, which can effectively simulate a reduced-gravity scenario. When loop is inclined by some angle θ to the vertical direction, the buoyancy force will reduce by a factor $\cos\theta$. Accordingly the mass flow rate through the loop is reduced, other parameters remaining the same. *Nu* was found to decrease with an increase in inclination angle, which indicate an inferior heat transfer performance of SCNCL for inclined loops (Cao and Zhang, 2012). At high heat flux conditions, effect of inclination angle on heat transfer is less pronounced (Chen et al., 2013a). For such cases *Nu* increases with increased heat flux and reduces slightly with increasing inclination. But at lower heat input conditions, inclination angle has relatively significant influence on the heat transfer rates (Chen et al., 2013d). With 15° inclination to vertical, average *Nu* for heat flux conditions of 60,000 W/m^2, 6000 W/m^2 and 600 W/m^2 was reported to be 2145, 184.5 and 21.61 respectively, showing the sharp deterioration at lower fluxes.

2.3.4. Effect of tube diameter

Tube diameter is directly related to the heat transfer surface area at both heating and cooling sections and also to the resistance offered to the flow. So higher heat flux is required for larger-diameter tubes in order to maintain the same level of temperature and flow rate. Figure 2-7 shows the variations of cooler and heater *Nu* number with heating wall temperature for two different tubes at 9 MPa pressure for a CO_2-based loop. *Nu* drastically increases with increase in tube diameter and decreases with higher of heating wall temperature (Cao et al., 2011; Chen et al., 2013a; Chen and Zhang, 2011). Heat transfer coefficient at the cooler section is found to be considerably higher than the same at heater section, apart from lower heating wall temperature.

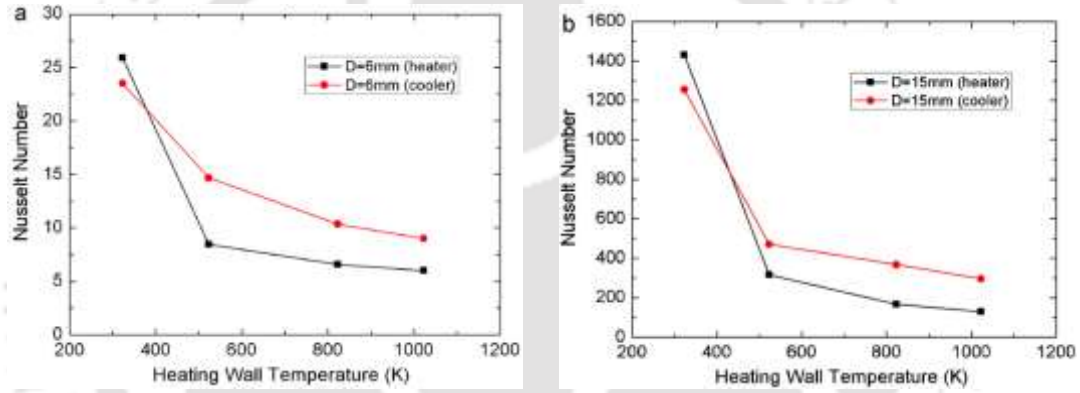

Figure 2-7. Variation of Nusselt number with diameter for (a) 6 mm and (b) 15 mm (Chen et al., 2013a).

Yadav et al., 2012b also numerically concluded that both mass flow rate and heat transfer rate increase with increase of loop diameter. Loop Reynolds number decreases with the increase in heating wall temperature and increases with tube diameter. Major variation in *Re* is, however, due to the change of viscosity, particularly around pseudo-critical point. Due to low viscosity at supercritical temperature, reverse flow can also occur for lower diameter loops. For larger diameter loops the chance of flow reversal is significantly low due to high flow velocity and resultant higher acceleration. Sadhu et al., 2018a numerically observed that, heat input can be amplified by increasing diameter of the loop for maximum mass flow rate. The heat transfer performance is greatly alter with varying diameter than height of the loop. Larger diameter loop has better performance than longer height loop.

2.4. Investigation on Flow Instability

Keller, 1966 was the first to theoretically find the periodic motion in a one dimensional model of rectangular NCL with point heat source and heat sink. He showed that under certain operating conditions, the system behaves like a self-excited oscillator. The effect of inertia was very negligible on such oscillations. That type of oscillations can occur simply requiring an interplay between frictional and buoyancy forces. The cause of instabilities in NCLs are meticulously discussed by Welander, 1967. The presence of thermal irregularities in the fluid is the reason of formation of unstable motion in the system. The irregularities amplify through the correlated variations in flow rate. A warm pocket of fluid creates maximum flow rate through the upper part and minimum flow rate going through the lower part of the loop. Flow rate in any natural circulation system being dependent on the interaction of forces and extremely sensitive to all involved system parameters, NCLs are always susceptible to instabilities. It can also be attributed to the non-linear nature of the phenomenon, as any change in the driving force affects the flow, which in turn affects the driving force itself, possible leading to either a self-correcting action or an oscillatory behavior. It is highly desirable to identify possible zones of instability in SCNCL operation, as unstable fluctuations can lead towards severe consequences in nuclear systems. Hence most of the studies on SCNCL have focused on stability evaluation and some of the important conclusions are summarized below.

2.4.1. Numerical Investigations

Two contrasting approaches have generally been followed for stability analysis. The linear or frequency-domain approach is based on developing the linearized version of perturbed conservation equations and identifying the nature of corresponding eigen values. On the contrary, the non-linear or time-domain approach numerically solves the complete transient form of governing equations and follow the temporal evaluation of system variables. Different research codes like SPORTS (Chatoorgoon, 2001), SUCLIN (Sharma et al., 2010c), NOLSTA (Sharma et al., 2010b), FIASCO (Jain and Rizwan-uddin, 2008, 2006), NAFA-LOOP (Archana et al., 2015) etc. were proposed with varying objectives. Use of system codes such as ANSYS-Fluent (Yadav et al., 2016a, 2016b, 2014) and RELAP5 (Debrah et al., 2013a, 2013b) can also be found for detailed transient analyses and non-linear stability characterization

respectively. To study the effect of heating structures and numerical diffusion on the dynamic behavior of SCNCL, 1D numerical codes following both the approaches were developed by Ambrosini, 2016; Carbone and Ambrosini, 2016, while Cheng and Yang, 2008, developed a theoretical approach named point-hydraulic model (PHM) for predicting the flow oscillation at supercritical operating condition of the system. More detailed discussion on concomitant literature is presented below.

2.4.1.1. Time-domain approach

Non-linear stability analysis generally involves the application of a small perturbation over the steady-state solution and subsequent evaluation of the transient equations over a prolonged duration of time. If the disturbance amplifies with time, the system is considered to be unstable. On the contrary, if the disturbance leads to decaying oscillations resulting in convergence of flow and other field variables back to the initial steady-state, corresponding system is considered to be stable. If the flow oscillations remain unchanged with time after a period of initial development, system is considered to be neutral, thereby predicting the threshold power for the system stability. Stability analysis code SPORTS was developed by Chatoorgoon, 1986 for investigating stability of two-phase flow systems, mostly at low pressure. It determines flow stability by introducing a perturbation in the inlet flow rate and executing real-time transients. The same code was modified by Chatoorgoon, 2001 to study the stability response of a rectangular loop with both distributed and point heat source and sink. The point heat source predicts instability much earlier than the distributed source. For identical conditions, stability threshold for point heat source and distributed source were found to be 3 MW and 4.5 MW respectively. In subsequent studies, Chatoorgoon et al., 2005a, 2005b examined the effects of several geometric and operating parameters on supercritical flow stability. They also included the effects of different working fluids, like CO_2 and H_2. Based on their results, it is concluded that stability characteristics of supercritical CO_2 were quite similar to the same of supercritical H_2O.

Jain and Rizwan-uddin, 2008 developed another nonlinear stability analysis code FIASCO using implicit finite difference scheme. Control-volume-based discretization in space and forward-difference scheme in time is employed, along with constant pressure drop boundary condition and

constant inlet conditions. Most of the transient analyses was carried out with a spatial grid size of 0.1 m and time step size of 0.35 s. Figure 2-8 presents the stable, neutrally stable and unstable time response for three different input power with CO_2 as working fluid. It was found that reduction in spatial grid size did not produce any significant changes on system stability, as the system remained stable at finer spatial resolutions producing spatially converged solutions. A shift in oscillations was observed, while the magnitude and frequency of oscillations remained nearly the same. Choice of time step, however, was identified to be very important, as a larger value can induce artificial stability. It was suggested to choose the time step in such a way that Courant number is close to unity. Similar role of tolerance in pressure boundary condition was also mentioned and a value of 10^{-6} MPa or less was prescribed, as a larger tolerance might suppress smaller perturbations. Predictions from FIASCO code deviated from the results reported by Chatoorgoon et al., 2005a, as the stability threshold was not obtained around the peak of mass flow profile, and such disagreement was attributed mostly to the undesirable dissipative and dispersive effects induced by large time steps.

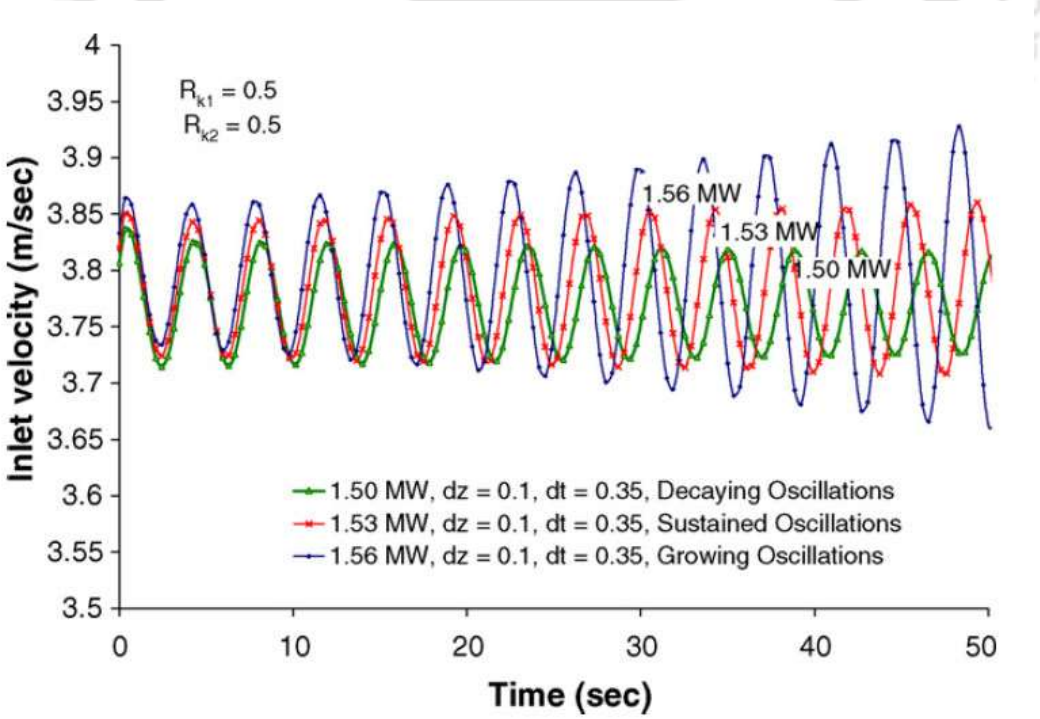

Figure 2-8. Transient responses for three different power levels (Jain and Rizwan-uddin, 2006).

Sharma et al., 2010c employed two different computer codes SUCLIN and NOLSTA to study the stability behavior of the loop with water as the working fluid. Control volume discretization in space using upwind scheme and forward difference in time were employed to discretize the conservation equations in NOLSTA. An obstruction coefficient was employed to consider minor pressure losses. Transient solution identified a stability threshold at 73.2 kW for 25 MPa system pressure and 633 K heater inlet temperature. In a subsequent study (Sharma et al., 2010a), NOLSTA code was applied for determining the stability characteristics of an open CO_2 loop used by Lomperski et al., 2004. The loop orientation was HHHC having ID of 13.88 mm and height of 2 m. Simulation results were validated with the experimental data of mass flow rate and heater outlet temperature. A stability threshold of 7.5 kW was predicted at 8 MPa and 297 K, while there was no instability found in the experiments. This deviation was attributed to the effect of wall capacitance. A sensitivity analysis was also carried using the code for investigating the effect of grid size and time step size. Instability increases in the system with increase in diameter, as that reduces the stabilizing frictional forces. It was also observed that power step-down increases instability, whereas unstable oscillations dies down with power step up. Dynamic response of a water-based SCNCL under transient variation in heater power was investigated by Tilak and Basu, 2015. Here, 1D conservation equations are solved numerically and stability threshold is estimated by following the nonlinear stability analysis approach. Step, ramp, exponential and sinusoidal-type of excitations were imposed on the heater power. The stability of the system is greatly fluctuated for each type of excitation imposed on the system. Rai et al., 2017, reported a numerical study of Ledinegg and density wave oscillation (DWO) in a vertical heater and vertical cooler configured loop. They were able to identify DWO under certain set of operating conditions, but Ledinegg instability was not observed.

2D numerical simulation of a supercritical CO_2 loop was carried out by Chen et al., 2010 to investigate the flow transitions and instabilities. Second order upwind scheme was used to discretize the conservation equation in finite volume method. Laminar flow model was considered with no-slip wall boundary and a structured non-uniform grid system was used to mesh the whole volume. Heat source temperature was varied in the range of 310-1023 K at a pressure of 9 MPa, while maintaining sink temperature constant at 298

K. A transition fluid average temperature was identified where the system changes from unstable repetitive-reversal flow to stable one-directional flow with further increase in temperature. Such critical transition fluid temperature was found to be near the second “pseudo-critical temperature” (defined as the average input wall temperature at which flow reversal frequency increases) at around 375 K, where the fluid properties experience major transitions with rise in temperature. Chen et al., 2012a extended the same model to investigate the effect of heat input condition on velocity and temperatures on supercritical and trans-critical CO_2 system. Numerical investigation was made with three different types of unsteady heat input, namely, sudden/quick increase, gradual/slow increase and sudden decrease. RNG k–ε model was included to introduce turbulent effect and heat sink was maintained at 290 K at an operating pressure of 9 MPa. It was found that slow increase of input heat flux induced less flow instability in the system than quick increase of the same, as quick increases could lead to greater velocity and temperature fluctuations. For sudden decrease in heat input, trans-critical CO_2 flow was found to be capable of quick slow-down, thus contributing to a safe system load-off implying less fluctuations. A similar supercritical/transcritical CO_2-based loop was also studied by Chen et al., 2013a in the pressure range of 7.5 MPa to 9 MPa. Source temperature was varied within 323.15 K to 1200 K, whereas sink temperature was also varied within 290 K to 300 K for different studies. Effects of heat source temperature, loop aspect ratio, loop diameter and its coupling effect with heat source temperature on system stability were investigated, along with the effect of constantly changing heat input condition during unsteady input. Unit value of aspect ratio, defined as the ratio of height to width of the loop, resulted in unstable system behavior, whereas the system was found to be more stable at higher and lower aspect ratios, as was reported by Cammarata et al., 2004. They considered aspect ratio in the range of 0.67 to 10.

RELAP5 was probably used for the first time by Debrah et al., 2013a to observe the stability phenomenon in a natural circulation loop with supercritical fluids. A simplified loop was considered with pipe diameter of 4.62 mm, similar to the one used by Chen et al., 2012b for experiments. Non-dimensionless scaling parameters introduced by Ambrosini and Sharabi, 2008 were also employed for the stability analysis and developed stability maps in terms of dimensionless numbers were confirmed by RELAP5

simulations. Two dimensionless groups were used, namely, N_{SPC} representing the dimensionless power-to-volume ratio and N_{TPC} representing non-dimensional fluid subcooling at heater inlet. Their mathematical expressions are given below.

$$N_{SPC} = \frac{\beta_{pc}}{C_{p,pc}} \frac{q^{''} \Pi_h L}{\rho_{in} \dot{m}_{in} A} \qquad N_{TPC} = \frac{\beta_{pc}}{C_{p,pc}} (h_{pc} - h_{in}) \qquad (2\text{-}7)$$

So-obtained stability maps (Figure 2-9) exhibited the dependence of a perturbation amplification factor on the dimensionless power-to-flow ratio and dimensionless heater inlet enthalpy provided a quantitative evaluation of degree of stability of the loop. For the addressed boundary conditions, the neutral stability line was found to be close to the line of maximum Froude number, though it is located at lower values of N_{TPC}. Presence of heat structures was found important to determine the level at which the unstable behavior could be reached. RELAP5 code suggested lower values of heat transfer coefficient compared to Dittus-Boelter correlation, which allowed to obtain unstable behavior closer to the observed operating conditions.

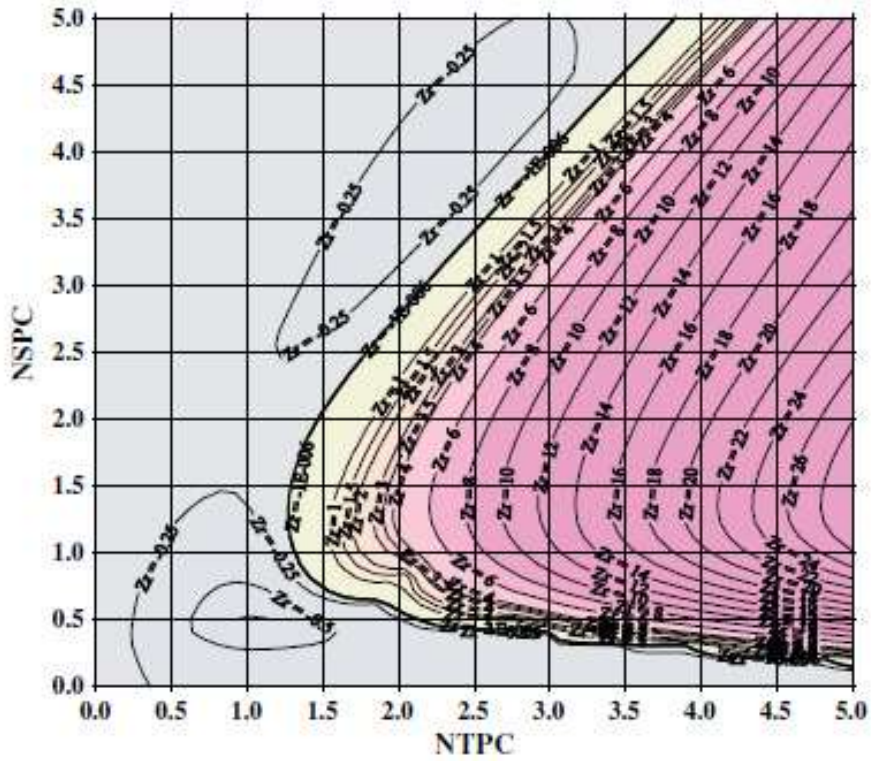

Figure 2-9. Stability maps obtained by RELAP5 simulation for the CIAE loop with 336 nodes (Debrah et al., 2013a).

2.4.1.2. Frequency-domain approach

In frequency-domain or linear approach, time-dependent conservation equations are perturbed over the steady-state operating point and linearized assuming the perturbation to be infinitesimally small. Real part of the eigen values of the resultant linearized perturbation equation determines the stability characteristics. If any of the eigen values has a positive real part, that indicates an unstable system, whereas a neutrally stable system has purely imaginary eigen values. A stable system has only negative real part for all eigen values. Stability predictions are then made by applying such well known methods as Bode plot, Nyquist plot, and root-locus technique. A linear model was developed by Chatoorgoon et al., 2005b and, comparing the results with the ones obtained from the SPORTS code, a difference of about 5% was indicated between the linear and non-linear methods. Sharma et al., 2010c used the same loop geometry as employed by Vijayan et al., 2010 for developing the linear stability code SUCLIN and the code was benchmarked for the loop of Chatoorgoon, 2001. Corresponding Nyquist plot at the inlet conditions of 25 MPa and 623 K is shown in Figure 2-10, which indicates a stability threshold at 4.2 MW.

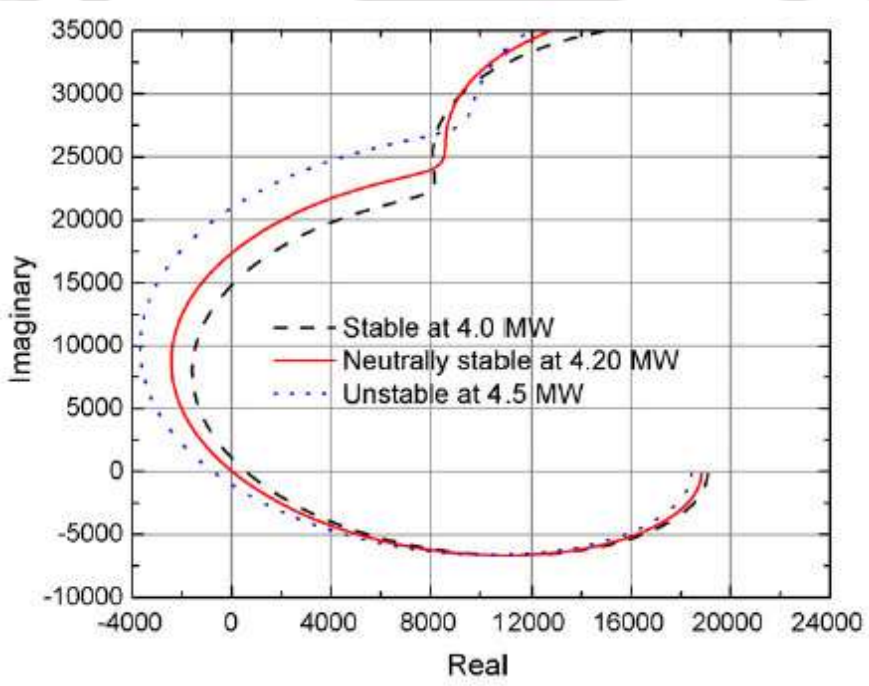

Figure 2-10. Nyquist plot developed by Sharma et al., 2010c for 25 MPa operating pressure and 623 K heater inlet temperature

A comparison was also made with predictions made by non-linear stability code NOLSTA. They were found to match qualitatively, but with a vast

quantitative difference. Unstable zone predicted by NOLSTA was found to be significantly greater than SUCLIN, as is shown in Figure 2-11 for a 14 mm diameter loop. The probable reasons behind the differences were identified as the followings.

✓ All the fluid properties were perturbed in non-linear analysis, whereas only enthalpy and specific volume perturbation was considered in linear stability analysis.

✓ Non-linear analysis accounts for friction factor perturbation, which was neglected in stability analysis.

✓ Perturbation induced in specific volume due to perturbation in enthalpy was considered in linear stability analysis, but not the perturbation due to pressure fluctuations.

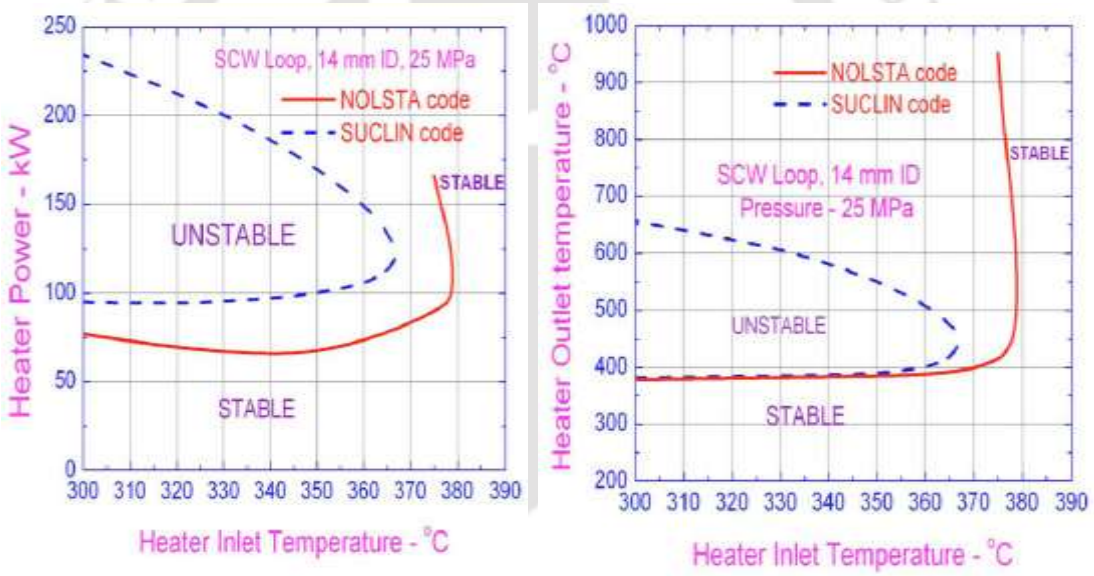

Figure 2-11. Comparison of stability maps developed by SUCLIN and NOLSTA for 14mm diameter loop (Sharma et al., 2010c).

The same code SUCLIN was employed by Sharma et al., 2010b to compare the simulated steady-state characteristics of UW-Madison loop with the results reported by Jain and Corradini, 2006. Stability maps created for the UW-Madison loop and for their in-house experimental facility were presented. It was observed that increase in loop diameter enhances the unstable zone, whereas increase in height showed similar effect. Local losses considered in cold leg stabilize the system better than that in hot leg. As increase in pressure increases the pseudo-critical temperature, both power and heater outlet temperature maps were seen to be moving slightly upwards.

2.5. Experimental Investigations

As per open literature, only limited number of experimental investigations was attempted with SCNCL, mainly due to the concern of handling high pressure and temperature in the laboratory environment. Before developing an experimental setup, scaling analysis is essential to identify the dimensions of setup. A fluid-to-fluid scale-down methodology was proposed by Marcel et al., 2009. It was observed that the variation in dimensionless enthalpy with dimensionless density for an appropriate mixture of R-125 and R-32 could accurately match the same for supercritical water. Another scale-down approach was proposed by Rohde et al., 2011, considering R-23 as the working fluid. As a subsequent extension, Joen and Rohde, 2012 developed an experimental facility named DeLight applying the above procedure and with HPLWR as the prototype. R-23 at 5.7 MPa was employed as the working fluid to study the coupled thermalhydraulic-neutronic stability of SCNCL. Accordingly, an artificial neutronic feedback scheme and a model for the heat transfer was implemented. No thermalhydraulic instability was observed over the chosen power range. But, within the operational plane, a clear zone of instability was found for the coupled neutronic–thermo-hydraulic mode.

One important test facility was set up in Bhabha Atomic Research Centre (BARC), India (Sharma et al., 2014, 2013, 2012, 2010a), in the form of a uniform diameter rectangular loop with 14 mm inner diameter and 21.34 mm outer diameter. Heating and cooling sections were provided on both horizontal and vertical arms, in order to avail the option of operating in either of four possible orientations. Experimentation was performed in the pressure range of 8-9 MPa with supercritical CO_2 to study the effect of orientation on both steady-state and stability behavior. No instability was observed with secondary-side coolant flow rate of 34 lpm. But, with lower coolant flow rate around 10-15 lpm, unstable oscillations were found at 500 W. Power step down from 1900 W to 300 W at 7.7 MPa and 10 lpm coolant flow rate, was found to have destabilizing impact. But instability died down with increasing power (Figure 2-12). Instability was observed in all the cases with heater inlet temperature near the critical point. A similar facility was developed by Swapnalee et al., 2012, as they observed sharp change in density around the pseudo-critical region leading to instability. Such instability was indicated

either to be of density wave or excursive type. The threshold of excursive instability was judged by checking for the occurrence of multiple steady-state solutions. Static instability was observed with supercritical water, whereas no instability was found with supercritical CO_2. Pressure was found to have a stabilizing effect, as it reduces the size of unstable region. At high pressures, instability was observed with very low inlet temperature. Yu et al., 2011, however, concluded that no Ledinegg instability could occur at supercritical pressure through the loop, as they experimented on a rectangular loop with a preheater and a heater, preheater being placed horizontally and heater vertically. The design pressure of the loop was 40 MPa and both the heaters were capable of providing 20 kW power. Cold-side temperature was maintained with secondary coolant flow rate. Numerical results obtained using the formulation of Chatoorgoon, 2001 were verified using their experimental data and less than 4% error was reported, which was attributed to the local loss coefficients. Kiss et al., 2017 developed a small-sized closed test facility and investigated the steady-state thermalhydraulics to understand the various cause of pressure drops in the system. Local pressure losses were found to depend strongly on the inlet temperature, but remained invariant to the system pressure.

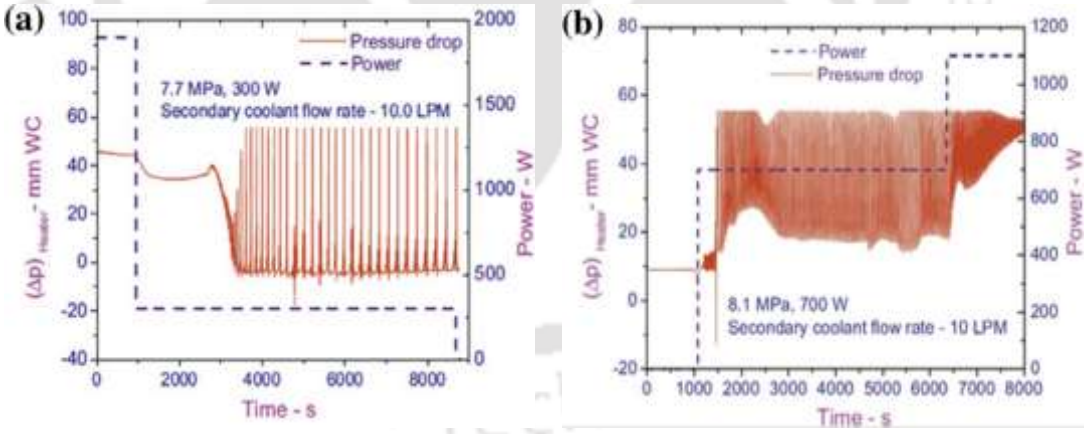

Figure 2-12. Experimental results obtained for pressure difference across a heater (a) at 300 W during power step-down and (b) at 700 W during power step-up (Sharma et al., 2013).

Chen et al., 2013c also developed a facility of SCNCL in the form of a uniform diameter rectangular loop with 8 mm ID and 10 mm OD. A DC electrical heat source was provided, along with a counter-flow cooler with maximum coolant flow rate of 15 lpm. The loop was designed to sustain a maximum pressure of 20 MPa. It was found that the flow pattern can change

from unstable sub-critical two-phase flow to stable liquid flow, and then to stable supercritical circulation with the increase of system initial pressure, the basic trend of stability response being dependent on initial pressure. Temperature difference between heater and cooler was found to be dependent on initial charging pressure of the loop and showed proportional effect on final system pressure. A higher temperature differential stabilized the loop. In the stable supercritical zone, the heat transfer performance of the cooler exhibited hardly any dependence on the bulk mean fluid temperature, whereas the heater showed better heat transfer performance for conditions close to the pseudo-critical point. In a further extension, Chen et al., 2013b employed the same facility to investigate the flow and heat transfer behavior of supercritical

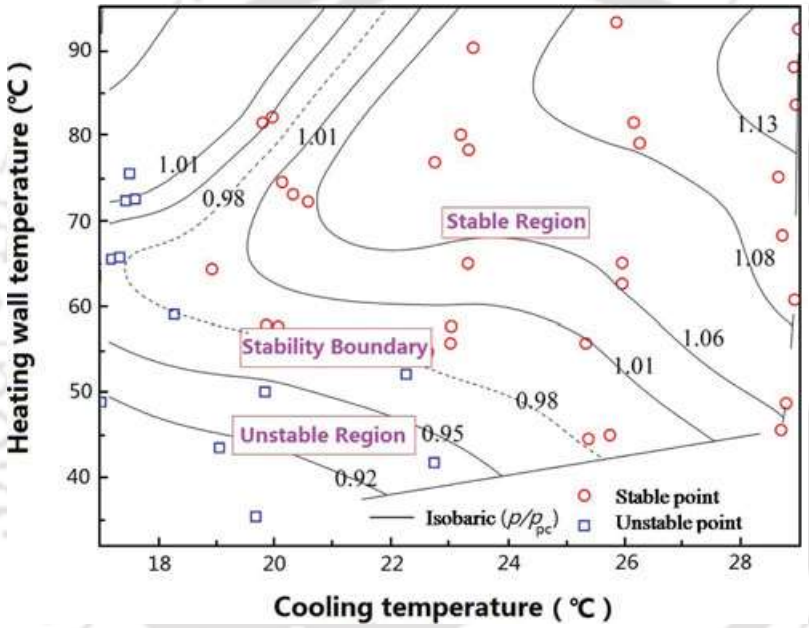

Figure 2-13. Stability map for CO_2 based SCNCL Chen et al., 2016.

and transcritical CO_2 system. Such systems were found to be capable of sustaining larger mass flow rate and heat transfer capacity compared to sub-critical fluid systems. Based on experimental observations, the flow in SCNCL was classified into three categories, namely, sub-critical single-phase gas flow with fluid temperature above boiling point and pressure below critical point, sub-critical liquid-gas two-phase flow with fluid temperature ranging across boiling point and pressure below critical value, and trans-critical or supercritical flow with both temperature and pressure above the critical value. The second category was found to be unstable, while no instability was observed for the supercritical flow. Stability for single-phase gas was found to be dependent on working pressure and temperature. Chen et al., 2016,

developed a general stability map for SCNCL (Figure 2-13), using the same experimental setup. It has been found that the reduced pressure lines divided the stability map to three different sections; stable, boundary and unstable flow region.

An experimental facility was developed by Chen et al., 2012b at China Institute of Atomic Energy in the shape of a vertical rectangle with 2.4 m width and 1.77 m height. Heat was supplied through an Inconel-625 electrical heater of 1.37 m length, located at the vertical right arm of the loop. Cooling was achieved by an annular heat exchanger of 20 mm outer diameter and 1.7 m length, mounted around the top horizontal arm. Their loop had an inner diameter of 4.62 mm and outer diameter of 6.46 mm. Operating at a pressure range of 24.2-25.2 MPa and heat flux range of 0-0.9 MW/m^2, they observed that, with linear increase in heater power, unstable fluctuations appeared around the maximum flow rate. That vividly characterized the separation between buoyancy-dominated and friction-dominated regimes. Reynolds number reached around 68,000, with mass flux of about 420 kg/m^2s at the maximum power level. Comparing the estimated heat transfer coefficient with Dittus-Boelter correlation, severe deterioration heat transfer deterioration was observed, with maximum degradation appearing while the order of buoyancy force and pressure gradient becomes the same. The highest degradation of 50% was reported for the value of buoyancy parameter around 2×10^{-6}. Comparisons were also made with four other forced-convection relations taking into account the property variations, with the Bishop's relation showing the closest predictions. Mostly dynamic instability was observed, which was attributed to the pressure pulses generated by the contact of subcooled liquid with superheated wall.

Their work was subsequently extended to a test section with 10.89 mm inner diameter (Chen et al., 2012c), as they experimented over the pressure range of 23.5-24.9 MPa and maximum wall heat flux of 0.45 MW/m^2. Onset of instability was found to shift to around 16 kW power supply and 380 °C outlet water temperature, compared to 11.6 kW and 370 °C respectively for the previous case. Oscillation amplitude was also found to be much lower, indicating towards a stabilizing role of increased inner diameter. Heat transfer, however, was found to get enhanced due to the larger diameter and lower mass flux, with the peak appearing close to the pseudocritical point.

None of the forced-convection heat transfer supercritical correlations was found to provide reasonable prediction over the whole working range, mostly due to the non-accountability of buoyancy force, non-uniform fluid temperature and flow instability. A test section of 7.98 mm inner diameter was also added in the follow-up work of Chen et al., 2013e. Possibility of static instability was observed when the flow rate reached a maxima at the outlet water temperature close to pseudocritical point. Convectional heat transfer relations were found not to be applicable for the new section as well.

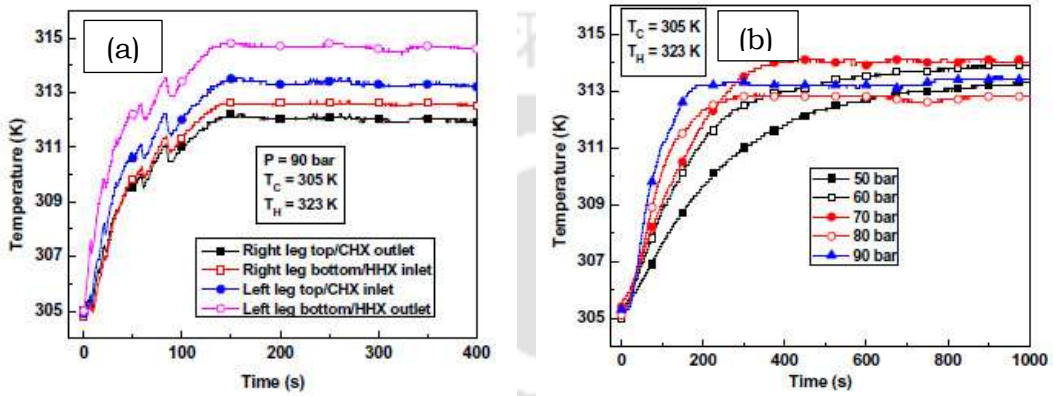

Figure 2-14. Variation of loop fluid temperature at (a) various locations and (b) left leg centre for different operating pressures (Yadav et al., 2017).

Yadav et al., 2017 also developed a test facility for supercritical CO_2 with two counter-flow heat exchangers with main loop pipe having ID of 7.3 mm and OD of 9.6 mm. The main loop was capable of sustaining pressure up to 95 bar. Temperature values were recorded with a time step of 0.5 s. It took approximately 150 s for a system maintained at 90 bar to attain the steady-state (Figure 2-14). Increased value of pressure help the system to attain steady-state quicker, thereby suppressing the start-up oscillations. Their simulation results were also in decent agreement with the experimental data. A liquid helium based U-shape NCL facility coupled with a cryocooler was developed by Song et al., 2013,. Experiments were performed for the condition of constant mass of helium inside the system. Fluid temperature and system pressure were reported to increase with the heat flux in the loop.

An experimental setup for CO_2 based SCNCL was established by Liu et al., 2015 at Nuclear Power Institute of China (NPIC). The loop was configured as a vertical heater and horizontal cooler one. The inner diameter of the heating and cooling sections was 10 mm, whereas the same for the adiabatic sections was 6 mm. The design temperature and pressure of the loop were

773 K and 30 MPa, respectively. Experiments were performed to investigate the influence of operating pressure, mass flux, bulk fluid temperature and heat flux, and subsequently a heat transfer correlation was proposed. Liu et al., 2016a, 2016b employed the same facility and investigated the steady-state characteristics of SCNCL. Both the enhancement and deterioration of heat transfer were observed. The maximum value of mass flow rate was obtained only when the heater outlet temperature greatly exceeds the pseudocritical temperature. In a further extension with the same facility, Liu et al., 2017 investigated the effects of various temperature sensitive thermal parameters on the characteristics of flow instabilities. Any increase in system pressure and coefficient of local resistance in cold section, and decrease of the same in the hot section, enhanced the stability of the system. An air-cooled CO_2 based SCNCL facility was built by Sadhu et al., 2018b, 2018c to operate with a much larger temperature range by using air as an external fluid for the heat exchanger section. For a 7 K temperature differential between the source and sink sections, Reynolds number was found to be around 10^4, which ensured the generation of a strong flow field in the system. For the sink section, an optimum velocity was identified for the air, below of which system pressure drastically increased, leading to system failure. The time required to reach steady-state during start-up and shut-down increased with reduction in loop charge for a given heater input.

Numerical and experimental analysis of sCO_2 based SCNCL have been reported by Sadhu, 2018. He considered both air and water as the secondary coolant for the numerical simulation, while only air-cooled loop was employed during experiments. Effects of different geometric parameters, loop charge, coolant velocity and coolant inlet temperature were investigated numerically. Increasing the loop diameter was reported to be a better option than increasing the height to have better heat transfer performance. Existence of an optima in loop charge, corresponding to the maxima in the thermal conductance of the heat sink, was experimentally observed for any heater power level. Mass flow rate was found to increase with heater power for a given charge level, indicating operation in the buoyancy-dominated regime. Experiments were also reported under transient conditions, exploring the effects of power step-up and step-down, accidental fan failure, complete power failure, loop charge, and loop asymmetry. Owing to the low critical temperature of CO_2, the physical state of the working fluid was found to

oscillate between two-phase and single-phase, even leading to partial condensation at the cooler outlet during shutdown. Asymmetry in configuration was found to impose a flow direction. However, no flow reversal or unstable fluctuations were observed over the entire range of test conditions.

One of the most critical issues in experimentation involving any NCL is the requirement of non-intrusive instrumentation. NCLs are characterized by low driving head due to the absence of any designated prime mover. Presence of any kind of intrusion, in the form of thermocouple bids or anemometer port, leads to additional pressure drop, which is highly undesirable. Unfortunately, none of the experimental studies available in open literature none reports any novel attempt of developing sensing tools suited exclusively for natural circulation based systems, rather than opting for only the conventional ones. Most of the researchers opted for an electric heater as the source (Chen et al., 2013b; Kiss et al., 2017; Sharma et al., 2014, 2013, 2012, 2010a; Swapnalee et al., 2012), while employing a variac for controlling the power input. Only a few works used a hot-side heat exchanger in the source section, and a thermostatic bath to control the concerned temperature (Yadav et al., 2017). The cooling section is invariably a tube-in-tube type heat exchanger, with water being the most common choice as the secondary coolant. Recently Sadhu et al., 2018 developed an air-cooled heat exchanger as the cooler. According to the level of temperatures involved, various types of thermocouples and resistance temperature detectors are use for measuring the temperature. Normally pressure gauges and pressure transducers are used for measuring the system pressure, whereas differential pressure transmitter is the most popular choice to get an indirect measurement of the mass flow rate of the loop. Scattered use of the coriolis mass flow meter can also be observed (Chen et al., 2016, 2013b), which is capable of providing highly accurate results, but at the expense of additional pressure loss.

2.6. Observation from Literature Survey

A quite comprehensive review of natural circulation loops working with supercritical fluids is presented above. Most of the reported works are theoretical in nature, spanning from primitive analytical models through simplified 1D simulations to high-end software applications. Experimental studies available in open literature is limited in number and corresponding database is far from complete. Numerical works have seen the development of

various codes like SPORTS, FIASCO, NOLSTA and SUCLIN as examples, mostly for stability characterization of SCNCLs. Some sparse application of commercial software like ANSYS-Fluent and RELAP5 can also be found in recent times.

Both theoretical and experimental observations indicate that the steady-state mass flow rate increases with power supply, till it attains a maxima, and decreases afterwards, quite similar to two-phase NCLs. Some of the early research suggested the stability threshold to correspond to the peak mass flow rate. It was identified later, however, not to be a perfect guideline. CO_2 as a working fluid was predicted to result in higher velocity magnitude, along with an asymmetric cross-sectional variation, and larger heat transfer rates compared to water, thereby indicating CO_2 as a better working medium. Quite a few of such observations were also supported by experimental data. A systematic effort has been put forward to summarize the influence of geometric and operating parameters on steady-state performance of SCNCL. Increase in loop height and diameter provides higher mass flow rate. Also the HHHC orientation results in highest mass flow rate among all possible configurations. Both mass flow rate and heat transfer rate increases with system pressure. With an increase in heater inlet temperature in an open loop, mass flow rate decreases. Inclination angle also has a similar effect. For high heat flux conditions, Nusselt number decreases with increasing inclination.

A thorough literature appraisal suggest that, both time-domain and frequency-domain approaches were employed for numerical stability predictions. Qualitative matching can be observed between the results obtained from the two approaches, but with a vast quantitative difference. Unstable zone predicted by the time-domain approach is generally larger than the same predicted by frequency-domain approach. Detailed parametric analysis found that the increase in diameter and height increases the instability in the loop. Local losses provided in the cold leg has a stabilizing influence rather than that in the hot leg. The need of optimizing the coolant flow rate was experimentally stressed upon, as lower coolant flow was found to enhance instability. A power step-up was observed to have a stabilizing effect on the loop compared to power step-down. RELAP5 simulations predicted that slow increase of input heat flux can induce less flow instability

than a quick increase. The nature of such dynamic response, however, is still an open topic of further analysis.

A detailed scrutiny of the available literature clearly shows that the researchers have tried to explore different aspect of SCNCL, starting from steady-state thermalhydraulics to intricate transient and stability response, following theoretical, computational and experimental loops. While several facets of this relatively-new, but with tremendous potential, technology of SCNCL have been documented over the last decade and half, there are still quite a few glaring gray areas, which must be addressed before its widespread commercialization. At the vary onset, the technologists must justify the need of adopting supercritical condition over the conventional subcritical systems and must establish the relative gain in heat transfer performance over the complicacies brought in by the drastic transformation experienced by the supercritical fluid. Nearly all the available studies dealing with supercritical system, both numerical and experimental, focus on demonstrating the enhancement or deterioration in heat transfer for a single fluid, without attempting to compare with another one working under the same conditions. It is more logical to assess the performance of different fluids, subcritical or supercritical, within the same regime of operating parameters, before deciding on a particular one. While water and CO_2 can be identified as the two most popular fluid among researcher, the disparity in there critical point values is really striking. Among the common fluids, CO_2 is characterized by one of the lowest critical temperature and moderate critical pressure. On the contrary, both values are quite extreme for water from lab-scale point of view. Therefore it is very much possible to envisage different thermodynamic states of CO_2, with water continuing to be compressed liquid, which are expected to present very contrasting heat transport characteristics. Hence a systematic performance comparison between natural circulation loops operating with different working fluids characterized by contrasting thermodynamic states, is the need of the hour, in order to establish the superiority of SCNCL as a heat transport system. The lack of reliable experimental data and consequent heat transfer correlations for SCNCL is another major area of concern. The requirement of non-intrusive instrumentation and the involvement of higher levels of pressure and temperature, often makes it difficult to have precise experimental measurement, despite the loop having a simple geometrical look and very specific areas of energy interaction. That can be recognized as the

principal reason for contrasting conclusions reported in literature. Therefore sophisticated experimentation with SCNCL should be attributed as another one with topmost priority. The knowledge base regarding the stability response of SCNCL is also quite thin and is expected to receive enhanced attention in the coming days.

2.7. Objectives of the Research

2.7.1. Computational investigation

✓ Development of a 3D numerical model of SCNCL for steady-state characterization and validation with available experimental data

✓ Transient analysis of SCNCL for evaluation of stability behavior

✓ Steady-state and stability performance comparison between different working fluids

✓ Dynamic performance assessment under periodic and aperiodic variation in operating parameters

2.7.2. Experimental investigation

✓ Scaling analysis to determine the dimensions of a lab-scale test facility with R134a as the working fluid

✓ Development of the experimental facility

✓ Experimental assessment of steady-state and stability behavior with variation in operating parameters such as input power, sink temperature, system pressure and tilt angle

✓ Comparison of experimental results with numerical simulation and possible development of thermalhydraulic correlations for SCNCL operation

Chapter 3: Development of Computational Model

3.1. Preamble

Appraisal of any phenomenon of scientific interest can be performed following either of two distinctly different approaches, namely experimental and theoretical. Experiments remain the primary mode of exploration since the pre-historic age and even more so while dealing with a spectacle with unknown physics. Real-time observations and subsequent analyses from a systematic experimentation can always be considered as a trustworthy source in enhancing the understanding about a system. There exits several factors, however, which can affect the accuracy of the experimental data. Lack of suitable measuring devices or the precision of the employed instruments can often limit the experimental conclusions just to an overall sense, while failing to provide any insight about the nature of local interactions. In this precise context, theoretical analysis comes into prominence, which can again be sub-divided into two broad categories as analytical and numerical. The former involves the classical method of solving the exact conservation equations over the domain of interest and finding a closed-form solution. But the precinct of the analytical mode is very reedy and its application remains circumscribed only to certain simplified cases, where the governing equations can be reduced to a smaller set. The Numerical mode allows the solution of the conservation equations in their most-convoluted form over a discretized domain, and also the incorporation of newer multiphysics and modern equation-of-state. Escalating growth in computational competencies has allowed the numerical simulation of rigorous thermophysical problems within a reasonable timeframe. The accuracy of the concerned output, however, is conditional, and can be contingent to numerous elements encompassing the computational domain, discretization scheme, nodalization, numerical solver, convergence criteria etc. The user must, therefore, be attentive to such details, and also ensure comparison with exiting experimental/analytical data to warrant the validity of the predictions.

The drastic variation in the thermophysical properties of the supercritical fluid around the pseudocritical point cannot be captured by any simple equation-of-state. Besides, the thermalhydraulics of SCNCL is yet to be explained properly. That makes the adoption of the analytical approach impracticable and hence the use of numerical simulation is very much prevalent in concerned literature, as has been elaborated in the previous chapter. A substantial part of the present thesis also comprises of the numerical investigation of SCNCL and hence it is important to describe the schemes and methodologies adopted thereof. The geometric dimensions of the base model have been identified following a systematic scale-down analysis, which is elaborated in §3.3. Both 3D and 2D numerical models are used for steady-state and transient analyses respectively. The commercial code ANSYS-Fluent 15 (ANSYS, 2015) is used to develop the computational model and also to perform the solution. Several other geometries are also considered, in order to explore the role played by the geometric variables. Each of them, however, can be considered as a variation of the base mode, with identical geometric orientation and change in any one of the dimensions. Comprehensive grid-dependency tests are performed to select the appropriate grid system for every such geometry. The selection of the turbulence model is one of the most important aspect in determining the success of the numerical predictions and the same is finalized after careful deliberation. Following sections logically unfold each such features of the numerical procedure followed in the present thesis.

3.2. Physical Geometry

According to the physical shape, a natural circulation loop can be classified into various categories as shown in Figure 1-6. The rectangular configuration is the most common one according to the literature and hence the same is adopted in the present work. Basic geometry of any rectangular NCL comprises of two horizontal and two vertical arms, connected together to have a continuous system of fluid motion. Heating and cooling sections can be mounted on any of the arms, as long as the sink is located higher than the source, in order to develop the favorable density gradient. Accordingly several orientations are possible, both symmetric and asymmetric, with each being characterized by distinct thermalhydraulic features. Here, heater and cooler are always placed at lower and upper horizontal arms of the loop respectively,

whereas other sections of the loop are ideally insulated. It is commonly believed that the configuration with heater and cooler in opposite horizontal arms (HHHC) is the most unstable among the four common designs. Chen et al., 2014 observed loops with vertical heaters to be stable over a wide range of power, while horizontal heating cases exhibited diverging oscillations. Instability was reported by Sharma et al., 2014 only for the HHHC configuration, during their experiment with four configurations. Hence, the same orientation is embraced in the present study. Before finalize the geometric dimensions of the rectangular loop a detailed scale-down analysis has been carried out, which is elaborated in next section. The final dimensions of the base model are obtained from this scale-down analysis. The base geometry is shown in Figure 3-2, where both the source and sink are placed at the middle of the concerned horizontal arms. And detail dimensions of the base model are shown in Table 3-3. Both 2D and 3D versions of the corresponding computational geometry have been developed in course of the present work. The 2D model is used specifically for transient analysis of SCNCL, whereas all other study have done with the 3D model. The material of the loop wall is considered to be stainless steel, with 1 mm thickness.

3.3. Scale-down Analysis of SCNCL

Scaling has been performed with respect to one prototype (Sharma et al., 2012), which is a rectangular loop with uniform diameter (13.88 mm ID and 21.34 mm OD). The material of the loop is SS-347. The loop has been operated at 8-9 MPa pressure with CO_2 as working fluid. Different orientations (HHHC, HHVC, VHHC and VHVC, where, H refers to 'horizontal' and 'heater', V refers to 'vertical' and C refers to 'cooler') of heater and cooler have been studied. It has been found that maximum and minimum mass flow rate is achieved for HHHC and VHVC orientation loop respectively. The available experimental data of HHHC orientation loop at 8.6 MPa operating pressure is used to scaling analysis for the current model. For model, loop fluid is considered R134a due to its lower critical pressure. Focus of this section is to develop a scale-down SCNCL model and numerically investigate the performance evaluation of model and prototype.

3.3.1. Mathematical equations

At the beginning of study, the appropriate equations have been identified, which express the flow and energy field of the loop. Thus, the

scaling process starts with the continuity, momentum and energy balance equations. The governing equations are summarize below,

3.3.1.1. Continuity equation

$$\frac{\partial \rho A}{\partial t} + \frac{\partial GA}{\partial z} = 0 \tag{3-1}$$

3.3.1.2. Momentum equation

$$\frac{\partial GA}{\partial t} + \frac{\partial}{\partial z}\left(\frac{G^2 A}{\rho}\right) + A\frac{\partial p}{\partial z} + \left(\frac{f}{D_{hy}}\right)\frac{G^2 A}{2\rho} + \rho g A \cos\phi = 0 \tag{3-2}$$

3.3.1.3. Energy equation

$$\frac{\partial \rho Ah}{\partial t} + \frac{\partial GAh}{\partial z} = \left(\frac{P_{hy}}{A}\right)\dot{q}'' A \rightarrow for\ heater \tag{3-3a}$$

$$= -\left(\frac{P_{hy}}{A}\right)h_{fc}(T - T_c)A \rightarrow for\ cooler \tag{3-3b}$$

$$= 0 \rightarrow for\ adiabatic\ pipe \tag{3-3c}$$

3.3.2. Non-dimensional Parameters

Following non-dimensional parameters are used to non-dimensionalizing the governing equations.

$$z^* = \frac{z}{L_t}, \quad G^* = \frac{G}{G_{PC}}, \quad t^* = \frac{t}{\left(\frac{\rho_{PC} L_t}{G_{PC}}\right)}, \quad h^* = \left(\frac{h - h_{PC}}{h_{PC} - h_{cr}}\right),$$

$$\rho^* = \frac{\rho}{\rho_{PC}}, \quad \mu^* = \frac{\mu}{\mu_{PC}}, \quad C_P^* = \frac{C_P}{C_{P,PC}}, \quad A^* = \frac{A}{L_t^2}$$

G_{pc} refers to the mass flux at the location where the system attains the pseudocritical point.

3.3.3. Non-dimensional form of governing equations

3.3.3.1. Continuity equation

$$\frac{\partial \rho^* A^*}{\partial t^*} + \frac{\partial G^* A^*}{\partial z^*} = 0 \tag{3-4}$$

3.3.3.2. Momentum equation

$$\frac{dG^* A^*}{dt^*} + \left(\frac{f L_t}{2D_{hy}}\right)\frac{G^{*2} A^*}{2\rho^*} + \left(\frac{Gr_{mPC}}{Re_{PC}^3}\right)A^* = 0 \tag{3-5}$$

3.3.3.3. Energy equation

Due to dissimilar boundary conditions for heating, cooling and adiabatic sections, the following non-dimensional energy equations are referred to corresponding sections,

For heater section

$$\frac{\partial(\rho^* A^* h^*)}{\partial t^*} + \frac{\partial(G^* A^* h^*)}{\partial z^*} = \frac{4\dot{Q}}{\Delta h L_t G_{PC} L_h} \tag{3-6}$$

For cooler section

$$\frac{\partial(\rho^* A^* h^*)}{\partial t^*} + \frac{\partial(G^* A^* h^*)}{\partial z^*} = -\frac{P_{hy} h_{fc}}{L_t G_{PC} C_{P,PC}} h^* \quad (3\text{-}7)$$

For adiabatic pipes

$$\frac{\partial(\rho^* A^* h^*)}{\partial t^*} + \frac{\partial(G^* A^* h^*)}{\partial z^*} = 0 \quad (3\text{-}8)$$

From equations (3-5), (3-6) and (3-7) total four non-dimensional groups have been found, which are listed in Table 3-1.

Table 3-1: Non-dimensional groups

Sl. No.	Non-dimensional groups	Physical significance
1.	$\frac{f L_t}{2D_{hy}}$	Modified Euler number (Eu_m): Relation between pressure force and inertia force.
2.	$\frac{Gr_{mPC}}{Re_{PC}^3}$	Modified Richardson number (Ri_m): Relation between buoyancy and flow shear term.
3.	$\frac{4\dot{Q}}{\Delta h L_t G_{PC} L_h}$	Non-dimensional Input Power (Γ): Relation between input power and flow rate.
4.	$\frac{P_{hy} h_{fc}}{L_t G_{PC} C_{P,PC}}$	Modified Stanton number (St_m): Relation between heat transfer and thermal capacity.

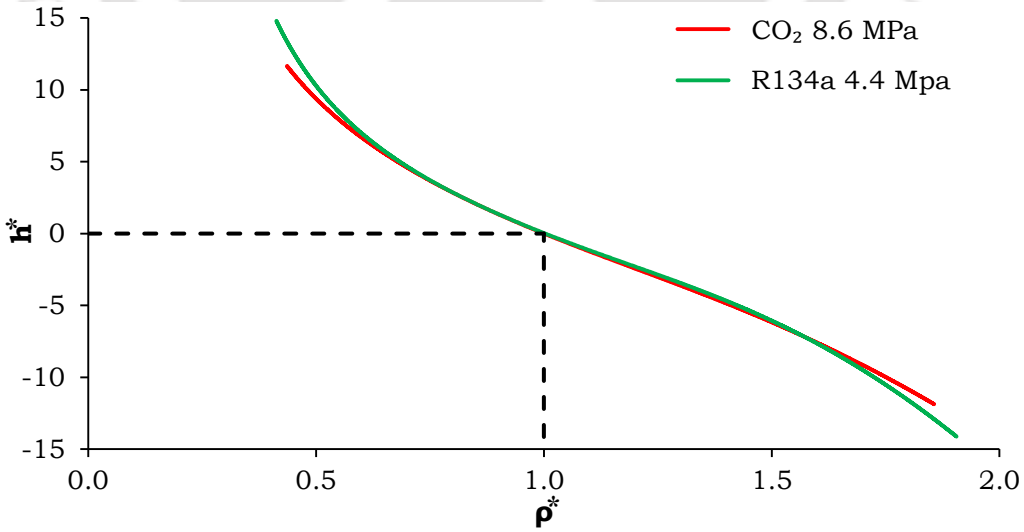

Figure 3-1. Non-dimensional property comparison of CO_2, R134a and water.

According to scaling laws, the non-dimensional groups are compared for both prototype and model. The experimental data of prototype loop is

available for 8.6 MPa system pressure. Therefore, to identify the scaling pressure of R134a, a non-dimensional property variation study has been carried out and compared with CO_2 at 8.6 MPa pressure, Figure 3-1 shows the same. It has been identified that the non-dimensional variation of enthalpy and density plot for R134a at 4.4 MPa is almost identical with CO_2 at 8.6 MPa pressure. Which ensures that, at the said pressure levels, both the fluids performed identically.

Table 3-2: Pseudo-critical properties of CO_2 and R134a

Properties	**CO_2 at 8.6 MPa**	**R134a at 4.4 MPa**
T (K)	311.05	378.25
ρ (kg/m^3)	479.27	513.51
h (kJ/kg)	341.97	395.05
C_P (kJ/kg-K)	17.095	16.64
λ (W/m-K)	0.0749	0.0557
μ (μPa-s)	34.233	34.988
β (1/K)	0.1367	0.2475

After non-dimensionalize the governing equations, several non-dimensional groups have been found (Table 3-1) and finally compared them for both model and prototype to compute the dimensions of the model. Table 3-2 contains the pseudocritical properties of CO_2 and R134a at 8.6 MPa and 4.4 MPa respectively, which are used in scaling analysis. Once, getting the dimensions of model (Table 3-3), a pair of 3D computational geometries for both prototype and model are developed in ANSYS-Fluent 15 and finally compared the numerical results for both the loops. Figure 3-2 shows the schematic diagram of the scaled down model. As expected, the geometrical parameters of the R134a loop having lower values with comparison to CO_2 based loop.

Most of the current numerical studies are based on this scaled down model ('base model'). According to requirement in studies, several 3D and 2D models have been developed for steady-state and transient analysis of SCNCL, following dimensions of the base model.

Table 3-3: Dimensions of the base model

Parameters	Dimensions (mm)
Diameter (D)	8
Height (H)	2120
Width (W)	1580
Radius of corner bends	5
Heater length (L_h)	1400
Cooler length (L_c)	1250

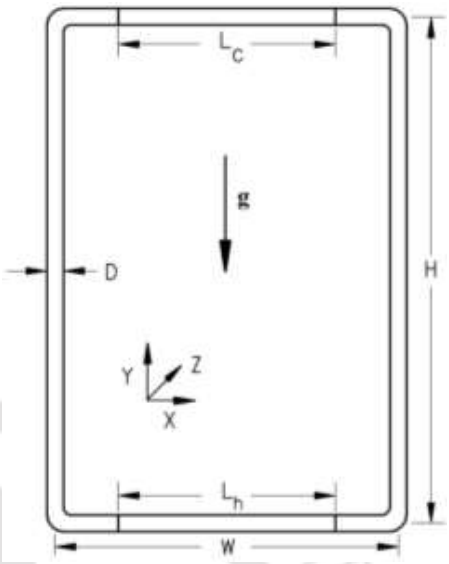

Figure 3-2. Schematic diagram of the base model

3.4. Conservation Equations and Mathematical Definitions

ANSYS-Fluent 15 is selected as the simulation tool for the present study. The governing equations are nonlinear partial differential equations describing the conservation of mass, momentum and energy, which are discretized using finite volume method. The standard form of the unsteady conservation equations are summarized below.

3.4.1. Conservation of mass:

$$\frac{\partial}{\partial t}(\rho) + \frac{\partial}{\partial x_j}(\rho u_j) = 0 \tag{3-9}$$

3.4.2. Conservation of momentum:

$$\frac{\partial}{\partial t}(\rho u_i) + \frac{\partial}{\partial x_j}(\rho u_j u_i) = -\frac{\partial p'}{\partial x_i} + \frac{\partial \tau_{ji}}{\partial x_j} + \rho g_i \tag{3-10}$$

Here modified pressure (p') and shear stress (τ_{ji}) are defined as:

$$p' = p + \frac{2}{3}\rho k + \frac{2}{3}\mu_t \frac{\partial u_k}{\partial x_k} \tag{3-11}$$

$$\tau_{ji} = \mu_{eff}\left(\frac{\partial u_i}{\partial x_j} + \frac{\partial u_j}{\partial x_i} - \frac{2}{3}\delta_{ij}\frac{\partial u_k}{\partial x_k}\right) \tag{3-12}$$

$$\mu_{eff} = \mu + \mu_t = \mu + C_\mu \rho \frac{k^2}{\varepsilon} \tag{3-13}$$

3.4.3. Conservation of energy:

$$\frac{\partial}{\partial t}(\rho h) + \frac{\partial}{\partial x_j}(\rho u_j h) = \frac{\partial}{\partial x_j}\left(\lambda_{eff}\frac{\partial T}{\partial x_j} + u_j \tau_{ji}\right) + S_E \tag{3-14}$$

Here,

$$\lambda_{eff} = \lambda + \lambda_t = \lambda + \frac{C_p \mu_t}{Pr_t} \tag{3-15}$$

where eddy viscosity is defined as,

$$\mu_t = C_\mu \rho k^2/\varepsilon \tag{3-16}$$

Here the volumetric energy source term (S_E) is taken to be zero in the adiabatic sections, thereby neglecting any heat leakage to the surrounding. Simulation results predict the Reynolds number for CO_2-based loop to be of the order of 10^5, which is essentially turbulent. That necessitates the use of a suitable turbulence model. A comparative approach and also detailed scan through the recent literature (Chen and Zhang, 2011; Yadav et al., 2012c, 2012b) identifies RNG k-ε model as the most suitable one and hence the same is selected here. Corresponding transport equations for turbulent kinetic energy (k) and energy dissipation rate (ε) can be presented as:

$$\frac{\partial}{\partial t}(\rho k) + \frac{\partial}{\partial x_j}(\rho u_j k) = \frac{\partial}{\partial x_j}\left[\alpha_k \mu_{eff}\frac{\partial k}{\partial x_j}\right] + G_k + G_b - \rho\varepsilon \tag{3-17}$$

and

$$\frac{\partial}{\partial t}(\rho\varepsilon) + \frac{\partial}{\partial x_j}(\rho u_j \varepsilon) = \frac{\partial}{\partial x_j}\left[\alpha_k \mu_{eff}\frac{\partial \varepsilon}{\partial x_j}\right] + C_{1\varepsilon}\frac{\varepsilon}{k}(G_k + C_{3\varepsilon}G_b) - C_{2\varepsilon}\rho\frac{\varepsilon^2}{k} - R_\varepsilon \tag{3-18}$$

In the above equations, G_k and G_b represent the generation of turbulent kinetic energy due to the mean velocity gradient and buoyancy effect respectively, while the quantities α_k and α_ε are the inverse of effective Prandtl numbers for the k and ε respectively. $C_{1\varepsilon}$, $C_{2\varepsilon}$ and $C_{3\varepsilon}$ are corresponding constants.

The value of the constants are as below

$C_{1\varepsilon}$ = 1.42, $C_{2\varepsilon}$ = 1.68, α_k = α_ε = 1.393 (Yadav et al., 2016b)

The degree to which ε is affected by the buoyancy is determined by the constant $C_{3\varepsilon}$ and calculated by using following equation

$$C_{3\varepsilon} = \tanh\left|\frac{v}{u}\right| \tag{3-19}$$

Here, v is the component of the flow velocity parallel to the gravitational vector and u is the component of the flow velocity perpendicular to the gravitational vector.

Generation of turbulent kinetic energy due to the mean velocity gradient is defined as,

$$G_k = \mu_t S^2 \tag{3-20}$$

Where, S is the modulus of the mean rate of strain tensor and defined as

$$S = \sqrt{2S_{ij}S_{ij}} \tag{3-21}$$

S_{ij} is the rate of strain tensor and defined as,

$$S_{ij} = \frac{1}{2}\left(\frac{\partial u_j}{\partial x_i} + \frac{\partial u_i}{\partial x_j}\right) \tag{3-22}$$

Generation of turbulent kinetic energy due to buoyancy is defined as,

$$G_b = \beta g_i \frac{\mu_t}{Pr_t}\frac{\partial T}{\partial x_i} \tag{3-23}$$

Where, β is the coefficient of thermal expansion and Pr_t is the turbulent Prandtl number for energy, which are defined as,

$$\beta = -\frac{1}{\rho}\left(\frac{\partial \rho}{\partial T}\right)_P \qquad \text{and} \qquad Pr_t = \frac{1}{\alpha} \tag{3-24}$$

The inverse of effective Prandtl numbers α_k and α_ε are estimated by using following relation.

$$\left|\frac{\alpha - 1.3929}{\alpha_0 - 1.3929}\right|^{0.6321}\left|\frac{\alpha + 2.3929}{\alpha_0 + 2.3929}\right|^{0.3679} = \frac{\mu_{mol}}{\mu_{eff}} \tag{3-25}$$

The term R_ε in the equation (3-18) is defined as

$$R_\varepsilon = \frac{C_\mu \rho \eta^3 \left(1 - \frac{\eta}{\eta_0}\right)\varepsilon^2}{(1 + \beta\eta^3)k} \tag{3-26}$$

Where, $\eta \equiv Sk/\varepsilon$, $\eta_0 = 4.38$, $\beta = 0.012$, $C_\mu = 0.0845$

Various terms have been defined during the post-processing stage to analyze the fluid flow and heat transfer phenomena. Mass flow rate at any cross-section is defined as,

$$\dot{m} = \int_A \rho \vec{V}_n dA \tag{3-27}$$

with $\vec{V}_n$ being the velocity normal to the concerned area. Area-averaged bulk temperature of the fluid can similarly be expressed as,

$$\bar{T} = \frac{\int_A \rho C_p T \, \vec{V}_n dA}{\int_A \rho C_p \, \vec{V}_n dA} \tag{3-28}$$

Steady-state Reynolds number (Re) and Grashof number (Gr) are commonly used to characterize NCLs. In the present context, they can be defined as,

$$Re = \frac{4\dot{m}}{\pi D \mu} \tag{3-29}$$

$$Gr_m = \frac{g\beta D^3 \rho^2 \dot{Q} H}{A\mu^3 C_p} \tag{3-30}$$

Here $\dot{Q}$ is the heat transfer rate from source to sink. All properties used in the above two definitions correspond to the system pressure and loop-averaged bulk mean temperature, the later being expressed as,

$$T_{avg} = \frac{1}{n} \sum_{i=1}^{n} \bar{T}_i \tag{3-31}$$

Here, i is the number of planes selected throughout the loop for such averaging, which is twenty in the present work.

3.5. Grid Generation and Sensitivity Analysis

Proper selection of grid system is a necessary component in any computational simulation. A system of structured grids is developed over the entire computational domain. In order to capture larger near-wall gradients of the flow variables, non-uniform grids are applied, with finer meshes close to the wall (Figure 3-3 and Figure 3-4). Finer axial meshes are employed at the heat-exchanging sections, as well as, at the corners, whereas slightly larger mesh resolution is used at the vertical arms. Grid sensitivity analysis is an important pre-requisite for any numerical analysis to ensure the correctness of the output. Thus, to alleviate any concern regarding the grid-reliance of the final solutions, each of the developed geometries are subjected to several grid structures. Simulations are performed with four different mesh structures for

the base model (Figure 3-2) and corresponding observations are summarized in Table 3-4 for sCO_2 loop with operating pressure of 8 MPa. Associated heater and cooler temperatures are 331 K and 315 K respectively. Corresponding cross-sectional views at the center of the source are shown in Figure 3-4. It is clearly evident that the increase in the number of cells from model 3 to model 4 yields less than 0.3% change in the magnitudes of loop-averaged quantities and steady-state mass flow rate. Consequently it is selected for simulation with the base model. Identical procedure is followed for each of the geometries described in the later chapters.

Table 3-4: Details of grid systems adopted for the base model

Model	**Model 1**	**Model 2**	**Model 3**	**Model 4**
Number of nodes	182000	249243	326836	414779
Number of cell	150075	211140	282555	364320
Average velocity (m/s)	0.577	0.571	0.567	0.566
Average temperature (K)	323.216	323.154	323.107	323.089
Mass flow rate (kg/s)	0.00606	0.00618	0.00626	0.00628

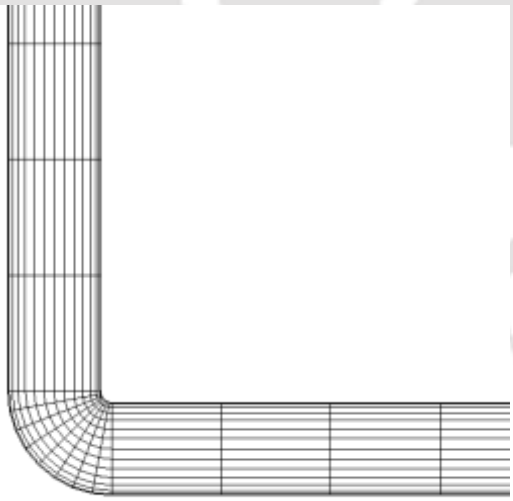

Figure 3-3. Grid distribution of bottom left corner of the loop

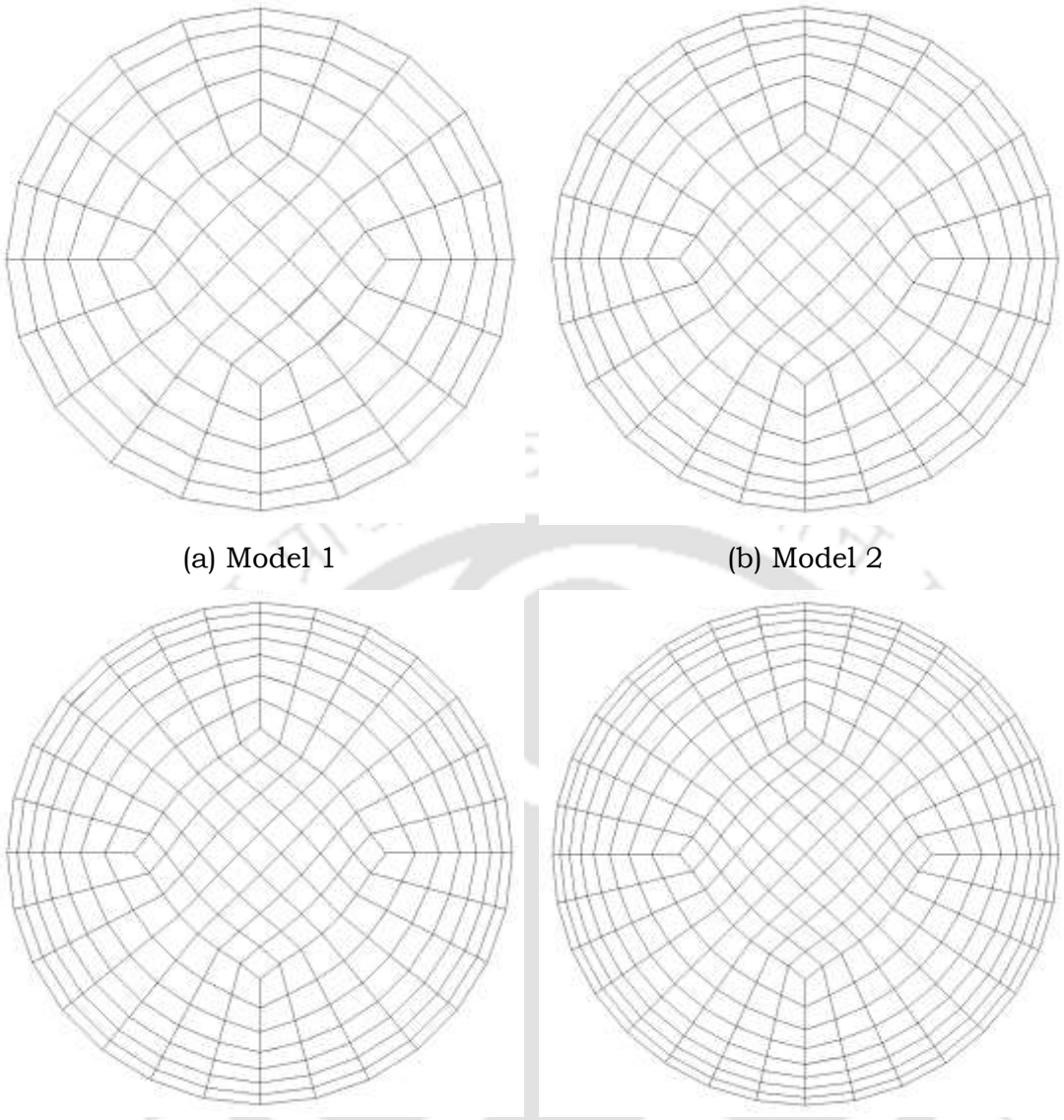

(a) Model 1 (b) Model 2

(c) Model 3 (d) Model 4

Figure 3-4. Cross-sectional mesh distribution at the center plane of the source for four different models

Skewness and orthogonal quality are two important properties for any mesh system, which measures its quality. The orthogonal quality for a cell is computed using the face normal vector; the vector from the cell centroid to the centroid of each of the adjacent cells, and the vector from the cell centroid to each of the faces. Its value ranges 0–1, with 1 being the best. Skewness, on the other hand, determines how close to ideal, i.e., equilateral or equiangular, a face or cell is. A value of 0 indicates the best cell. The average skewness and orthogonal quality of the selected model are 0.12 and 0.981 respectively, which signifies good mesh quality. Concerned cross-sectional grid distribution at the source center is shown in Figure 3-4. Precise illustration of the flow in

the near-wall region is governed by effective prediction of wall-bounded turbulent flow and the same can be ensured with proper choice of two dimensionless quantities, namely, y^+ and y^*. The former depends on the distance between the wall and its nearest cell, and is defined similar to local Reynolds number.

$$y^+ = \rho u_\tau y/\mu \tag{3-32}$$

where $u_\tau = \sqrt{(\tau_w/\rho)}$ is the friction velocity, τ_w is wall shear stress and y is the distance of first layer from boundary. Definition of y^* is nearly identical and is more commonly used with standard wall functions. The range of y^* values for which wall functions are suitable depend on the overall Reynolds number of the flow (ANSYS, 2015).

$$y^* = \rho C_\mu^{1/4} k^{1/2} y/\mu \tag{3-33}$$

where value of C_μ is 0.085 and k is the turbulent kinetic energy.

Relevant literature (Gharbi et al., 2012) suggests the positioning of the first grid point in the log-law region, to have a y^+ value greater than 30 with standard wall functions. The selected grid system allows an average y^+ and y^* values of about 46.88 and 46.89 respectively among all the simulated cases, which can be considered to be adequate.

3.6. Thermo-Physical Property Estimation for Supercritical Fluids

As the present work concerns several different working fluids and also under conditions varying from sub- to supercritical, accurate estimation of local thermodynamic and transport properties is of utmost importance. Critical point parameters for water, CO_2 and R134a are summarized in Table 3-5. Beyond this thermodynamic state point, any supercritical fluid exhibits substantial variation in its properties, particularly around the pseudocritical temperature Figure 1-7, which itself is a function of pressure. The variation is moderate for the single-phase medium, but can be significant in deciding the interaction between buoyancy and friction. Therefore accurate property estimation plays a vital role for precise simulation of any natural circulation based device, particularly recognizing the fact that the flow is initiated and sustained by thermally-induced density gradient. Friction being the

restraining force, exact estimation of the dynamic viscosity is also essential. Therefore it is critical to ensure the accuracy of the nodal property values accessible to the code over the entire range of parameters under consideration. Property functions inbuilt to Fluent are suitable generally for subcritical fluids only and hence additional reinforcement is necessary. The NIST standard reference database (NIST, 2011) is employed for calculating required thermodynamic and transport properties of all the involved fluids, which calculates properties at each node as functions of local pressure and temperature. Hence, instead of selecting the fluid from the available material list in a Fluent session, NIST real gas model is activated within the Fluent environment and appropriate fluid is selected from there. The default phase is vapour, which is correct for supercritical state fluids (CO_2 and R134a). While simulating with single-phase liquid water, however, the phase need to be set as liquid.

Table 3-5: Critical properties of the working fluids

Fluid	**Pressure (MPa)**	**Temperature (K)**	**Density (kg/m³)**
Water	22.064	647.096	322.0
CO_2	7.377	304.128	467.6
R134a	4.059	374.21	511.9

3.7. Numerical Scheme of Solution

Choice of numerical schemes and grid structure plays pivotal role on the success of any computational platform. Conservation equations and the selected turbulence model are solved simultaneously in ANSYS-Fluent 15 platform using implicit finite volume method. Convective terms in the momentum, energy and turbulence equations are discretized following the second order upwind scheme. Pressure Staggering Option (PRESTO) scheme is used for the pressure terms, while the PISO algorithm is followed to solve for the pressure-velocity coupling. No-slip boundary condition is selected for the walls, while assuming standard wall functions for precise estimation inside the boundary layer (Launder and Spalding, 1974). Axial conduction of tube wall has also been taken into consideration. A convergence criterion of 10^{-6} is selected for the residual of the energy equation and 10^{-3} for residuals of all other quantities. The flow field is energy-dominated and hence a higher

convergence level for the energy equation was felt necessary during simulation.

3.8. Selection of Turbulence Model

The prime motivation of this section is to explore the different turbulence models available in ANSYS-Fluent 15 and identify the suitable one for SCNCL. Total five numbers of turbulence models have been selected for this study, namely, $k-\varepsilon$, $k-\omega$, $k-kl-\omega$, SST and Reynolds stress. The $k-\varepsilon$ and $k-\omega$ models are subdivided into three (Standard, RNG and Realizable) and two (Standard and SST) sub-categories respectively. To find out the best turbulence model, simulations have been performed for all the above mentioned models. For the simulation, operating condition of the system is chosen as 10 MPa pressure and 305 K sink temperature, with CO_2 as the working fluid. Constant heat flux boundary condition is selected and the heater power is accordingly varied over a wide range of 0.1-6 kW. Figure 3-5 shows the variation in mass flow rate with input power for different turbulence models.

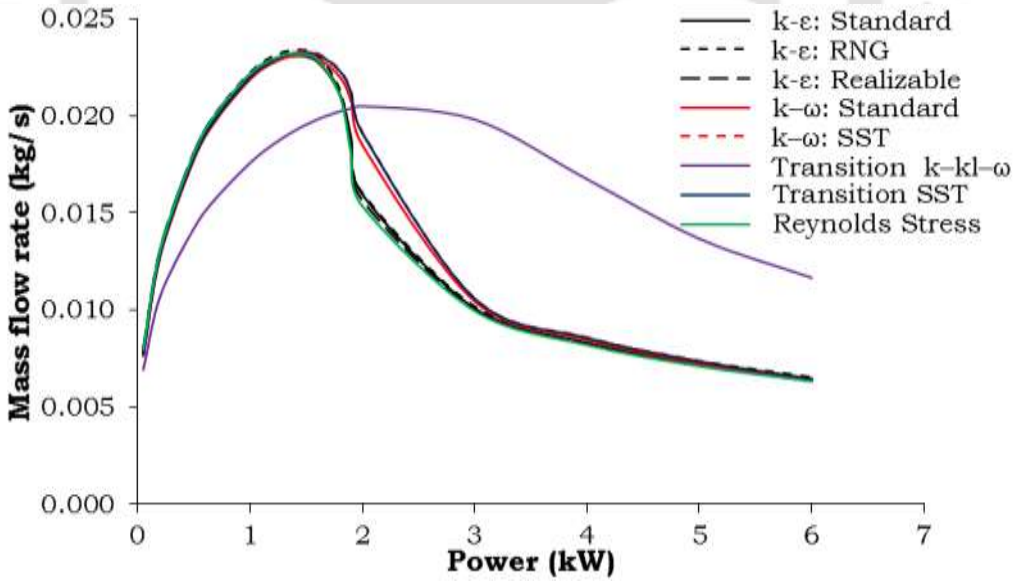

Figure 3-5. Mass flow rate for various turbulence models

Comparison of non-dimensional parameters are shown in Figure 3-6, where the simulated results are also compared with the experimental correlation of Swapnalee et al., 2012 and experimental data of Lomperski et al., 2004. Figure 3-5 and Figure 3-6 show the admirable closeness of

numerical results for more or less all the turbulence models available in the fluent code and experimental results. Only the numerical results of transition $k-kl-\omega$ turbulence model is exceptionally diverges from the other results. Hence, for the consistency with available literature, RNG k-ε model is selected as turbulence model for further simulation of present computational study (Chen and Zhang, 2011; Yadav et al., 2012c, 2012b).

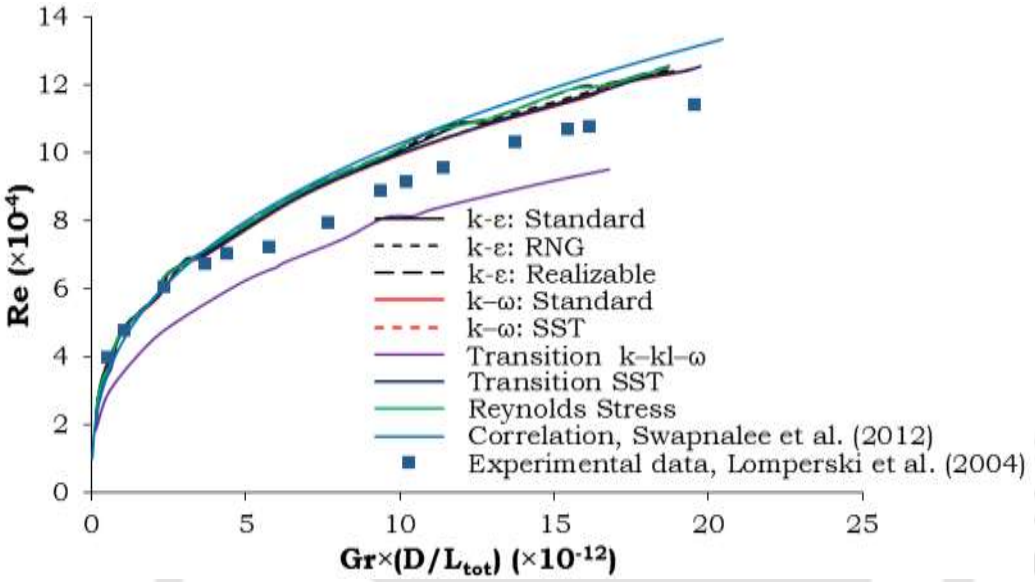

Figure 3-6. Comparison of numerical and experimental data

3.9. Validation of Numerical Model

The final, but utmost important, aspect of any numerical model is its validation. Any numerical procedure converts a continuous domain into a discrete one through the process of discretization, thereby raising the possibility of truncation and discretization errors intruding into the final solution. Besides, certain degree of modeling errors is also possible because of the incorrect replication of a physical system into a computational one. Hence, to check the correctness of the model, it is necessary to compare the predicted results from the developed computational model with experimental/analytical data from reliable literature, to authenticate the code before proceeding with further simulation. Present thesis work concerns both single-phase and supercritical fluid systems, and hence validation is attempted with both kinds of loops.

The current study is involved with several operating conditions and hence a details validation process will be addressed before discussion of main

matters in each chapter for numerical work. All the validation process will be discuss in upcoming topics are the comparison of Reynolds and modified Grashof numbers.

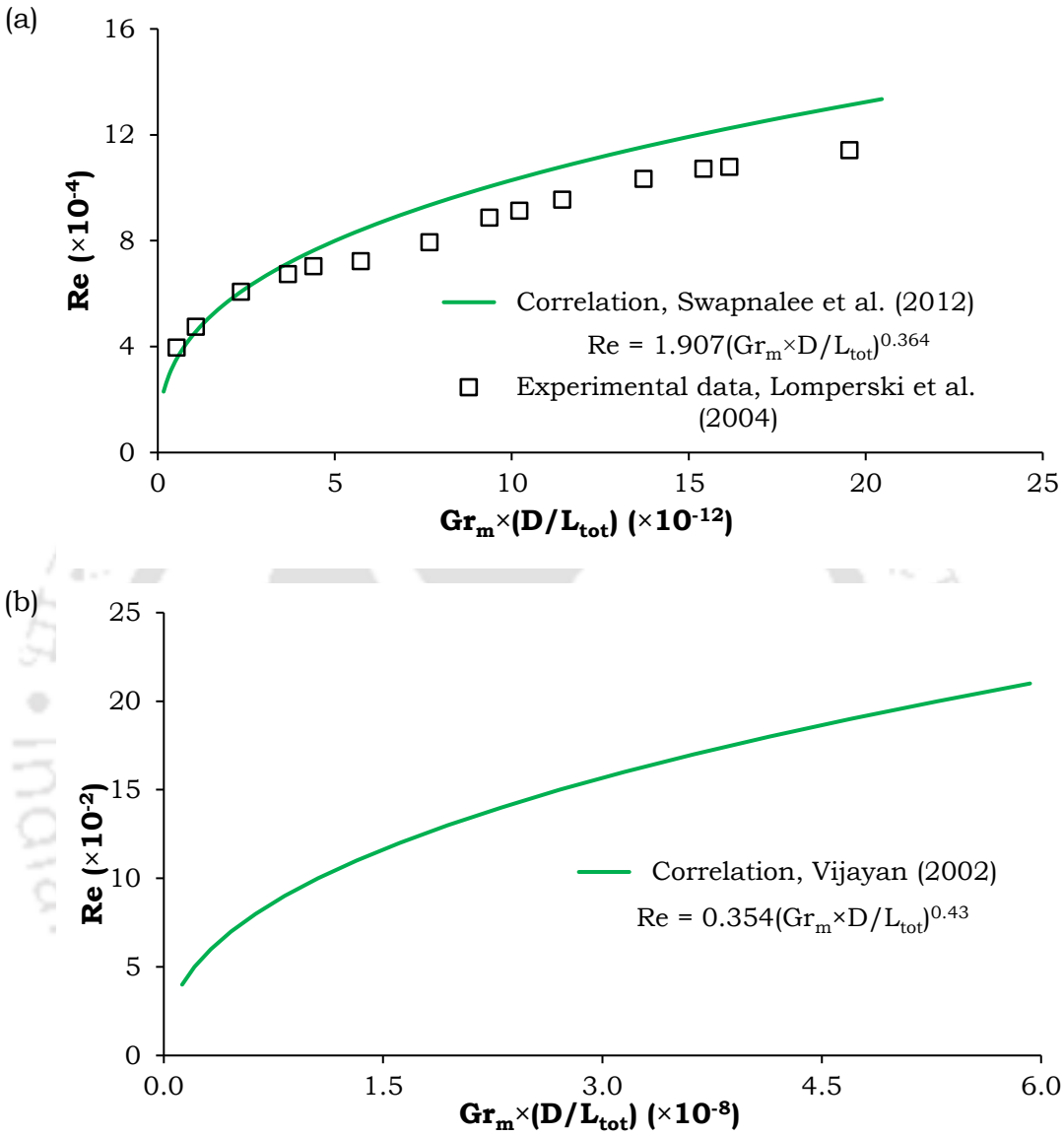

Figure 3-7. Available experimental data for validation of (a) SCNCL and (b) single-phase water based NCL

Experimental data of Lomperski et al., 2004 and experimental correlation of Swapnalee et al., 2012 are used for supercritical condition, whereas Vijayan, 2002 experimental correlation is used for single phase water (Figure 3-7) .

3.10. Summary

The computational modeling study begins with a significant down scaling analysis to finalize the dimensions of the base models. There are

several 3D computational models with various sets of dimensions are developed according to the requirement of study, albeit, all are follows base model. 2D model with identical dimensions of 3D model is used specifically for transient analysis of SCNCL. Structured non-uniform grid system is employed in the present work, with finer mesh near the wall to capture larger gradients of field variables. For grid dependency analysis, four different mesh structures are developed for the base model and simulation have been performed for each of them, finally the numerical results are compared to identify the suitable one. A detailed discussion is documented over the several boundary conditions are employed in the present study. Validation of numerical model with available experimental data is an important task in numerical study. Each chapter involving with numerical approach has a detailed discussion over validation of the model. Here some available experimental works are pointed out, which are used for addressing the validation in the upcoming chapters.

Chapter 4: Thermalhydraulic Characterization of Temperature-coupled NCL

4.1. Preamble

Basic operating principle of any NCL involves the development of flow field by thermally-induced buoyancy force, with the common objective being the transmission of thermal energy from the source to the sink. The high-temperature zone can be created either in heat-flux-supported or temperature-specified mode. While most of the large-scale industrial applications concern heater with specified heat flux, NCLs with definite source and sink temperatures can also be found in solar heaters, heat pipes and micro-coolers. For any given set of such boundary conditions, the overall thermalhydraulic response of the system will certainly depend on the working fluid. Present chapter, therefore, focusses on identifying the most favorable working state of the fluid in a temperature-coupled NCL, with an inherent objective of understanding the advantages gained on imposing supercritical condition in an NCL under a given set of operating condition.

The heat transfer aspect of SCNCL has received more attention in recent times, as the role of heat structures and nature of energy addition/removal on the stability response is under scrutiny (Debrah et al., 2013b). Due to the strong temperature dependence of thermo-physical properties under supercritical conditions, around the pseudocritical point in particular, both buoyancy and frictional forces contemplate non-linear relationship with temperature. Accordingly the thermalhydraulic behavior is decided by the involved temperature range. Yadav et al., 2012c, 2012b found enhancement in both flow rate and heat transfer rate at higher temperature levels for a rectangular SCNCL. Larger temperature differential between heater and cooler was observed by Chen et al., 2013b with increase in heater power. In a subsequent work (Chen et al., 2013c), large values of heat transfer coefficient were estimated in the heating section, nearly comparable with boiling loops, which was also in consensus with the experimental study of

Tokanai et al., 2010. 2D numerical model of Cao and Zhang, 2012 correlated loop thermalhydraulics to several factors inclusive of heater-to-cooler temperature differential, system pressure, pipe diameter, geometric orientation and loop inclination. The role of local buoyancy forces, developed due to asymmetric temperature distribution across any particular cross-section in both heating and cooling sections, was stressed upon by Zhang et al., 2010. .

Therefore it is very much evident that the topic of steady-state thermalhydraulic of SCNCLs for different working fluid under identical operating conditions are not very well explored until date. Hence the present chapter deals with various working fluids under identical operating condition. Single-phase water is the most preferred fluid there due to its availability and non-toxic nature. Excellent heat transport capabilities of transcritical CO_2 and low critical pressure levels of R134a have also attracted engineers as possible alternatives. Present work, therefore, focuses on the thermalhydraulic comparison of the performance of water, CO_2 and R134a as the working medium in NCL under identical set of operating conditions. Parameters are selected so as to maintain water under single-phase liquid condition, while R134a is at supercritical pressure. Selected temperature ranges generally allow R134a to remain below concerned pseudocritical limit, thereby ensuring "liquid-like" density level for this fluid. State of CO_2 remains sub- to supercritical based on selected system pressure. Velocity and temperature profiles at different sections of the loop are compared, along with heat transfer coefficient at specific locations. Effort is made to identify the best working fluid from heat transfer point of view.

4.2. Validation of Numerical Model

The base geometry shown in Figure 3-2 is adopted throughout the present chapter and the computational model detailed in chapter 3 is followed here for all the simulations. It is important to compare the results predicted by the developed computational model with relevant literature to validate the code before proceeding with further simulation. As the present study encompasses both single-phase and supercritical systems, two different sets of validation are attempted with. Simulations are performed with water for three different pressure levels, namely, 6, 8 and 10 MPa. Source and sink temperatures are varied within the range of 275 K to 371 K. Concerned

pressure values being well below the critical pressure limit and selected temperature ranges being lower than corresponding saturation temperatures, water remains as single-phase liquid throughout the loop.

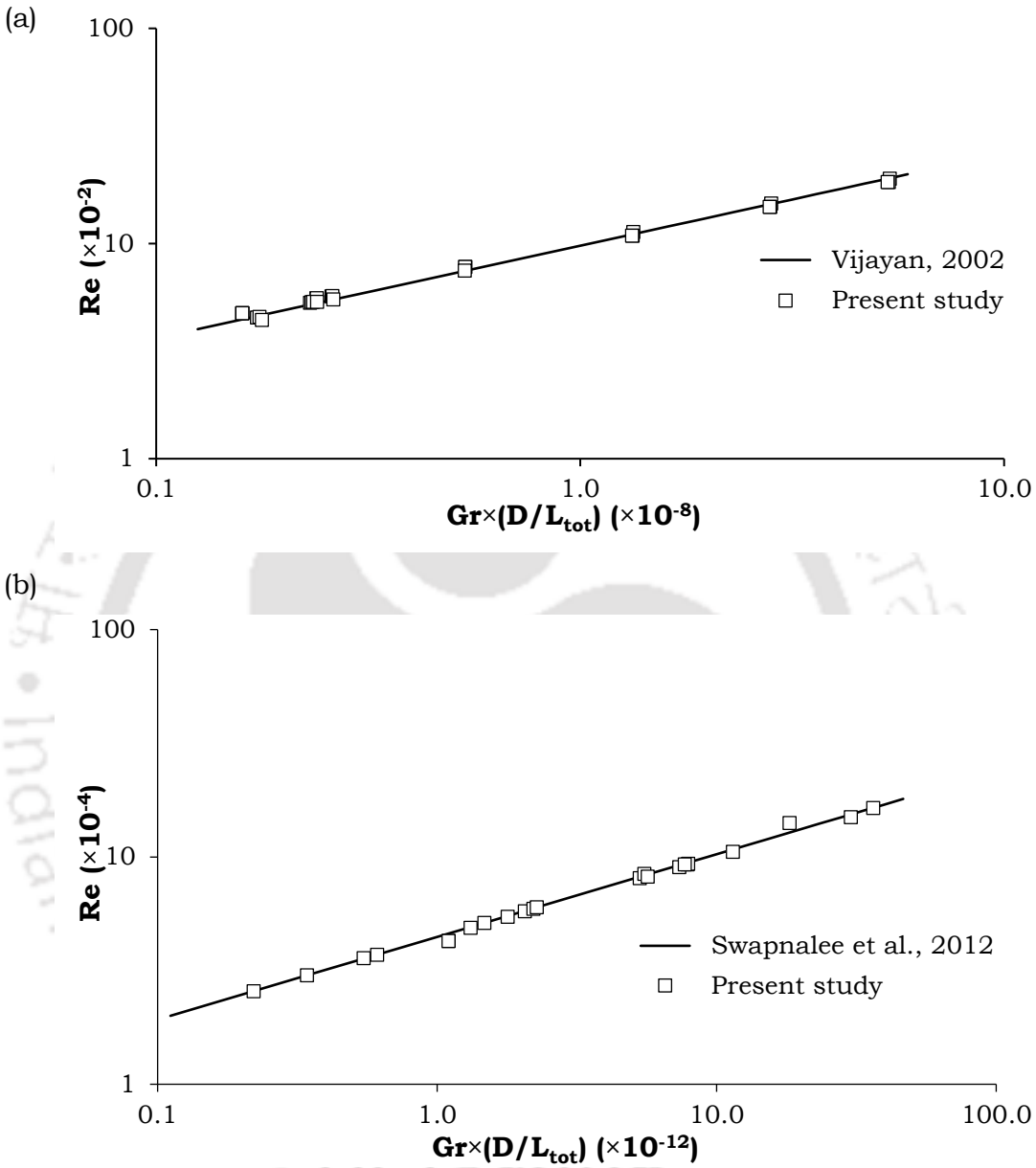

Figure 4-1. Validation for (a) single-phase water (Vijayan, 2002) and (b) subcritical-to-supercritical CO_2 (Swapnalee et al., 2012).

Resultant dataset is compared with the experimental correlation of Vijayan, 2002 and excellent degree of conformity can be observed (Figure 4-1a). Result obtained from the present study can be correlated in a power law form as, $Re = 0.4782\,(Gr_m D/L_{tot})^{0.414}$, which is quite similar to the one proposed in (Vijayan, 2002). For the selected ranges of pressure and temperature, condition of CO_2 varies from sub- to supercritical pressure.

Concerned predictions are compared with the experimental data of Swapnalee et al., 2012 and amicable agreement is obtained, as can be seen from Figure 4-1b. Here the predicted results can be correlated as, $Re = 1.6775\,(Gr_m D/L_{tot})^{0.3681}$, which is again analogous to the experimental one (Swapnalee et al., 2012), thereby endorsing the correctness of the developed model.

Two grossly different types of simulations are carried out to explore the relative influences of source and sink temperatures. The first set considers the increase in heater temperature from 331 K to 371 K at constant sink temperature of 315 K, whereas the other envisages the reduction in cooler temperature from 315 K to 275 K at constant source temperature of 331 K. It is pertinent to mention here that such temperature range can be of particular interest in engineering applications such as the solar water heaters (Chen and Zhang, 2014), air-conditioning systems (Kim et al., 2009), ground-coupled geothermal heat pumps (Rieberer, 2005) and thermal expansion pumps for fluidic transport (Adams et al., 1995), to name a few. Secondary heat transport loops of nuclear reactors or power cycles can also be viewed as a potent application, albeit with slightly raised source temperature level (Pearson, 2004; Zhang et al., 2006).

4.3. Comparison of Thermalhydraulic Parameters

The phenomenon of natural circulation is generally governed by an interplay between buoyancy and friction, with inertia having negligible effect under the steady-state condition. To study the thermalhydraulics of any NCL, it is essential to envisage the temperature and velocity distribution over the length of the loop. Temperature and velocity profiles at the centre of the source with CO_2 as the working fluid under different conditions of pressure and source temperature are presented in Figure 4-2. For smaller source-to-sink temperature differential, cross-sectional temperature variation is fairly uniform. However, with increase in source temperature, asymmetry develops in the profile, with lower temperature being predicted closer to the bottom wall of the tube. The fluid attains the heater temperature only close to either walls, while the temperature in other sections remains well below that, particularly at higher source temperatures. Effect of pressure is much less pronounced compared to the heater temperature, with increase in asymmetry at higher pressure levels. For an increase in system pressure from 6 to 10 MPa with 371

K source temperature, minimum fluid temperature drops nearly by 8 K. The radial location of the appearance of the minimum fluid temperature, however, remains nearly unaffected with change in pressure or source temperature. The temperature profile is well complemented by the asymmetric velocity

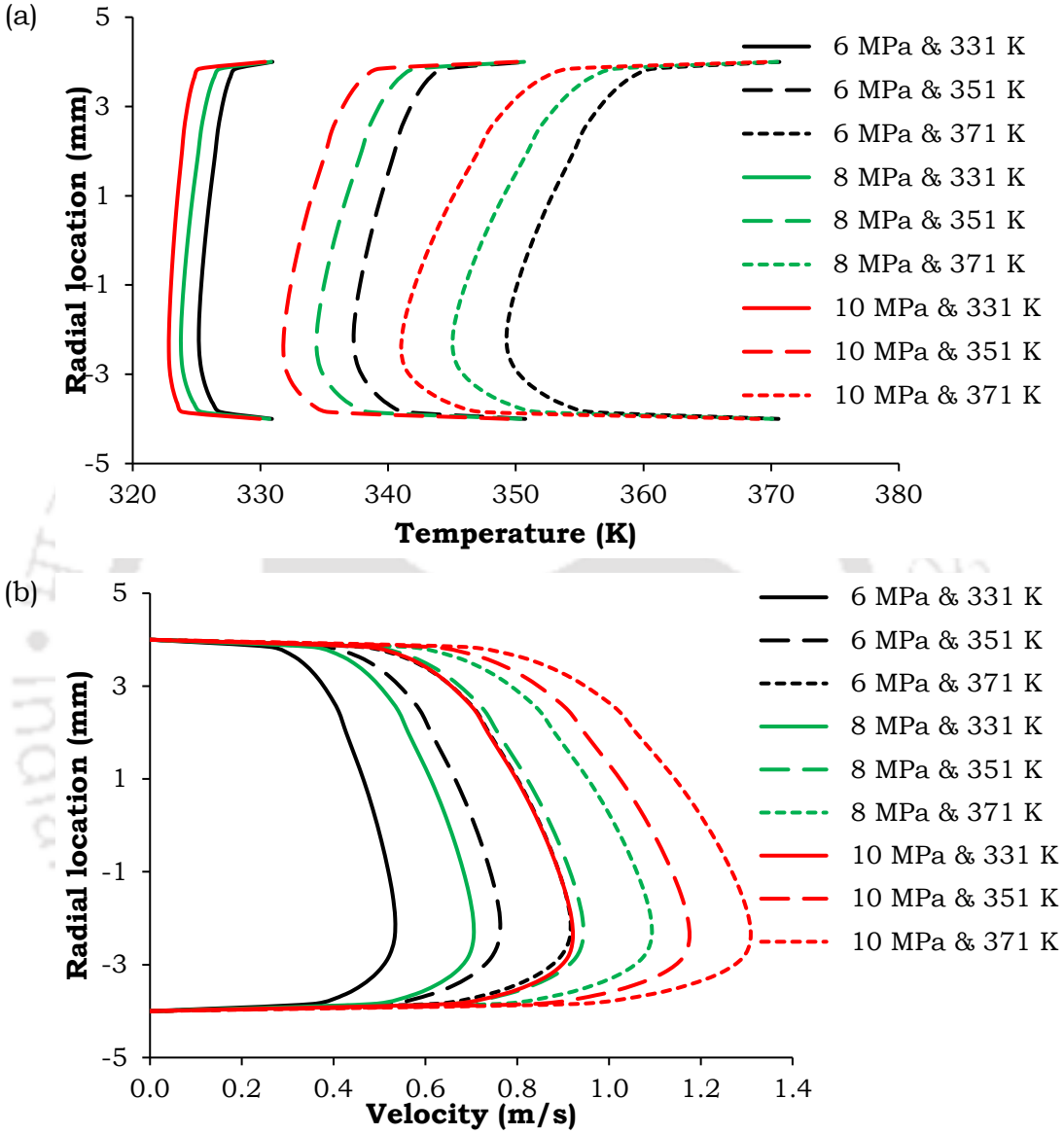

Figure 4-2. (a) Temperature and (b) velocity profiles at source centre with CO_2 as working fluid at different pressures and source temperatures (T_h) for T_c = 315 K

variation, as the radial location of largest velocity closely matches with the same for minimum temperature. It manifests the role played by the local buoyancy force at any cross-sectional plane. Fluid near the heater wall is at higher temperature level and so at lower density compared to the cooler fluid around the centreline. That sets up an upward radial flow velocity. Similar phenomenon happens in the cooler section as well, but with downward radial

velocity and denser fluid near the wall (Figure 4-3). As a result, fluid near the lower wall of the heater and upper wall of the cooler directly drives the local

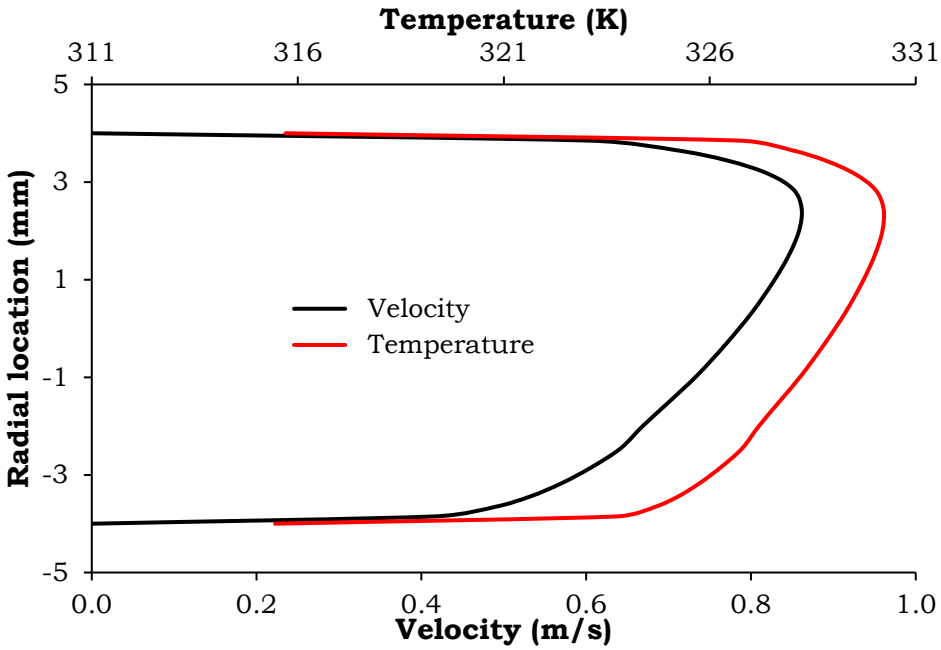

Figure 4-3. Temperature and velocity profiles at sink centre with CO_2 as working fluid at 8 MPa pressure with T_h = 351 K and T_c = 315 K

heat and mass transfer processes, leading to enhanced heat transfer. Present discussion can further be reinforced following fluid temperature contours at the source centre. A particular case is presented in Figure 4-4. Fluid can attain the imposed source temperature of 371 K only very close to the wall and a substantial temperature gradient can be observed across the thermal boundary layer, the thickness of which varies along the periphery. Lowest temperature zone is located quite close to the bottom wall, with highly-compressed isotherms below the same, indicating severe temperature gradient in the lower part of the tube. Isotherms are more relaxed in the upper part, signifying lower rate of heat transfer. The opposite scenario is true for the sink, with the asymmetry shifted towards the upper half and large temperature gradient close to the upper wall.

The asymmetric nature is more prominent with reduction in sink temperature. As the lowest temperature falls below concerned pseudo-critical point, with the source temperature remaining well above that, loop fluid experiences substantial density variation between the hot and cold leg of the loop, leading to considerable development in the buoyancy field. Fluid density variation over any particular cross-section in the heater or cooler region can

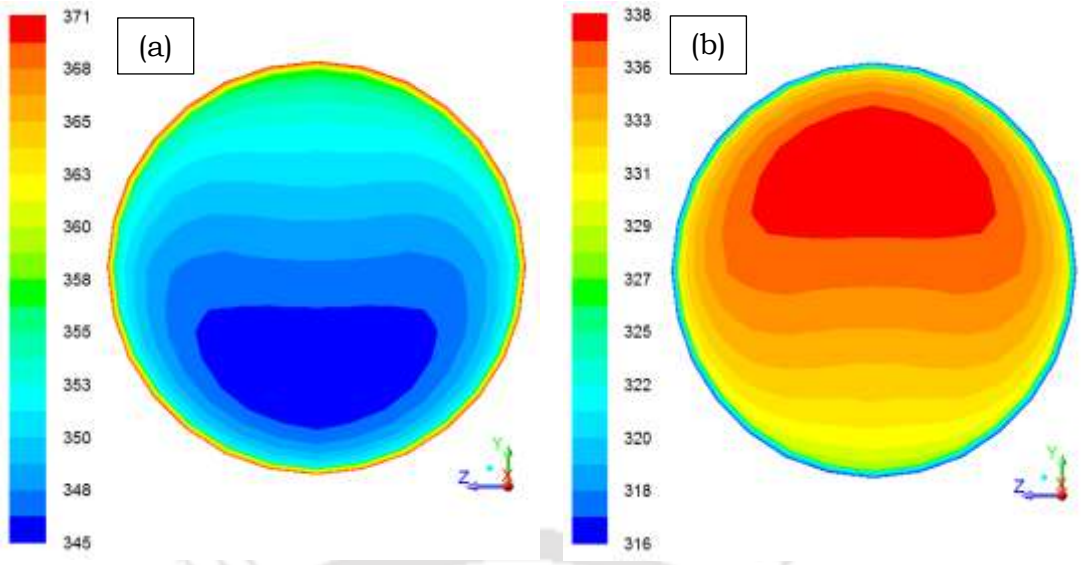

Figure 4-4. Cross-sectional temperature contours at (a) source and (b) sink centres with CO_2 as working fluid for p = 8 MPa, T_h = 371 K and T_c = 315 K

also be quite sizeable. As a pressure level of 8 MPa is just above the critical point for CO_2, such property variation is significantly more compared to the pressure level of 10 MPa. The immediate effect is a reduction in heat transfer rate, as is evident by the lower temperature levels of loop fluid at 8 MPa compared to 10 MPa (Figure 4-5a). Local buoyancy field is also enhanced due to such density variation, leading to larger velocity levels. The deviation is particularly prominent when the operating condition is reasonably close to the pseudo-critical zone. 8 MPa pressure level for CO_2 is closer to its critical pressure (7.377 MPa) compared to 6 and 10 MPa. A sink-side condition of 295 K is also slightly below the pseudocritical point at 8 MPa (~ 307.8 K). This particular situation corresponds to rapid changes in fluid properties, and so provides the largest magnitude of velocity (Figure 4-5b).

Objective of the present study being the identification of the preferred fluid through thermalhydraulic comparison, simulations are performed with both R134a and water under identical operating conditions. Selected conditions are well below the pseudocritical values of R134a (about 411.4 K at 8 MPa) and so it behaves as a supercritical fluid with “liquid-like” density level, showing quite regular nature of property variation and hence no inconsistency in velocity or temperature profiles unlike CO_2. Radial temperature variations at the source centre for the R134a loop with changes in sink temperature and system pressure are presented in Figure 4-6a. The effect of pressure is found to be minimal, with the profiles getting clustered

depending on the imposed temperature ranges. A lower sink temperature reduces the minimum fluid temperature across the pipe section and also enhances asymmetric nature due to the local buoyancy effects, fairly analogous to the CO_2-based loop. However, the nature of velocity or temperature contours are markedly different with water as the loop fluid. Selected conditions maintain single-phase liquid water throughout the loop, leading to larger rates of heat transfer owing to higher thermal conductivity. Energy supplied by the source can be distributed across the fluid layers more uniformly, minimizing the local buoyancy effects. Hence quite symmetric

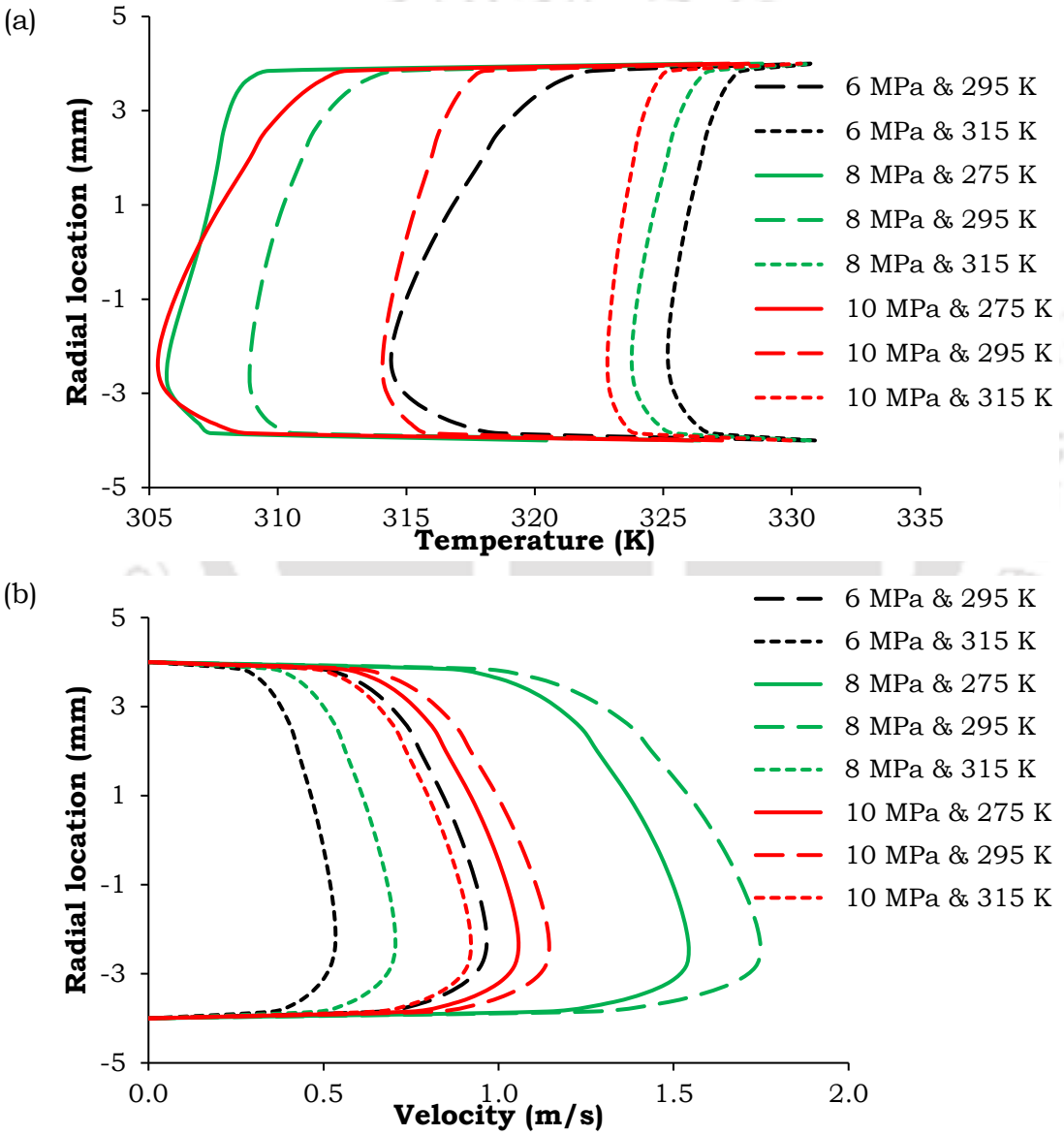

Figure 4-5. (a) Temperature and (b) velocity profiles at source centre with CO_2 as working fluid at different pressures and sink temperatures (T_c) for T_h = 331 K

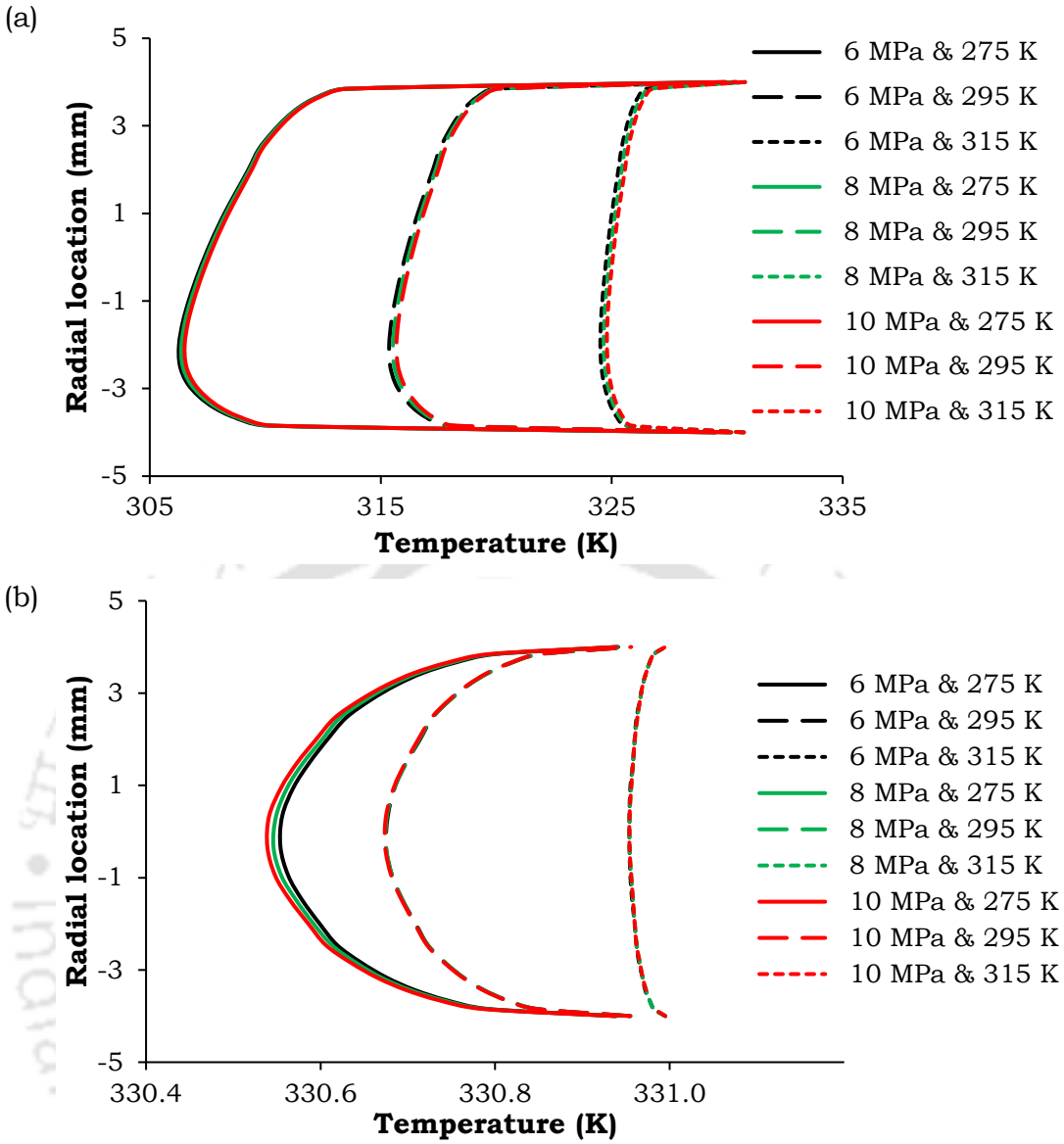

Figure 4-6. Temperature profiles at source centre with (a) R134a and (b) water as working fluid at different pressures and sink temperatures (T_c) for T_h = 331 K

temperature profiles can be observed across the tube, with influence of pressure being inconsequential (Figure 4-6b). For lower source-to-sink temperature differential, nearly uniform fluid temperatures can be obtained, whereas a fully-developed parabolic profile is achieved for larger differences. The magnitude of variation in temperature across the pipe section, however, is nearly negligible, indicating greater energy diffusion across fluid layers compared to CO_2 or R134a. Velocity profiles for both the fluids also follow similar trends. Temperature contours at the source centre with R134a and water under identical working conditions are presented in Figure 4-7. Lowest

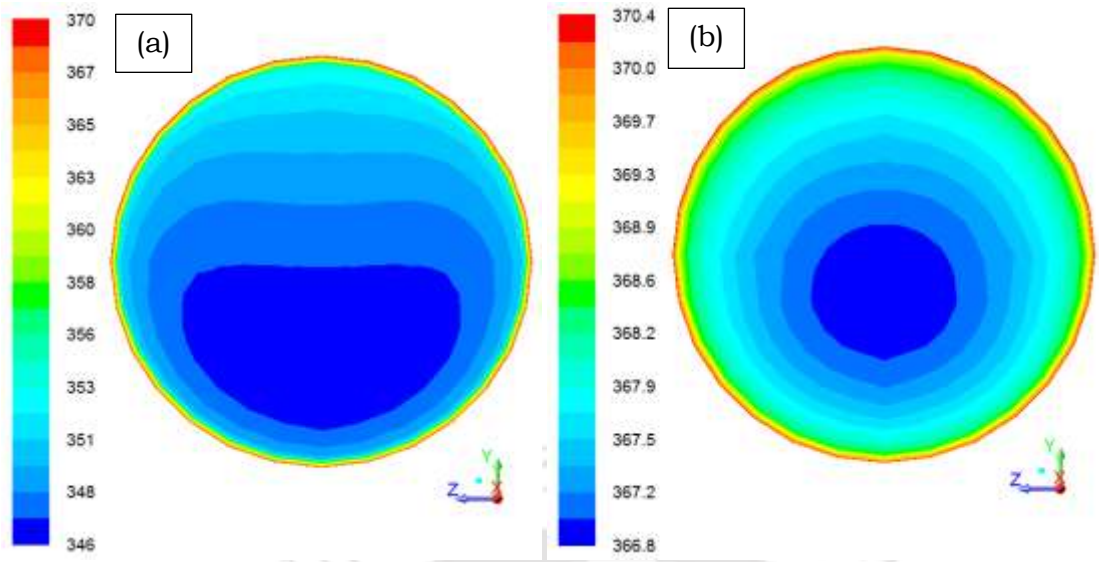

Figure 4-7. Cross-sectional temperature contours at source centre with (a) R134a and (b) water as working fluid for p = 8 MPa, T_h = 371 K and T_c = 315 K

temperature zone for R134a is located quite close to the lower wall, with compressed isotherms below that, signifying larger temperature gradient in the bottom section of the tube. On the contrary, temperature contours for water is reasonably uniform, as the lowest temperature zone is positioned

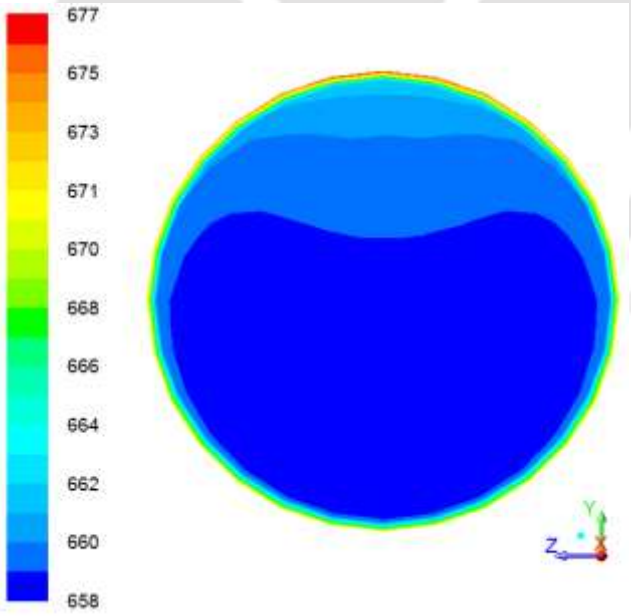

Figure 4-8. Cross-sectional temperature contours at source centre with water as working fluid for p = 25 MPa, T_h = 688 K and T_c = 628 K

slightly below the centre and well-distributed isotherms all over the cross-section. Magnitude of the smallest temperature associated with water is also

substantially higher than the same for CO_2 (Figure 4-4) or R134a, indicating larger heat diffusion rate with water.

In order to establish the role of property variation across a single cross-section and local buoyancy effect under supercritical condition, one simulation is performed with supercritical water and corresponding temperature contours at the source centre is presented in Figure 4-8, along with the operating conditions. The asymmetric nature is clearly visible, with the lowest temperature zone positioned very close to the bottom wall. The corresponding condition being well apart from the present scope of the work, any further discussion is hence avoided.

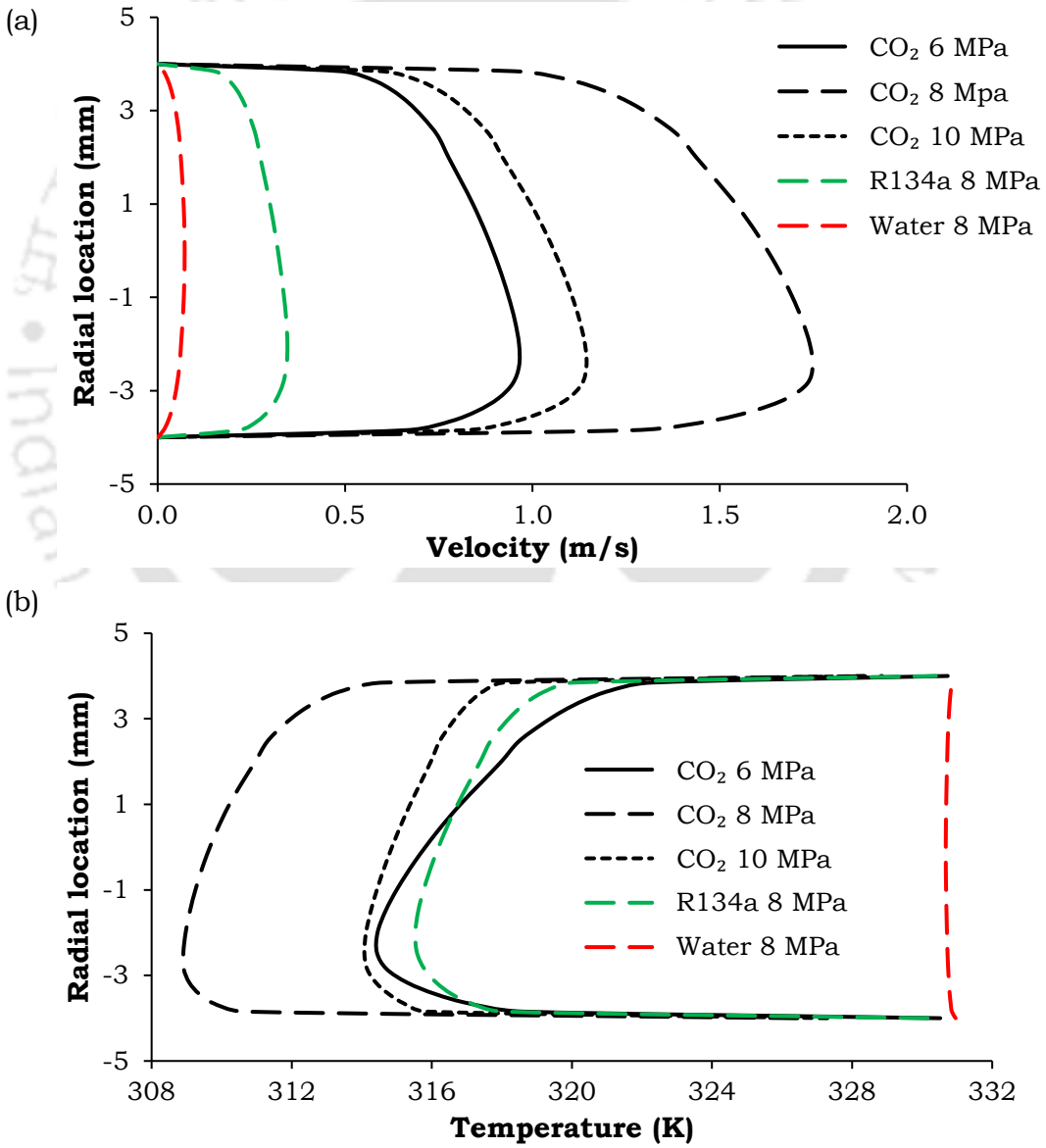

Figure 4-9. (a) Velocity and (b) temperature profiles at source centre with three different working fluids for T_h = 331 K and

A direct comparison of velocity and temperature profiles for all the three fluids is drawn in Figure 4-9 under identical operating conditions. Due to the single-phase liquid nature of water loop, driving buoyancy force is quite small, yielding low flow rates. As the selected condition allows CO_2 to pass across the pseudocritical point, considerably larger velocity can be achieved due to substantial variation in fluid density, particularly at pressure levels slightly above critical. For a system pressure of 8 MPa, maximum flow velocity with CO_2 is as much as 25 times higher than the same with water. Flow velocities with R134a lies in between and can be about 5 times of water. Velocities in water and R134a loop are nearly invariant of pressure, because of near-incompressible nature of both fluids within selected range of operating conditions. The water loop, in fact, can be operated at any lower pressure level, as long as the attainment of saturation temperature is avoided. Velocity values with CO_2, however, varies significantly with pressure. Increase in system pressure from 8 to 10 MPa causes about 35% reduction in the maximum velocity at the source centre. When the sink temperature is above the pseudocritical point, density variation for CO_2 is much lesser, producing lesser flow velocities and so the difference in magnitude with water loop is much smaller. Still, for all the considered combinations of operating parameters, CO_2 delivers the highest velocity and water the least at any section of the NCL. The velocity profiles contemplates the temperature profiles reasonably well (Figure 4-9b). Single-phase liquid nature of water ensures large heat transfer coefficient, resulting in negligible temperature variation over the cross-section. Significant temperature variation exists for both CO_2 and R134a. Rapid reduction in thermal conductivity for 8 MPa yields deterioration of heat transfer coefficient, leading to the lowest fluid temperature.

4.4. Comparison of Mass Flow Rate

Figure 4-10 demonstrates the effect of source and sink temperature on mass flow rate. As expected, flow rates for water and R134a are nearly independent of system pressure. With increase in source temperature, R134a predicts the largest flow rate at 8 MPa pressure. At 10 MPa, however, CO_2 delivers the largest flow rate till a certain temperature range. Highest flow rate is achieved with CO_2 loop while reducing the sink temperature, as long as the sink temperature is well-below the pseudocritical point. The buoyancy force

in single-phase NCL linearly increases with temperature differential and hence induces near-linear increase in mass flow rate. Condition being far away from pseudocritical point, the same is also true with R134a. But the properties of CO_2 being strongly temperature-dependent, development of buoyancy field depends on the involved temperature range. Density drops rapidly around the pseudocritical point, producing a peak of the volumetric expansion coefficient. Therefore, when the fluid crosses the pseudocritical temperature during its passage through the heater, a high density differential is developed, yielding a strong buoyancy field. Any increase in flow rate also enhances the frictional resistances, while viscosity can drop sharply at higher temperatures. Large

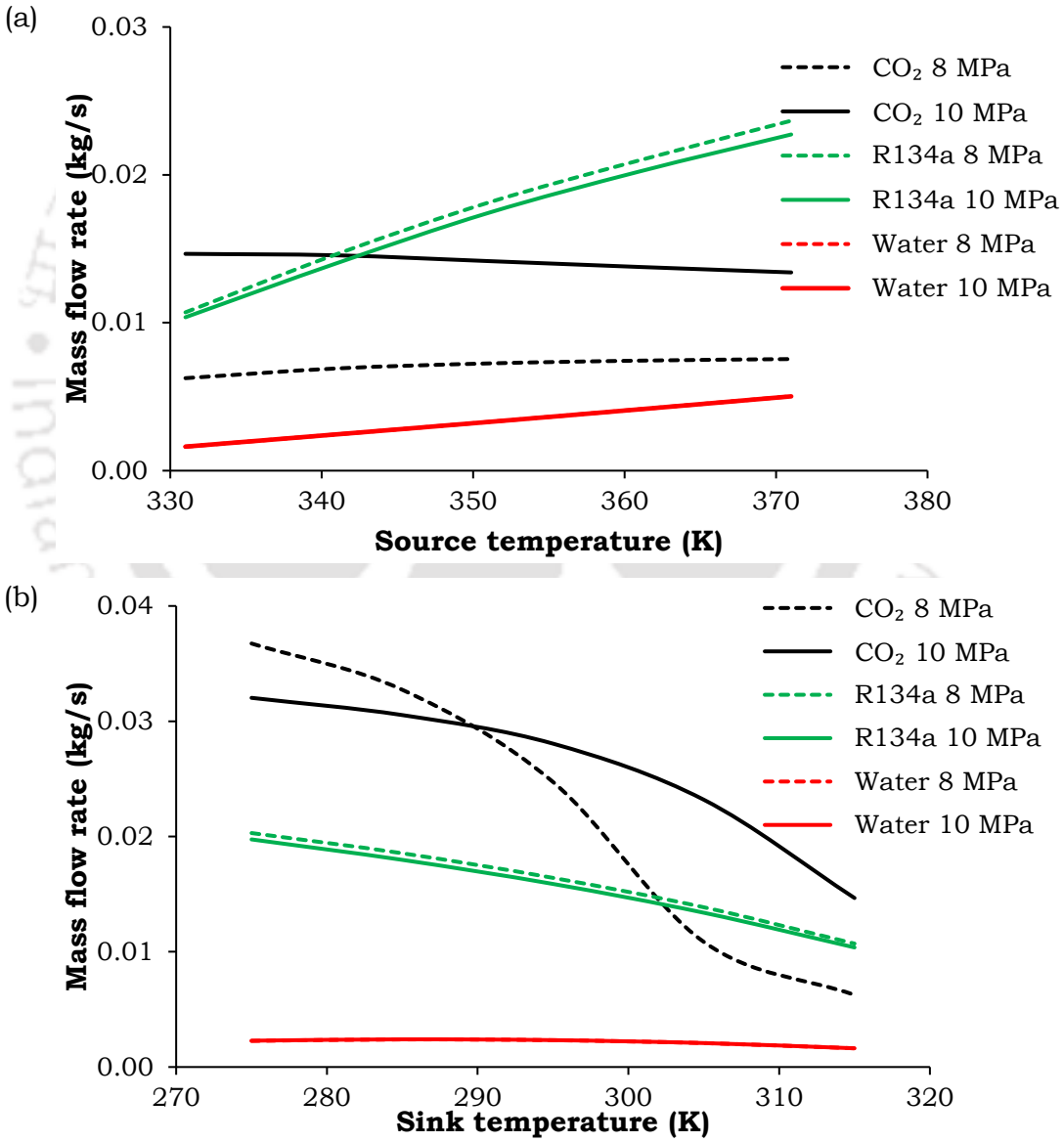

Figure 4-10. Variation of loop mass flow rate with (a) source temperature for T_c = 315 K and (b) sink temperature for T_h = 331 K with three different working fluids

reduction in density in the riser can substantially enhance the kinetic head for any given flow rate. Combination of these two opposing effects resolves the final loop flow rate. When the sink condition is close to the pseudocritical temperature, viscous forces are dominated by the buoyancy forces, instigating enhancement in flow rate. The reverse condition is true for conditions well away from pseudocritical zone, as is evident in all situations with R134a and also with CO_2 under certain conditions.

4.5. Mass Inventory Requirement

Mass inventory can occasionally be a consideration in practical

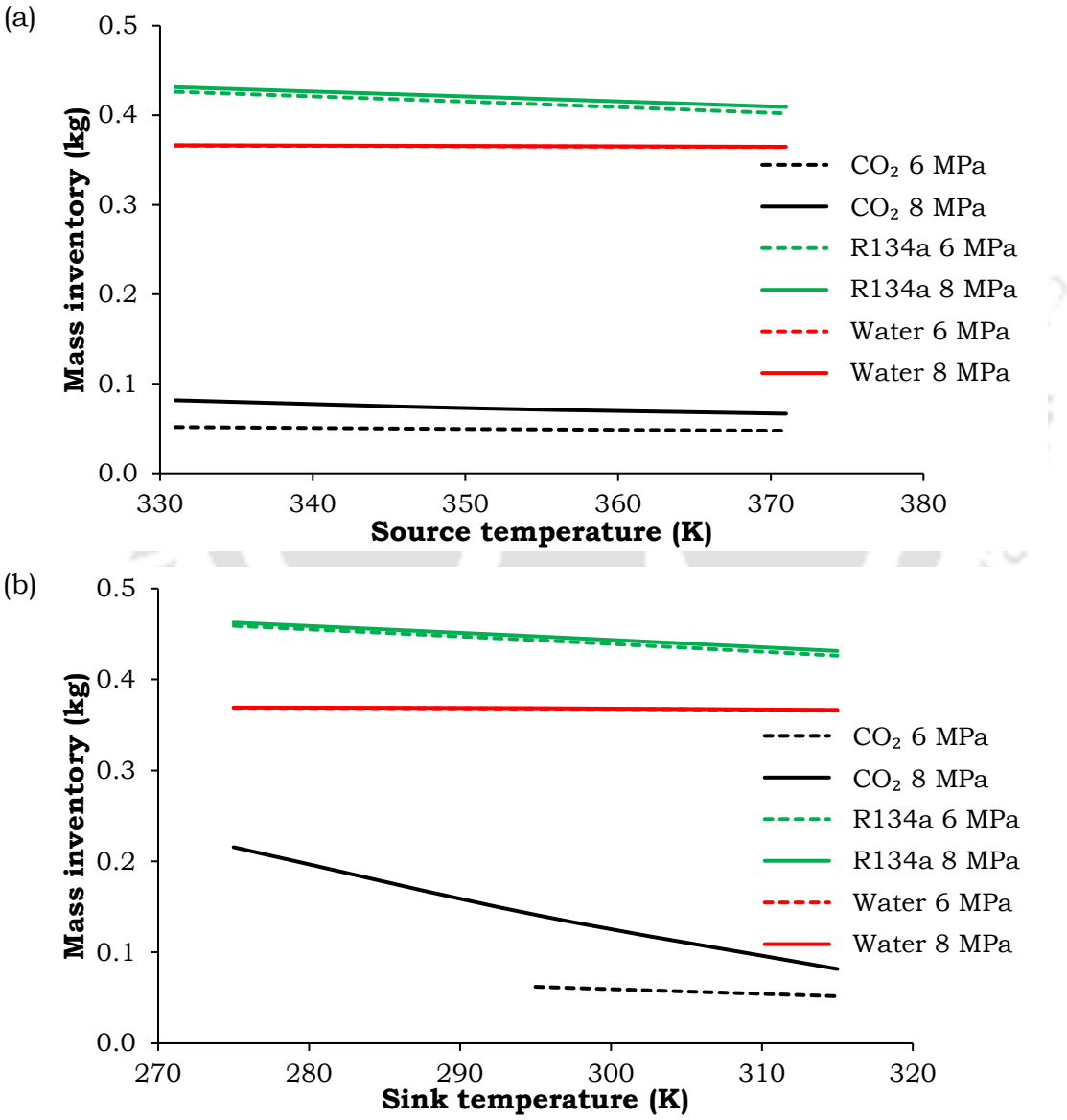

Figure 4-11. Variation of mass inventory with (a) source temperature for T_c = 315 K and (b) sink temperature for T_h = 331 K with three different working fluids

operation, as it determines the minimum mass of fluid required for operation and the corresponding storage obligation. Inventory requirement is directly related with the operating condition of the system. The total volume of the loop being specified, the mass inventory can be viewed to be proportional to the average fluid density, or in torn, the average value of the bulk-temperature. A reduction in the later value is expected to increase the inventory requirement. That is possible either by lowering the sink temperature for a constant temperature source or by reducing the source temperature for a constant temperature sink, for a loop with isothermal heater and cooler. The former option will also lead to an increase in the temperature differential, thereby enhancing the effective buoyancy force and hence the flow rate. Therefore, it is possible to simultaneously have lower mass inventory and higher flow rate with this option. However, the other option will reduce the effective buoyancy, thereby reducing the inventory requirement at the cost of lower flow rate. Concerned variation with source and sink temperatures are presented in Figure 4-11. CO_2 consistently provides the least inventory, while R134a is the highest. Inventory requirement for CO_2 reduces quite sharply with rise in sink temperature, particularly for 8 MPa system pressure, due to large flow velocities and augmented local buoyancy effects. Therefore supercritical CO_2 can be viewed as a more preferable fluid from both mass flow rate and inventory requirement point of view, particularly when the desired system pressure is slightly above the corresponding critical value.

4.6. Heat Transfer Aspects

The situation is, however, noticeably different from heat transfer point of view. Effect of source and sink temperatures on average heat transfer coefficient at source with all the three fluids at 8 MPa pressure level is presented in Figure 4-12. Local Nusselt number values are calculated using the dimensionless temperature gradient prevailing at the tube surface and that is employed in estimating the concerned heat transfer coefficient. Water is single-phase liquid and hence exhibit very high heat transfer coefficient. R134a is in supercritical condition, but the considered temperature range is well below the pseudocritical temperature (about 411.4 K at 8 MPa). So it also behaves nearly like a single-phase medium with poor thermal conductivity, resulting in very low heat transfer coefficient. Under identical conditions, heat transfer coefficient for water can be as much as 6 times that of R134a. With

increase in source-to-sink temperature differential, heat transfer coefficient moderately increases with R134a, while it remains nearly the same for water. When the sink temperature is higher than pseudocritical temperature for CO_2 (about 307.8 K at 8 MPa), its heat transfer performance is very poor compared

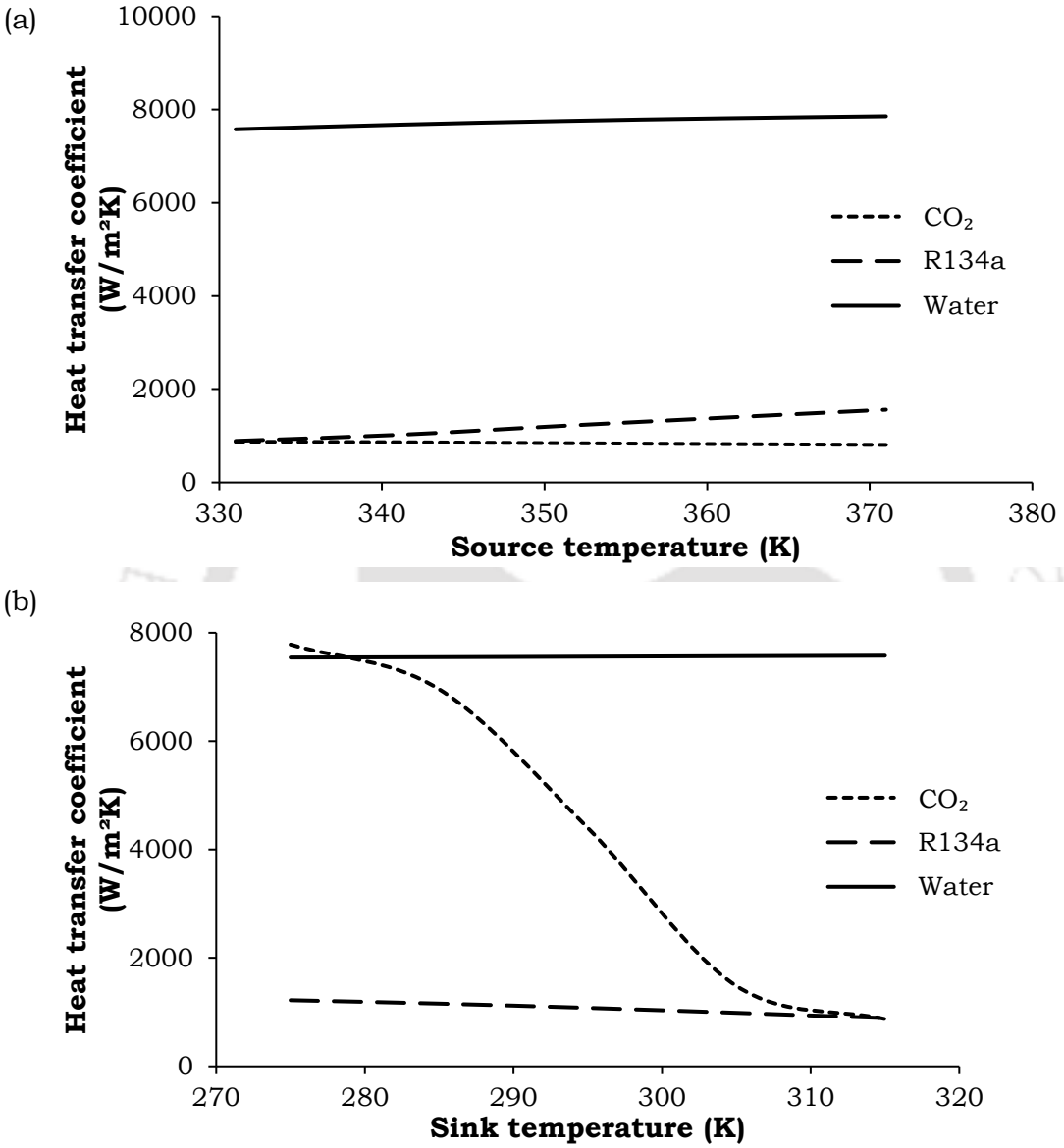

Figure 4-12. Variation of heat transfer coefficient at source with (a) source temperature for T_c = 315 K and (b) sink temperature for T_h = 331 K with three different working fluids at p = 8 MPa

to water and can even be inferior to R134a, due to poor thermal conductivity. However, when CO_2 crosses the pseudocritical point within the heater, it experiences a sharp drop in thermal conductivity, along with a small intermediate peak (Figure 1-7). The consequence is evident from Figure 4-12b, as heat transfer coefficient is comparable with water for low sink temperatures and drops sharply with any increase thereof. It emphasizes the role of local

buoyancy in enhancing both mass and heat transfer rate. Such behavior is, however, found only for supercritical pressure levels close to the critical value. Heat transfer coefficient generally increases with system pressure (Figure 4-13). When the sink condition is higher than pseudocritical, heat transfer coefficient monotonically decreases with larger source-to-sink temperature differential and the concerned gradient is much steeper at higher pressure levels. Rapid deterioration in heat transfer coefficient can be found when the working fluid is made to cross the pseudocritical temperature, as is explained earlier.

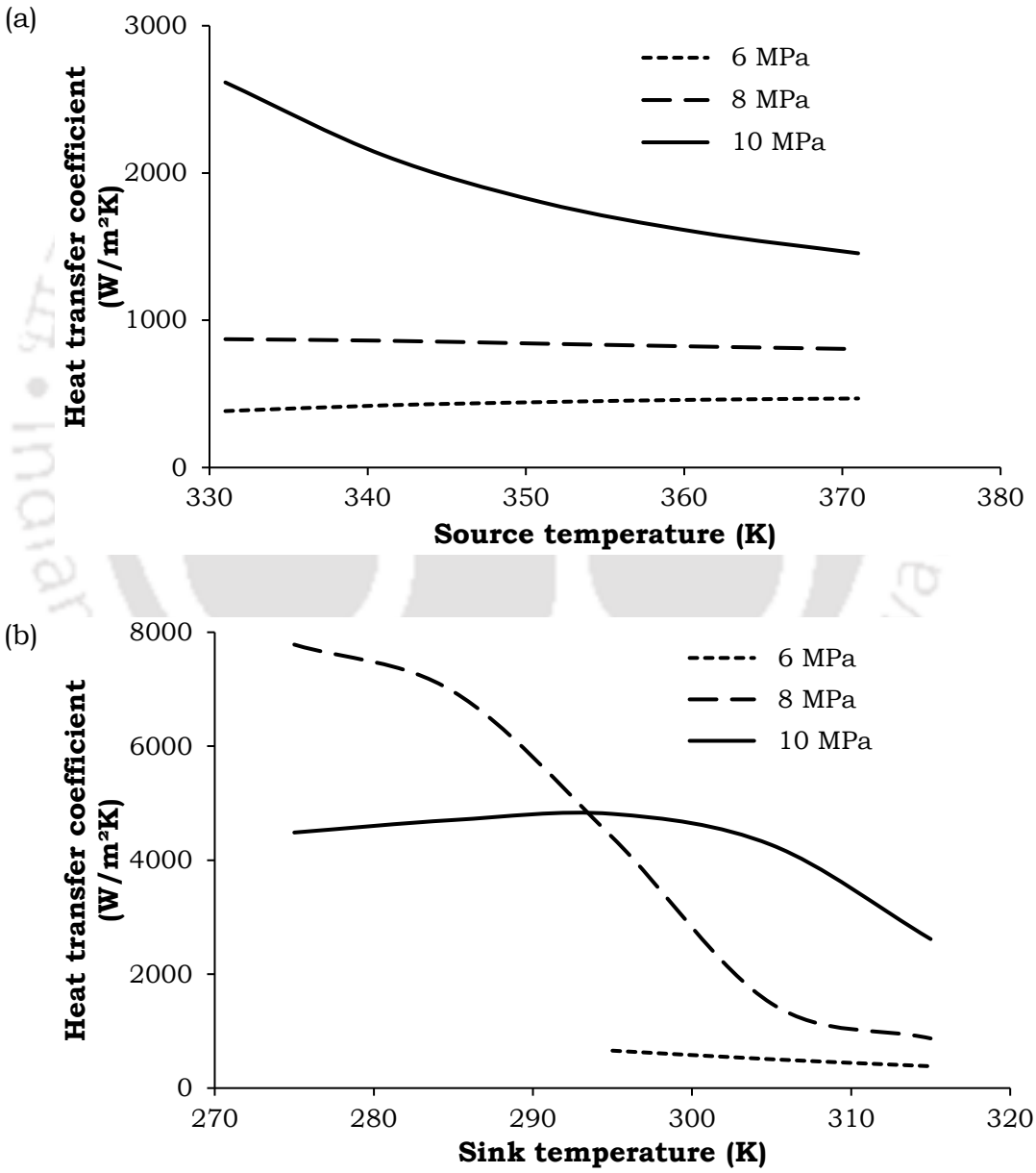

Figure 4-13. Variation of heat transfer coefficient of CO_2 at source with (a) source temperature for T_c = 315 K and (b) sink temperature for T_h = 331 K at three different pressure levels

NCL under consideration has temperature-coupled boundary condition and hence the rate of heat transfer from source-to-sink depends on both mass flow rate and heat transfer coefficient. Figure 4-14 presents the variation of the rate of heat transfer with source and sink temperature for all the three fluids at two different pressure levels. Large heat transfer coefficient for water and high mass flow rate for R134a help achieving large power transmission

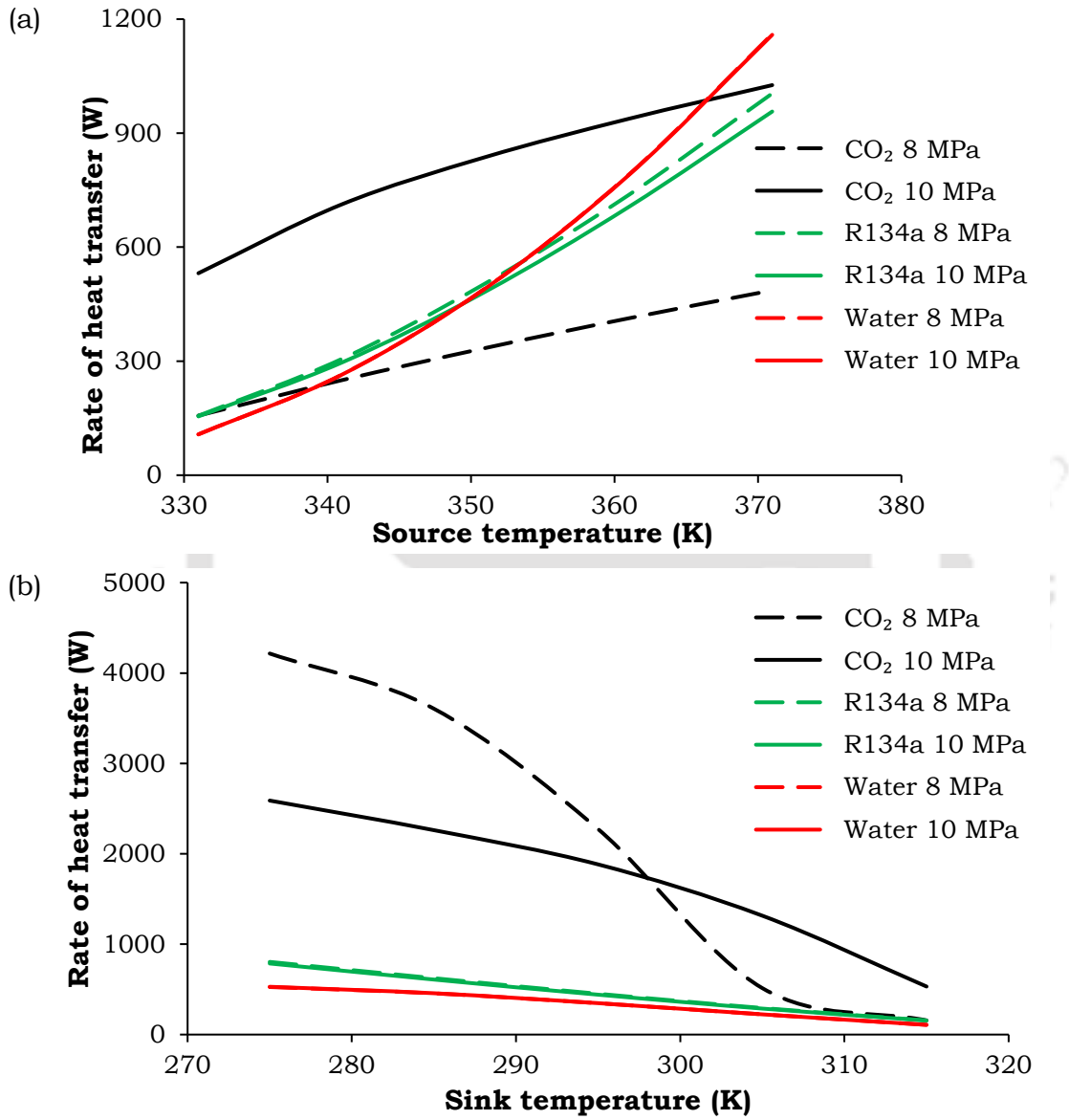

Figure 4-14. Variation of rate of heat transfer at source with (a) source temperature for T_c = 315 K and (b) sink temperature for T_h = 331 K with three different working fluids

with either of the working fluids. The same increases continuously with enhanced source-to-sink temperature differential, without any significant influences of system pressure. Till a certain limit of source temperature, R134a provides greater rate of heat transport. However the steeper profile for

water owing to the substantially higher heat transfer coefficient, results in larger power transport with water at higher level of source temperatures. Rate of heat transfer for the CO_2-based loop is dependent on the working temperature limits. When the sink temperature is higher than the pseudocritical value, both heat transfer coefficient and mass flow rate being low, CO_2 at 8 MPa can transfer energy at a very low rate. At 10 MPa, however, CO_2 exhibits the largest flow rate till a certain source temperature limit. Corresponding heat transfer coefficient values are also much higher than 8 MPa (Figure 4-13). Therefore CO_2 loop at 10 MPa is able to provide the largest heat transfer rate for almost the entire range of source temperature considered here. On the other hand, when the sink temperature is well below pseudocritical, extremely high rates of heat transport can be obtained with CO_2 loop, which can be as high as 8 times that of water at 8 MPa. But the rapid deterioration in heat transfer coefficient, as the sink temperature approaches the pseudocritical point, is also reflected in the heat transfer rate, which shows a sharp decline with increase in sink temperature. Still the amount of power transmitted by the CO_2-loop is higher than other two fluids for the conditions considered in present study. Therefore supercritical CO_2 as a working fluid is able to provide favourable heat transmission characteristics for majority of the conditions. The use of CO_2-based loops can specifically be suggested at higher system pressures and large source-to-sink temperature differential, with the sink temperature being well below the pseudocritical limit and the source temperature being well above the same. However it demonstrates inferior performance for system pressure close to the critical point and with sink temperature higher than pseudocritical at corresponding pressure.

4.7. Epilogue

The present chapter deals with three different working fluids to ascertain the suitability of employing supercritical condition for a given set of operating parameters. Here, Dirichlet boundary condition has been imposed at both source and sink throughout the study to explore the thermalhydraulic performance of a rectangular NCL. Source and sink temperatures and system pressure are selected as the control variables. For the chosen operating conditions, CO_2 is in sub- to supercritical state, while R134a is at supercritical pressure and water is single-phase liquid. Both single-phase and supercritical

results are validated with available literature to have amicable agreement. Asymmetric temperature and velocity profiles can be observed across flow sections, particularly with larger source-to-sink temperature differential, due to local buoyancy effects. Such asymmetry is the largest with CO_2 as the working fluid, whereas water shows a near-uniform profile. Under identical operating condition, CO_2 exhibits the highest velocity magnitude at any particular cross section and also the lowest temperature value, with the radial location of largest velocity and lowest temperature conforming each other well. Largest velocity is achieved with the system pressure slightly above the critical. Mass flow rate increases with increase of temperature differential between heater and cooler for both water and R134a. Variation for CO_2 is strongly dependent on both system pressure and imposed temperature range. CO_2 also exhibits the smallest mass inventory requirement among the three fluids considered here. Single-phase liquid nature of water yields the highest heat transfer coefficient, which remains nearly constant for the selected ranges of pressures and temperatures. When sink-side condition is below pseudocritical, CO_2 produces heat transfer coefficient comparable with water. However, a sharp deterioration is observed with change of state from trans-critical to supercritical. Rate of heat transfer for both R134a and water are directly proportional to the temperature difference between heater and cooler. CO_2 provides the largest heat transfer rate at higher pressures and also when the sink temperature is reasonably below the pseudocritical value.

In view of the above observations, a guideline can be proposed about the choice of working fluid depending on the prevailing operating conditions. CO_2-based SCNCL can be identified as the preferred option from heat transfer point of view only for pressures reasonably above its critical value, and with source and sink temperatures lying on either side of the pseudocritical temperature corresponding to the system pressure. However, if the pressure approaches critical limit for CO_2 (~ 7.38 MPa) or the sink temperature is around or above the pseudocritical value, single-phase loop can be a better choice. Consistent thermalhydraulic performance and possibility of operating at reduced system pressure are added incentives for the water-based system. R134a, despite being a supercritical fluid, cannot be suggested as a feasible option for the ranges of parameters explored here, owing to lesser heat transfer rate and larger inventory requirement. Therefore the adoption of supercritical condition can be suggested only under favorable set of operating conditions.

Chapter 5: Characterization of Heat Flux Supported NCL-Appearance of FiHTD

5.1. Preamble

The mode of heating is a critical factor on steady-state thermalhydraulics of SCNCL. Both Dirichlet and Neuman mode are of equal importance, based on the application. Rectangular loops with Dirichlet boundary condition imposed at both source and sink has already been explored in the previous chapter. Heating in specified heat flux mode, however, is more common in important engineering applications, such as nuclear reactors, refrigeration and electronic chip cooling. Present chapter, therefore, discusses the steady-state thermalhydraulics of a rectangular NCL, where, heating is envisaged in constant heat flux mode and cooling is through a constant temperature sink. Computational investigation for comparative thermalhydraulic analyses is performed to propose a guideline for selecting the working fluid and nature of the loop, subcritical or supercritical, under identical levels of operating parameters like pressure, heating power and coolant temperature. The 'base model' (Figure 3-2) is considered as computational model in the current chapter, where, both heating and cooling sections are placed in horizontal arms. Due to favourable thermophysical properties and environmental conformity, water, CO_2 and R134a are selected as possible working fluids. Working conditions are selected so as to maintain water as single-phase liquid, while the others vary between sub- to supercritical state based on involved pressure and temperature ranges.

The first analytical model of single-channel SCNCL was developed by Chatoorgoon, 2001 with both distributed and point heat source and sink. Steady-state flow rate was found to increase till a maxima and decrease afterwards. In subsequent studies of Chatoorgoon et al., 2005b, 2005a, influences of various geometric parameters on the stability behaviour of the loop with different working fluids were investigated. Trends of steady-state profiles for both CO_2 and H_2 were found to be similar to water, which is consistent with the observations reported later by the implicit finite difference

model of Jain and Rizwan-uddin, 2008. Cao and Zhang, 2012 developed a numerical model to study the thermalhydraulics of SCNCL and reported the same to depend on several factors like operating pressure, loop diameter, source-to-sink temperature differential and loop inclination to vertical, if any. A 3D rectangular model of SCNCL was developed by Yadav et al., 2012c, 2012b to compare flow and heat transfer behaviour of subcritical single-phase water and sub- to supercritical CO_2. For identical operating conditions, CO_2 exhibited higher velocity and higher heat transfer rate.

Appraisal of literatures suggest that a thorough steady-state thermalhydraulic analysis of SCNCL for different working fluids with heat flux coupled condition are still not explored properly. Thus, it is imperative to perform a comparative thermalhydraulic analysis of loops under identical operating conditions, to check the viability of opting for a supercritical system and also to propose a guideline for selecting the nature of the loop, subcritical or supercritical, based on the requirement of energy transport. Therefore, present chapter consists a detail steady-state analysis with considering CO_2, water and R134a as loop fluid. The results are compared for all the fluids under identical operating condition. Influences of operating parameters like system pressure, input heat flux and coolant temperature on loop thermalhydraulics are ascertained for all the three fluids with focus on performance comparison.

5.2. Validation of Numerical Model

Three different pressure levels are selected for the present study for all three fluids, namely 6, 8 and 10 MPa. Due to the lower critical pressure of R134a (~ 4.06 MPa), a few simulations are also performed at two additional pressure levels of 4.2 and 5 MPa solely for this fluid. Selected conditions are well below the critical pressure of water (~ 22.06 MPa) and hence water flows as single-phase liquid till the saturation temperature limit is breached. Generally the heat flux and coolant temperature criteria are selected so as to maintain water as liquid for all the simulated conditions. The 6 MPa pressure is below critical pressure of CO_2 (~ 7.38 MPa), while the other two levels are supercritical. R134a loop is always supercritical, but the highest fluid temperature can be below or above the pseudocritical value, based on the imposed conditions, thereby allowing NCL simulation under all of subcritical, transcritical and supercritical situations. For all pressure levels, sink

temperature varies in the range of 285 to 315 K, whereas the supplied heat flux corresponds to input power in the range of 50 W to 8 kW.

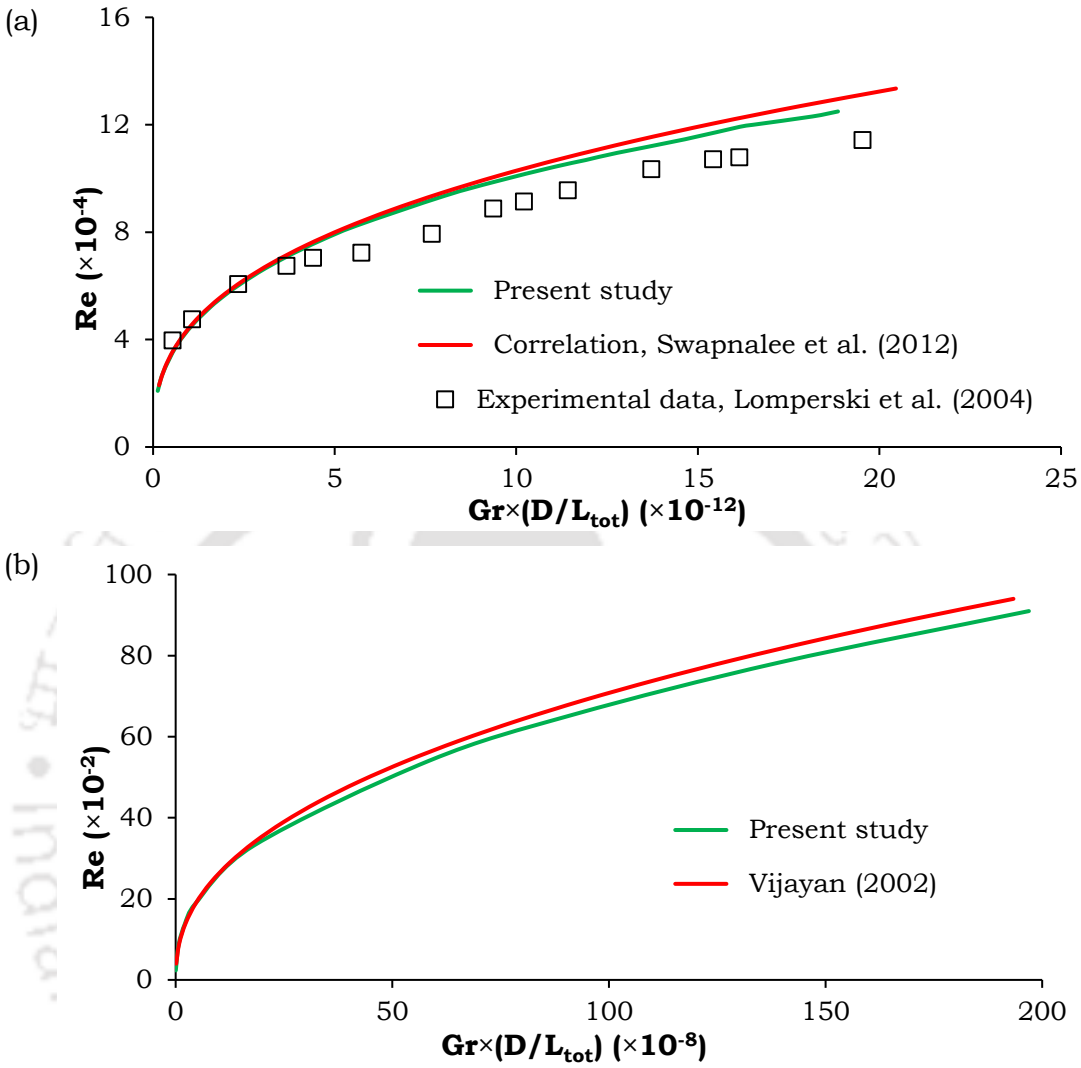

Figure 5-1. Comparison of present model prediction with existing literature for (a) supercritical CO_2 loop and (b) single-phase water loop

Experimental validation is mandatory for any numerical model to judge its correctness and hence present predictions are compared with the experimental correlation proposed by Swapnalee et al., 2012. They studied the influence of heater and cooler orientation by choosing four different combinations and with both water and CO_2 as working medium. Operating pressure and range of input power were 8.6 MPa and 203.7-2391.7 W respectively during experimentation with supercritical CO_2 in HHHC configuration and a comparison is drawn here precisely with that particular dataset. As can be observed from Figure 5-1a, excellent conformity is achieved over the complete range of parameters considered on a non-dimensional

plane. Direct comparison is also drawn with the experimental data of Lomperski et al., 2004 and present model is able to attain better accuracy than the earlier correlation, particularly at higher power levels, while the matching is exact at lower powers. That establishes the capability of the employed computational model. Lack of complete geometrical information about the cooler-side of the experimental facility of Lomperski et al., 2004 thwarts any further attempt to refine the computational model for enhanced validation at elevated power levels. Predictions for the single-phase water loop are also compared with correlation proposed by Vijayan, 2002 and again satisfactory agreement can be observed over the entire range Figure 5-1b.

5.3. Effect of Operating Pressure and Sink Temperature on Steady-State Thermalhydraulic of SCNCL

One of the most important concern with supercritical fluid operation is the involvement of severe temperature and hence the selection of wall material. Maximum value of steady-state wall temperature depends both on heat flux and working fluid, and occasionally on system pressure. Generally the maximum fluid temperature is expected to appear at the outlet of the heater section and hence the variation in cross-sectional averaged temperature at that particular location with heater power is presented in Figure 5-2 for CO_2 at a sink temperature of 305 K and three different pressures. Maximum temperature increases only moderately till a certain power level for all the pressures, with rapid increase in corresponding mass flow rate. However, the mass flow rate drops beyond a maxima and continues with a decreasing profile, while a steep rise in maximum temperature can be observed. Buoyancy is the driving potential in any NCL and that depends on the fluid density difference between the vertical arms. For a specified sink condition, temperature differential across the heater increases with input power, with the lowest temperature being around the sink temperature only. So, for supercritical pressures, with rise in heater power, the fluid is made to pass through the pseudocritical point inside the horizontal arms. Density drops sharply around the pseudocritical point, resulting in a peak of the volumetric expansion coefficient (Figure 1-7). It is very much possible to have the fluid temperature well above pseudocritical in the hot leg of the loop and significantly below that in the other vertical arm. That creates significant density difference across the heater, resulting in rapid growth in the flow rate

and only small temperature rise of the fluid across the heater. However at larger powers, the lowest temperature stays above the pseudocritical point and so the developed buoyancy field is small, resulting in lower mass flow rate. With increase in system pressure, pseudocritical temperature increases,

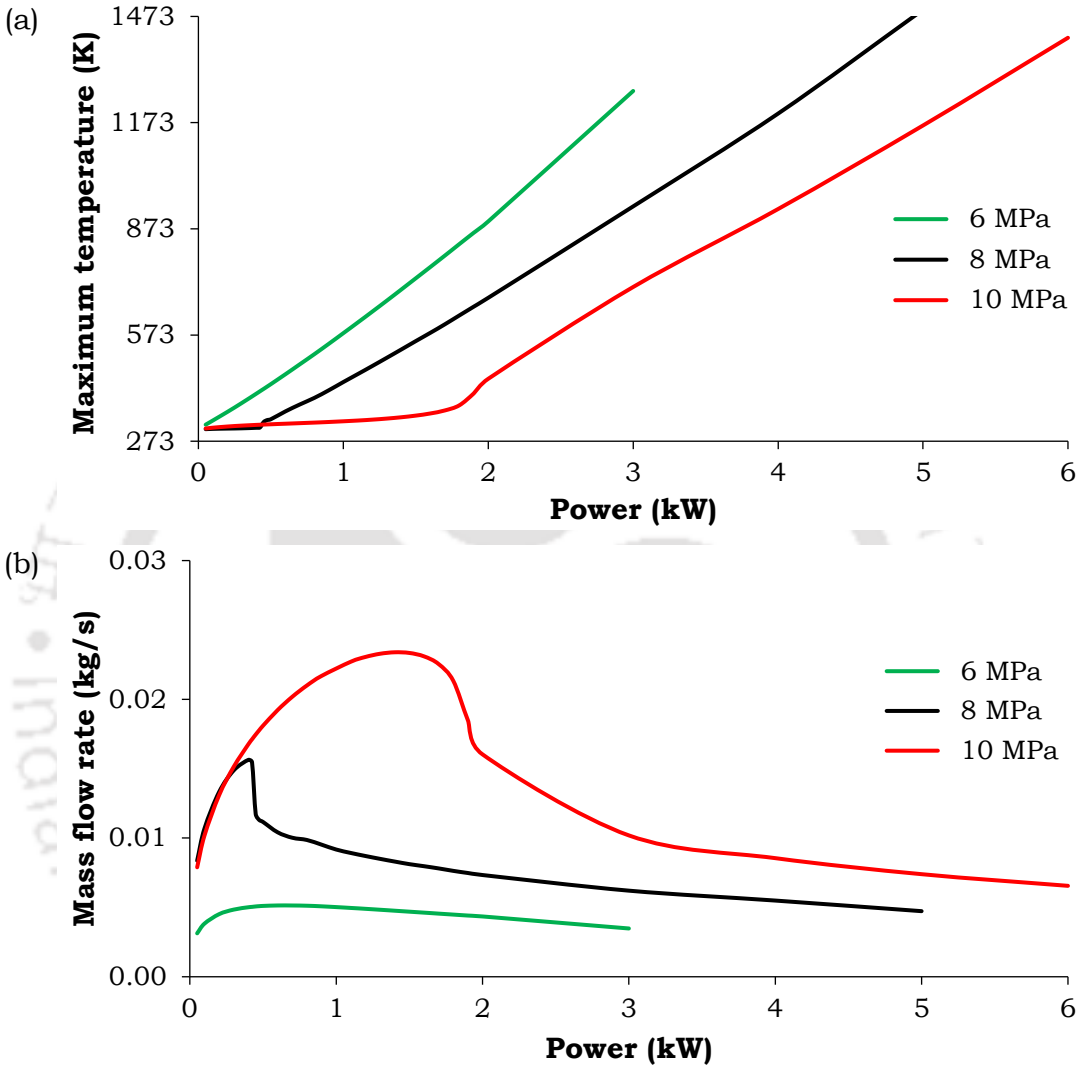

Figure 5-2. Variation in (a) maximum fluid temperature and (b) mass flow rate of CO_2 based loop with power and system pressure for constant sink temperature of 305 K

thereby allowing larger power ranges of operation with increasing mass flow rate. While the maximum flow rate appears only around 0.4 kW of power at 8 MPa pressure, the same corresponds to about 1.4 kW at 10 MPa, allowing much wider span of operation. The above argument, however, does not hold for 6 MPa pressure, which is subcritical, with a saturation temperature of about 295.13 K. Sink temperature being higher than this limit, the loop behaves like a single-phase one, with superheated vapor as the working

medium. That explains the reason of having low mass flow rate with monotonic variation and larger wall temperature for any given power level.

In fact, a small increase in loop flow rate can be observed at 6 MPa for initial increase in the power level, while the same monotonically decreases thereafter. The reason for the same can be elucidated following the variation of superheated CO_2 vapor properties (Figure 5-3). As density decreases nearly linearly with rise in fluid temperature, driving buoyancy is continually weakened. However, an initial drop in viscosity can be observed, before the eventual rise following a minima around 311 K at 6 MPa. Hence the resisting friction also decreases at the lower power level, instigating the rise in loop flow rate over a short span of power. Beyond that range, however, mass flow rate reduces both due to the reduction in buoyancy and rise in friction.

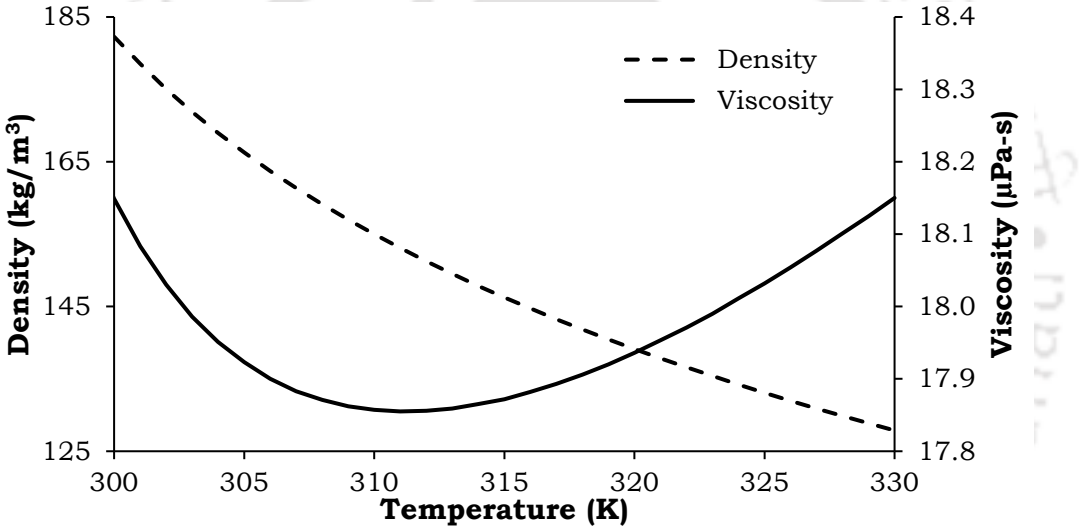

Figure 5-3. Effect of temperature on density and viscosity of superheated CO_2 vapour at 67 MPa (NIST,2011)

The appearance of maxima in mass flow rate is more pronounced at lower sink temperatures (Figure 5-4). A cooler sink allows the lower temperature with CO_2 to stay below the pseudocritical value till much larger power levels. Accordingly the mass flow rate continues to rise over a larger range of input power, the maximum temperature being limited to moderate values. Highest mass flow rate appears for a power value as high as 3 kW with sink temperature of 285 K at 8 MPa system pressure, which is nearly twice of that for 295 K sink temperature. However, as the power supply increases beyond that maxima, a drastic reduction in flow rate can be observed, due to the sharp deterioration in driving buoyancy. Accordingly the maximum fluid temperature inside the loop experiences a jump, which can amount from 150

K to 500 K, based on operating conditions. That is of serious concern from loop safety point of view, as the elevated temperature level can be detrimental for the wall material and hence may lead to tube rupture and overall system failure. Therefore it is essential to limit the operation of the CO_2-based loop below the power level corresponding to the maxima of mass flow rate.

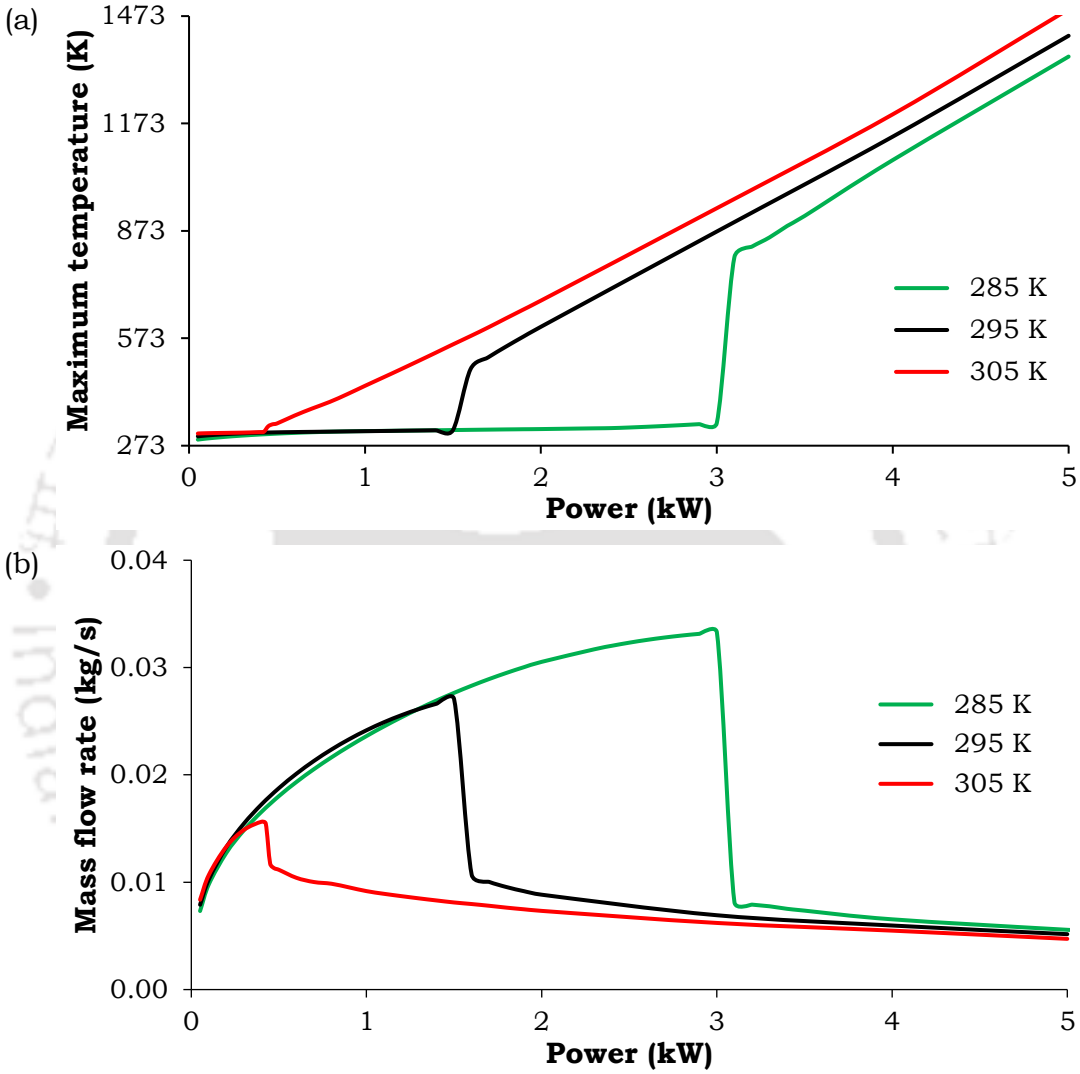

Figure 5-4. Variation in (a) maximum fluid temperature and (b) mass flow rate of CO_2 based loop with power and sink temperature for constant system pressure of 8 MPa

Effect of such drastic change in mass flow rate on the thermal field can be recognized by comparing the temperature contours at the source centre for two different situations (Figure 5-5). With only 10 W rise in the input power, CO_2 experiences about 346 K temperature variation in a single cross-section, compared to just about 10 K in the other case. Axial profile in bulk temperature over the entire loop length for sCO_2 and water for two different

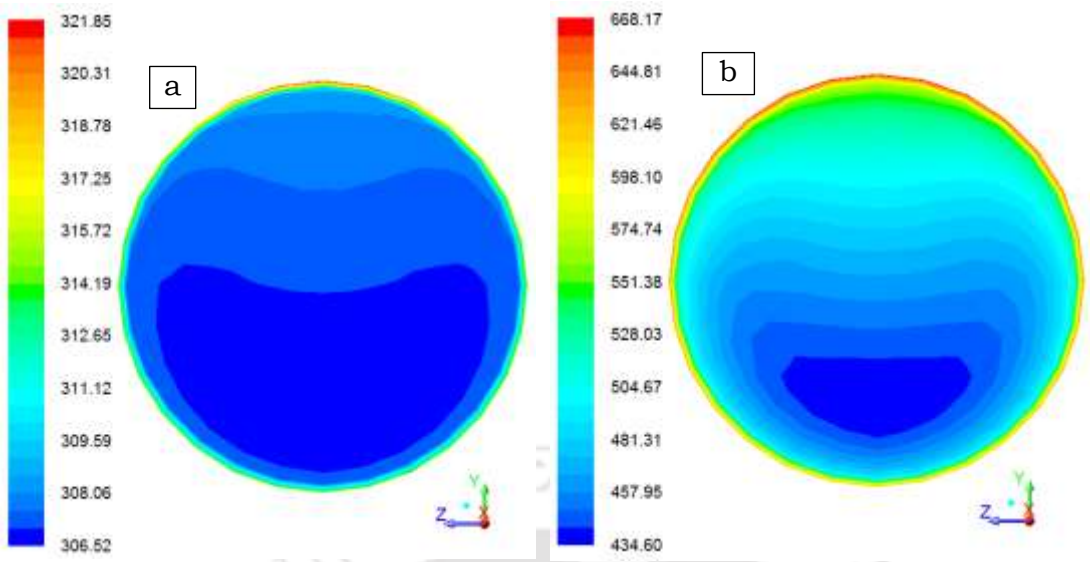

Figure 5-5. Source-center temperature contours of sCO_2-based loop for 8 MPa pressure and 285 K sink temperature and different input powers (a) 3.09 kW and (b) 3.10 kW

conditions are compared in Figure 5-6. In case of 3.09 kW input power, large mass flow rate results in moderate temperature variation for sCO_2 over the loop and about 87 K lower value of maximum fluid temperature compared to water. However, with only 10 W increase in power, heater inlet temperature can clearly be seen to be above the pseudocritical value, resulting in substantial temperature variation across the loop. The maximum value of bulk temperature for sCO_2 can be about 249 K higher than the same for water under identical operating conditions.

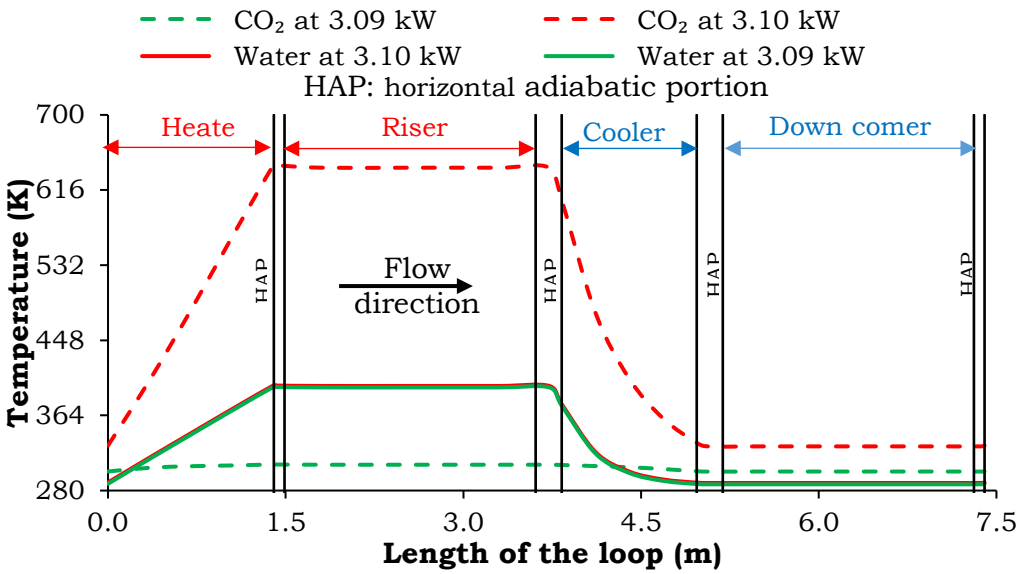

Figure 5-6. Axial profile of fluid bulk temperature for 8 MPa pressure and 285 K sink temperature and different input powers.

The situation is contrasting with R134a as working medium. Despite the pressure being above critical, lowest fluid temperature generally remains well below the pseudocritical limit (~ 441.5 K at 8 MPa) throughout the loop, giving a liquid-like representation of the working medium and hence a regular variation in density. With increase in power supply, the average density difference between the riser and downcomer section increases, encouraging a continuous rise in mass flow rate (Figure 5-7). The maximum fluid temperature also increases simultaneously, albeit at a much slower rate compared to CO_2. Only after attaining a significantly higher power level, the lowest temperature crosses the pseudocritical limit, forcing a reduction in driving buoyancy. Consequently the mass flow rate starts decreasing

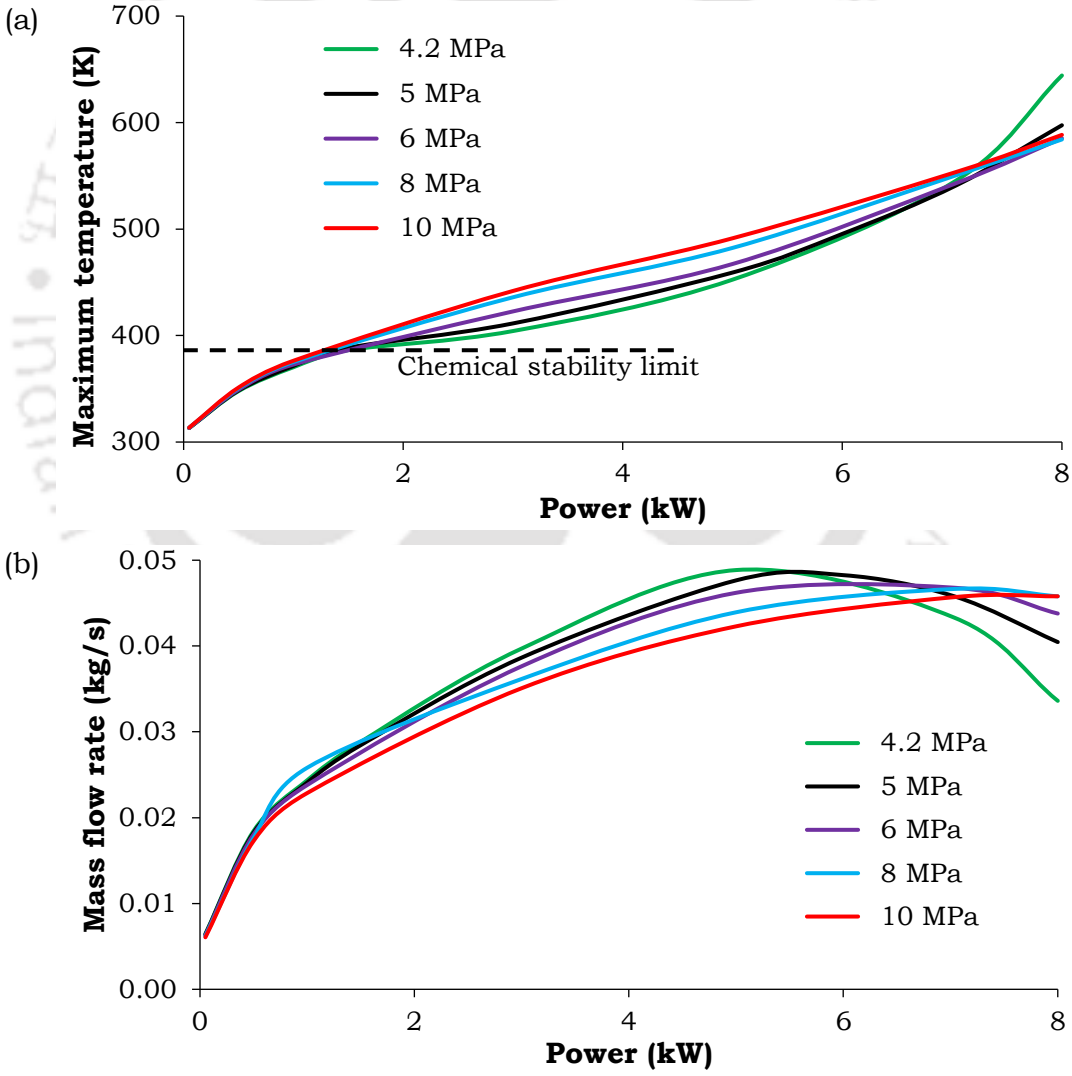

Figure 5-7. Variation in (a) maximum fluid temperature and (b) mass flow rate of R134a based loop with power and system pressure for constant sink temperature of 305 K

gradually and maximum fluid temperature rises at a faster rate. That phenomenon is more apparent for system pressure values closer to the critical limit, due to the lower pseudocritical temperature at lower pressure levels. For pressure levels higher than 6 MPa, both flow rate and fluid temperature profile exhibit monotonic variation over the complete range of power under consideration. The effect is also less pronounced with lower sink temperatures (Figure 5-8), as R134a requires larger power input to cross the pseudocritical limit, and hence allows wider span of operation. In fact, the effect of sink temperature is prominent only beyond the maxima in mass flow rate for any system pressure. One important factor that requires special mention here is the unstable chemical nature of R134a beyond 115 °C (Zhao and Jiang, 2011). So, despite the maximum fluid temperature being well below the same predicted with CO_2 as working fluid at higher powers, the operation of R134a loop is practically limited only to low powers, as is indicated in Figure 5-7a. The CO_2 loop, however, can exhibit substantially higher values of maximum temperature even for such powers, particularly with lower system pressures and higher sink temperatures, and hence R134a is a better option within such power range from material safety point of view.

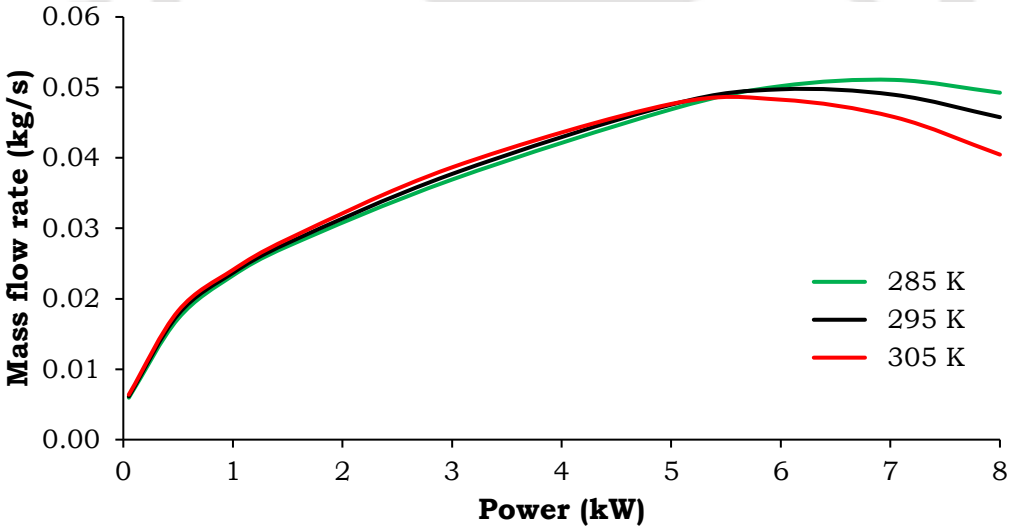

Figure 5-8. Variation in mass flow rate of R134a based loop with power and sink temperature for constant system pressure of 5 MPa

Variation of mass flow rate and maximum fluid temperature with heater power for a water loop is presented in Figure 5-9 for different pressures and sink temperatures. Due to the near-incompressible nature of liquid water, pressure has hardly any effect on loop thermalhydraulics. With rise in power supply, temperature differential across the heater and hence the driving

buoyancy force increases, causing a monotonic growth in mass flow rate and only moderate rise in maximum fluid temperature. Higher water temperature reduces both density and viscosity in the riser section. That enhances buoyancy and reduces friction, with both factors aiding the increase in flow rate. A lower sink temperature results in larger viscosity in the downcomer

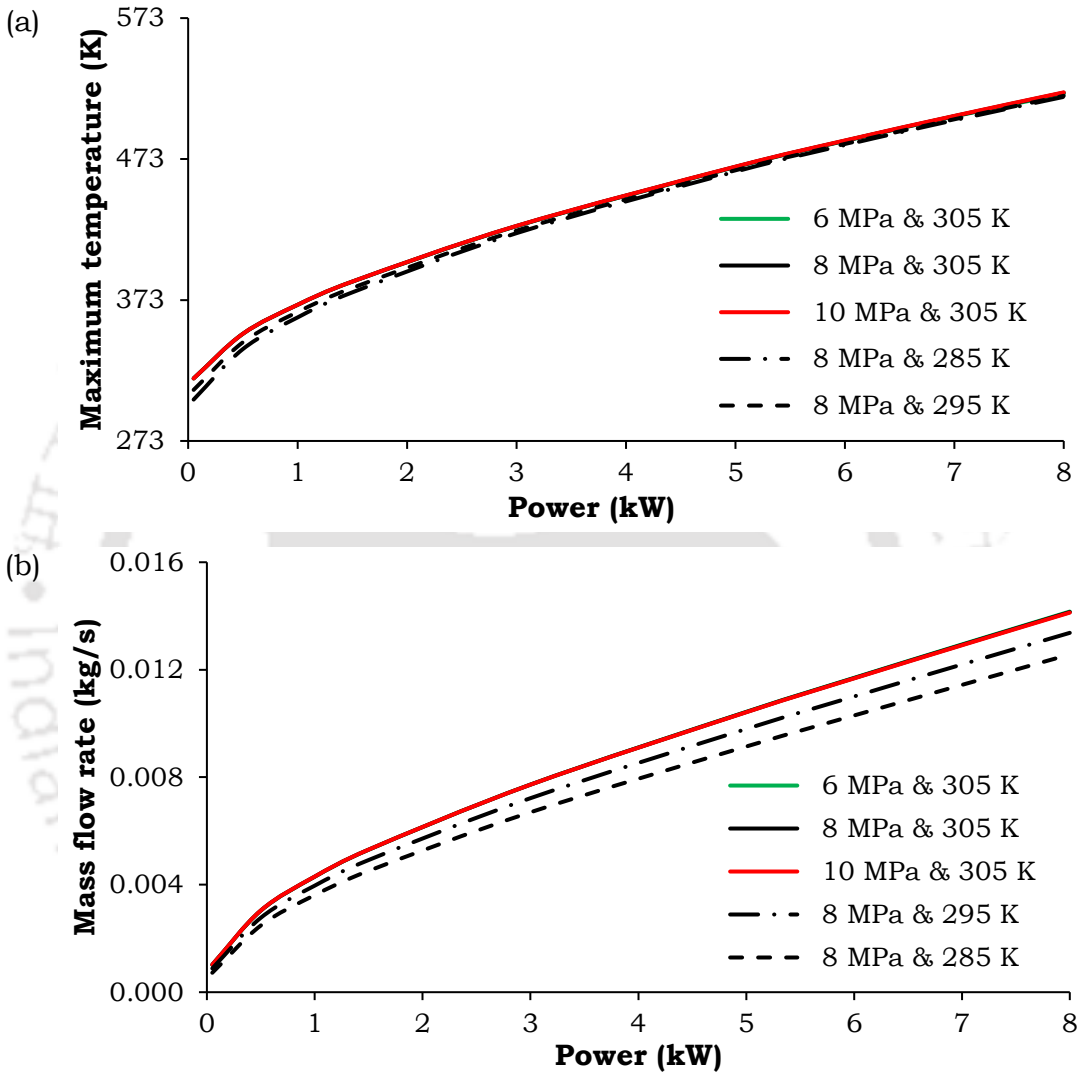

Figure 5-9. Variation in (a) maximum fluid temperature and (b) mass flow rate of water based loop with power, system pressure and sink temperature

section and so larger frictional losses, which is manifested by the corresponding drop in flow rate. For identical system conditions, the mass flow rate for the water loop is significantly lower compared to R134a and CO_2-based loops. The maximum temperature is also lower, in general, compared to R134a loop. It can, however, be greater than the same for a CO_2 loop based on operating conditions. As pressure has little effect on water-based loop, so similar behaviour can be obtained at lower pressures as well. Still it is required

to operate at a higher system pressure to maintain a safe distance away from saturation temperature of water and thus eliminate the possibility of boiling.

5.4. Appearance of Flow Induced Heat Transfer Deterioration (FiHTD)

Heat transfer coefficient for any fluid generally depends on local Reynolds number (Re) and Prandtl number (Pr), along with thermophysical properties. Cp exhibits a narrow peak around the pseudocritical point (Figure 1-7) and continually decreases with a moderate gradient on further heating. As the average fluid temperature across the sink remains nearly invariant to heater power till the maxima of mass flow rate and keeps on increasing thereafter, area-averaged Pr is also expected to fall monotonically. Rapid variation in loop mass flow rate allows significant changes in average Re, making it the dominating factor in deciding the average heat transfer coefficient under any condition and that is manifested by its in-phase variation with mass flow rate for supercritical CO_2 (Figure 5-10a). It is interesting to note that, despite lower value of maximum mass flow rate, peak heat transfer coefficient is much higher at 8 MPa system pressure compared to the same at 10 MPa. That can be attributed to the steeper property variation at pressure levels close to critical.

The variations at lower sink temperatures, however, are even more drastic (Figure 5-10b). Heat transfer coefficient steadily increases with heater power till the maxima is attained and then exhibits a sharp decline, which is even steeper at lower T_c. Power level corresponding to such fall in heat transfer matches well with the decrease in loop flow rate and increase in peak fluid temperature. Hence that particular power level can be identified as the initiation of heat transfer deterioration in SCNCL (HTD), which till date has mostly been acknowledged for forced-flow-based supercritical channels (Kao et al., 2010; Liu et al., 2013a, 2013b). It also corresponds to a rise in maximum fluid temperature and so is directly related to the material-related safety concerns. Therefore the HTD location is an important landmark during any SCNCL operation and heater power should be regulated to maintain below this limit, in order to have higher mass flow rate and heat transfer coefficient, while maintaining lower fluid temperature level. It is important to mention here that the term HTD is commonly employed for forced flow channels with wall heating to signify drastic reduction in heat transfer coefficient and

simultaneous increase in wall temperature, without any significant change in fluid temperature, while the flow rate remains constant. The situation is a bit different for SCNCL, as the fluid temperature may exhibit sharp rise due to the reduction in flow rate. The natural circulation version of HTD is, in fact, deterioration in heat transfer coefficient as a consequence of a deterioration

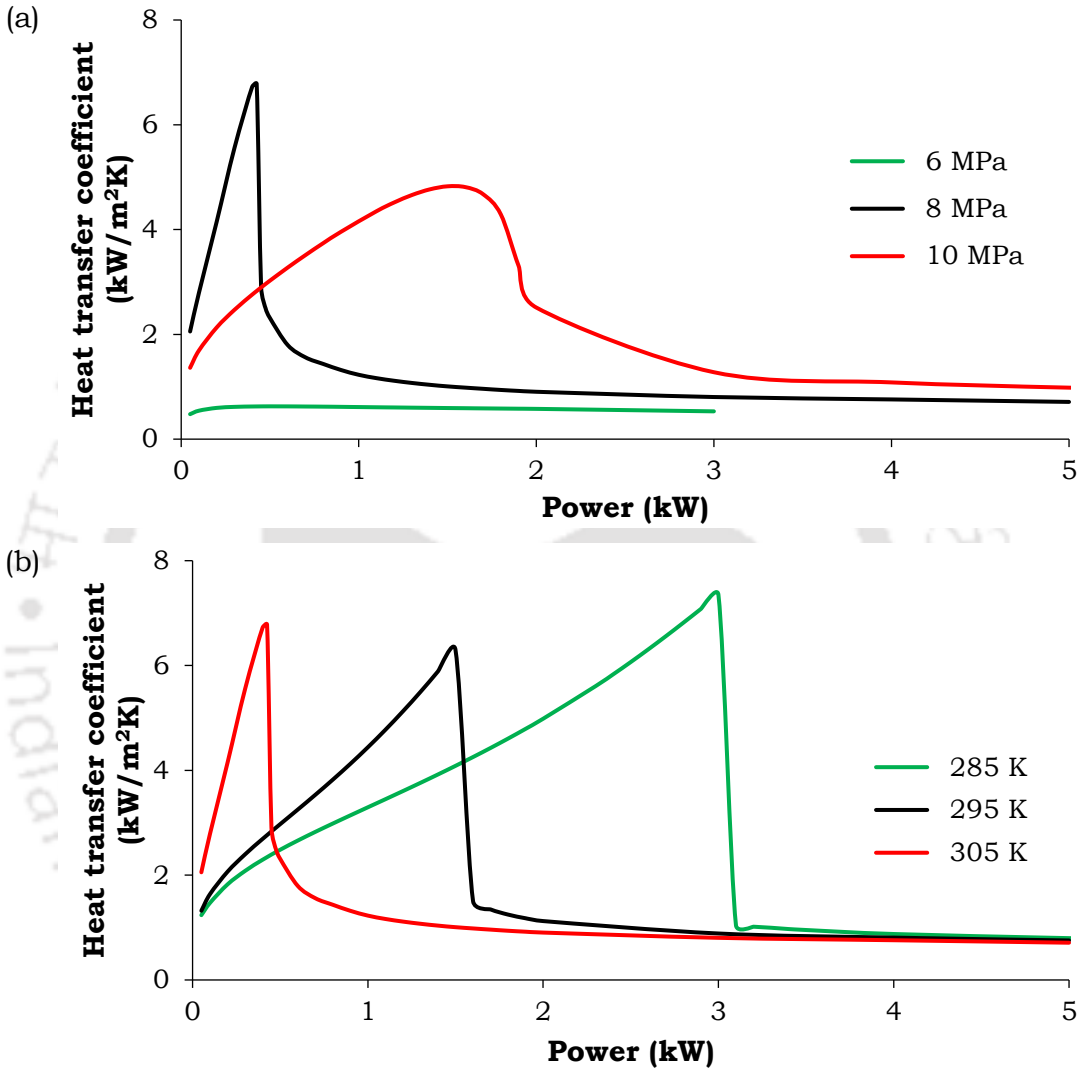

Figure 5-10. Variation in average heat transfer coefficient of CO_2 based loop with power for (a) constant sink temperature of 305 K and (b) constant system pressure of 8 MPa

in mass flow rate and therefore can also be termed as flow-induced heat transfer deterioration (FiHTD) to differentiate it from forced flow systems. The foregoing discussion can further be reinforced by following the axial variation in sink-side heat transfer coefficient for two specific conditions on either side of the maxima in mass flow rate. The profiles for 2.5 kW and 3.5 kW corresponding to 8 MPa pressure and 285 K sink temperature are presented in Figure 5-11. Maximum fluid temperature for the first case is about 323.7

K, only marginally higher than pseudocritical temperature (~ 307.8 K at 8 MPa), while the same is about 914.9 K for the later situation. Accordingly the local heat transfer coefficient close to the inlet plane of the sink is approximately thirteen times higher for 2.5 kW power input than the other case. The same varies substantially along the length, due to the reduction in fluid temperature. But the heat transfer coefficient at the exit plane remains nearly four times higher, signifying considerably larger heat transport capability. For 3.5 kW power supply, local heat transfer coefficient consistently exhibits a very low value throughout the sink, resulting in markedly higher fluid temperature level. Hence the maxima in mass flow rate for CO_2-based SCNCL under any particular set of operating conditions can categorically be earmarked to correspond to the initiation of FiHTD in the loop. It can also be concluded that SCNCLs are more susceptible to such undesirable consequences with higher sink temperature and for supercritical pressures close to the critical limit.

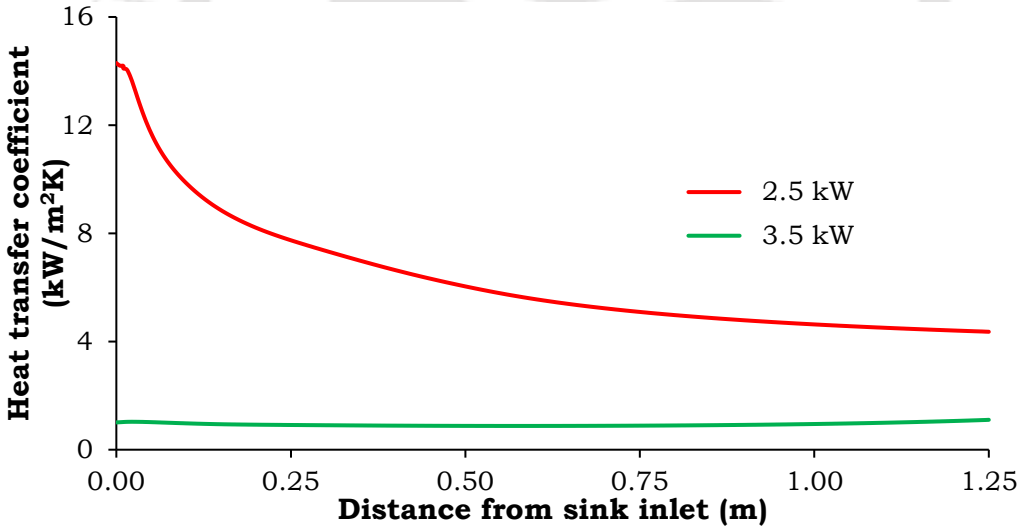

Figure 5-11. Axial variation in area-averaged heat transfer coefficient along the sink of CO_2 based loop for 8MPa system pressure and 285 K sink temperature

The variations in heat transfer coefficient for water and for R134a at lower power levels are more regular due to the single-phase nature of the working fluids, as has been discussed earlier. R134a loop attains the maxima in mass flow rate only at higher powers and for system pressures close to the critical point, forcing a subsequent reduction in heat transfer coefficient (Figure 5-12a). Possible appearance of FiHTD at 5 MPa system pressure is suggested for input powers greater than 7 kW. However fluid temperature

under such levels of power are not practicable for R134a. Even such tendency towards FiHTD can completely be eliminated by lowering the sink temperature. Pressure dependence of properties being relatively negligible, water loop exhibits monotonic rise in heat transfer coefficient over the entire power range at each of the considered pressure levels (Figure 5-12b). Low mass flow rate and hence the low *Re* induces lesser heat transfer coefficient with reduction in sink temperature.

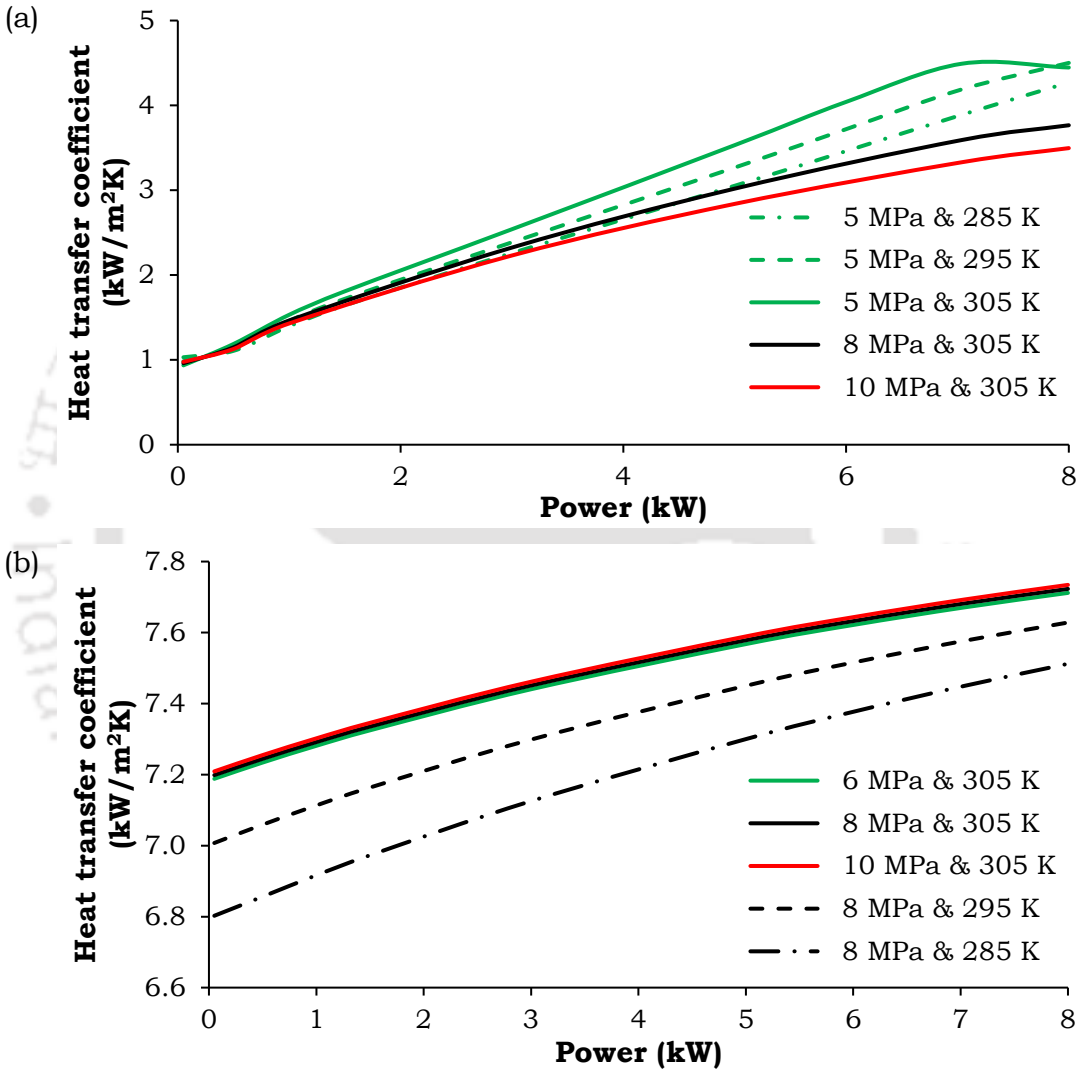

Figure 5-12. Variation in average heat transfer coefficient of (a) R134a and (b) water based loop with power, system pressure and sink temperature

In order to facilitate a direct comparison between the performances of the three working fluids, maximum fluid temperatures and heat transfer coefficients are compared for two different sets of operating conditions in Figure 5-13. Single-phase water consistently exhibits the highest heat transfer coefficient over the entire range of input power considered. Temperature level

for R134a is quite similar to water, despite significantly lower heat transfer coefficient. Parameters for CO_2, however, are strongly influenced by the

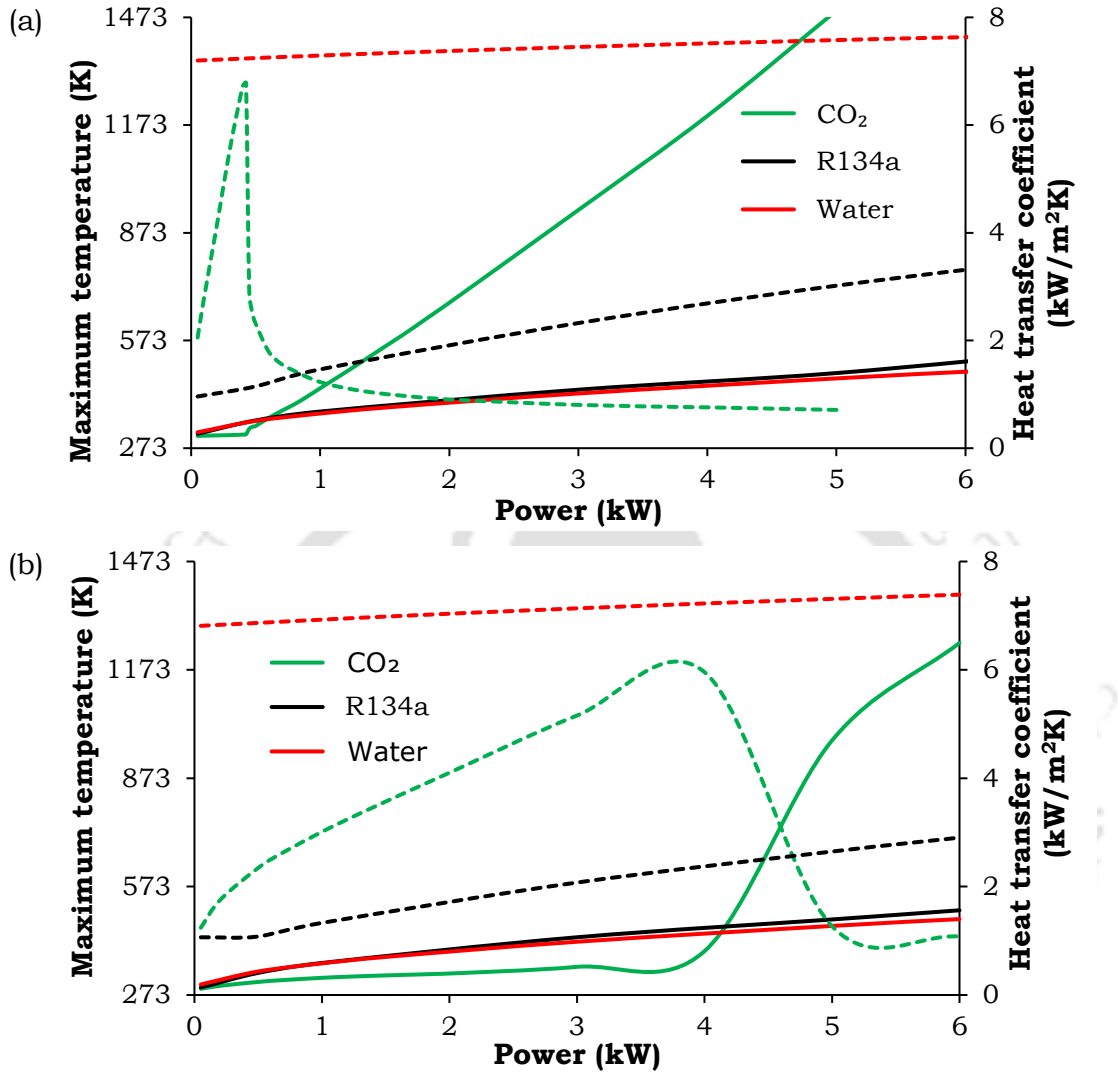

Figure 5-13. Variation in maximum fluid temperature (continuous line) and heat transfer coefficient (dashed line) with power for identical operating conditions. (a) 8 MPa and 305 K, (b) 10 MPa and 285 K

operating conditions and generally governed by the power level corresponding to the appearance of FiHTD. Rapid increase in heat transfer coefficient for CO_2-based loop prior to the FiHTD location guarantees the T_{max} value to be the lowest among the three fluids with identical power supply. Beyond FiHTD, however, T_{max} sharply rises with CO_2 as the working fluid and water provides the smallest value of T_{max}. It is important to note that the largest value of average heat transfer coefficient achievable with SCNCL is still smaller than water-based loop. Despite the lower heat transfer coefficient, CO_2 and R134a-based systems are able to maintain maximum fluid temperature comparable with that of water due to much higher mass flow rates (Figure 5-14). Flow rate

with both the alternated fluids show similar variation with input power, till the appearance of FiHTD in SCNCL, and can be as much as eight times to

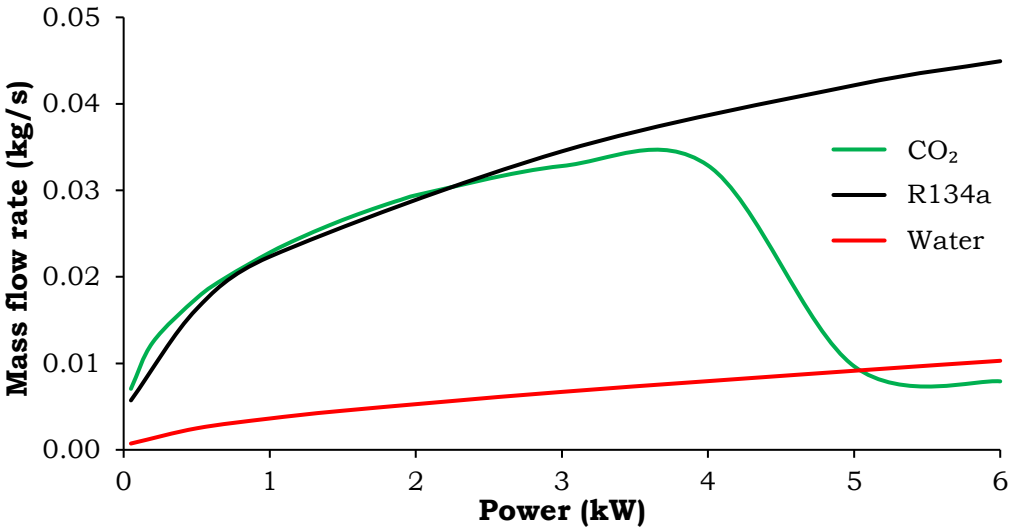

Figure 5-14. Variation in mass flow rate with power for identical operating conditions of 10 MPa system pressure and 285 K sink temperature

that of water. Therefore, from material safety point of view, supercritical CO_2 can be identified as the preferred option for working fluid till the FiHTD location and water beyond that. With increase in system pressure and reduction in sink temperature, initiation of FiHTD is delayed, thereby substantially enhancing the allowable power level for CO_2-based SCNCL operation.

Along with the thermal aspects, another important consideration during operation of NCLs is the mass inventory, as that provides a measure of the requisite quantity of fluid and associated storage issues. Corresponding

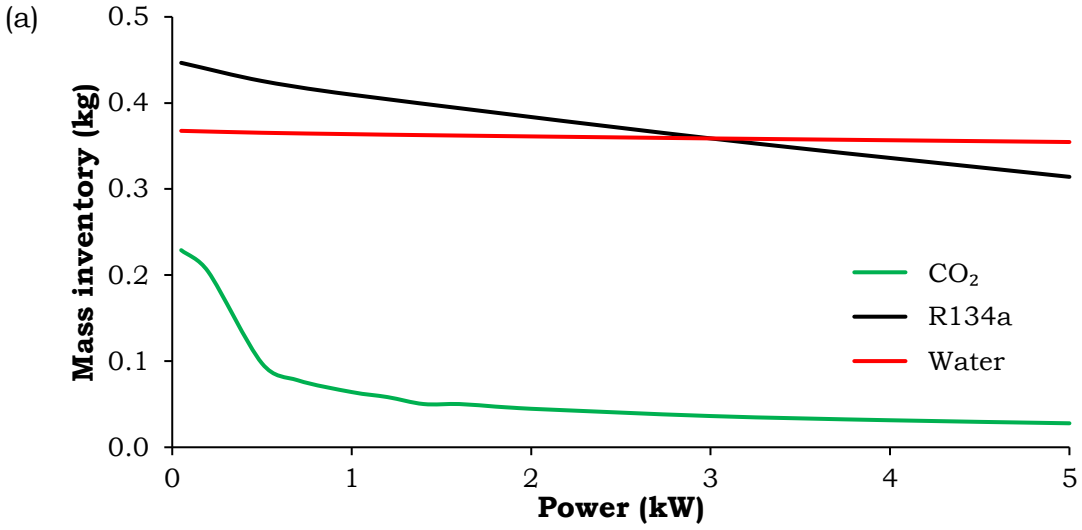

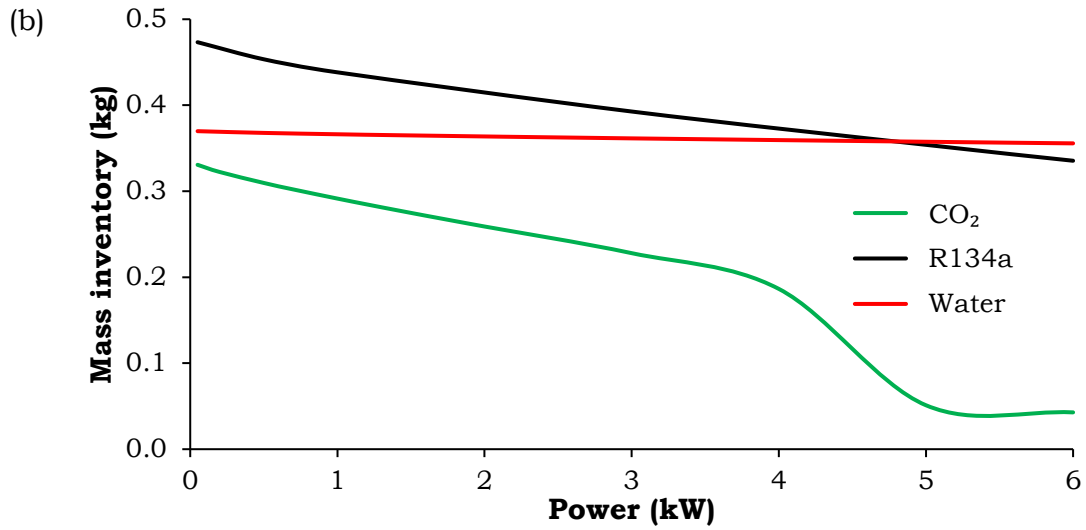

Figure 5-15. Variation in mass inventory with power for identical operating conditions. (a) 8 MPa and 305 K, (b) 10 MPa and 285 K

variations with heater power for all the three fluids are presented in Figure 5-15 for two different sets of operating condition. CO_2 consistently requires lesser inventory and even more so at higher powers. It is interesting to notice that the inventory requirement for R134a is lesser than water at larger powers. Considering similar nature of T_{max} variation, R134a can therefore be a more prospective fluid at larger powers.

5.5. FiHTD for Different Working Fluids

Till this juncture, the focus has been on comparing the performance of three working fluids under identical set of operating conditions, in an effort to identify the one with superior thermalhydraulic performance. The supercritical fluid, in general, exhibits excellent performance when it is allowed to cross the pseudocritical temperature within the heat-exchanging sections. The prime attraction of using supercritical fluids for heat transport is their radical property variation around the pseudocritical point, as that corresponds to a low inventory requirement, owing to a peak in volumetric expansion coefficient and high specific heat, and high heat transfer coefficient. Small change in the operating conditions though may force the system towards FiHTD, as discussed. Different fluids, however, have different critical point parameters, making a fluid-to-fluid comparison extremely difficult, at least in the dimensional form. An effort, therefore, is taken in this section to facilitate the comparison of the behavior of different working fluids under supercritical condition.

The first step thereof is to recognize the identical operating conditions across different fluids. The entire phenomenon of natural circulation being governed by the variation in thermophysical properties, it is absolutely mandatory to ensure similar nature of temperature-dependence of the concerned properties. Following definitions of dimensionless density and enthalpy are considered here.

$$\rho^* = \frac{\rho}{\rho_{PC}} \qquad \text{and} \qquad h^* = \left(\frac{h - h_{PC}}{h_{PC} - h_{cr}}\right) \qquad (5\text{-}1)$$

Six different fluids are selected for the comparison, namely, CO_2, H_2O, R134a, C_3H_8, N_2 and NH_3. Variations in their dimensionless density with dimensionless enthalpy at certain pressure levels are shown in Figure 5-16. It is very much evident that over a substantial range of temperature around the pseudocritical point, each of the selected fluids can exhibit identical property variation, subjected to an appropriate choice of pressure for every individual fluid. For example, CO_2 at 8.6 MPa can successfully simulate water at 23.5 MPa, and hence it is logical to expect a lab-scale loop working with CO_2 at 8.6 MPa to closely replicate an industrial loop based on water at 23.5 MPa, subjected to other constraints.

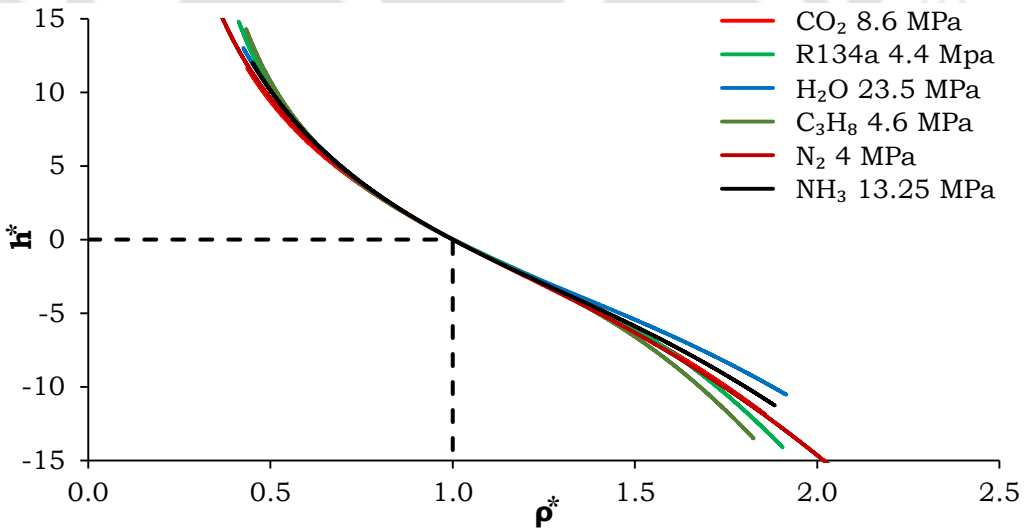

Figure 5-16. Variation of non-dimensional properties.

Every fluids have different critical point, thus a specific supercritical condition for one fluid is perform differently for other fluids. For a particular condition, the degree of supercritical is changed with alteration of working fluid. Thus it is better to compare the results of different loops which are functioned with scaled operating conditions. Therefore, a fluid-to-fluid scaling

analysis have been performed here with several fluids, CO_2, H_2O, R134a, C_3H_8, N_2 and NH_3. A detailed scale down analysis has been performed in Chapter 3. To non-dimensionalizing the governing equations, several non-dimensional parameters are used (Section 3.3.2.). The experimental data is available for sCO_2 based loop operating at 8.6 MPa pressure. Thus, with consideration of 8.6 MPa sCO_2 as base condition, a non-dimensional property variation study have been performed to find out the scaled pressures for other fluids. To facilitate the same, non-dimensional density and enthalpy are used as scaling properties. Figure 5-16 shows the property characteristic curves for different fluids. It has been recognized that the non-dimensional variation of enthalpy and density plots for selected fluids are almost identical with CO_2 at 8.6 MPa pressure. Which confirms that, at the said pressure levels, the fluids have comparable behavior. Once, getting the scaled pressure, pseudocritical temperature can be find out from variation of specific heat with temperature plot for the corresponding pressure. Here, the process of non-dimensionalizing the temperature is similar to non-dimensional enthalpy (Section 3.3.2.). Finally compared non-dimensional temperatures with CO_2 to get the scaled temperature.

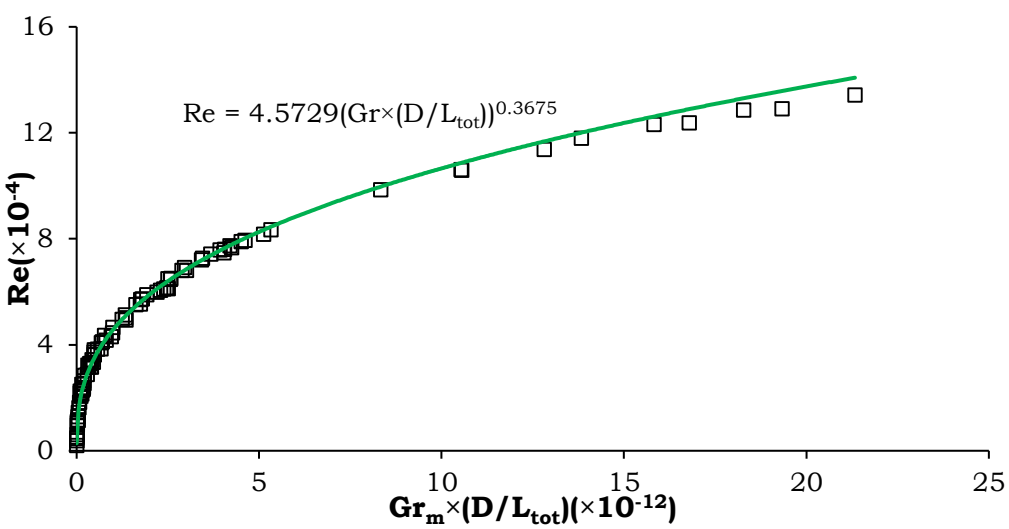

Figure 5-17. Supercritical correlation for SCNCL.

The main goal of this specific study is to discover the correlations and non-dimensional number, which can signify the SCNCL. In the open literature many correlations are available, which are mainly for a single fluids, operating in various conditions. Sometimes, geometric parameters are also varied for a single fluid loop. Still, there is no such correlation exist which is usable for different working fluids of SCNCL. Hence, in the present section of the current

study a correlation has been developed with consideration of several supercritical fluids with scaled operating condition, the same is shown in Figure 5-17. The generated results for different fluids are followed an identical pattern and configured correlation can be used for various fluids, which are working at supercritical condition.

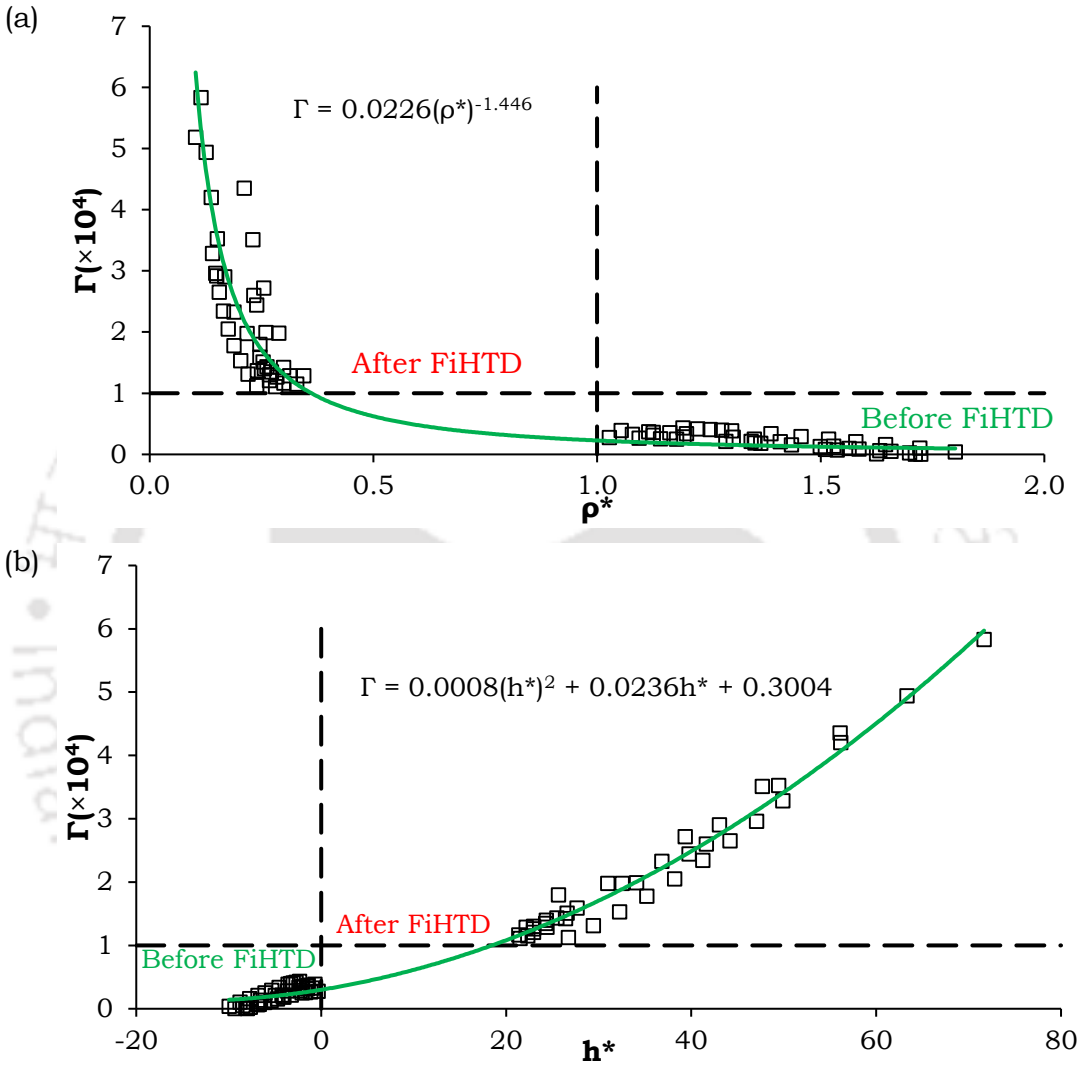

Figure 5-18. Variation of non-dimensional Input Power (Γ) with non-dimentional (a) density and (b) enthalpy

There are numerous non-dimensional groups are identified in scale down analysis of SCNCL in Chapter 3 (Table 3-1). Among them, group three is coined as Non-dimensional Input Power (Γ) and corresponding data are explored in Figure 5-18. A strong and undoubted observation is found from the results, for any fluid FiHTD is occurred when the value of Γ is more than 10^{-4}. For a healthy operation of SCNCL, the value of non-dimensional density and enthalpy are should be higher than “1” and less than “0” respectively. By

crossing the said values, the most unwanted event FiHTD is initiated in the system. The correlations of Su with non-dimensional density and enthalpy are also configured and shown in Figure 5-18.

5.6. Epilogue

According to design of the system the mode of heating can be alter, and hence both the options are equally important. Previous chapter was dealt with Dirichlet type of heating, whereas, in the current chapter Neuman mode of heating applied thoroughly to ascertain the thermalhydraulic viability of employing supercritical condition of working fluid for any particular combination of operating parameters. Water, CO_2 and R134a are selected as the working fluids. Water remains as single-phase liquid over the complete range of chosen working parameters, whereas the others vary from sub- to supercritical states. Predicted results are found to be in consensus with data from literature. Maximum fluid temperature, loop flow rate and average values of sink-side heat transfer coefficients are compared, as thermal safety of the wall material is of prime concern. Mass flow rate for SCNCL increases with input power, till the lowest fluid temperature inside the loop remains lower than the pseudocritical temperature corresponding to the system pressure. Rapid rise in flow rate can be observed when the fluid crosses the pseudocritical point during its passage through the heater section, owing to the substantial density difference between the two vertical arms. Beyond a maxima, mass flow rate in SCNCL drops drastically, with corresponding jump in the maximum fluid temperature. The effect is more pronounced with higher sink temperatures and for system pressures close to the critical point. For pressure levels considerably away from the critical point, monotonic rise in flow rate can be observed, quite similar to the single-phase NCLs. Power level corresponding to the appearance of FiHTD can be increased by raising pressure and lowering sink temperature, if possible, thereby expanding the zone of SCNCL operation with increasing heat transfer coefficient. A mechanism can also be devised to manoeuvre the sink temperature with heater power for delaying the appearance of such deterioration. Single-phase water-based loop presents monotonic profile of mass flow rate, magnitude of which is well-below the same of SCNCL till the appearance of FiHTD, leading to elevated temperature level. Heat transfer coefficient for single-phase water-based NCL is consistently higher than SCNCL, owing to higher thermal

conductivity of the working fluid. Under identical operating conditions, fluid temperature level for the CO_2-based loop is the lowest among the three fluids till the appearance of FiHTD and hence supercritical condition can be adopted. Beyond the power level corresponding to FiHTD, however, single-phase NCL is a safer option. Mass inventory requirement is the lowest for CO_2-based loop. At higher powers, inventory requirement for R134a is lesser than water, with similar order of maximum temperature and hence R134a can be a prospective fluid under such situations, provided the chemical stability limit is adhered with. Several correlations for SCNCL are developed from fluid-to-fluid scaling study. A generalized non-dimensional number 'Γ' (Non-dimensional Input Power) is coined for SCNCL, which directly signify the working zone of SCNCL. At any condition for several fluids, FiHTD is occurred at Γ is higher than 10^{-4}. The condition for a healthy operation of SCNCL is SCNCL is $\rho^* > 1$ and $h^* < 0$ respectively.

Overall it can be summarized that the sCO_2-based SCNCL can be a superior choice, as long as the power level can be limited to the FiHTD, owing to the higher flow rate and lower fluid temperature levels. However, if the expected power range of operation goes beyond the FiHTD constraint, single-phase water-based loops are clearly better option, due to the consistent behavior. High pressure requirement can be another deterring issue for SCNCLs. Also the stability analysis and dynamic performance assessment needs to be carried out for SCNCL before drawing a final conclusion and that can be viewed as the next step of research.

Chapter 6: Guidelines for Selection of Geometric Parameters in SCNCL from FiHTD Point of View

6.1. Preamble

An elaborate discussion on the deterioration of mass flow rate in SCNCL, accompanied by rapid decline in the heat transfer coefficient, has been presented in the previous chapter. It is generally recognized as the consequence of fluid temperature crossing the pseudocritical limit throughout the loop and sets a practicable limit for operation of SCNCL. Present chapters aims at reconnoitering the dependence of such flow-induced deterioration on the associated geometric parameters, with an aim of identifying the guidelines for a safer design. Accordingly a computational model of a rectangular loop, with source and sink in opposite horizontal arms, is developed and employed to explore the influence of geometric variables, including diameter, height, width, inclination, corner bends, and heating and cooling lengths and their orientations. Additionally, a numerical fluid-to-fluid scaling analysis has been performed to discover the correlations and non-dimensional number to signify the performance of SCNCL.

The non-toxic and non-explosive nature of sCO_2, coupled with its favorable transport properties, has propelled it in the forefront of supercritical research over last couple of decades and SCNCL is no exception. Parameters like input power, height and heated length of the loop were found to affect the loop thermalhydraulics significantly. Subsequently several researchers have explored the role of geometric variables on both steady-state thermalhydraulics and stability characteristics. Chen et al., 2013a numerically studied a 2D SCNCL to inspect the influence of inner diameter, aspect ratio, inclination and orientation of heater and cooler. Loop operating temperature was found to greatly affect the heat transfer efficiency of the system, with higher efficiency corresponding to the larger diameter loop. A thorough investigation for various loop diameters was made by Chen and Zhang, 2011, as they reported the stabilized flow to correspond to larger

diameter loops. Flow in any NCL is initiated by buoyancy, which decreases with increased inclination to vertical plane, leading to reduced flow velocity and inferior heat transfer performance of the loop (Cao and Zhang, 2012; Chen et al., 2013d). At lower heat fluxes, inclination greatly affects the flow field and average value of Nusselt number, while the effects are not so significant for larger heat fluxes. The system was found to be more unstable, with occasional flow reversals, for lower heat fluxes. Orientation of the loop, in terms of the relative positioning of the heater and cooler in particular, has also been reported to have substantial influence (Chen et al., 2014; Swapnalee et al., 2012). Due to higher effective vertical distance between the heater and cooler, maximum mass flow rate is found to correspond to the geometry with horizontal heater and cooler, whereas it is minimum with both being vertical (Sharma et al., 2012). Therefore it is clearly evident that the geometric parameters can have important role in determining the thermalhydraulic nature of SCNCL. Besides, the appearance of FiHTD distinctly affects the fluid transport and associated raise in fluid temperature is better to be avoided due to material safety concerns. That necessitates a comprehensive study to understand the role of geometric variables on the thermalhydraulic characteristics of SCNCL in general and FiHTD in particular.

6.2. Computational Model Development

Focus of the present study being on recognizing the role of associated geometric parameters, several 3D computational models with various sets of dimensions are developed. The base geometry, along with corresponding nodalization information, has already been discussed earlier (Figure 3-2) and the same is reproduced in Figure 6-1 for immediate reference (regeneration of Figure 3-2). Here, both the source and sink are placed at the middle of the concerned horizontal arms. The source is subjected to constant heat flux, distributed uniformly over the entire length of the heater. A constant temperature boundary condition is imposed on the sink, which can be visualized to be housed in an isothermal bath. Remaining areas of the loop are ideally insulated, restricting any thermal interaction with the ambient. Other geometries embraced for computation are generally designed through methodical adjustment of the base model (Table 6-1). The material of the loop wall is considered to be stainless steel, with 1 mm thickness.

Table 6-1: Summary of the range of parameters explored

Parameters	Dimensions (mm)
Diameter (D)	4 – 8
Height (H)	530 – 4240
Width (W)	395 – 3160
Radius of corner bends	5 – 20
Heater length (L_h)	1000 – 1500
Cooler length (L_c)	1000 – 1500

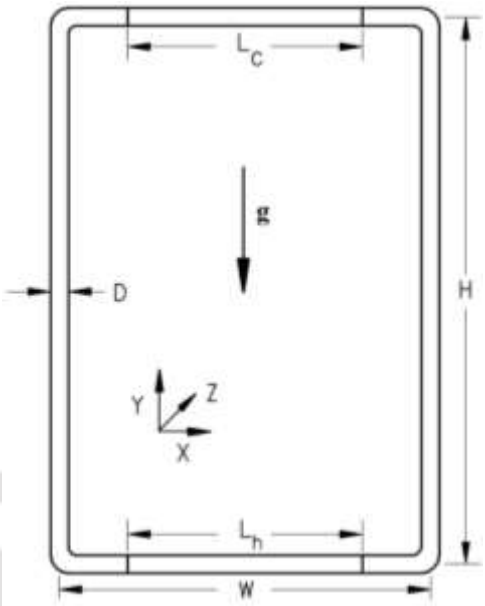

Figure 6-1. Schematic representation of the rectangular loop under analysis

For meticulous understanding of the influence of the associated geometric variables, systematic variation in each of these parameters is attempted. Table 6-1 summarizes all the dimensions explored in course of the study. While varying the magnitude of any particular parameter, all others are maintained at the value as in the base model, unless stated otherwise. Separate computational models are developed for each case, while ensuring the grid-independent nature of the solutions. Other computational aspects, such as the turbulence model, schemes for discretization and property estimation, remain identical to the base geometry.

6.3. Loop Diameter

Any change in the loop diameter directly affects the volume of fluid participating in energy transport, as well as the surface area available for heat exchange in both source and sink. Frictional resistances are inversely proportional to the diameter. Accordingly the thermalhydraulics in a smaller-diameter loop is strongly influenced by the friction, even in the buoyancy-dominated regime, resulting in smaller flow rate and a greater rise in the fluid temperature across the heater. Figure 6-2 presents the profiles of mas flow rate with power for three different loop diameters. For a given heater power, flow rate of sCO_2 becomes more than double with only 2 mm increase in diameter. Higher levels of fluid temperature also administers an early

initiation of FiHTD, characterized by the decline in both mass flow rate and heat transfer coefficient. While a loop with 4 mm diameter suffers the deterioration around 0.8 kW power, 8-mm-diameter loop can sustain larger flow till about 2.2 kW. The maximum value of flow rate and heat transfer coefficient attained by the larger-diameter loop are also substantially higher. Associated influence on the temperature and velocity levels can be perceived from Figure 6-3. Appearance of asymmetry in the flow stream within the heat-exchanging sections of SCNCL is well-established in literature (Yadav et al., 2012b), and the same can be inferred here as well. For the same power input, while the bulk fluid in the 4-mm-diameter loop can experience nearly 90 K variation in temperature in a single cross-section, it is less than 4 K for the one with 8 mm diameter. Substantial property variation is the result of such thermal asymmetry, developing local buoyancy effects. For the situation shown in Figure 6-3a, fluid can suffer nearly 18% change in density and 16% in thermal conductivity, which leads towards this asymmetry. The consequence is more-than-double increase in the velocity values for the slimmer loops compared to others, despite stronger local friction.

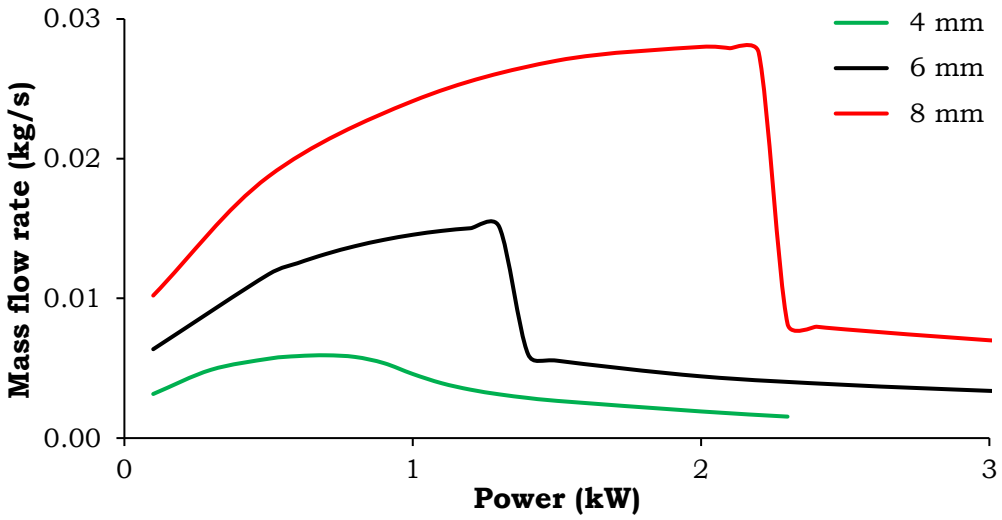

Figure 6-2. Variations in mass flow rate with heater power for three different loop diameters

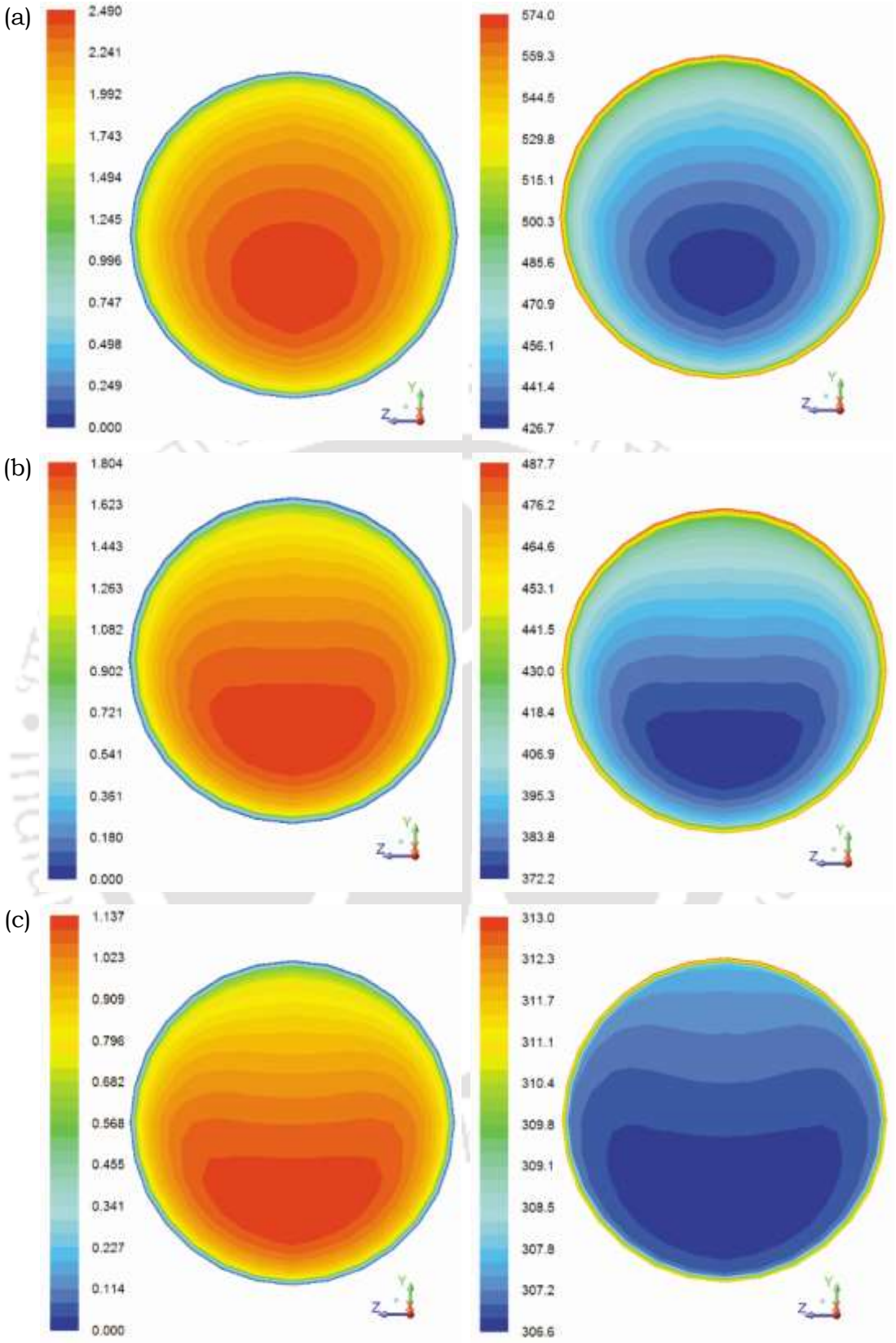

Figure 6-3. Velocity (left) and temperature (right) contours at the source center with 1.5 kW power supply for three different loop diameters: (a) 4 mm, (b) 6 mm and (c) 8 mm

6.4. Loop Height

Height or the vertical length scale is a very important parameter for determining the behavior of any natural convection based device. Flow in SCNCL is initiated and sustained by buoyancy, which linearly varies with height. Therefore a taller loop is expected to experience larger flow rate, and subsequently greater heat transfer coefficient. The same can be observed from Figure 6-4. Increase in the height from 0.53 m to 2.12 m, causes about 50% enhancement in the flow rate for 1 kW heater power. Larger flow rate allows the taller loop to sustain operation with lower temperature level over a wider span of power supply and hence the appearance of FiHTD is delayed significantly. Near-identical values of the average heat transfer coefficient can be observed for all loops till the maxima.

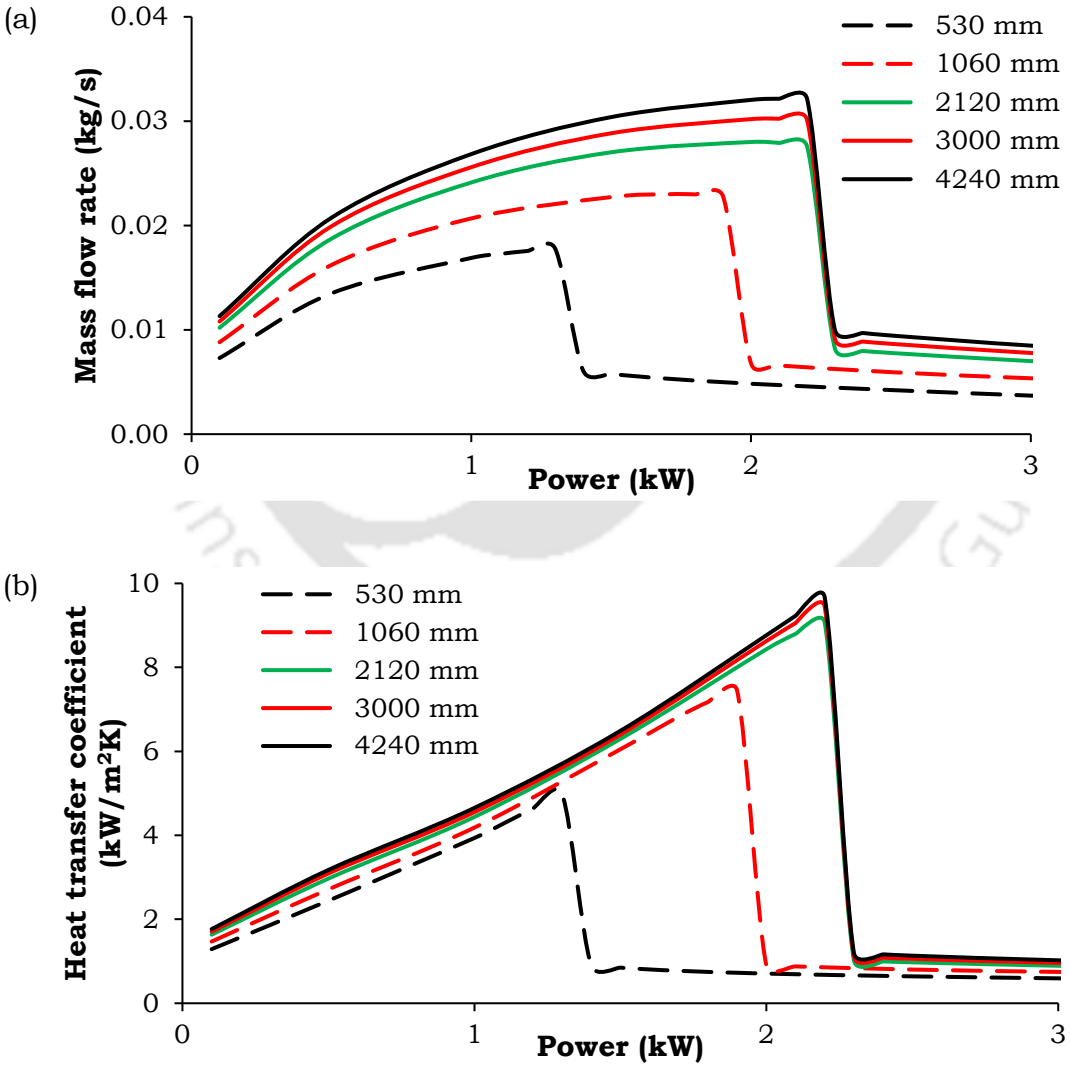

Figure 6-4. Variations in (a) mass flow rate and (b) sink-side average heat transfer coefficient with heater power for different loop heights

However, an increased height also lengthen the total flow path, imposing larger frictional resistances to the flowing stream. Concerned effect is progressively more apparent for larger heights and the friction acquires the dominating role beyond a certain level. As can clearly be observed from Figure 6-4, the gain in buoyancy is more compared to friction for a change of H from 1.06 m to 2.12 m, causing about 29% rise in the peak flow rate. However any further increase in H seems to hint towards a friction-dominated behavior. While both mass flow rate and average heat transfer coefficient grow marginally at identical power levels, their respective peaks correspond nearly to the same magnitude of heater power. That indicates the presence of an optimum loop height from FiHTD point of view, as any increase in height beyond 2.12 m for the present geometry is not able to yield any tangible benefit, and therefore better be avoided.

6.5. Width

Any change in the length of the horizontal sections has a direct influence on the frictional forces, as it alters the length of the flow path, without affecting the buoyancy development. Therefore increasing W, while holding other dimensions the same, is likely to have consequence qualitatively similar to that of reducing the diameter. Figure 6-5 compares the profiles for

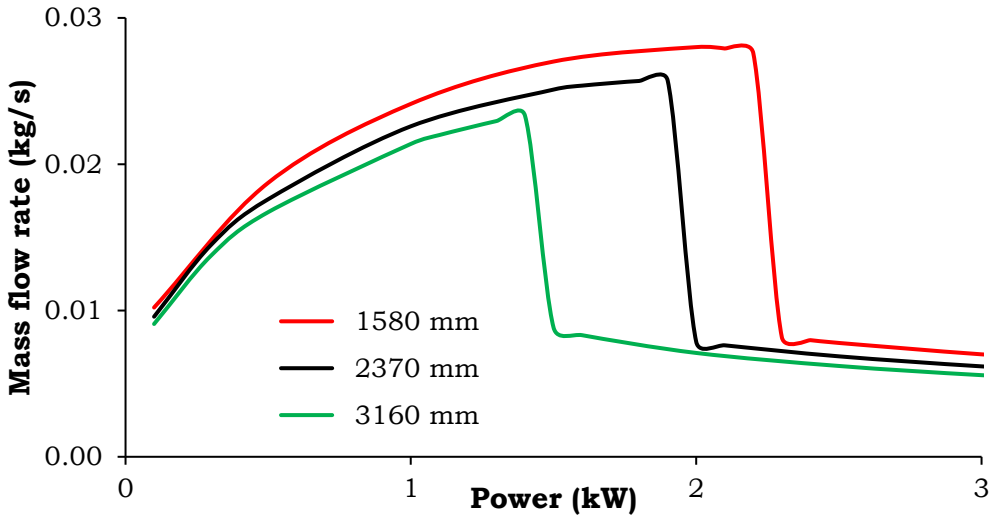

Figure 6-5. Variations in mass flow rate with heater power for three different lengths of the horizontal arms

loops with three different widths. Continuous reduction in the flow rate can be clearly observed with increased W, which is accompanied by higher temperature level and subsequently an early initiation of FiHTD. 50%

enhancement in the width advances the power corresponding to FiHTD by about 0.5 kW, along with nearly 15% decline in the largest heat transfer coefficient, which definitely limits high-power operations.

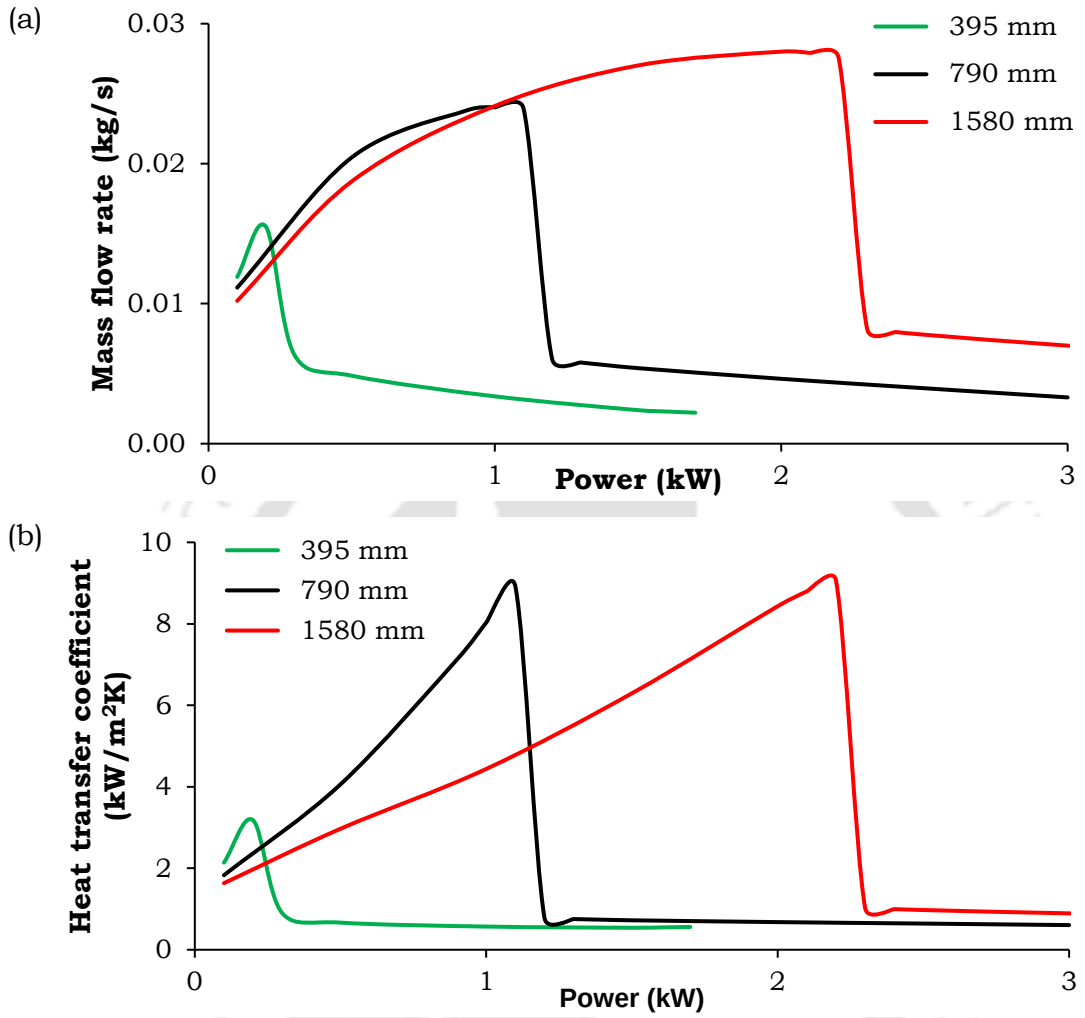

Figure 6-6. Variations in (a) mass flow rate and (b) sink-side average heat transfer coefficient with heater power for three different loop widths

Any reduction in the width from the base dimensions can affect the length of the heat-exchanging sections as well. Therefore a study is attempted considering three different loop widths, namely 395, 790 and 1580 mm, with the latest being the base geometry. In the former two models, lengths of the heating and cooling sections are decided by maintaining the same width-to-heater/cooler length ratio, as in the base model. Here both the surface area available for heat transfer and total frictional length change proportionately with W. At lower powers, mass flow rate is smaller for the wider loops, emphasizing the role of enhanced friction. Rapid increase in the mass flow rate can be observed for the all the geometries (Figure 6-6), with subsequent

rise in the heat transfer coefficient. However, FiHTD appears around a power level of merely 0.2 kW for the slender loop with 395 mm width, compared to about 2.2 kW in the base model.

A loop with larger width suffers from elevated friction, while longer lengths of the concerned heat-exchanging sections allow a relatively moderate temperature gradient, as can be seen from Figure 6-7. For 1 kW power input, the loop with 395 mm width experiences a temperature jump of about 270 K across the source, while the same is less than 5 K for the other two. Despite such a large change in both temperature and enthalpy, effective temperature level being well-above the pseudocritical limit, only about 33 kg/m^3 change in density can be observed. Due to the gas-like nature, the viscosity in the riser arm is found to be noticeably greater than that in the downcomer (Figure 1-7). Both this factors combine to produce weaker buoyancy and stronger friction, and hence lower mass flow rate, despite smaller frictional length. *Pr* is limited to around 0.7 throughout the loop, yielding very low heat transfer coefficient as well. For other two cases, the fluid crosses T_{pc} within heater, resulting in large density variation (~180 kg/m^3) and significant reduction in viscosity at the riser, in the range of 24-33%. That allows large flow rate and delay the appearance of FiHTD.

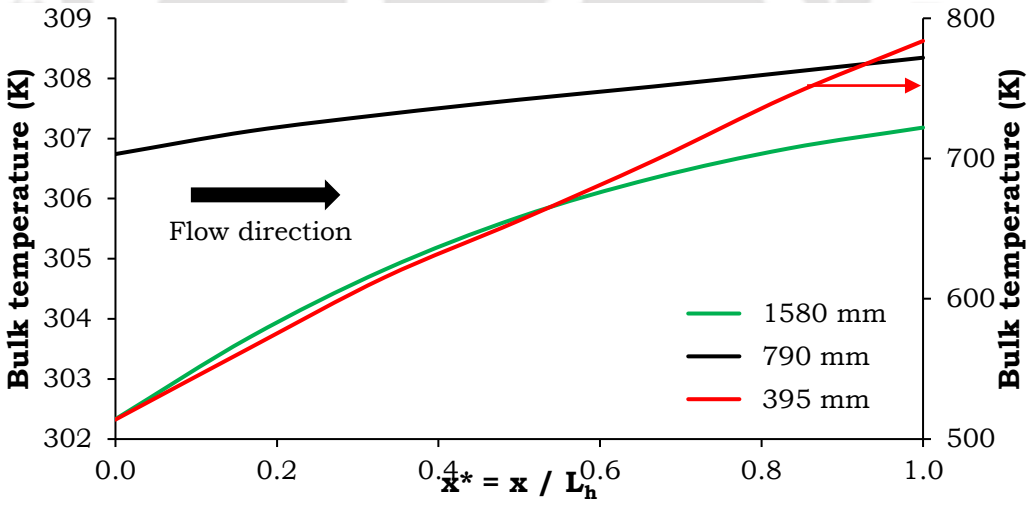

Figure 6-7. Variations in bulk fluid temperature along the heater with 1 kW power supply for three different loop widths

6.6. Heater and Cooler Length

For a given power input, imposed heat flux is directly proportional to the length of the heater. Therefore a shorter heating section enforces a steeper gradient in axial temperature profile. It, however, leads to similar change in

the fluid temperature, and hence in properties, for a specific mass flow rate. With other dimensions remaining unchanged, the loop, therefore, is expected to experience near-identical buoyancy and frictional fields, resulting in analogous macroscopic behavior. The same can be demonstrated from Figure 6-8. Profiles of average heat transfer coefficient with power for four different loops, varying only in terms of the length of the heater, seemingly overlap with each other. Similar nature can also be observed with mass flow rate variation, with hardly any distinguishable change on the initiation of FiHTD. So it can safely be concluded that the length of the heater has no significant influence on the loop thermalhydraulics and hence it can be optimized based on other design criteria, such as, the material issues and thermal stress on structures.

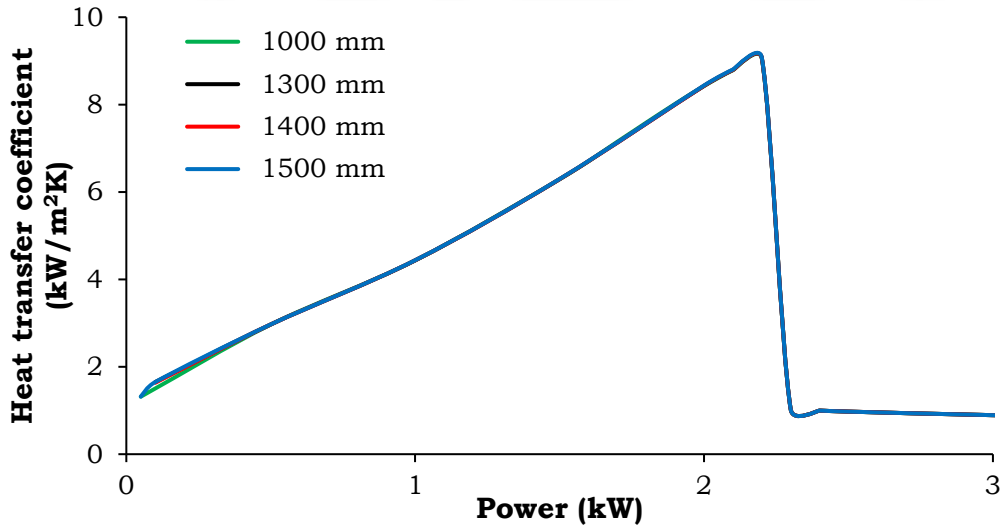

Figure 6-8. Variations in sink-side average heat transfer coefficient with heater power for different heater lengths

Cooling being done in convective mode, change in the length of the cooler demands an update in the prevailing heat transfer coefficient, as the power imposed to the fluid in the heater has to be completely discharged to the sink under steady-state. Accordingly a shorter cooler produces an increased value of the average heat transfer coefficient (Figure 6-9). For example, reducing L_c from 1.25 m to 1 m causes about 15% rise in the average heat transfer coefficient for 1 kW heater power. While that has barely any effect on the mass flow rate, FiHTD is initiated for a significantly lower power level. Peak value of the average heat transfer coefficient initially growths with rise in L_c, till it attains some maximum level, and starts declining thereafter. Such a nature can be explained following the profiles of bulk temperature

along the sink. As presented in Figure 6-10, the reduction in temperature is limited within a narrow band of 3-5 K for the three selected geometries. Such a small temperature differential causes near-identical change in density and viscosity values, and hence yields similar flow rates. However, the corresponding variation in *Pr* is quite palpable. While the concerned decline is around 18% for L_c = 1.25 m, it escalates to nearly 60% for L_c = 1.5 m, which leads to overall decline in average heat transfer coefficient.

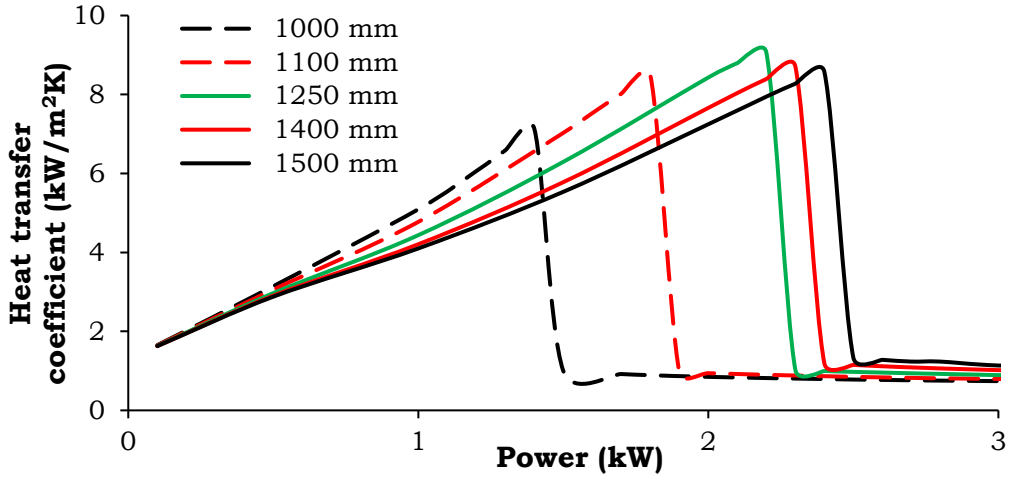

Figure 6-9. Variations in sink-side average heat transfer coefficient with heater power for different cooler lengths

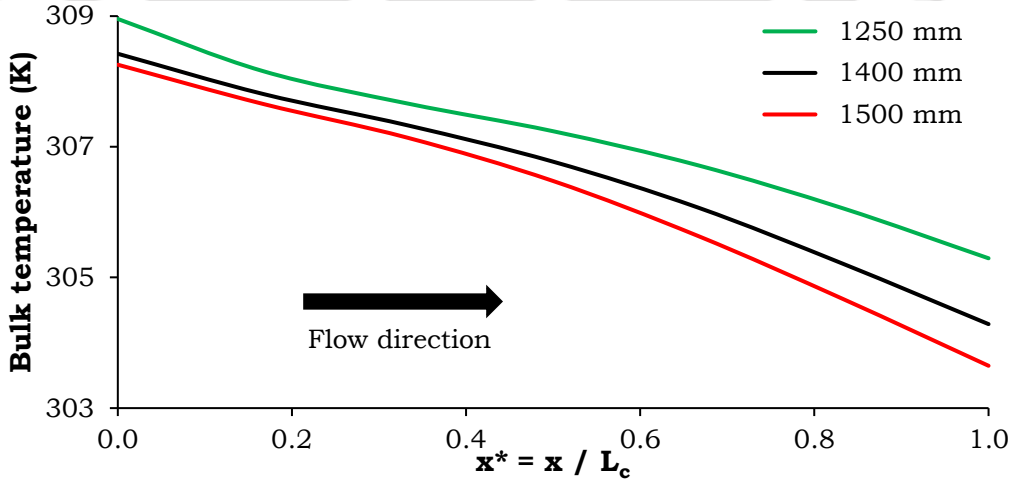

Figure 6-10. Variations in bulk fluid temperature along the cooler with 2 kW power supply for three differ-ent cooler lengths

6.7. Corner Bends

The horizontal and vertical sections are connected by right-handed elbows of specific radii, in order to yield the rectangular shape. Generally the

specification of the bend is not expected to hamper the overall loop performance significantly and the same can be observed in the present case. Major contribution of a bend, however, is to impart the centrifugal action on the flow stream, creating asymmetry in the profiles owing to the enhanced

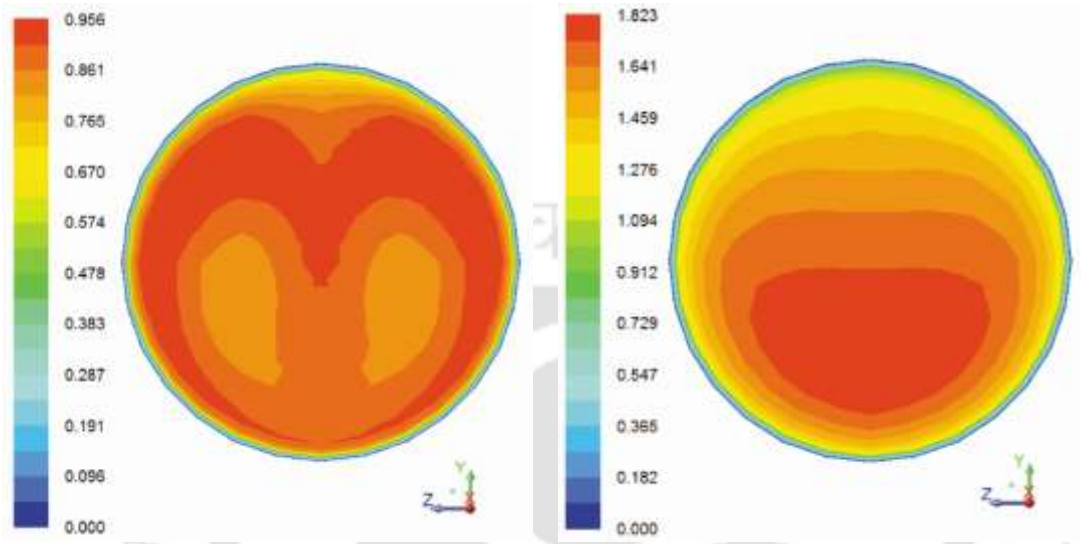

(a) Plane upstream to heater inlet (b) Plane downstream to heater exit

Figure 6-11. Temperature contours at two different planes of the bottom horizontal arm with 2 kW power supply.

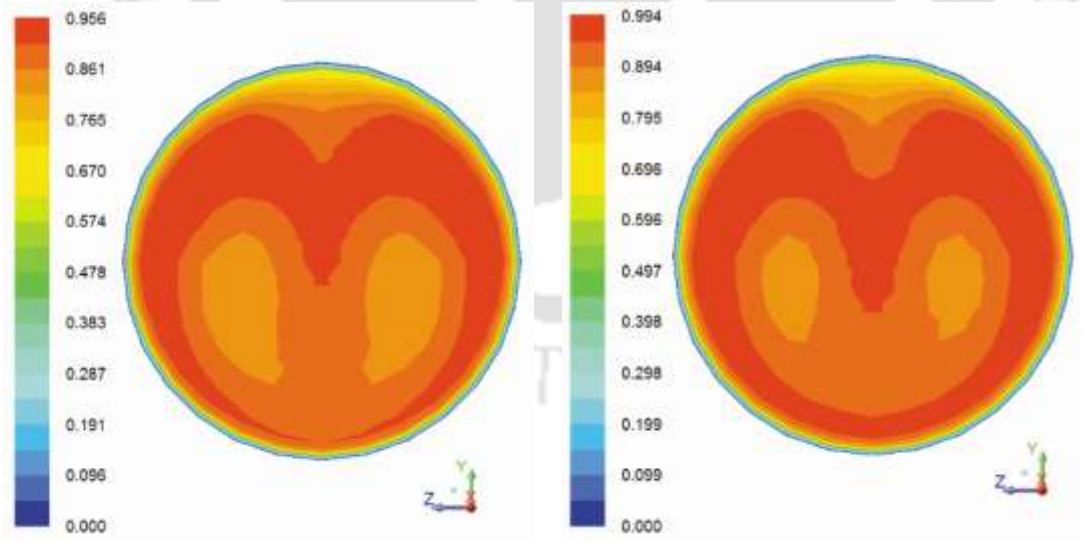

(a) Bend radius = 5 mm (b) Bend radius = 15 mm

Figure 6-12. Effect of bend radius on the temperature contours at a plane immediate upstream to the heater with 2 kW power supply.

velocity along the outer surface of the tube. As mentioned earlier, the presence of asymmetry in SCNCL is a common observation and the same is ascribed to

the presence of the local buoyancy, particularly when the bulk fluid temperature is reasonably close to T_{pc}. In order to isolate the effect of bend and local buoyancy, the velocity contours are presented in Figure 6-11 for two different planes, one immediately upstream to the heater inlet and the other just downstream to the heater exit. While significant amount of asymmetry is evident in the later, it is rather uniform in the former, with a distinct low-velocity zone near the upper wall, which happens to be the inner surface for the lower horizontal arms. This symbolizes the deceleration of the fluid in proximity of the inner surface because of the presence of bend. The largest velocity magnitude at the heater exit is also virtually double to that in the upstream plane, because of the added momentum gained through energy interaction with source. The extent of the centrifugal action, and hence the resultant asymmetry in the upstream plane, increases with the bend radius (Figure 6-12), with moderate rise in the largest velocity magnitude.

6.8. Role of Relative Positioning of Source and Sink

When both the source and sink are placed at the mid-location of the respective horizontal arms, the loop is symmetric in nature. Therefore it is not possible to realize the flow direction a priori, as flow is equally probable in either directions. For a real-life facility, the final direction generally depends on the mode of energy addition and the local irregularities encroached during the fabrication stage. Mathematically it can be envisaged as a problem with two possible solutions, with the eventual one being dependent on the direction

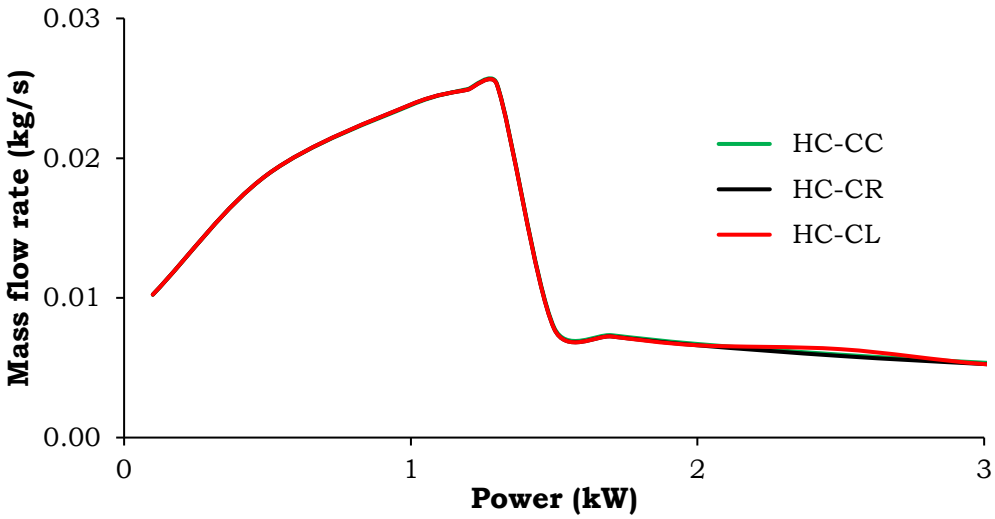

Figure 6-13. Variations in mass flow rate with heater power for three different positions of the cooler in the top horizontal arm

of error propagation. Breaching the symmetry in the configuration is anticipated to impose a pre-defined flow direction and may have an effect on the steady-state thermalhydraulics. In order to explore the same, a specific model is developed with both source and sink having 1 m length, whereas the other dimensions remain identical to the base model. Locating the heater at the center of the bottom horizontal arm, three different positions of the cooler are explored and concerned profiles of mass flow rate variation with power are presented in Figure 6-13. Here HC refers to the heater at the central location, whereas CC, CR and CL represents the central, right and left positions of the cooler respectively. The changes in the position does not affect the effective buoyancy and frictional forces, and hence induce no significant effect on the macroscopic behavior of the system.

One noticeable influence the positioning of source and sink has is on the flow direction. It is impossible to predict the flow direction in a symmetrical loop. However, for a non-symmetrical one, generally a pre-defined direction exists. For example, when the heater is shifted towards left and the cooler towards right, high-temperature fluid leaving the heater will always tend to climb through the nearest vertical arm. The reverse is true for the cooler fluid exiting the sink, thereby inducing a left-to-right or clockwise circulation. Following similar logic, it can easily be predicted that the loop with heater towards right and cooler towards left will present anti-clockwise motion. The same can be demonstrated following the velocity vectors at the relevant

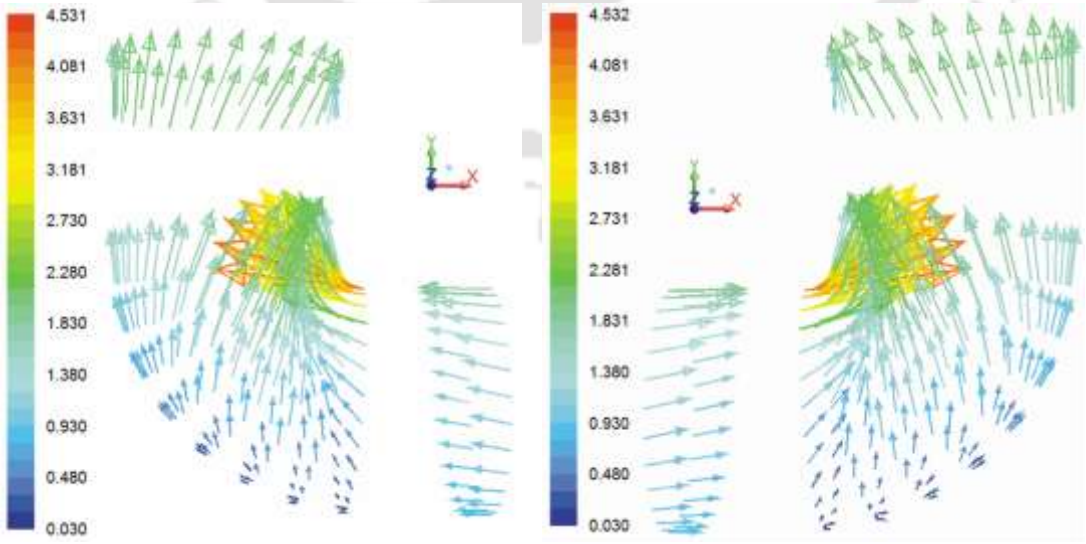

(a) Lower left corner for HL-CR configuration

(b) Lower right corner for HR-CL configuration

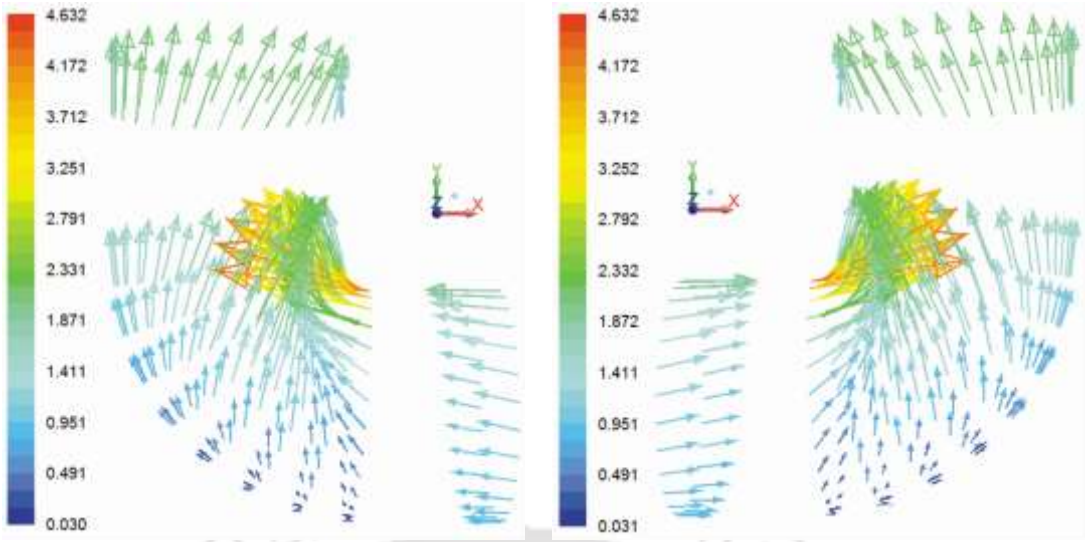

(c) Lower left corner for HL-CL configuration

(d) Lower right corner for HR-CR configuration

Figure 6-14. Effect of the relative positioning of source and sink on the velocity vectors with 2 kW power supply

corners of the bottom horizontal arm, as is shown in Figure 6-14. However, when the heater and cooler enforces opposite flow direction, the positioning of the heater is found to be the governing factor (Figure 6-14c-d).

6.9. Effect of Inclination Angle

The most effective way of altering the buoyancy force, without disturbing the frictional length, is to provide an inclination to the loop. An inclined loop lowers the vertical distance between the source and sink. When the loop is subjected to a tilt angle θ to vertical, effective buoyancy force will also be reduced by a factor of $\cos\theta$. As the order of frictional resistances remain unchanged, such tilting reduces the driving force in the loop, leading to lower rate of circulation. In the present study, inclination is considered in both $x-y$ and $y-z$ planes (Figure 6-15). Figure 6-16 presents the mass flow rate variation with power. A tilt angle of 60° to vertical in the $x-y$ plane results in nearly 20% decline in the flow rate around 1 kW heater power. That is accompanied by an equivalent reduction in the average heat transfer coefficient, as was indicated by Cao and Zhang, 2012. Chen et al., 2013d identified the role of inclination to be more prominent at lower heat fluxes. The same can also be observed here. For lower heat fluxes, i.e., before the appearance of FiHTD, the deviation in mass flow rate profiles are quite substantial. However, the profiles are much closely-spaced in the post-FiHTD zone. For any given inclination angle, the average elevation difference between

the source and sink is higher for the loop tilted to the $y-z$ plane, resulting in comparatively larger driving potential. Accordingly, such a loop predicts slightly higher flow rate compared to a loop inclined to the $x-y$ plane for any power level and the deviation continues to increase with the tilt angle. It is interesting to observe that the power level corresponding to the initiation of FiHTD is insensitive to any such tilting. Lowering of the mass flow rate, however, can have a big impact on the temperature level of the loop, particularly in the post-FiHTD regime. As shown in Figure 6-17, largest fluid

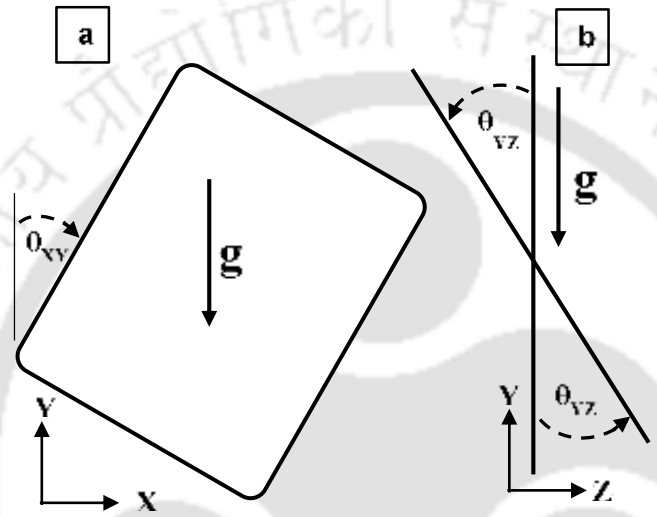

Figure 6-15. Schematic representation of the loop inclined to (a) x-y and (b) y-z planes

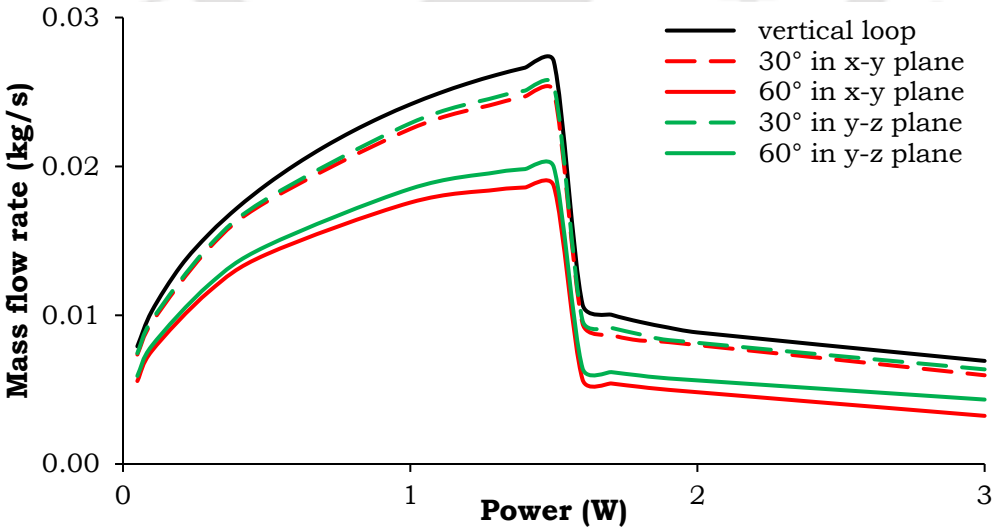

Figure 6-16. Variations in mass flow rate with heater power for different inclination angles

temperature inside the loop can be as much as 200 K higher for a loop 60°-tilted in the $x-y$ plane, compared to a vertical one, around 2 kW heater power. It can raise serious safety issues during operation and hence needs to be handled carefully.

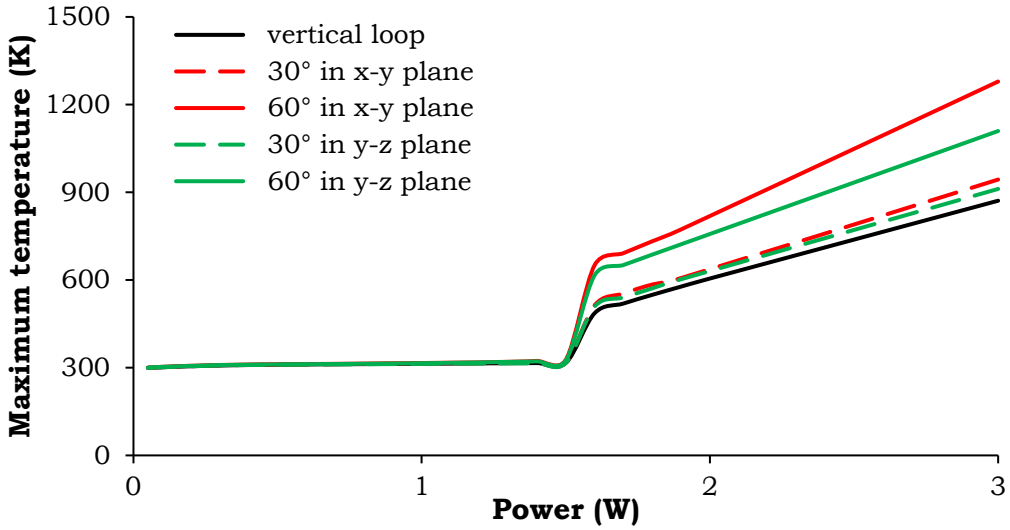

Figure 6-17. Variations in maximum bulk fluid temperature with heater power for different inclination angles

6.10. Epilogue

This chapter consists a thorough computational investigation of a CO_2-based rectangular SCNCL, with the primary focus being on identifying the role played by the associated geometric parameters on the thermalhydraulic behavior. Adopting the standard computational procedure, it is aimed to propose some guidelines about deciding the safer loop dimensions considering the appearance of FiHTD. Here, loop diameter can be viewed as the most influencing parameter. Smaller-diameter loop imposes larger friction, reducing the flow rate and thereby enforcing an early initiation of FiHTD. Thermal asymmetry in any particular cross-section, as well as the local velocity magnitude, can be substantially larger for smaller-diameter loops. However, increased diameter results in larger material requirement, as well as greater space and cost consideration, and therefore some trade-off may become necessary. Change in loop height affect both buoyancy and frictional fields. Buoyancy being the dominant force initially, mass flow rate and power level corresponding to FiHTD keeps on increasing with height till some optimum level. Hardly any tangible benefit can be observed beyond that and hence it is important to locate such optimum, possibly through systematic simulations. Change in horizontal length, without affecting the heat-

exchanging sections, has similar effect of reducing the diameter. So the extent of the adiabatic horizontal sections should be smallest possible. Variation in heating length, while maintaining rest of the loop the same, hardly imposes any noticeable change. On the contrary, rise in cooler length delays the appearance of FiHTD quite significantly due to the lower level of heat transfer coefficient. Therefore it is better to fabricate both the source and sink covering the entire of respective horizontal sections. Positioning of the source and sink in the horizontal arms does not influence the gross thermalhydraulic characteristics, apart from imposing a pre-defined flow direction. Effect of the corner bends is found to be restricted only in introducing minor asymmetry in profiles due to the centrifugal action. Despite reduction in driving buoyancy and hence the flow rate, providing inclination to the loop is found to have insignificant influence on the FiHTD. Therefore it can be treated as an effective option of stability control, without affecting the regime of operation under steady-state and that can be projected as the next step of research in the context of the present study.

Chapter 7: Experimental Characterization of a Rectangular SCNCL

7.1. Preamble

Experimental investigations on R134a based NCL with supercritical operating conditions are presented in this chapter. After thorough literature appraisal, it has been comprehended that, very few experimental studies on SCNCL are available in open literature, where mostly CO_2 and water are used as working fluid. The motivation of this study is to fill this gap and perform experiments for other fluids. Accordingly an experimental setup has been developed in IIT Guwahati. To enlarge the field of experimental analysis of SCNCL, several sets of experiment have been performed using R134a as a working fluid. Experimental studies have been carried out to understand the steady-state and transient behaviour of SCNCL with supercritical R134a.

The zone of operation of SCNCL is above critical point, therefore, the system operating pressure and temperature is very high compared to conventional system. Thus, the operating conditions become the prime constraints to perform the experimental investigation of SCNCL. It is a serious concern to do the experiment with supercritical water at above 22.5 MPa pressure. Nevertheless, some researchers did experimental analysis by overcoming all the barriers. Chen et al., 2013c, 2013b performed experimental work on sCO_2 based SCNCL to study the steady-state thermalhydraulics and stability behavior at different pressure ranges. Sharma et al., 2012 did experimental work to study the effect of heater and cooler orientation on steady-state behavior of a CO_2-based NCL. The leading force for initiation of flow field in the NCL is buoyancy, and which decreases with increase of inclination with vertical plane of the loop and thus both the flow velocity and heat transfer performance of the loop decreases (Chen et al., 2013d). Yadav et al., 2017 also studied the influence of inclination angle in thermalhydraulics of SCNCL experimentally. It was found by them that the heat transfer rate was decreased with the increase of tilt angle in x-y and y-z plane. At low heat flux condition, influence of inclination greatly affect the flow filed and average Nu

value, while at higher heat flux condition the effects are not significant. Orientation of heater and cooler greatly affect the flow pattern and thermalhydraulics of the system (Swapnalee et al., 2012). Down scaling study for a supercritical water loop has been done by Rohde et al., 2011, with consideration of R-23 as working fluid. A detailed literature review over experimental study of SCNCL has reported in § 2.5 of chapter 2.

The focus of this chapter is to experimentally investigate the steady state and transient behaviour of SCNCL, employing with supercritical R134a. Due to the non-toxic and environment-friendly natures of R134a, it has been identified as possible substitutes of water, particularly for lab-scale test facilities or smaller energy transport systems. R134a exhibits a low critical pressure, which making it relatively easier to achieve supercritical condition with compared to water. Before development of test facility a systematic scale-down analysis has been carried out and finalized the dimensions of the set-up (see § 3.3). Influence of sink temperature, operating pressure, inclination angle and input heating power are thoroughly investigated. There is no instability observed for the selected range of operating condition. At the end of study, some experimental results are compared with numerical results and a decent match is observed.

7.2. Design and Development of Components

Before developing an experimental setup, scaling analysis is essential to identify the dimensions of setup. Thus, a fluid-to-fluid scale-down analysis has been carried out to finalize the dimensions of R134a based loop on § 3.3. Scaling process begins with the identification of governing equations for flow field and then non-dimensionalizing them. Several non-dimensional groups (Table 3-1) are identified from non-dimensional equations and compared for model and prototype (Sharma et al., 2012). Finally, model dimensions are found from this comparison and shown in Table 7-1. Figure 7-1 shows the schematic representation of corresponding rectangular loop.

After completion of scaling analysis, the second stage of experimental study is to design and development of experimental set-up. According to scaling analysis, experimental setup of present study is a rectangular loop, where four tubes are connected together. Heating and cooling sections were chosen symmetrically around the center location of lower and upper

horizontal arms of the loop. The schematic view of experimental setup with various components is shown in Figure 7-2.

Table 7-1: Dimensions of the model

Parameters	**Dimensions (mm)**
Diameter (D)	8
Height (H)	2120
Width (W)	1580
Radius of corner bends	5
Heater length (L_h)	1400
Cooler length (L_c)	1250

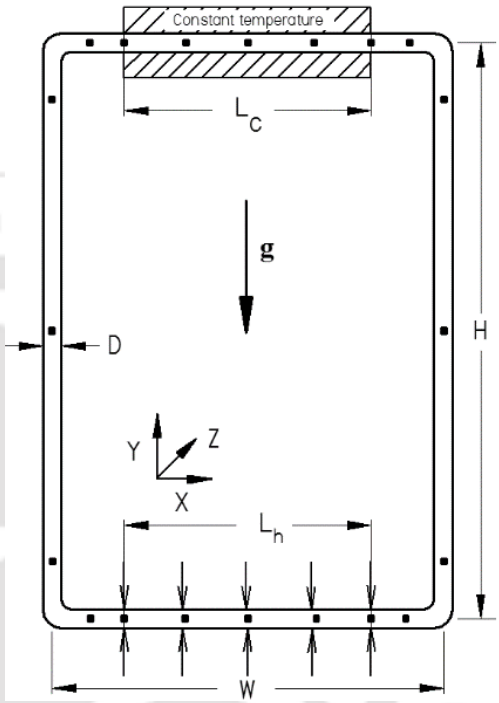

Figure 7-1. Schematic of the model

Here, 10 mm outer diameter SS 316 tube with 1 mm thickness is used to construct the loop. The length of vertical arm is 2120 mm, whereas the horizontal arm is 1580 mm. The heater portion is mounted on the lower horizontal arm of the loop. Similarly, the cooler portion is mounted on the upper horizontal arm of the loop. The heater and cooler lengths are 1400 and 1250 mm respectively. The cooler is a dual tube type heat exchanger. Where, outside diameter of outer tube is 38 mm. Heater is constructed by electric heating elements and controlled with a variac.

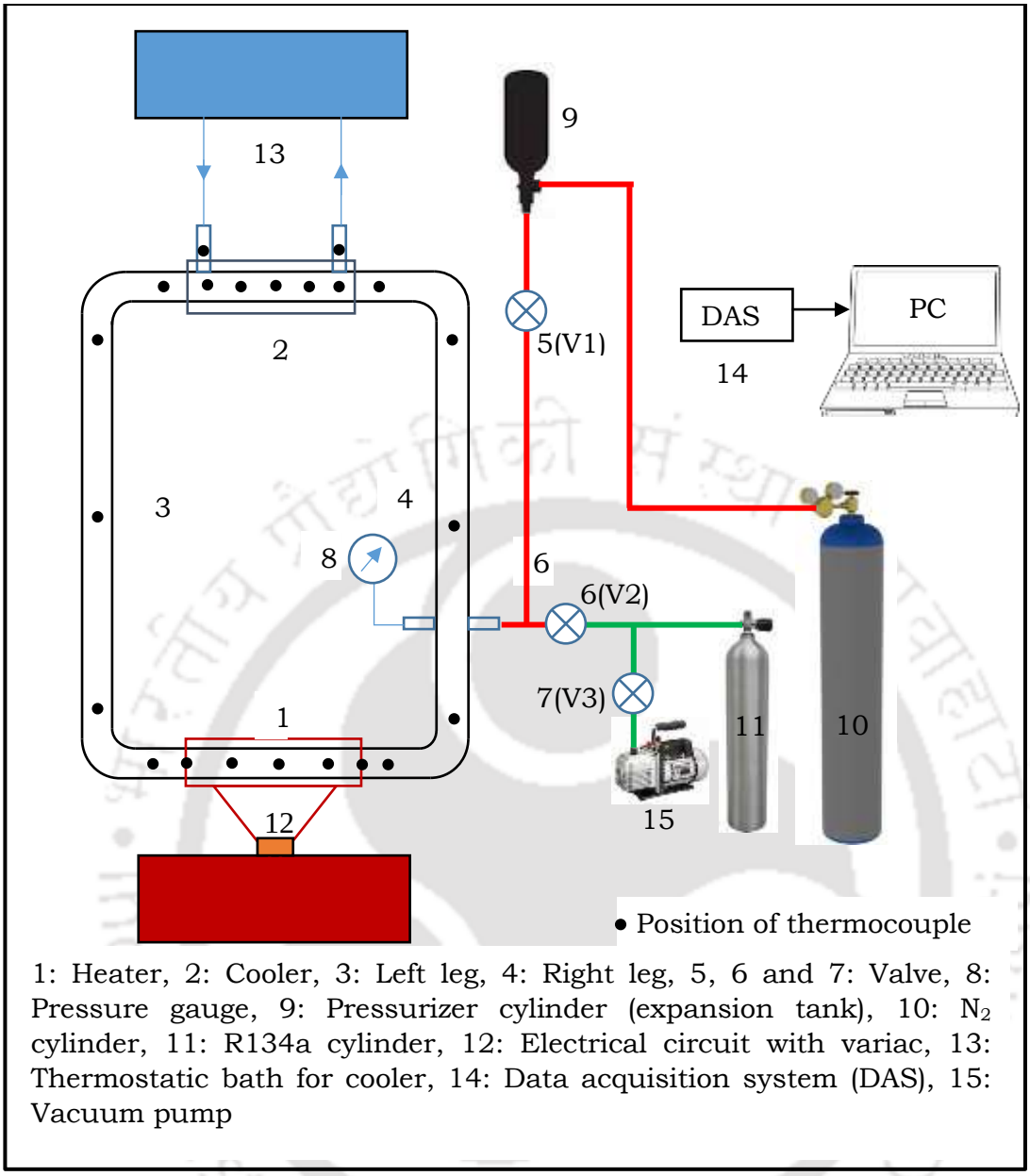

1: Heater, 2: Cooler, 3: Left leg, 4: Right leg, 5, 6 and 7: Valve, 8: Pressure gauge, 9: Pressurizer cylinder (expansion tank), 10: N_2 cylinder, 11: R134a cylinder, 12: Electrical circuit with variac, 13: Thermostatic bath for cooler, 14: Data acquisition system (DAS), 15: Vacuum pump

Figure 7-2. Schematic of experimental setup

7.2.1. Main structure

The main structure of experimental setup is the component which hold the rectangular loop with cooler and heater. The structure was manufactured in such a way that the loop can rotate in x-y as well as y-z plane within the structure. The material of main structure is high quality mild steel.

7.2.2. Heater

The basic idea of making a heater is wrapping a heating coil around the pipe. Therefore it is necessary to select an electrically insulating material

between heating coil and SS tube on which heating coil wrapped and which ensures no conducting electricity to the set up. At the same time insulating material should have good thermal conductivity, otherwise it prevents flow of heat from heating coil to the tube surface. For serving the above purpose, a mixture of Aluminum oxide and Sodium silicate were used as electrical insulation and thermally conductive material. When Aluminum oxide and sodium silicate is mixed in an appropriate proportion, a paste is formed. At room temperature this paste does not get solid, but it becomes a very hard material after some amount of heating to it. The paste are applied over the tube surface according to heater length, where the heating coil is to be wrapped around, and then heating is applied to make it hard. Only the portion left uncover where thermocouple is to be set. This composite material worked pretty well as electrical insulation and thermally conductive material. Figure 7-3 shows the pictorial view of heater.

Figure 7-3. Heater

To regulate the power in the heater a 15 Ampere variac is used. Nichrome wire with melting point 1400 °C is used as heating coil. To measure the temperature on the different points of heater, five numbers of K-type thermocouple are used (Figure 7-2).

7.2.3. Power input circuit

Power input circuit (Figure 7-4) is the combination of variac, multifunction meter, temperature controller and Nichrome wire. Variac is the heart of the power input circuit, which regulates the input power. Multifunction meter is used for measuring the input power (in Watt) of heater directly. To control the maximum temperature of the heater, i.e, as a safety instrument, temperature controller is used in the circuit. Temperature controller disconnects the circuit when temperature level is reached at a predefined point.

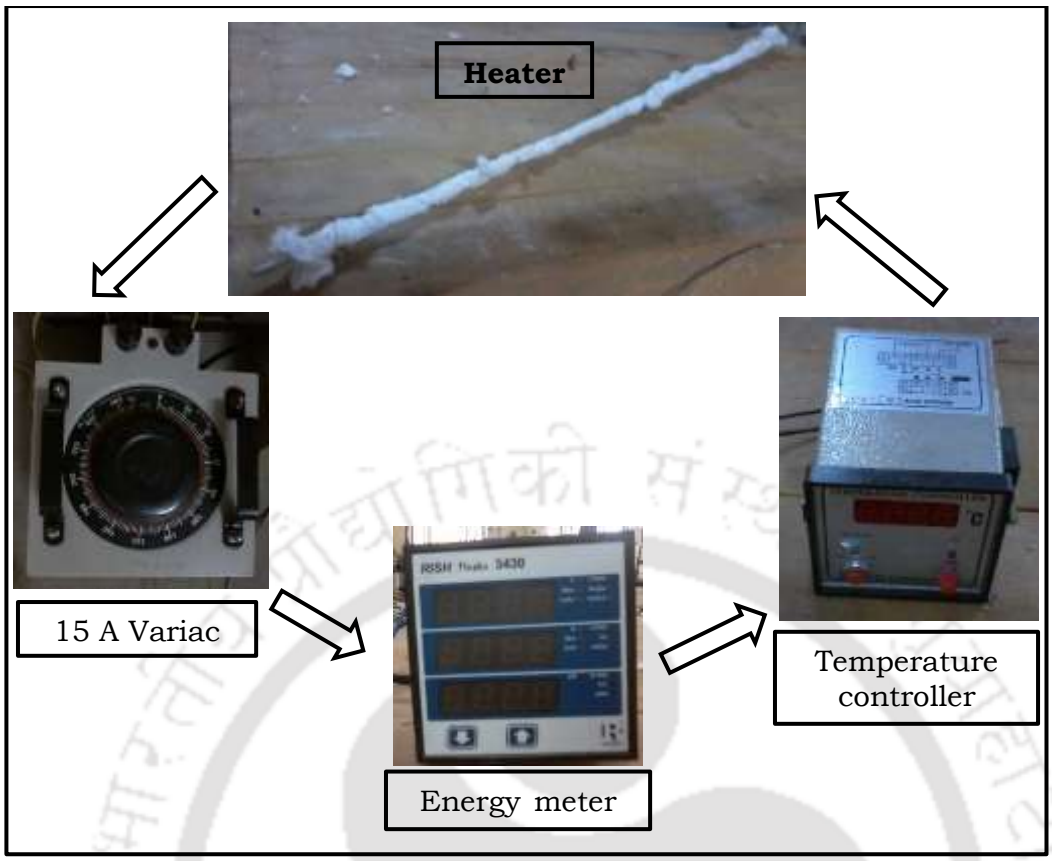

Figure 7-4. Power input circuit

7.2.4. Cooler

In the current experimental study a double pipe heat exchanger is used as heat sink or cooler. Figure 7-5 shows the pictorial view of heat exchanger with recirculation cooler. Outside diameter of outer and inner tubes of heat exchanger are 38 mm and 10 mm. Since it is a double pipe heat exchanger, therefore the annulus portion on both sides is covered with a pair of metal caps in which the sealing is done to prevent the leakage of the heat exchanger fluid with the help of M-seal. Two small parts of 10 mm tube is attached on the outer tube as inlet and outlet of heat exchanger fluid. There are five thermocouples which are used to measure the location wise temperature of inner tube within heat exchanger. The thermocouples are fixed on the surface of the inner tube with the help of a thermocouple attaching machine. A small portion of the thermocouple is exposed in the cooling fluid, therefore this exposed area is coated with proper insulation. Now, the thermocouple wires that are attached to the inner tube are brought out to the outside of the heat exchanger through three holes that are drilled on the outer tube surface. M-seal was applied to seal those three holes. Another pair of thermocouples is

inserted in the inlet and outlet of the heat exchanger to measure the inlet and exit temperature of the cooling fluid.

7.2.5. Cooling water connection

The cooling circuit is the combination of cooler, thermostatic bath and insulated pipes; which are used for making connection of inlet and outlet of the cooler. Thermostatic bath have an inbuilt pump and it continuously supply lower temperature water to the cooler and extract heat from there.

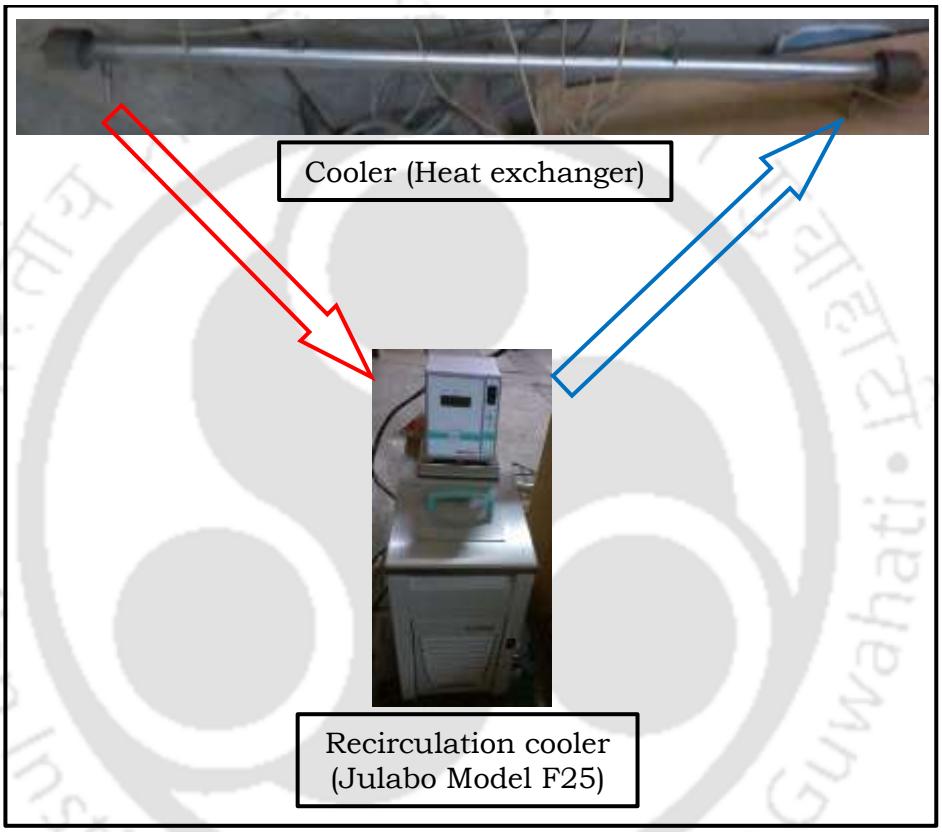

Figure 7-5. Cooler connection

After completion of fabrication of setup, whole loop with heater and cooler insulated by using 50 mm thick mat type ceramic wool. All set of performed experiment for current study have been done by using R134a as working fluid. A double stage rotary vacuum pump is used to evacuate the loop before injection of R134a into it. N_2 gas is used to pressurize the system upto required pressure levels. Specially, one inverted cylinder is used as pressurizer to damp the increase pressure at the time of operation.

7.2.6. Calibration of thermocouple

To measure the temperature throughout the loop, total twenty numbers

of K-type thermocouples are attached in the system at various location and two additional thermocouples are set at the inlet and outlet of cooler. Before using a thermocouple, it is essential to calibrate it to check the accurateness. For calibration of thermocouple an identical arrangement like actual system is assembled. One end of thermocouple is set in a small tube as similar way of thermocouple set at main loop and other end set in DAS. The tube is set with inlet and outlet port of recirculation cooler with the help of two plastic pipes. And water is flowed into the tube as similar as R134a flow in main loop. Initially recirculation cooler set at 15 °C, when cooler temperature reaches at 15 °C then both the temperatures are recorded, i.e., the temperature of cooler and thermocouple. After recorded one reading, allow to increase cooler temperature by 1 °C and repeat the process upto 95 °C. The temperature readings are got by thermocouple and recirculation cooler are compared in Figure 7-6. The calibration study of the thermocouple presented the perfectness of use of K-type thermocouple.

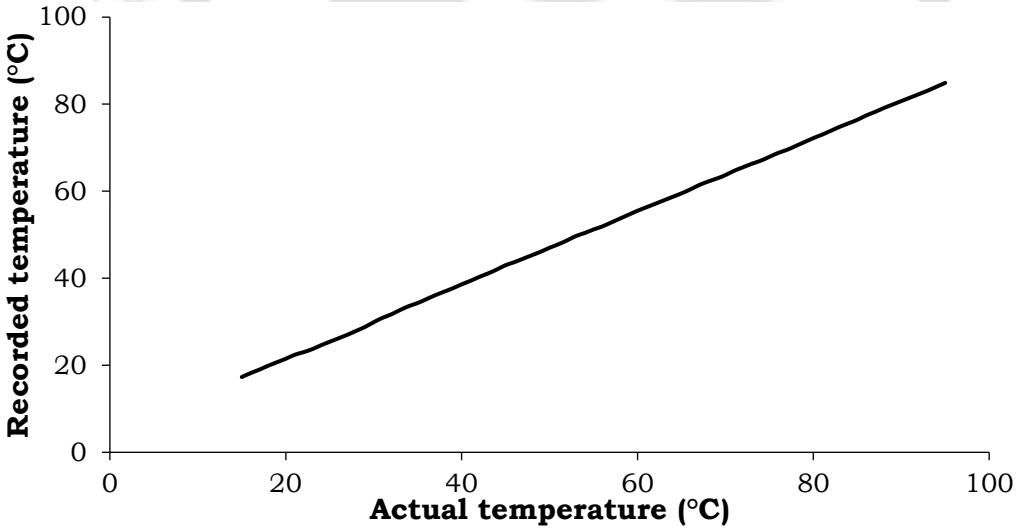

Figure 7-6. Calibration chart of thermocouple

7.2.7. Experimental procedure

The minimum operating pressure of the present set of experimentation is 50 times of atmospheric, which is a huge amount of pressure. Thus, additional attention should be required at the time of operation. Before starting the operation, following steps need to be strictly maintain.

1. A double stage rotary vacuum pump is connected to the loop to extract air from the system. At the time of air extraction, the regulators of N_2 and R134a cylinder must be closed while all valves (V1, V2 and V3) are in open condition (Figure 7-2).

2. After extracting air, the valve V3 is closed while other two valves remain open. Then, the regulator of R134a cylinder is opened to allow the gas to insert in the loop. At the time of injecting fluid in the system, cooling circuit is started to cool the fluid, which ensures the largest mass of gas inject in the loop.

3. Once the loop as well as pressurizer cylinder are filled with maximum amount of R134a, valve V1 and V2 are closed and N_2 cylinder's regulator is opened slowly to inject N_2 upto the pressurizer cylinder. The required amount of system pressure is gain by pouring N_2 into the pressurizer cylinder. After getting required pressure level in regulator outlet pressure gauge, the regulator of N_2 cylinder is closed and is kept the system untouched for some time. Because, initially N_2 mixes with R134a in the pressurizer cylinder, but due to high density difference between them within some time N_2 goes up and R134a goes down in the pressurizer cylinder. After sometime, valve V1 is slowly opened to pressurize the loop and thus N_2 cylinder regulator pressure gauge readings goes down, therefore the system does not get the required level. To fill-up this gap, the same procedure is repeated till it reaches the exact operating pressure.

4. After getting required pressure for experimentation, the heater circuit is switched on to begin the operation. Heater circuit consists of a Variac, multifunction meter, temperature controller and heating coil.

In the present experimentation three different pressure levels have been chosen, which are 5, 6 and 7 MPa. One USB type Agilent make data acquisition system (DAS) is used for recording the readings of 22 K-type thermocouple and the data's are stored for every ten seconds. The pictorial view of experimental setup is shown in Figure 7-7.

Figure 7-7. Pictorial view of experimental setup

In the present study, several experiments have been performed for various operating parameters. Specially, operating pressure and sink temperature are most significant parameters in case of SCNCL. The operating parameters and their ranges are presented in Table 7-2.

Table 7-2: Range of operating parameters

Parameters	Range
Operating pressure	5 – 7 MPa
Cooler temperature	15 – 35 °C
Tilt in x-y plane	30 – 60 degrees
Tilt in y-z plane	30 - 60 degrees
Heater power	0 – 1200 W

7.3. Numerical Comparison of Model and Prototype: Operating at Scaled Conditions

Before final preparation of experimental setup, a set of primary numerical simulations have been carried out to get the basic idea about the thermalhydraulic behaviour of the loop. To compare the numerical results for model and prototype, two different 3D models have been developed and simulated by using ANSYS-Fluent 15. Supercritical R134a and CO_2 are selected as working fluids for model and prototype respectively. Simulations are carried out for various input heat flux conditions, with scaled operating pressure and sink temperature. Various schemes of numerical solution, generation of mesh, grid sensitivity analysis and selection of turbulence model are thoroughly discussed in chapter 3.

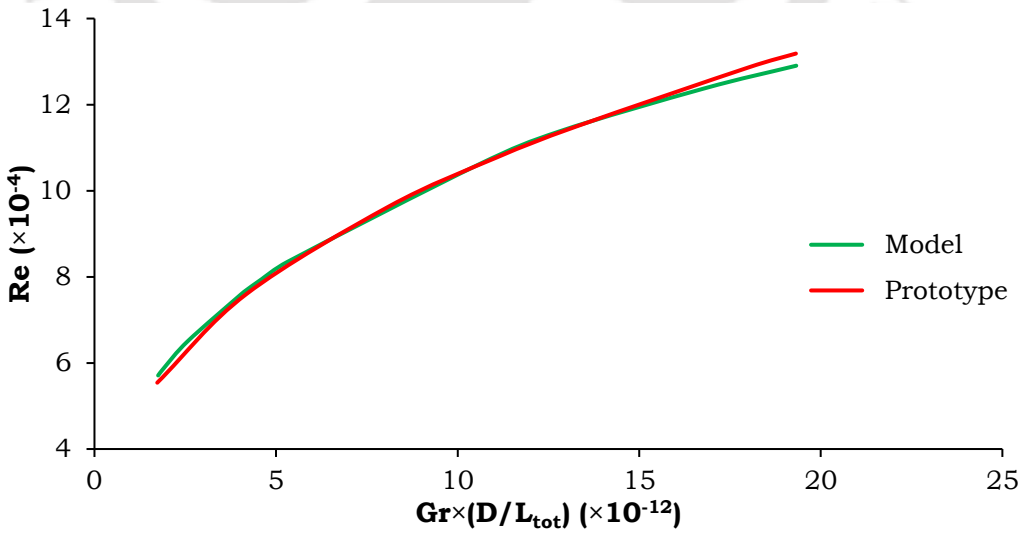

Figure 7-8. Comparison of non-dimensional results for model and prototype

Comparison of non-dimensional parameters for scaling analysis is a good practice. For serving the purposes, non-dimensional results (Re versus

modified Gr) are compared for both the model and prototype and an excellent conformity is achieved over the complete range of parameters considered on a non-dimensional plane. Figure 7-8 shows the admirable closeness of numerical results for model and prototype, which confirms the correctness of the corresponding study.

Table 7-3 shows the comparison of non-dimensional parameters for both the loops. Here, boundary conditions for the simulation are considered as scaled pressure (8.6 and 4.4 MPa), sink temperature (295 and 369 K) and source heat flux (20 and 25.57 kW/m^2) for both prototype and model. A potential endorsement is establish from this results, which ensures the exactness of scaling study. Figure 7-9 shows the source center velocity and contour plots for both model and prototype. The asymmetric variations are evidently shown for both the cases. The main reason of development of such profile is for the presence of local buoyancy. This significantly affects the heat transfer characteristic of the system. The fluid present near the wall of the heater is at a higher temperature and at lower density, compared to the cooler bulk fluid near the centerline. Considering the large density variation experienced by the supercritical fluid, the near-wall fluid can have noticeably lower density than the bulk, generating a strong local buoyancy and subsequently setting up a local upward motion. The same phenomenon occurs at the cooler also, but with downward radial velocity which is due to the cooler and denser fluid near the wall. As a consequence to such local phenomenon, fluid near the upper wall of the sink and lower wall of the source directly energize the heat and mass transfer into the main stream, leading to enhanced heat transfer at those locations.

Table 7-3: Non-dimensional groups for prototype and model for scaled operating conditions

Groups	**Prototype**	**Model**
Eu_m	505.518	949.075
Ri_m	0.00868	0.00869
Γ	0.0269	0.0287
St_m	0.00134	0.00169

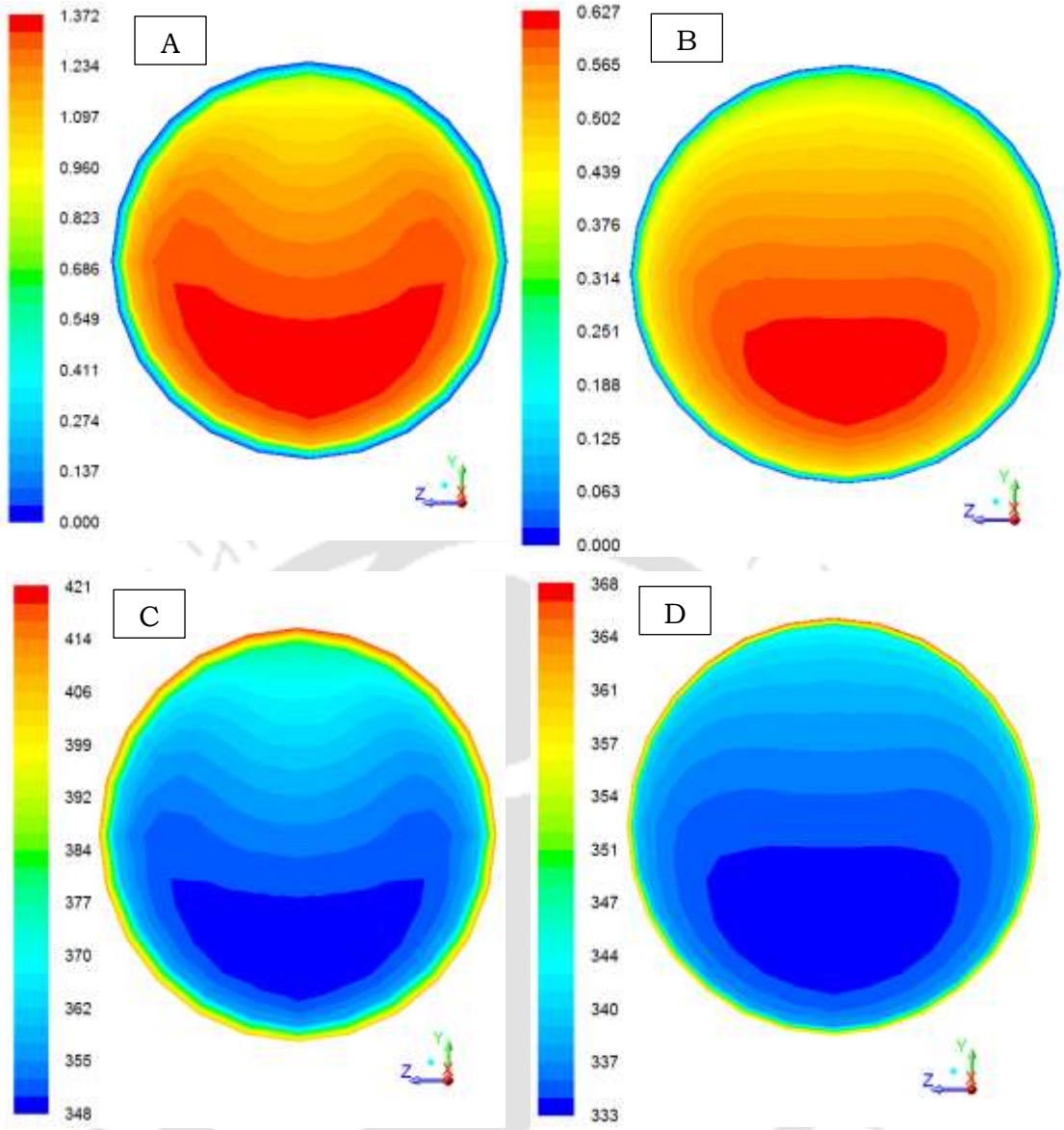

Figure 7-9. Source center velocity (A & B) and temperature (C & D) contours of prototype (A & C) and model (B & D)

Figure 7-8 and Figure 7-9 are shows the conformity of model and prototype. The range of non-dimensional numerical results are almost identical for both the cases (Figure 7-8). The presence of local buoyancy or broadly asymmetric profiles on both model and prototype ensures the similarity of the systems. After getting this confirmation, the foundation of experimental setup has initiated.

7.4. Results and Discussion

The motivation of present experimental study is to identify the thermalhydraulic characteristic and stability behaviour of SCNCL. For the present study each experiment has been performed on supercritical condition

of R134a. The critical temperature and pressure of R134a are 101.2 °C and 4.06 MPa respectively, thus, the selected pressure levels for most of the cases are 5 – 7 MPa. Thorough investigation have been done to observe the influences of pressure, tilt angle on both the planes (x-y and y-z) and sink temperature on thermalhydraulic of SCNCL.

In this experiment mass flow rate of supercritical R134a has calculated by energy balance equation across the heater,

$$\dot{m} = \frac{\dot{Q}_{th}}{C_p \Delta T} \tag{7-1}$$

Where, ΔT is the inner surface temperature difference between heater outlet and inlet sections. Temperatures are measured by using thermocouples and which are placed at the outer surface of the tube. To compute the inner surface temperature of the tube following conduction equation is used (Jo et al., 2014),

$$T_{w,i} = T_{w,o} - \frac{q'' t}{2\lambda} \tag{7-2}$$

Where, $T_{w,i}$ and $T_{w,o}$ are the inside and outside wall temperatures of the heater respectively. t and λ are the thickness and thermal conductivity of the heater material. $q'' = \frac{Q_e}{A_h}$ = average heat flux, where, Q_e and A_h are the electric power and area of the heater. Here, assuming that the electric power is ideally converted to thermal power. The thermal conductivity of SS 316 according to temperature is presented in Table 7-4.

Table 7-4: Thermal Conductivity of SS 316 with Temperature (https://goo.gl/h9seK4)

Temperature [°C]	20 °C	100 °C	200 °C	300 °C	400 °C	500 °C
λ [W/m- K]	14.0	14.9	16.0	17.3	18.6	19.9

Whatever the precaution may be taken, there are always some errors in the experimental study. Thus, a through uncertainty analysis is required to properly present the accurate experimental results and the same is shown in Appendix A.

Most of the experimental results are compared with simulated data, here simulations have been performed by using ANSYS-Fluent 15. To serve the purpose, a 3D model is developed with similar dimensions of experimental

loop and are simulated for identical operating conditions as experiment. Both the results are significantly matches with each other, only few results are not matches quantitatively, but the deviation is limited to less than 15%.

7.4.1. Variation of temperature at different location

Experimental loop have four different sections, namely, heater, cooler, riser and downcomer. Figure 7-10 shows the center wise temperature distribution with time for these four sections until reaching steady-state. The input power, cooler temperature and operating pressure for this specific experiment are 500 W, 25 °C and 6 MPa respectively. Here, heat transfer takes place directly on heater and cooler sections, whereas, riser and downcomer sections are behave like a path of passing heat from heater to cooler and vice versa. The maximum and minimum temperature occurs at outlet zone of heater and cooler sections. The riser is transferring this maximum temperature fluid from heater outlet to cooler inlet. Whereas, downcomer transferring the minimum temperature fluid from cooer outlet to heater inlet. Because of that, the temperature difference between heater and cooler center is much less than the difference between riser and downcomer center. Additionally, the result shows that the system is stable for the applied condition. Yadav et al., 2017 have also been found a stable system, whereas Chen et al., 2013c have observed small periodic waves in temperature profile of the heater wall.

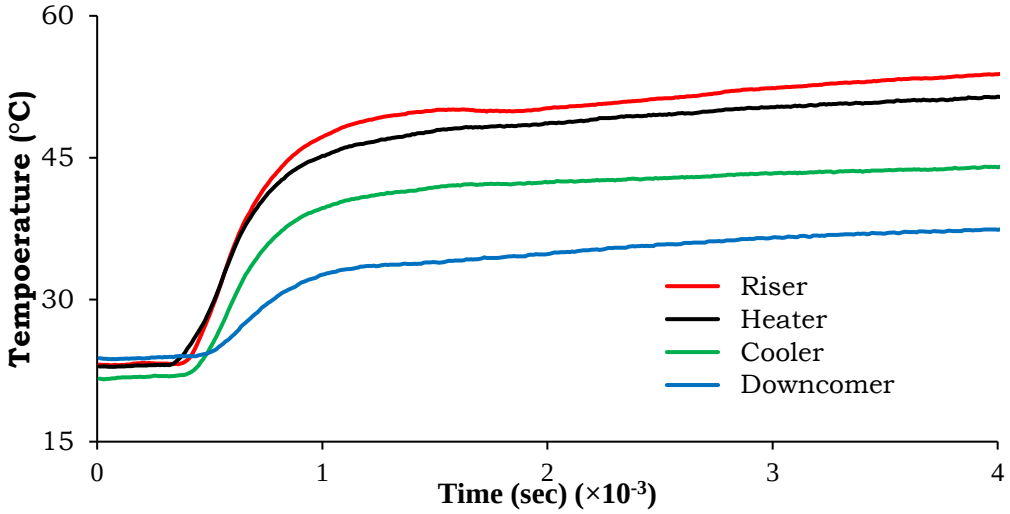

Figure 7-10. Variation of temperature at different location (operating codition: 6 MPa, 500 W and 25 °C)

Building a perfect insulated system, is one of the most important challenge of any experimentalist. Due to making or using wrong insulation, energy is lost which is not expected, because energy is the most vital and expensive matter of the recent world. Thus a study is essential for ensuring the correctness of applied insulation (Sadhu et al., 2018b; Yadav et al., 2017). For this experimental study, 50 mm thick mat type ceramic wool is used as insulation material. Temperature distribution of top and bottom sections of riser and downcomer (adiabatic) are presented in Figure 7-11, which indicates the perfectness of insulation. Temperature difference between top and bottom sections are less than 0.2 °C, which ensures that, the system is highly insulated.

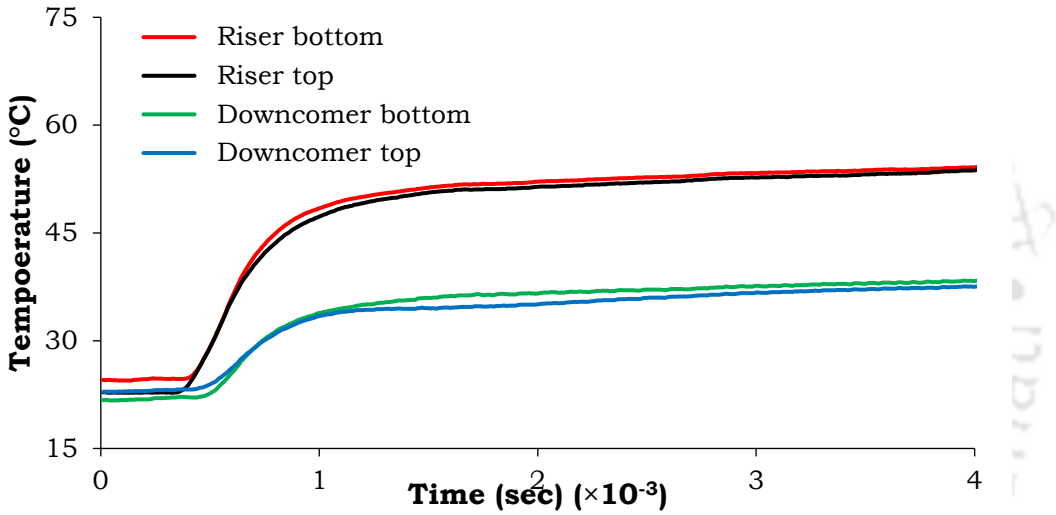

Figure 7-11. Top and bottom section temperature of riser and downcomer (operating codition: 6 MPa, 500 W and 25 °C)

7.4.2. Effect of sink temperature

Sink temperature is one of the most important parameter for any type of NCL. Hot fluid coming from heater is cooled down in this heat exchanging section. Rate of cooling is estimated according to sink temperature and thus, thermalhydraulics of NCL is highly dependent on it. Figure 7-12 shows the variation of mass flow rate with power for different sink temperature, at 6 MPa operating pressure of the loop. The chosen temperatures are 15 °C, 25 °C and 35 °C with 3.75 LPM (liter per minute) of water flow through the cooler for all the cases. The numerical results are compared with the experimental results and a decent contrast is observed. Mass flow rate is increased according to the increase of power for a constant sink temperature. And it is also increased

with the increase of sink temperature for constant power. Kiss et al., 2017 were performed an experimental study for supercritical water based SCNCL and identical observations made.

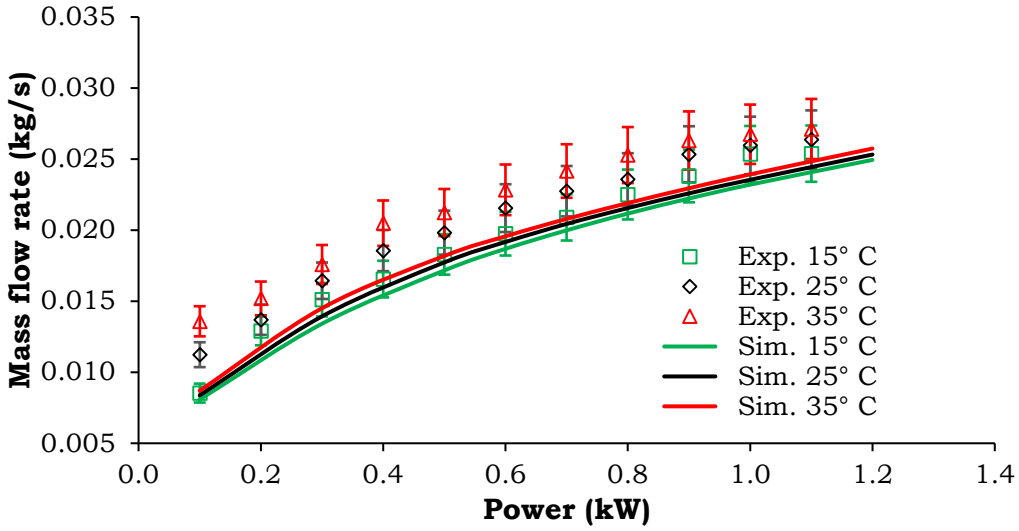

Figure 7-12. Mass flow rate for different sink temperature (operating pressure is 6 MPa)

7.4.3. Effect of tilt

Study over a vast range of tilt angle is more practicable. Because, in real cases, the system can be tilted in any of the planes. Thus the experimentation have been performed for both the planes for 30, 45 and 60 degrees.

7.4.4. Tilt on x-y plane

Buoyancy is the driving force of any NCL, which is dependent on both the density gradient between heater and cooler as well as the vertical distance between them. Mass flow rate is varies according to available buoyancy force in the system. Vertical distance is maximum in case of vertical loop ('0' degree) and hence this type of loop generate the highest mass flow rate. According to increase of tilt angle, center wise or average vertical distance between heater and cooler decreases. Consequently buoyancy force is also reduced and hence mass flow rate is decreases with increase of tilt angle (Figure 7-13). The operating condition for this special experiment is considered as 6 MPa system pressure and 25 °C sink temperature. Numerical simulations are performed for identical operating condition with experiment, finally both the results are compared and a decent comparison is observed (Figure 7-13) (Chen et al.,

2013d). Figure 7-14 shows the variation of heater inlet and outlet temperatures for different tilt angles on x-y plane for a constant power (500 W) input system, which operated at 6 MPa pressure and 25 °C sink temperature. It has been found that all the temperature levels are shifted due to the shifting of buoyancy force according to the tilt angle (Yadav et al., 2017).

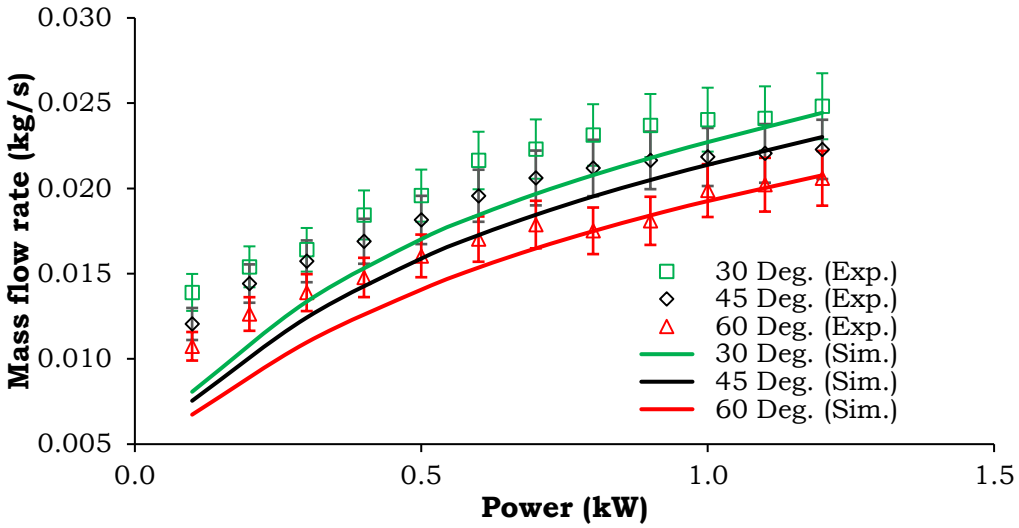

Figure 7-13. Mass flow rate for various tilt angle in x-y plane (operating condition: 6 MPa and 25 °C)

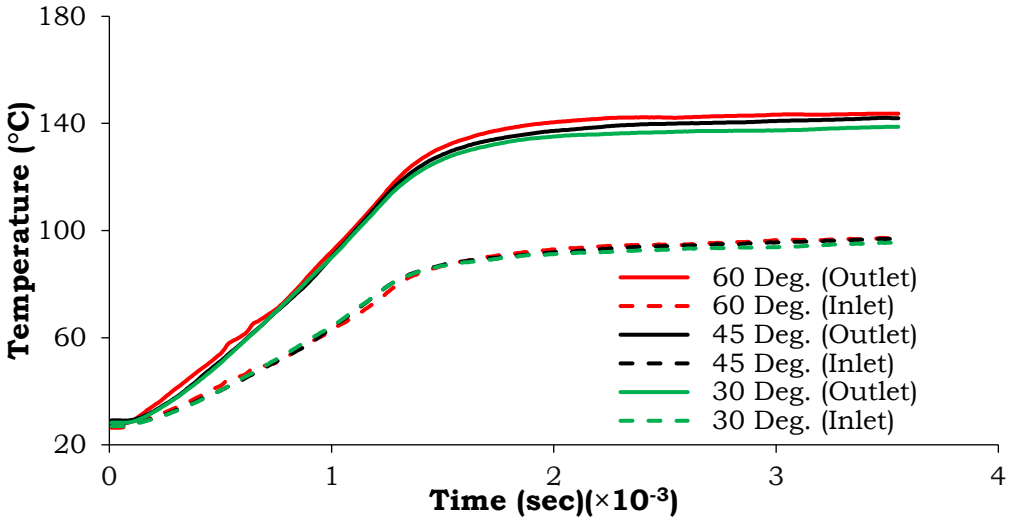

Figure 7-14. Heater inlet and outlet temperature according to tilt angle in x-y plane (operating codition: 6 MPa, 1200 W and 25 °C)

7.4.5. Tilt on y-z plane

Vertical distance between heater and cooler reduces by making tilt, not only in x-y plane but also in y-z plane. The influence of tilting in y-z plane is

less pronouncing than x-y plane. Tilting in x-y plane means, the flow direction is predefined. Thus the flow rate is highly deflect in this case. Whereas, after tilting in y-z plane, the system remains in symmetric in nature. Figure 7-15 shows the corresponding variation of mass flow rate according to the tilt angle in y-z plane. Here also, numerical data compared with experimental results. The operating conditions for both the systems are chosen as 6 MPa pressure and 25 °C sink temperature and both the results shows a decent comparison. The similar type of results have also been found in experimental observation of Yadav et al., 2017.

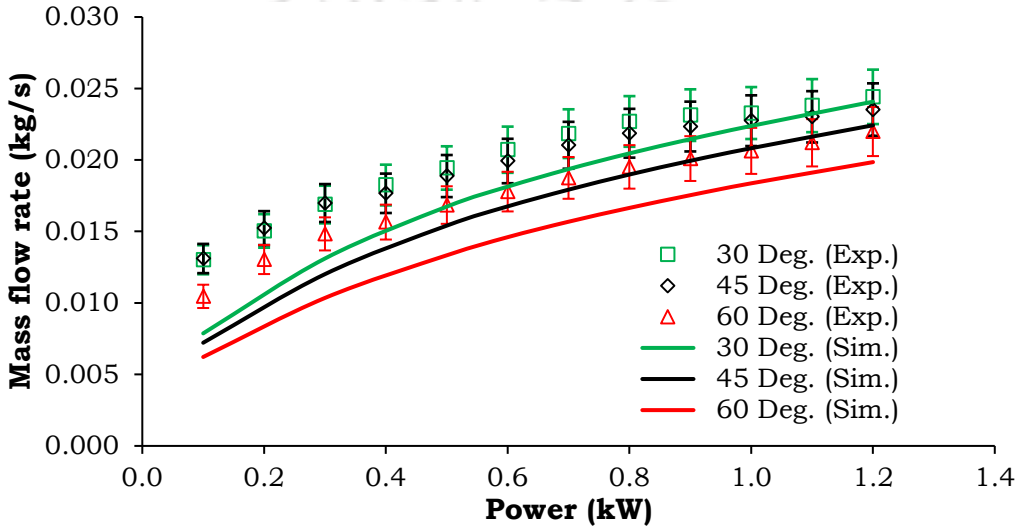

Figure 7-15. Mass flow rate for various tilt angle in y-z plane (operating codition: 6 MPa and 25 °C)

7.4.6. Effect of pressure

The most influencing parameters for investigating the thermalhydraulics of any NCL is doubtlessly pressure. State of the working fluid changes with change of this parameter, like sub-critical to supercritical. Present experimentation has been conducted for supercritical pressure of R134a (critical pressure 4.06 MPa), hence selected pressure levels are 5, 6 and 7 MPa. The experimental and numerical results are compared and a moral match is obtained from this comparison, which is shown in Figure 7-16. Mass flow rate is decreased with the increase of operating pressure of the system (Kiss et al., 2017; Yadav et al., 2017). The thermophysical properties of any fluids largely vary near the critical point of that fluid and which are basically the function of pressure. For supercritical condition, most of the thermophysical properties are decreases with increase of pressure. Thus, due

to decrease of density, the available buoyancy force is decreased with further increase of pressure and the result is mass flow rate is reduced.

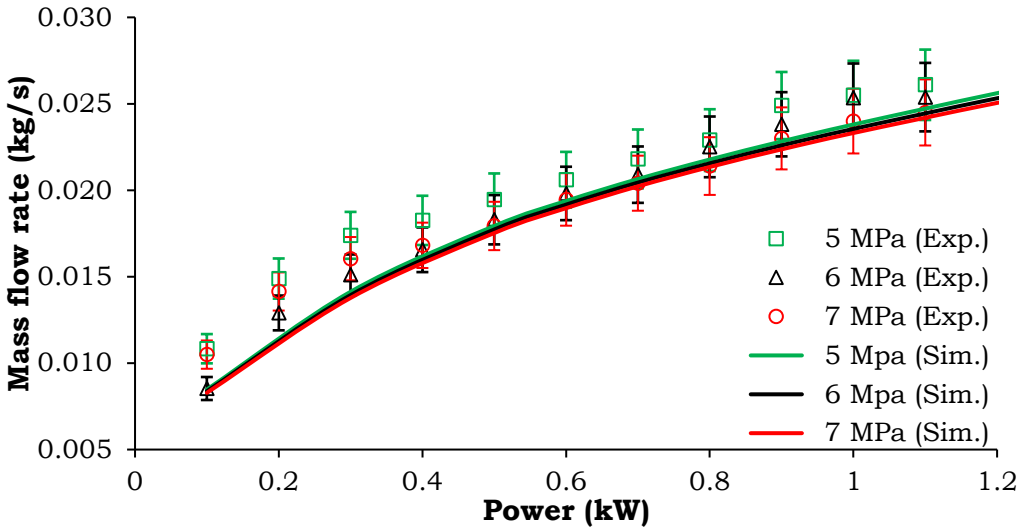

Figure 7-16. Variation of mass flow rate for different pressure levels with constant sink temperature 25 °C

7.4.7. Loss-of-coolant experiment

LOCA (loss-of-coolant accident) is a well-known term in the field of nuclear power generation. It is a common cause of nuclear reactor failure when the flow of coolant through the reactor seizes under some uncontrolled or unforeseen circumstances (https://goo.gl/BPsUD6). For the nuclear reactors designed in the forced-flow mode, there is always a possibility for the prime mover to malfunction, leading to a rapid increase in the fluid temperature level. A system operating in natural circulation mode is always expected to enhance the passive safety features because of the absence of any pump and natural variation in the fluid properties being the reason of the origin of flow. In course of the present experimental study, an effort is made to simulate a loss-of-coolant kind of situation, by suddenly tripping the flow of the cooling fluid. The objective of this particular test is to explore the transient response of the system following such an occurrence and to understand the amount of time an operator may have to react against such a scenario. The operating conditions are selected as 500 W input power, 25 °C cooler temperature and 6 MPa system pressure. An initially-quiescent system is subjected to these conditions and is allowed to reach the consequent steady-state, which is maintained over a significant time span. At the instant of 4000 s since the commencement of the experiment, the pump of the cooler side is

suddenly switched off and subsequent response from the loop has been recorded. A temperature limit of 120 °C has been pre-decided as the cut-off point, considering the safety aspect. As can be seen from Figure 7-17, the maximum wall temperature requires a further 2000 s to attain the cut-off limit, thereby allowing sufficient response time to the operator. Fluid and wall temperature at all the important junction points keep on rising steadily, albeit with different slopes. The difference between temperature at heater outlet and cooler outlet decreases quite substantially, from about 43 °C at 4000 s to about 21 °C around 6000 s. That indicates a continuous drop in the temperature differential between the two vertical arms and hence reduced potential for natural circulation flow. Beyond 5800 s, fluid temperature remains nearly constant during its passage through the cooler. Despite a possible reduction in flow rate, the rise in fluid temperature across the heater seems to decrease significantly, which probably is a sign for the system to approach the pseudocritical point. Finally it can be concluded that, despite the loos-of-coolant scenario, the system is able to sustain natural circulation flow over a considerable duration of time, providing sufficient response time to the operator.

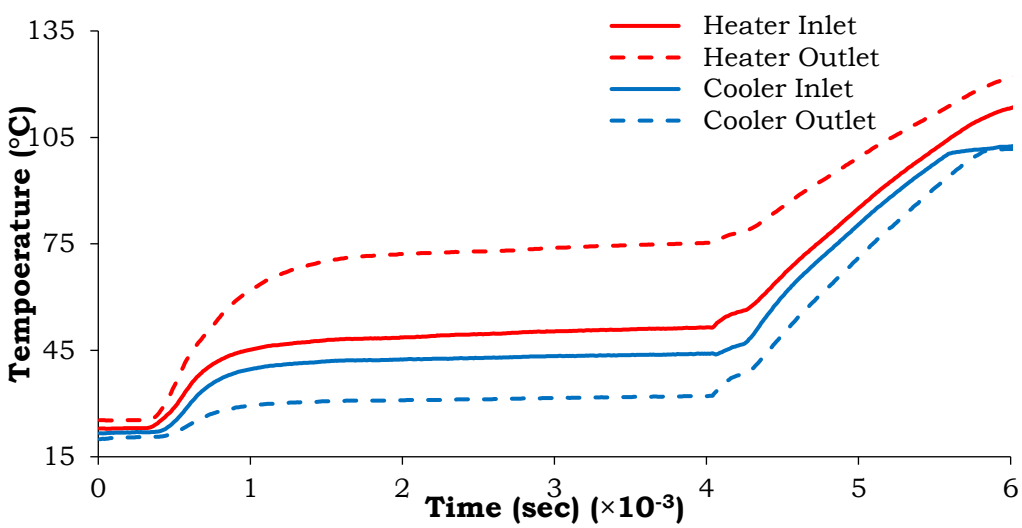

Figure 7-17. Heater and Cooler temperature for loss-of-coolant condition (operating codition: 6 MPa, 500 W and 25 °C)

7.4.8. Inspection of insulation leakage

Already mentioned that, making or assembling a proper insulated system is a challenge of an experimenters. Insulation is a primary aspect of a heat transfer based system (Sadhu et al., 2018b; Yadav et al., 2017). To

inspect the quality of insulation used in the present experimental setup, one special experiment has been conducted here. The system is initiated to run for 1200 W power, 25 °C cooler temperature operating and 6 MPa pressure. Once the system is reached at steady-state, both heater and cooler are shutdown at same instance and allow the system to reach normal/initial condition. The required time for reaching back the system to its initial position is estimated the quality of insulation. Figure 7-18 shows the elapsed time for come back a system to its initial condition, which is basically the measure of perfectness of the insulation used. It has been found that more than 15 hours is required for cool down to normal temperature, which ensured the good quality of insulation. Similar type of experiments were performed by Sadhu et al., 2018b and Yadav et al., 2017 and the corresponding observations are highly favor with present one.

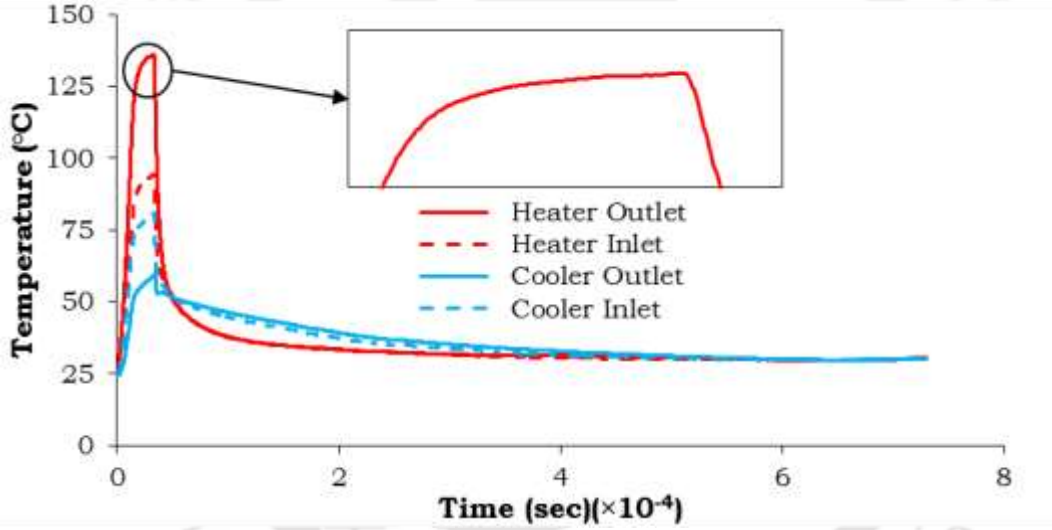

Figure 7-18. Inlet and outlet temperature of heater and cooler (operating codition: 6 MPa, 1200 W and 25 °C)

7.4.9. Sudden increase/decrease of load over a steady state system

Steady load on any system is an ideal condition, but in reality the load is frequently changed from small to a moderate value and sometimes it is abruptly changed to a big value (power on/off situation) which is off course unexpected. Thus, according to real situation, an experimental investigation is essential to study the system behaviour, mostly stability performance of the system for such circumstances. Figure 7-19 shows the results for sudden increase and decrease of the input power for the source section. Here, system

is running in steady-state condition for 800 W input power and 25 °C cooler temperature with 6 MPa operating pressure. Suddenly the input (power on) power is increased from 800 W to 1200 W and hold it for 5 minutes and then again it is changed to 800 W and continue for second steady state. For sudden decrease (power off) case, input power reduce from 800 W to 0 W (switch off the heater) and hold it for 5 minutes and then again it is changed to 800 W and continue the operation. For the chosen conditions, no unstable results are found in the experiments and for both the cases the system is remains in the stable condition. The result is extremely comparable with the transient temperature profile of Sadhu et al., 2018c.

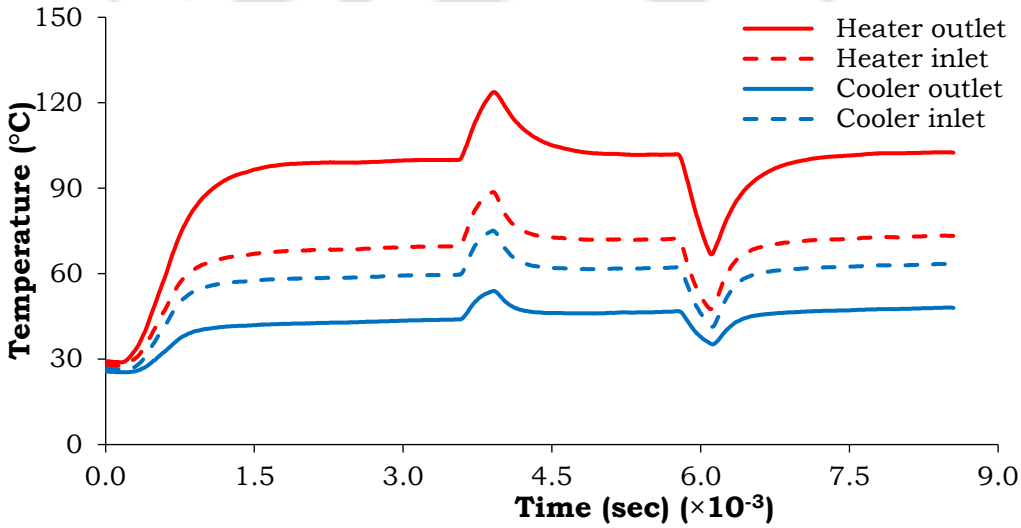

Figure 7-19. Temperature distribution for sudden increase/decrease of load (operating codition: 6 MPa and 25 °C)

7.4.10. Step input load

Figure 7-20 shows the temperature distribution of heater and cooler inlet and outlet for step input load condition. In this experiment the system is started at 100 W power condition and then load is increased by multiplier of 100 W upto 1200 W. The system holds for 10 minutes for each load condition and after concluding the last step allow the system to goes steady-state. The system operating pressure and cooler temperature are considered as 6 MPa and 25 °C respectively.

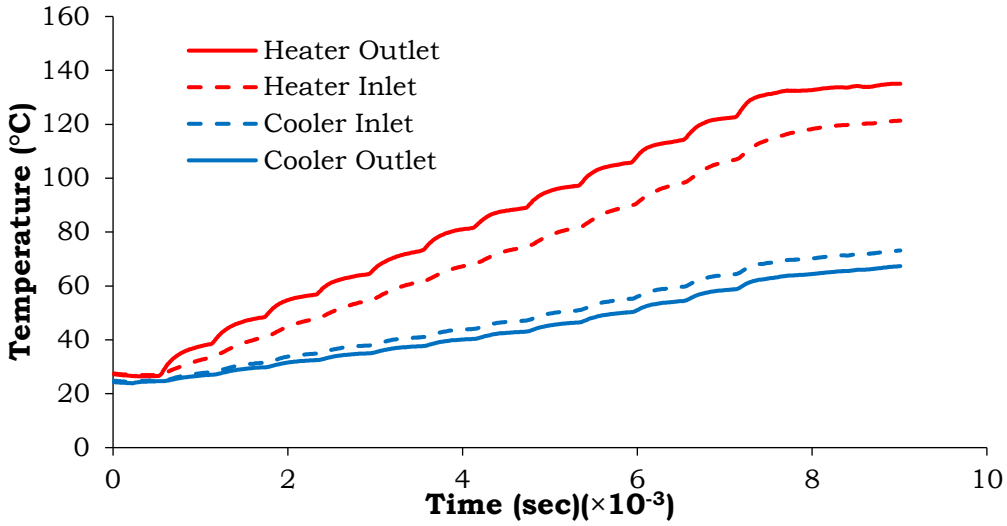

Figure 7-20. Temperature distribution for step input load (operating codition: 6 MPa, 100-1200 W and 25 °C)

The result shows that the system is stable for the selected operating conditions. Here, influencing parameter is heater power, thus heater responses quickly than cooler. Therefore, the temperature differences across heater is significantly more than cooler. Identical observation was made by Yadav et al., 2017 for varying hot water inlet temperature.

7.5. Epilogue

To enlarge the field of experimental analysis of SCNCL, a R134a based laboratory model is designed and fabricated in IIT Guwahati. Thorough experimental investigation have been performed for various operating parameters. Qualitatively as well as quantitatively good agreement exhibits for experimental and simulated data. Both the results are significantly matches with each other, only few results are not matches quantitatively, but the deviation is limited to less than 15%. The most influencing parameter for any type of NCL is sink temperature. The rate of cooling is assessed according to sink temperature and hence the thermalhydraulics of NCL is highly dependent on it. Mass flow rate is increased according to the increase of power for a constant sink temperature loop. One of the most important influencing parameters for investigating the thermalhydraulics of any NCL is doubtlessly pressure. Due to change of operating pressure the state of the working fluid is changes sub-critical to supercritical state. Due to decrease of density, the available buoyancy force is decreased with further increase of pressure and the result is reduced mass flow rate.

The buoyancy force dependent on both the density gradient between heater and cooler as well as the vertical distance between them. Center wise or average vertical distance between heater and cooler decreases with increase of tilt angle. Vertical distance is maximum in case of vertical loop and hence this type of loop generate the highest mass flow rate. The flow direction can be predefined by tilting the loop in x-y plane. Thus the flow rate is highly deflect in this case. Whereas, after tilting in y-z plane, the system remains in symmetric in nature and hence the influence of tilting in y-z plane is less pronouncing than x-y plane. Experimentally dynamic performance analyses have been performed by sudden increase and decrease of the input power for the source section. For the selected range of study, no unstable results are found in the experiments and for both the cases the system is remains in the stable condition. In case of step input load condition, the influencing parameter is heater power, thus the heater responses more quickly than the cooler. Therefore, the temperature differences across the heater is significantly more than the cooler. A detailed experimental analyses have been confirmed that the system is stable for all the selected operating conditions.

Chapter 8: Transient Simulations of a 2D SCNCL for Stability Appraisal

8.1. Preamble

Since the last few decades several research work have been carried out to investigate the thermalhydraulic as well as stability behaviour of NCL. In the current chapter, a comprehensive transient analysis has been carried out to observe the stability performance of an SCNCL. Consequently, a 2D computational model of rectangular NCL is developed and used to explore the transient nature of the same. Here, sCO_2 is considered as working fluid with 10 MPa operating pressure. The system exhibited both stable and unstable performances. Influence of sink temperature on transient analysis of SCNCL is thoroughly investigated and a wide-ranging stability map is prepared. Both the stability threshold can be crossed by varying sink temperature and heating power. The SCNCL always remains in single phase state and experiences a huge density variation for a small temperature changes near the pseudocritical point. This is the main possible reason that may pushed the system towards instabilities alike to those have been noticed in two-phase flow heated channel.

Similar to two-phase loop, SCNCL also experiences large changes in density across the heating section and for this reason, this may be susceptible to flow instabilities similar to those observed in two-phase system. The non-linear stability code SPORTS was developed by Chatoorgoon, 1986 for stability analysis of a two-phase NCL. This code (SPORTS) was again used in first analytical as well as numerical model of SCNCL by Chatoorgoon, 2001. The single-channel SCNCL model has been developed for supercritical water, where heat source and heat sink are point as well as distributed. A definite flow instabilities was observed in this study which is different from its two-phase counter parts and author recommended experimental study to confirm or deny this finding. Chen et al., 2016, 2013c, 2013b performed experimental work on SCNCL to study the flow and heat transfer characteristics and also stability behaviour at different pressure ranges. Thermalhydraulic and

stability behavior of NCL depends on various parameters like, temperature gradient between heater and cooler, operating pressure, geometrical parameters, orientation of heater and cooler, tilt angles of the loop etc. Numerically as well as experimentally transient analysis of CO_2 based SCNCL have been carried out by Yadav et al., 2017, 2014. Effect of operating pressures, inlet temperatures of water, tilt angles on system stability are examined thoroughly. Effects of source and sink temperature and loop diameter on system stability was investigated by Chen et al., 2013a at supercritical and transcritical conditions of NCL. Numerical study over the flow instabilities and dynamic behavior of SCNCL are performed by Jain and Rizwan-uddin, 2008, 2006. Effects of source temperatures on the flow transition and instabilities of the system, while sink temperatures are constant was carried out by Chen et al., 2010. Sharma et al., 2010c, 2010b reported linear and nonlinear stability analysis of water based SCNCL. For that purposes, two separate codes were developed, namely, SUCLIN and NOLSTA. They have discussed the effect of diameter, loop operating pressure and heater inlet temperature on steady-state and stability behavior of supercritical water based SCNCL. The larger diameter loops are more unstable than smaller diameter loop in terms of heater power. Influence of unsteady heat input in the form of gradual/slow and sudden/quick increase and sudden decrease in input power for trans-critical NCL were numerically investigated by Chen et al., 2012a. The possibility of generating instability is more in case of quick increase of input heat flux than slow increase. In subsequent study, Chen et al., 2013d have done a numerical as well as experimental investigations to identify the influence of inclination angle of the loop on system stability. It has been identified that at low heat flux condition the system is unstable, but the system is stable when input heat flux is high. They have not found any unstable behaviour of the system in case of experimental study.

In the present chapter, investigations are focused on transient analysis of sCO_2 based SCNCL, to find out a gross idea about stability performance of the system. Instabilities in SCNCL, associated with the two-phase-like property variation of single phase supercritical fluid, near the pseudocritical point have not been fully explored. Therefore, in the current study an investigation of flow stability phenomena in an NCL with supercritical fluid is carried out. The final goal of this study is to produce stability map for SCNCL

to identify the stable zone of operation. Stability of the system depends on several parameters like, pressure, sink temperature, input heat flux, loop aspect ratio, presence of heating structure and many more. With stability analysis, a detailed dynamic performance evaluation study have also been carried out in this chapter. The system stability also depends on the time and types of perturbation. To apply the perturbation in input heat flux of the system several UDFs are used.

8.2. Physical Geometry

For transient study of SCNCL, a 2D rectangular model has been developed and investigated with identical dimensions of base model (Figure 3-2). The main aim of use of 2D model is to reduce the computational cost of simulations. By using 2D model, the number of cell in grid system is greatly reduced which significantly minimized the time of simulation. Here, heater and cooler sections are located at the top and bottom horizontal arms respectively, whereas the vertical arms are assumed to be ideally insulated. System pressure is tuned at 10 MPa, such that CO_2 attains at supercritical state. The physical dimensions of the current 2D model is identical with the dimensions of base model of 3D geometry, which is shown in Table 3-3. Primarily, steady-state results are generated for both the models (2D and 3D) with identical operating condition and compared thoroughly. Figure 8-1 shows the variations of steady-state mass flow rate with input power of 2D and 3D

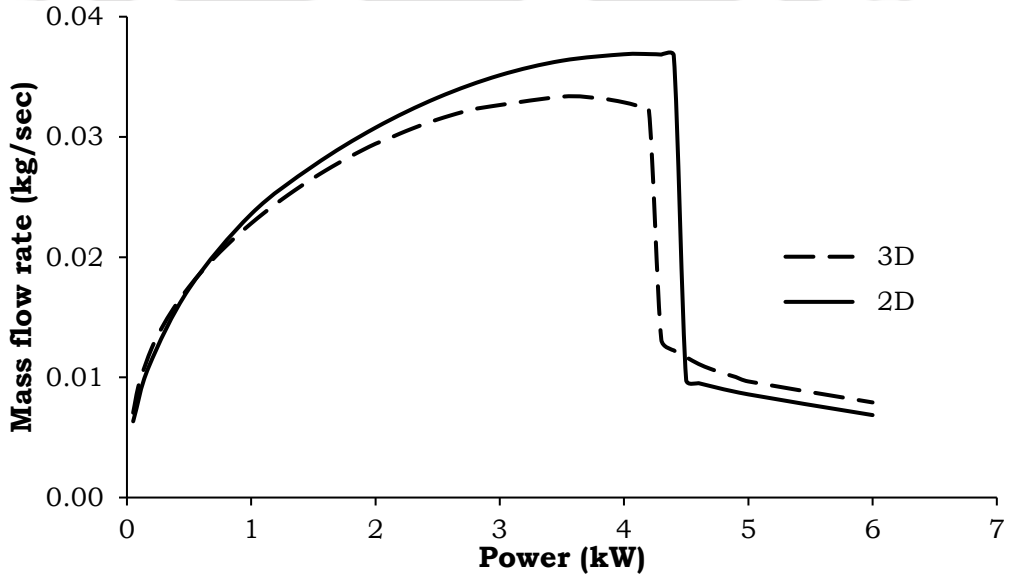

Figure 8-1. Variations of mass flow rate with input power for 2D and 3D models (285 K sink temperature and 10 MPa system pressure)

models, both are operating at 10 MPa system pressure and 285 K sink temperature. The results for 2D model slightly deflected from 3D results, due to nonappearance of θ variation of flow properties. To reduce computational cost, the elimination of θ variation of flow properties have been allowed and goes for further simulations.

8.3. Grid Generation and Mesh Sensitivity Analysis

Structured non-uniform grid system is developed to engulf the entire computational domain, with finer meshes near the wall for acquiring larger

Table 8-1: Details of 2D grid systems

Model	Model 1	Model 2	Model 3
Number of nodes	41902	83722	125624
Number of cell	40880	81680	122560
Average velocity (m/s)	1.184	1.179	1.174
Average temperature (K)	322.973	322.927	322.901
Mass flow rate (kg/s)	2.213	2.241	2.255

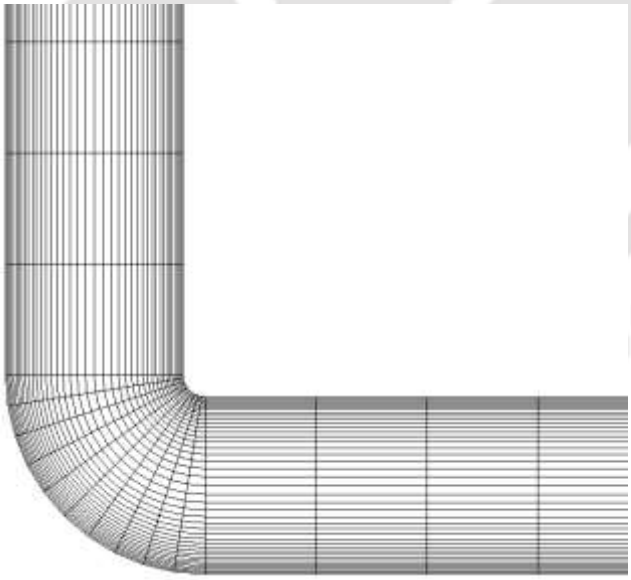

Figure 8-2. 2D Grid system for transient analysis

gradients of field variables within concerned boundary layers. To alleviate the concern with the grid-reliance of the final solutions, each of the developed geometries are subjected to several grid structures. Table 8-1 summarizes the details of three different mesh structures employed for the transient study.

Corresponding cross-sectional views at the center of the source are shown in Figure 8-2. It is clearly evident that the increase in the number of cells from model 2 to model 3 yields less than 0.3% change in the magnitudes of loop-averaged quantities and steady-state mass flow rate. Important mesh properties like average skewness and orthogonal quality are also found to be satisfactory for model 2 and consequently it is selected for simulation.

8.4. Time Step Refinement Analysis

For the study of transient analysis of SCNCL, a 2D model of rectangular NCL has been developed and simulated by using ANSYS-Fluent 15. It has been known to all that the first footstep of any transient analysis is time step refinement study, which is more likely as grid independence study. For the same, three different times are selected as time step, which are 1, 0.1 and 0.01 seconds. The operating condition of the system was selected as 700 W/m^2 source heat flux, 355 K sink temperature and 10 MPa pressure. The outcomes of time step analysis are shown in Figure 8-3 and after fully scrutinize the results 0.1 second has been selected as time step for further simulation. All the subsequent simulations are performed with 10 MPa system pressure.

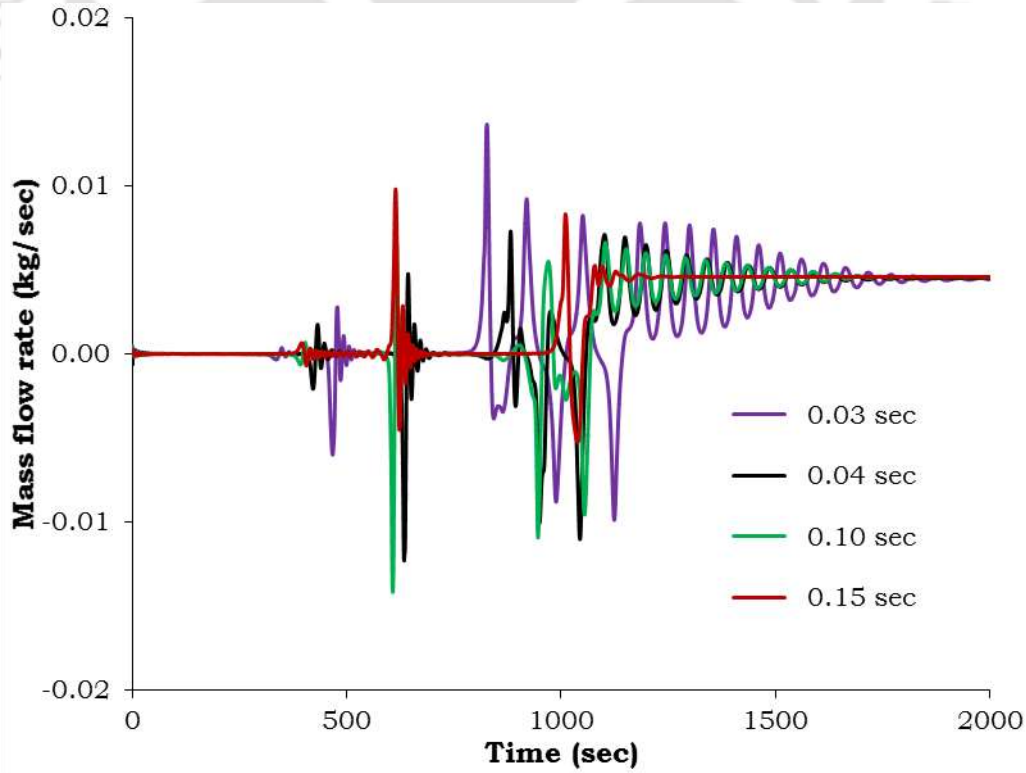

Figure 8-3. Time step refinement analysis

8.5. Results and Discussion

Flow rate in any natural circulation system being dependent on the interaction of forces and extremely sensitive to all involved system parameters, NCLs are always susceptible to instabilities. It can also be attributed to the non-linear nature of the phenomenon, as any change in the driving force affects the flow. Which in turn affects the driving force itself, possible leading to either a self-correcting action or an oscillatory behavior. It is highly desirable to identify possible zones of instability in SCNCL operation, as unstable fluctuations can lead towards severe consequences in nuclear systems. Hence most of the studies on SCNCL have focused on stability evaluation.

The most important and essential part of the numerical study is the validation of the numerical model with available experimental data. Thus, the developed 2D model has been validated with the experimental data. One of the main reason for requirement of validation is that all the numerical results are estimated by the iterative process and hence it is an approximate value. Thus, to check the correctness of the model, it is necessary to compare the predicted results from developed computational model with the relevant experimental or analytical data to authenticate the code before proceeding for further simulation. Operating condition of the computational model for generation of numerical results for validation is needed to be identical with main part of investigation, even it is same for the generation of dimensionless results. Hence, operating pressure and sink temperature of the model for validation are chosen as 10 MPa and 285 K respectively for various input heat flux. The numerical results were compared with the experimental data of Lomperski et al., 2004 and the experimental correlation of Swapnalee et al., 2012. Both the above mentioned models are three dimensional and operated in supercritical condition with sCO_2 as working fluid. Here, non-dimensional numbers are compared for all the loops and results are shown in Figure 8-4. It has been observed from Figure 8-4 is that, an amicable agreement is achieved over the complete range of parameters considered on a non-dimensional plane. The fruitful results of validation study is endorsed the use of the computational model for subsequent study.

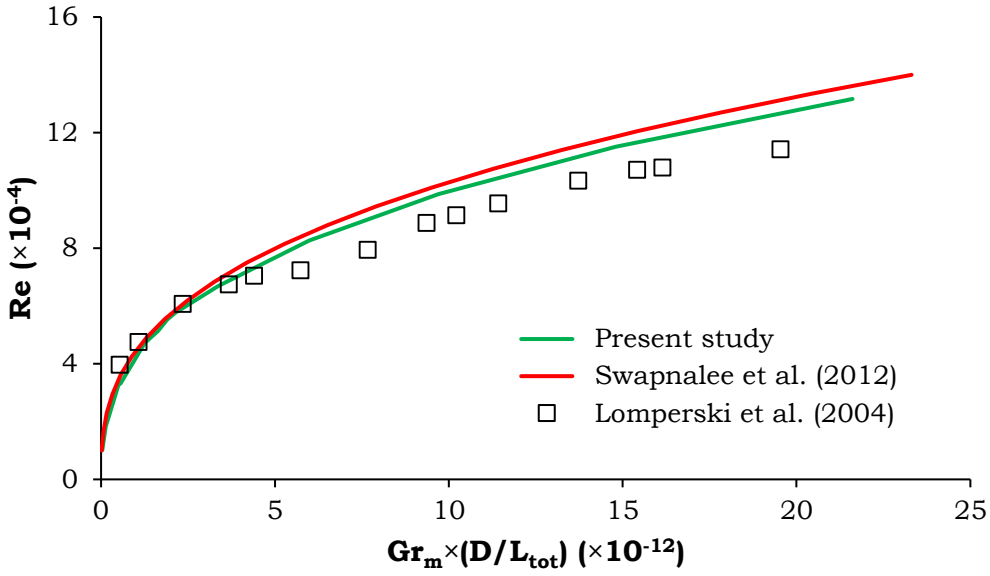

Figure 8-4. Comparison of present model (2D) prediction with existing experimental data in literature

8.6. Stability Analysis of SCNCL

Both, the static or dynamic both type of instability may be occurred in the operation of SCNCL. In case of the steady-state instability, by applying a small perturbation over the steady-state condition the system goes to another steady-state condition. Only steady-state governing equations are sufficient to find out the threshold for this type of instability. On the other hand, if a small perturbation over steady-state condition makes the system with sustained or diverging flow oscillations, then the system is considered to be under dynamic instability. The inertia and feedback effect take an active role for creation of dynamic instability in SCNCL. To find out the threshold for dynamic instability the time dependent conservation equations must be solved.

In this chapter the stability analysis has been performed by nonlinear approach. Time dependent conservation equations of mass, momentum and energy are solved in time domain by using ANSYS-Fluent 15. The simulations begin with a 'zero' initial condition and continued with time step of 0.1 second. Here, the system is considered stable, unstable and neutrally-stable (Figure 8-5) according to the amplitude of flow oscillation.

- ✓ Stable: amplitude of flow oscillation dies out with time.
- ✓ Neutrally-stable: amplitude of flow oscillation is constant with time.
- ✓ Unstable: amplitude of flow oscillation increases with time.

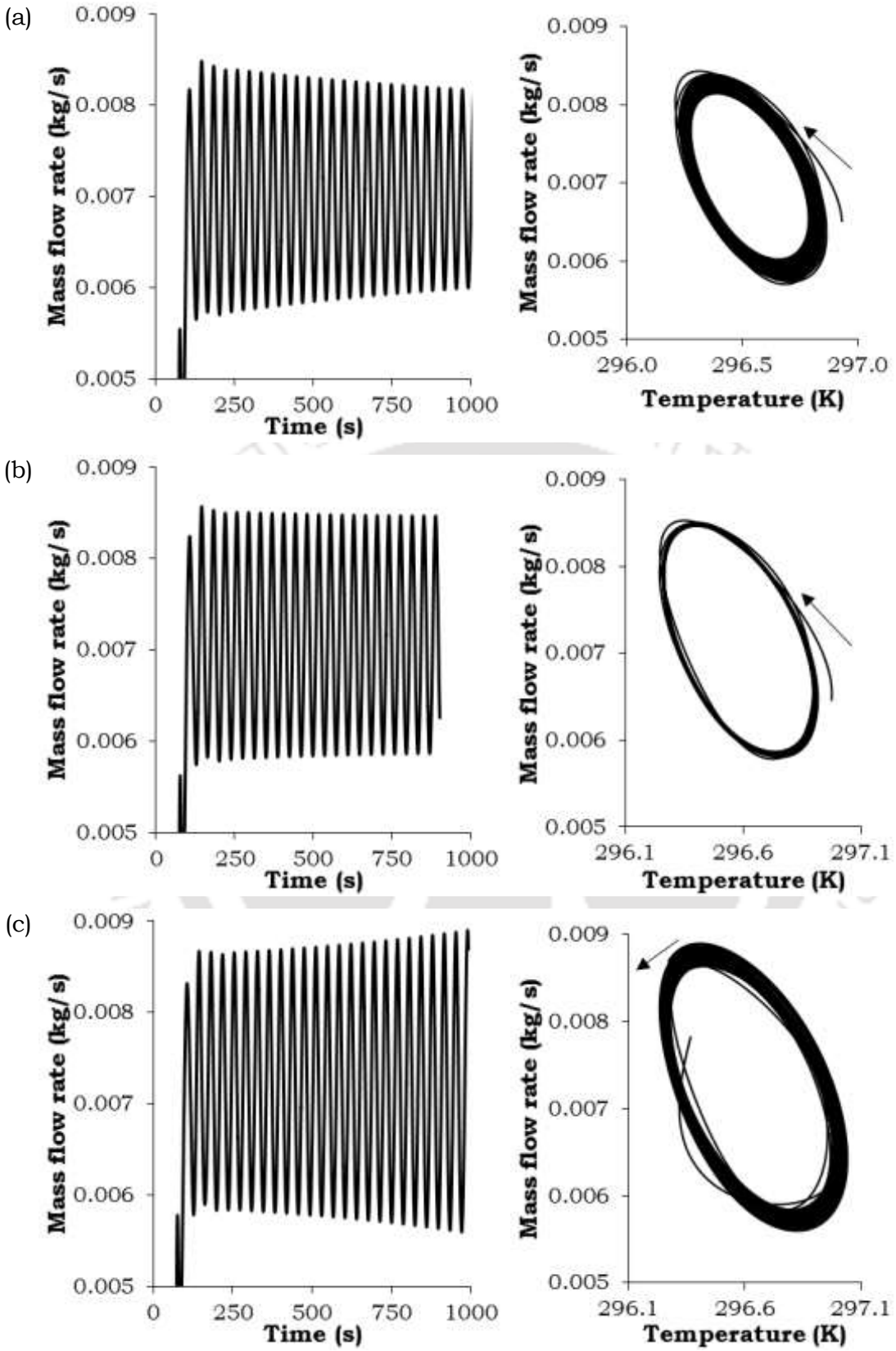

Figure 8-5. (a) Stable (1600 W/m^2) (b) neutrally-stable (1650 W/m^2) and (c) unstable (1700 W/m^2) systems and corresponding phase portrait at 295 K sink temperature and 10 MPa operating pressure.

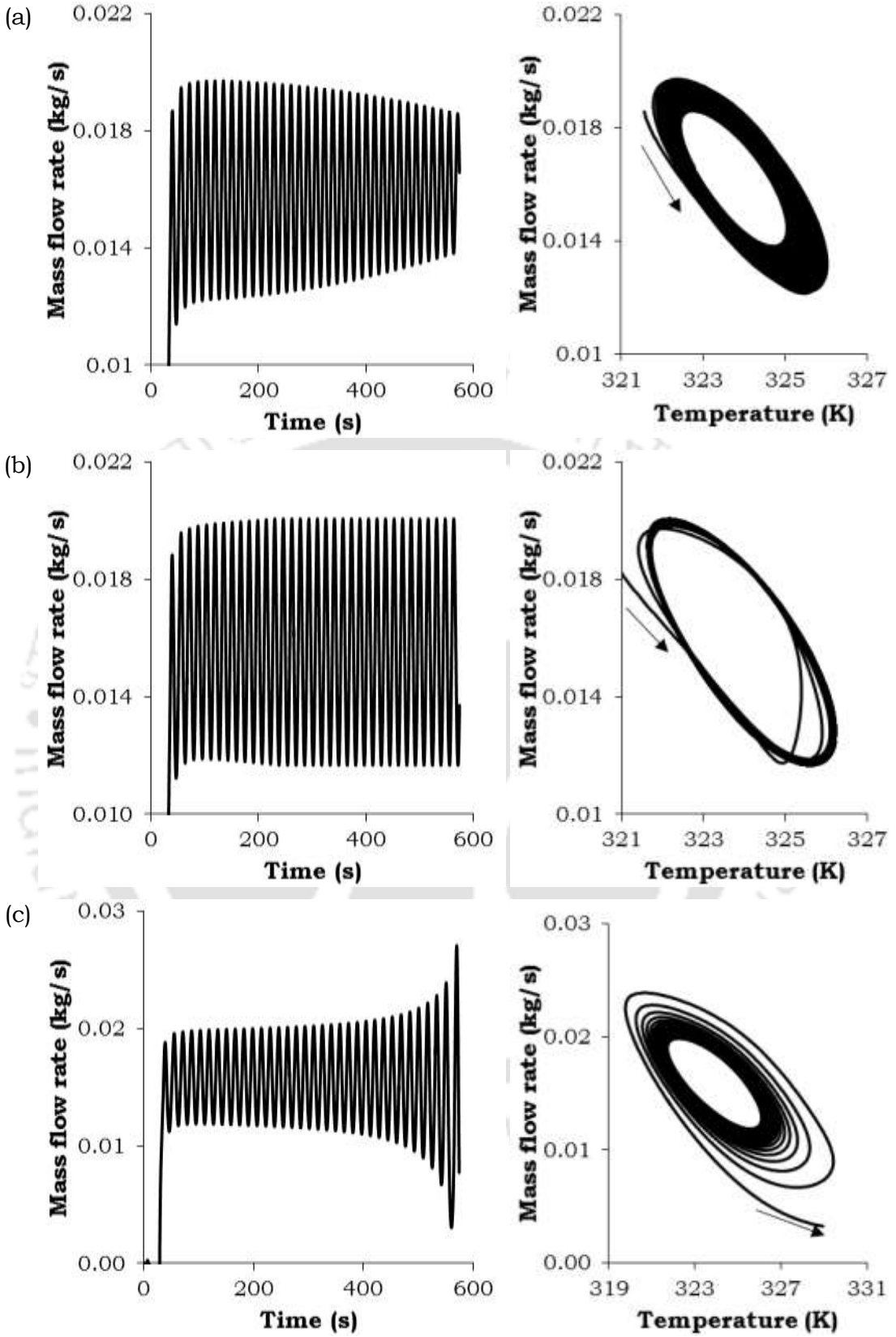

Figure 8-6. (a) Stable (11700 W/m^2) (b) neutrally-stable (11650 W/m^2) and (c) unstable (11600 W/m^2) systems and corresponding phase portrait at 315 K sink temperature and 10 MPa operating pressure

The neutrally-stable points take a crucial role in generation of stability map. Here two different stable zones are observed, namely lower and upper lower stable zone. Figure 8-5 and Figure 8-6 are shown with the three different stability conditions, for two different sink temperatures, which are 295 K and 315 K respectively. The corresponding phase portraits confirm the behavior of stability of the loop.

The stable zones are separated from the unstable zone by the line named as threshold. Thus, two different thresholds are observed, namely the lower and the upper threshold. The system goes from stable to unstable region by crossing the lower threshold at a low power level, due to the erratically change of buoyancy force. Similarly, the system goes from unstable to stable zone by crossing the upper threshold at a high power level, due to the occurrence of active frictional force. The buoyancy and the frictional forces are interplay between each other and make a balance for stable system. In any type of NCL, instability occurs due to the unevenly growing or diminishing of the buoyancy or frictional forces. The haphazardly change of former one is increases the possibility of instability. It has been found that the density changes across the heater section for lower threshold power is large and hence, generated buoyancy force is higher than optimum. As a result the system goes to unstable zone. Figure 8-7 is a combination of steady-state and transient results, which shows the instability threshold points on a steady-state mass flow rate curve. Here, the input power for the upper threshold is directly related with the sink temperature of the system. Whereas, the lower threshold powers are hardly changed with the sink temperature.

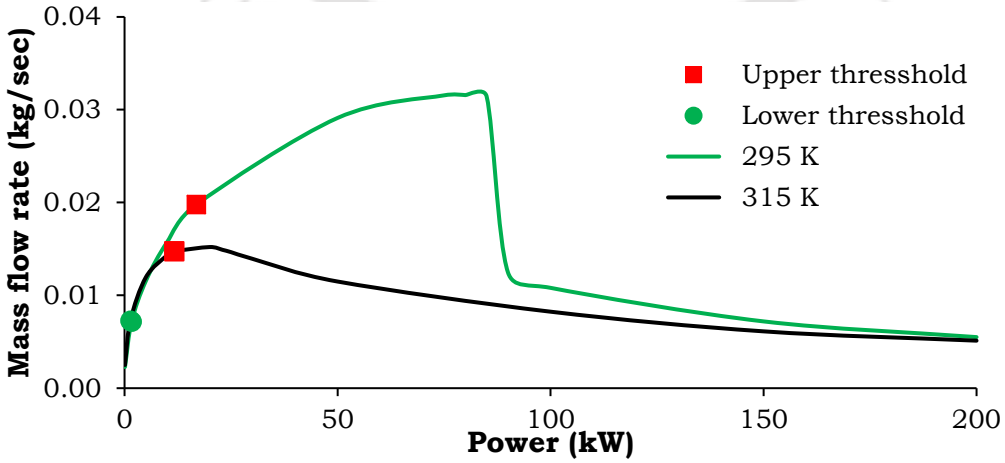

Figure 8-7. The location of upper and lower threshold for different sink temperatures and 10 MPa operating pressure

After tracking out the neutrally-stable points for different sink temperatures, they are joined together to obtain stability map (Figure 8-8). The unstable zone is reduced with increase of sink temperature and after a certain condition no unstable zone is observed. The unstable zone is massive for low sink temperature condition due to the large density gradient over the loop. For the same input heat flux condition, the temperature differential between the heater and the cooler is high for low sink temperature system. Hence, the density differences between the two vertical arms are also very high, which causes the generation of fluctuating buoyancy force. This creation of uneven buoyancy force is the prime cause of such happening. With the increase of sink temperature, the generation of this fluctuating force is reduced and the unstable zone is diminished.

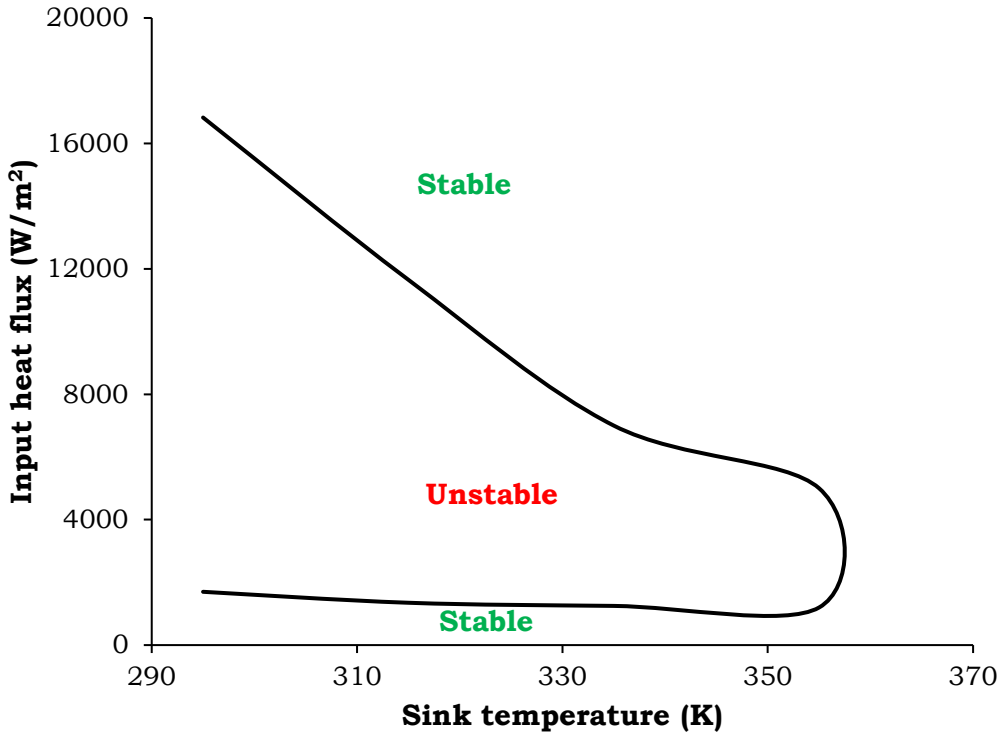

Figure 8-8. Stability map of sCO_2 based loop at 10 MPa operating pressure

8.7. Analysis of Flow Transients

Any stable systems becomes unstable by crossing the stability threshold for both the zones. The flow field of unstable zone recognized in the current study, behaves like Lorenz chaotic flow (Ambrosini, 2008; Jiang and Shoji, 2003; Ridouane et al., 2010). The temporal evolution of mass flow rate for 11500 W/m² input heat flux are shown in Figure 8-9, which represents a

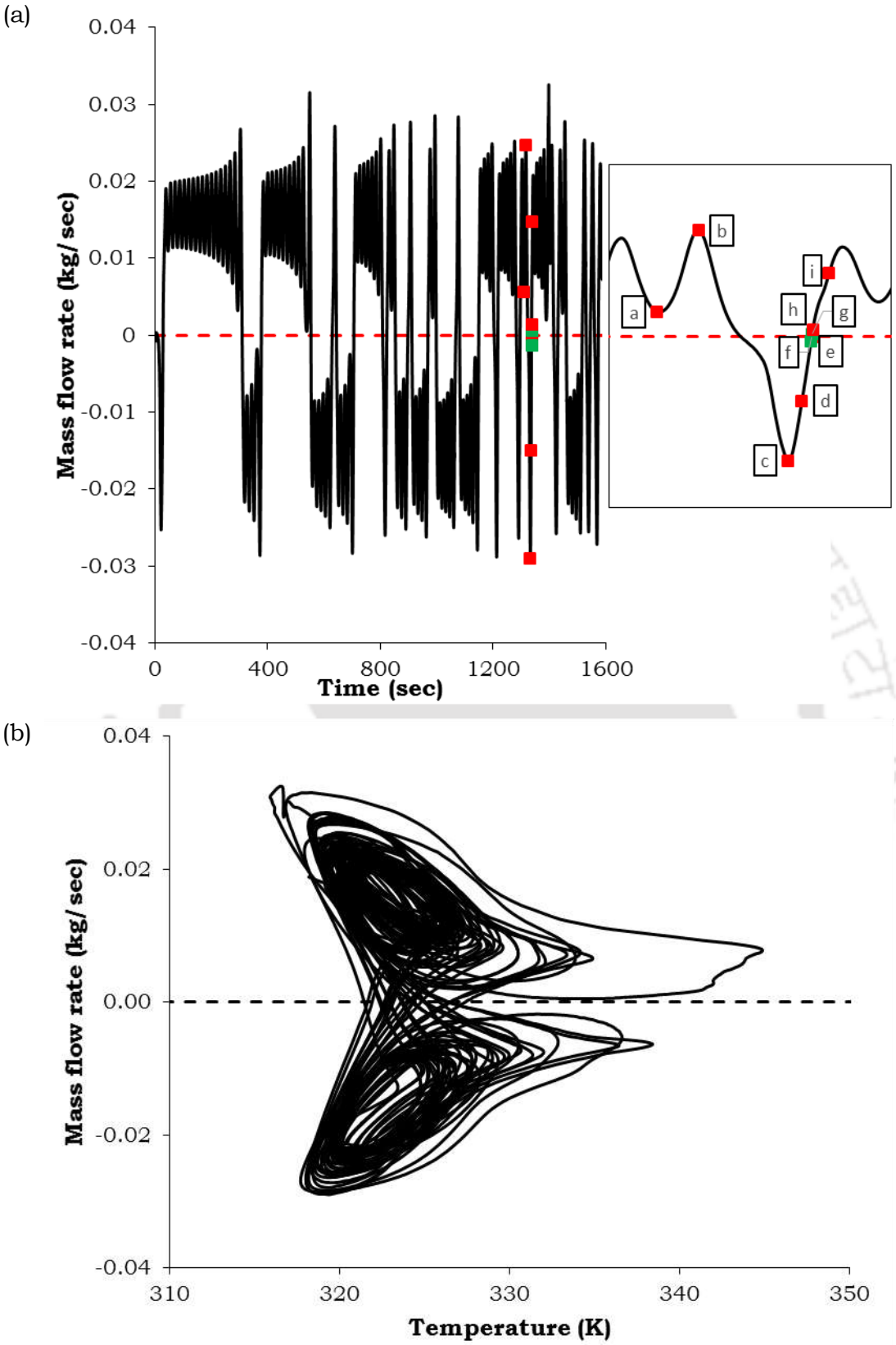

Figure 8-9. Temporal variation of (a) mass flow rate (Lorenz chaos) and corresponding (b) phase portrait (operating condition: 10 MPa pressure, 315 K sink temperature and 11500 W/m^2 input heat flux)

typical variation of the x variable in the original three-variable Lorenz model. The sign of the mass flow rate is changed when the flow direction is altered. Here, positive and negative values of the mass flow rate indicates the direction of flow in CW and CCW respectively. The corresponding phase portrait confirms the existence of bidirectional pulsing flow (Jiang and Shoji, 2003; Misale et al., 2011). Before changing the direction, the mass flow rate oscillates with growing magnitude until it reaches an optimum amplitude. Once, the highest or critical amplitude occurs, then the flow changes its direction and a new sequence begins with a new sets of oscillations. Generally, after changing the direction of flow, oscillations grows gradually until the next change, but if the first peak in a given direction is huge, then the flow direction reverses rapidly without additional increases in oscillation amplitude.

The occurrence of flow reversal and Lorenz chaos can be explained by following the positive feedback mechanism (Chen et al., 2010; Jiang and Shoji, 2003). Assuming the system is in equilibrium state and flow is in CW direction, and an anomalous warm pocket of fluid is considered in outlet zone of the heater section. Due to the additional hot condition of warm pocket the generation of buoyancy force is higher and thus a positive acceleration in the CW direction is added and speeding up the flow rate. Because of the higher flow rate this pocket cools less on its journey across the sink section and emerges from the cooler as warmer fluid than it was in its previous journey. As a result, buoyancy force presence in downcomer section is reduced and the speed of the fluid is slowed down. The motion of the fluid is decelerated, but continues to flow in CW direction and hence time of heat up is more while passing the heater section. Upon arriving again at the same location, the pocket is get once again warmer than former condition, by a larger amount than before. This time, the occurrence of buoyancy force to accelerate the fluid flow is higher than previous pass, since the instability has been magnified. Again, while crosses the sink section, less time is required to cool off the pocket than the previous pass and the instability continues to grow, decelerating the CW flow. Amplification continues until the buoyant force generated by the pocket at riser grows large enough, that, as a result cooler inlet and outlet fluid temperature becomes same and thus causing the flow to stop. With no flow in the loop, once again the temperature gradient between heater and cooler sections grows undisturbedly, and at an optimum condition flow begins on any direction and is repeated the behaviour indefinitely.

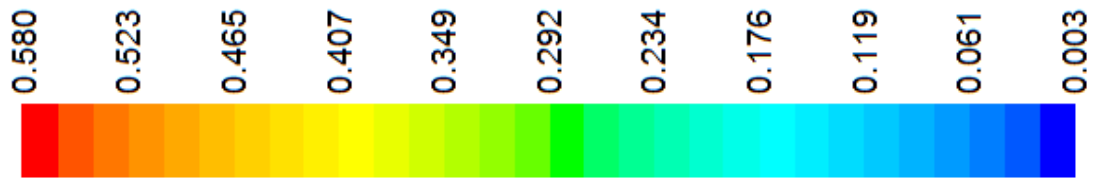

Color map for 1308.5 sec

(a) 1308.5 sec

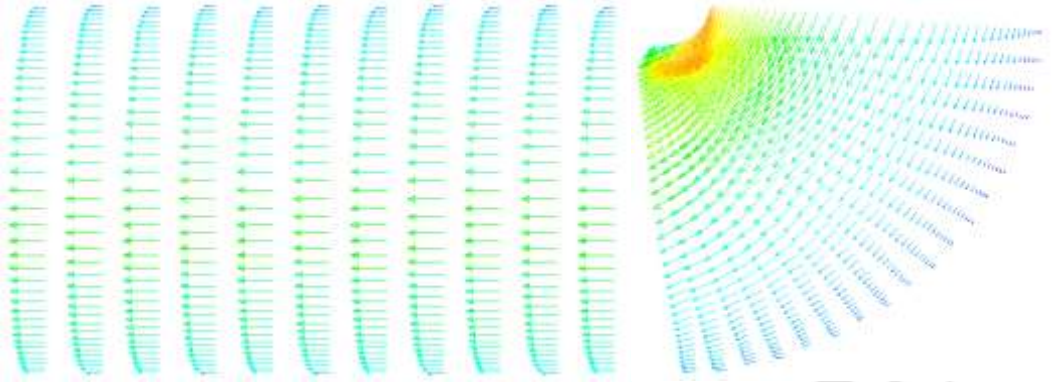

(b) 1315.8 sec

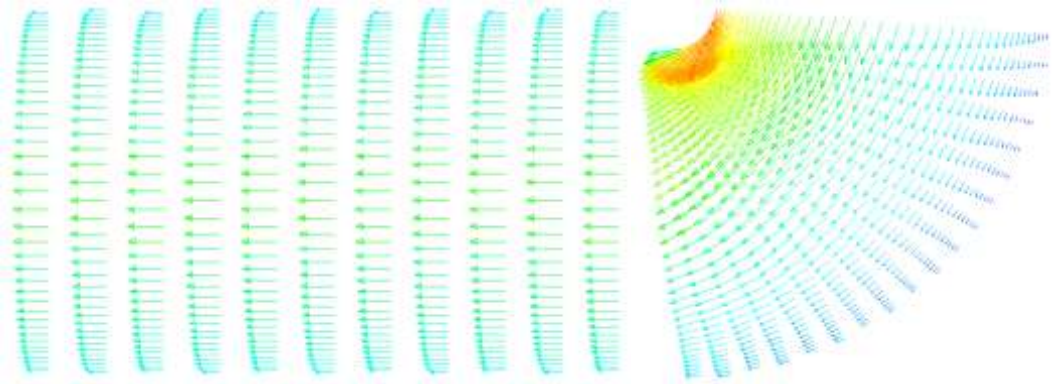

(c) 1331.7 sec

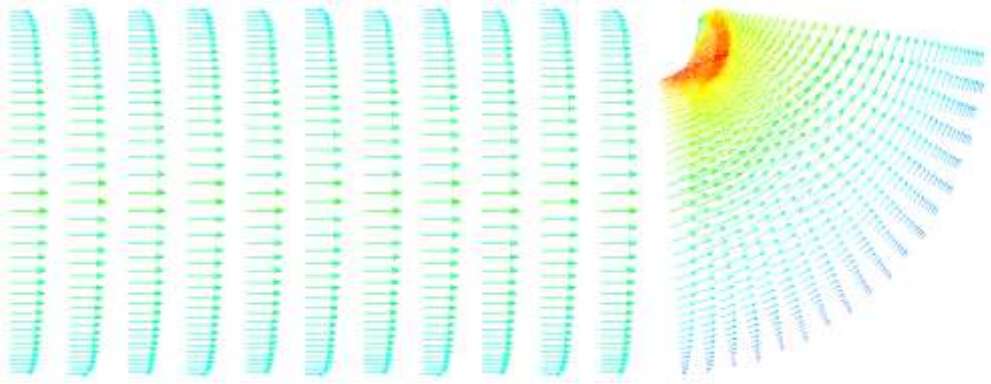

(d)

1334.
2 sec

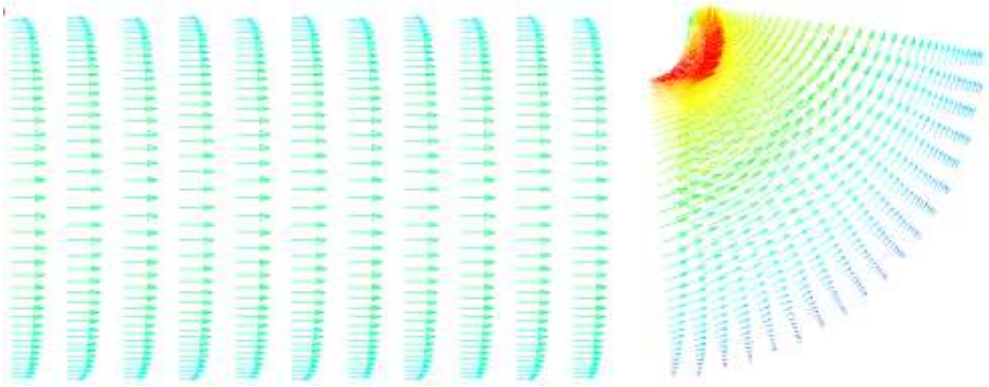

(e)

1335.
8 sec

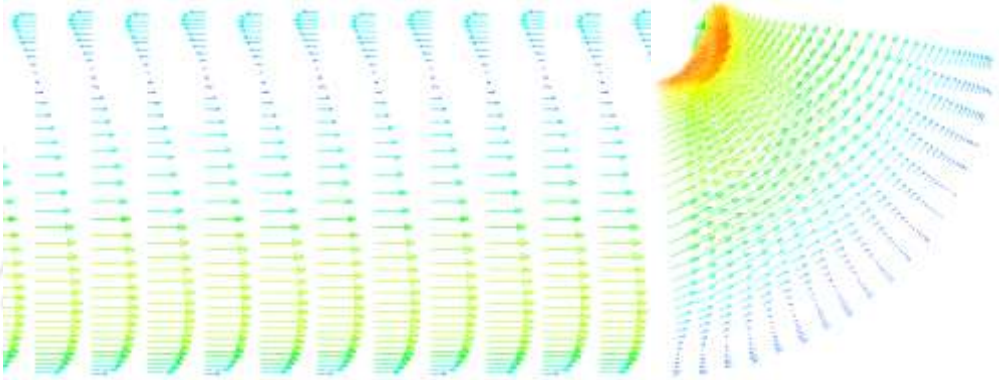

(f)

1335.
9 sec

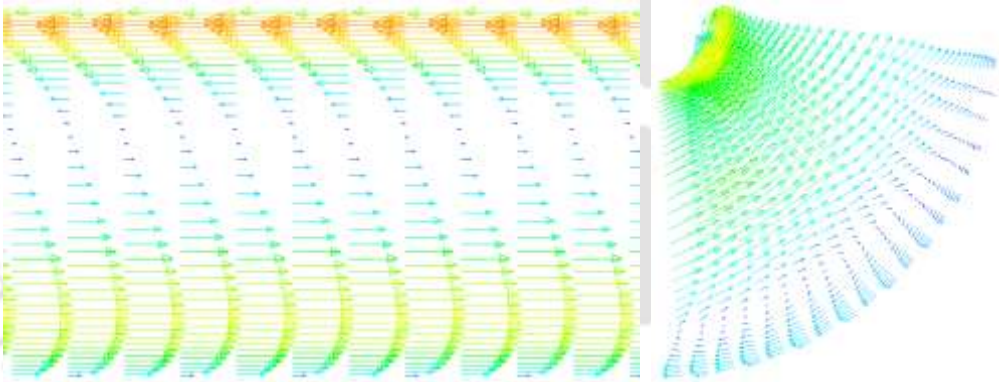

(g)

1336.
0 sec

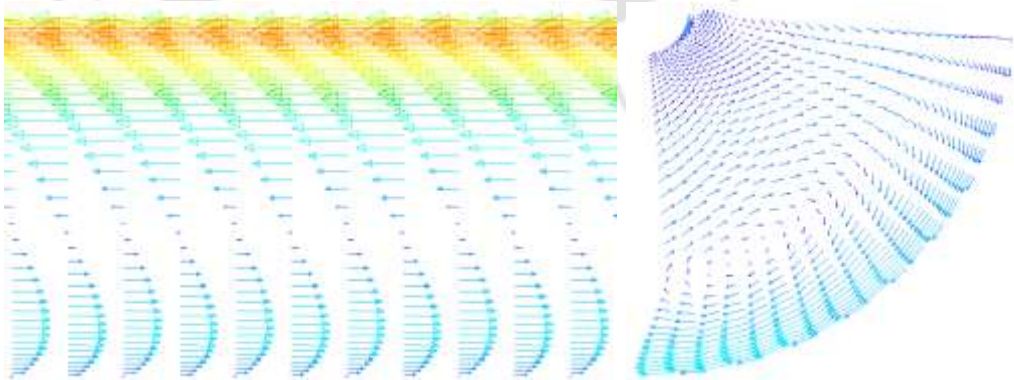

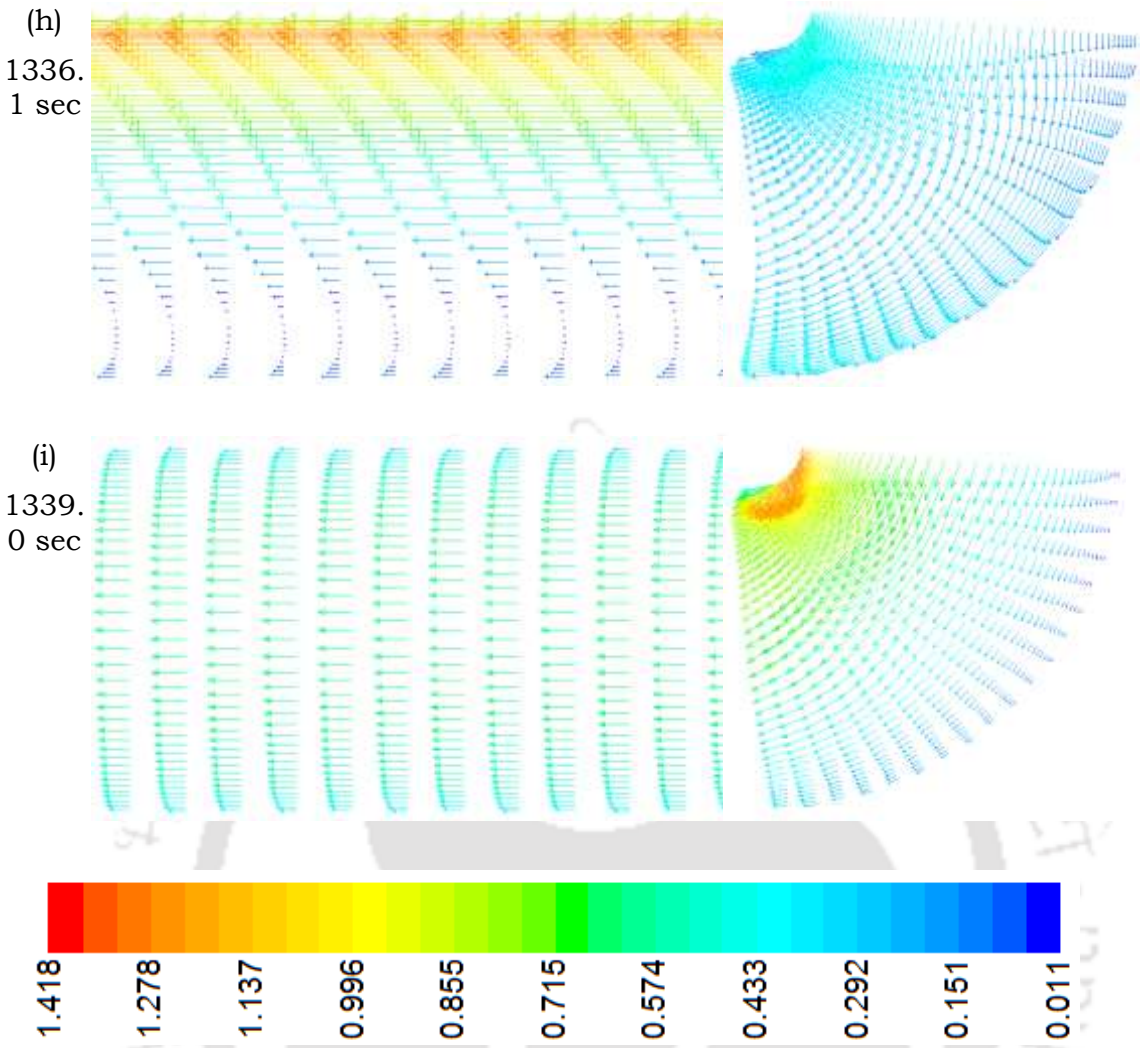

Color map for 1339.0 sec

Figure 8-10. Vector plots for the points a, b, c, d, e, f, g, h and i of the Figure 1-9 (a).

To observe the flow field in the loop, the vector plots of mid-portion of the source section and elbow section of bottom right corner of the loop are plotted in Figure 8-10. The color maps are included here for two optimum cases (1308.5 and 1339.0 second), others are included between these ranges. Figure 8-10 a, b and c are shows the vector plots for three different optimum condition corresponding to points a, b and c in Figure 8-9. The direction of mass flow rate of points a and b are CW, while for point c is CCW. The flow behavior during the transition from CCW to CW is shown in Figure 8-10 d, e, f, g, h and i. The points are selected for vector plots are d, e, f, g, h and i in Figure 8-9. Figure 8-10 d and i represents the fully developed CCW and CW mass flow rate at the instants of t = 1334.2 s and t = 1339.0 s respectively. Point's e and f are in CCW and g and h are in CW mass flow rate condition

with increment of 0.1 second time, and the nature of flow observed is chaotic in nature. At the time of changing the flow direction, the vortex are occurred at elbow sections of the loop, while in horizontal and vertical sections flow changes gradually from CW to CCW. Due to the presence of local buoyancy, the fluid near the upper wall of the heater section and the lower wall of the cooler section are affected first and changes its direction from the corresponding locations.

8.8. Dynamic Performance Assessment of SCNCL

The operating condition of any practical power system is always expected to undergo frequent changes to synchronize with the demand network. SCNCLs being prone to instability and such swift alteration of power can always induce unstable fluctuations on the system. Thus, according to the stability analysis point of view, the observation of system responses for dynamic input power is an utmost important fact (Tilak and Basu, 2015). Therefore, to observe the dynamic behavior of SCNCL, the system is subjected to a few standard variation in heater power. Here, all the simulations are performed for dynamic performance evaluation over a stable solutions (base conditions) and then observed the nature of system response. With respect to stability map (Figure 8-8), two arbitrary stable points (700 W/m^2 and 17050 W/m^2 on lower and upper stable zones respectively) are chosen for different sink temperatures (355 K and 295 K) and then changed the power levels to unstable zone (1500 W/m^2 and 15000 W/m^2) by various possible ways. Input heat fluxes are mainly altered by three ways, which are directly, gradually (10 sec) and slowly (30 sec) to final state and then continued. Some cases are considered where the system again comes back to its initial input condition by same rate and then continued. Also few special cases are considered, where the system holding 10 seconds in changed input level and then comes back to initial condition with identical rate and then continued.

Figure 8-11 a and b are show the real situation of 700 W/m^2 and 1500 W/m^2 input heat flux condition, when simulated directly from 'zero' initial condition. Here, the first case is clearly evident of the stable system, whereas the second one is unstable system. To observe the dynamic response of the

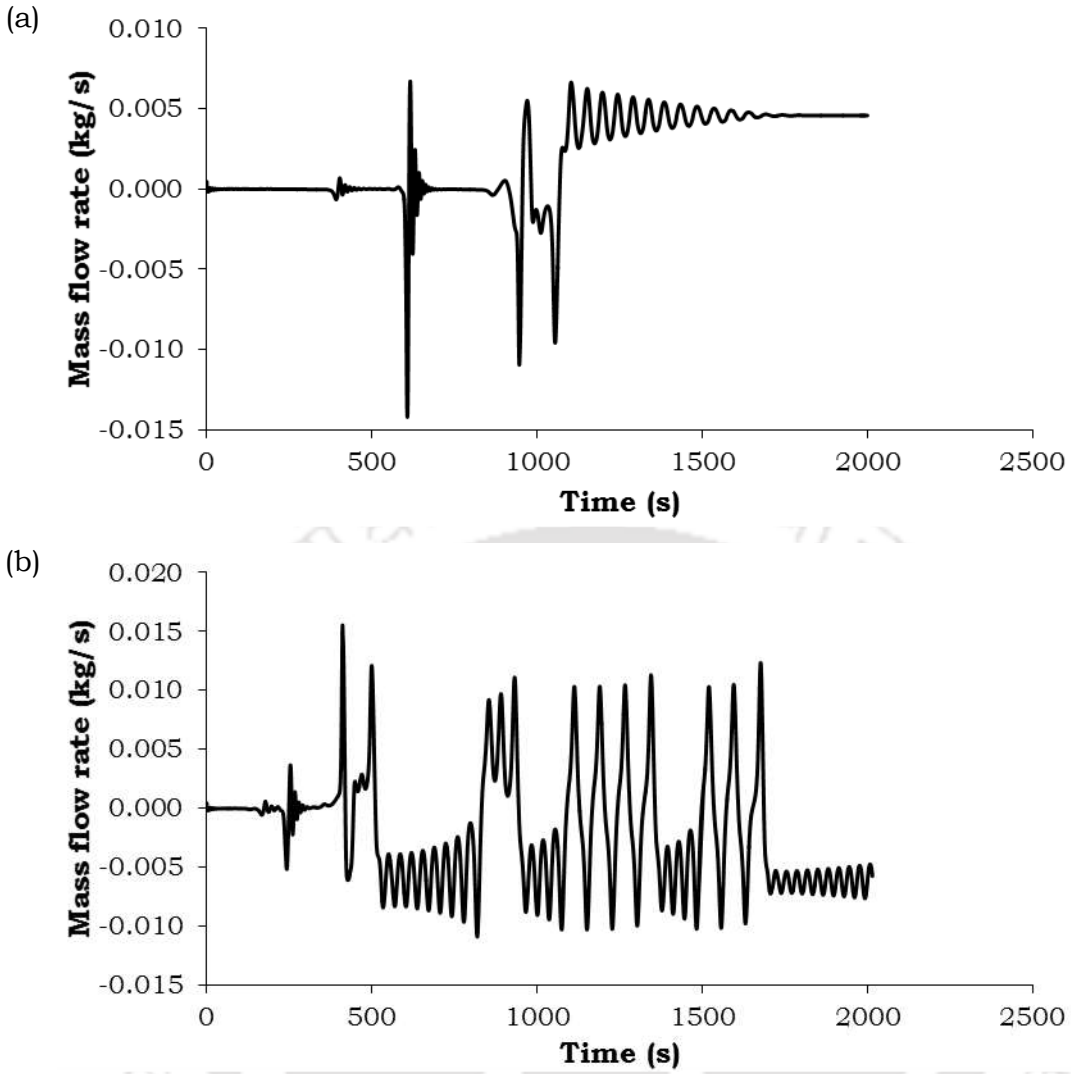

Figure 8-11. Mass flow rate distribution for (a) 700 W/m^2 and (b) 1500 W/m^2 heat flux and 355 K sink temeperature

system, 700 W/m^2 input heat flux condition is chosen as 'base case' for lower threshold. Broadly, 'base case' is basically a point placed in bottom stable zone or below the lower threshold of the stability map. The main aim of this study is to observe the system performance after applying a perturbation to the 'base case'. Hence, after selecting the 'base case' input heat flux changed to 1500 W/m^2, which is basically a point placed on purely unstable zone (in Figure 8-8). Various types of UDF are used to make this unsteady heat flux input condition for source section. A detailed discussion over different process of altering input heat flux are thoroughly reported in the upcoming sections.

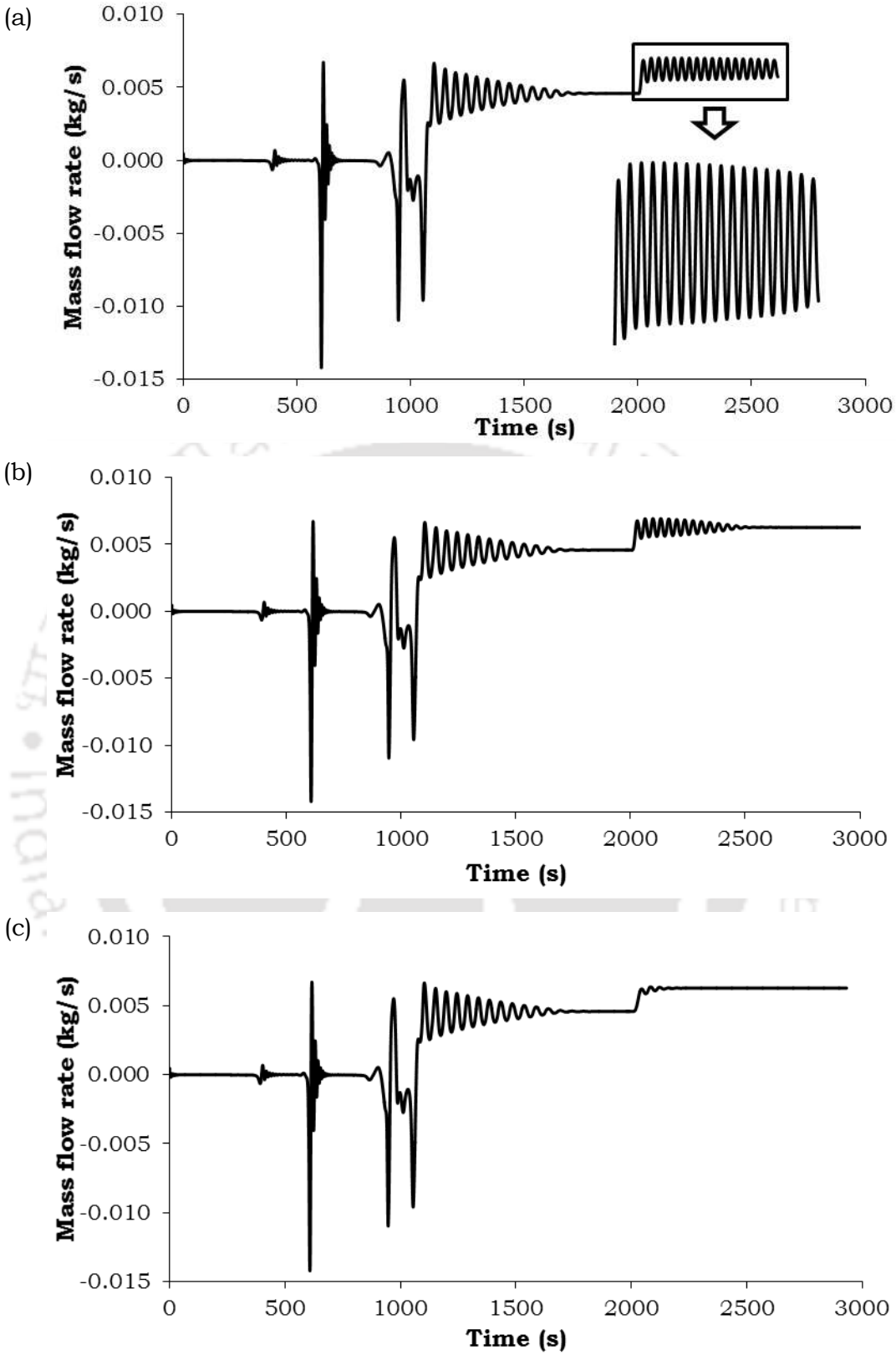

Figure 8-12. Heat flux inreases from 700 W/m^2 to 1500 W/m^2 by (a) directly (b) gradually (in 10 seconds) and (c) slowly (in 30 seconds), then continued at that condition for further simulation

The first variation of the process of altering input heat fluxes are three types, which are directly, gradually (10 sec) and slowly (30 sec) to final state and then continued. All the above mentioned input heat flux altering processes are shown in Figure 8-12. In this cases, the final heat fluxes are different from the initial heat fluxes. Figure 8-12 a, b and c are show the process of changing heat flux by directly, gradually and slowly respectively. In all the cases, the systems are found in stable condition. The second variation of the process of altering input heat fluxes are two types. Similar to first variation, here also system goes to 1500 W/m^2 condition by gradually and slowly increasing the of heat fluxes by means of UDF (Figure 8-13). Here the

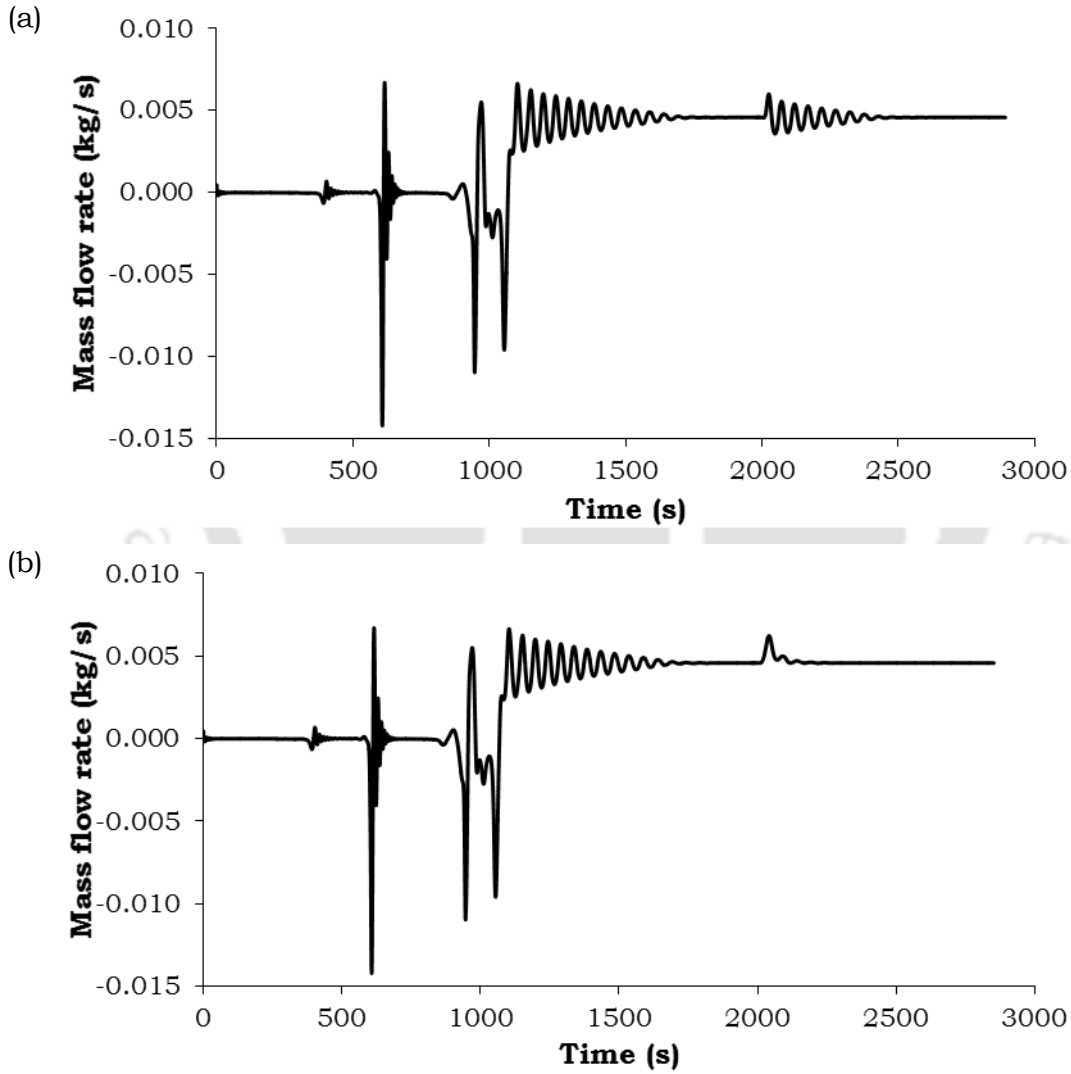

Figure 8-13. Gradually increase heat flux from stable base condition to1500 W/m^2 in (a) 10 seconds and (b) 30 seconds, after that again decrease to 700 W/m^2 in (a) 10 seconds and (b) 30 seconds and continued for further simulation.

only difference is that, the system again comes back to its initial input condition (700 W/m^2) by same rate and then continued with this condition. Here, the initial and the final input heat fluxes are same. In this situation also both the cases finally goes to stable condition.

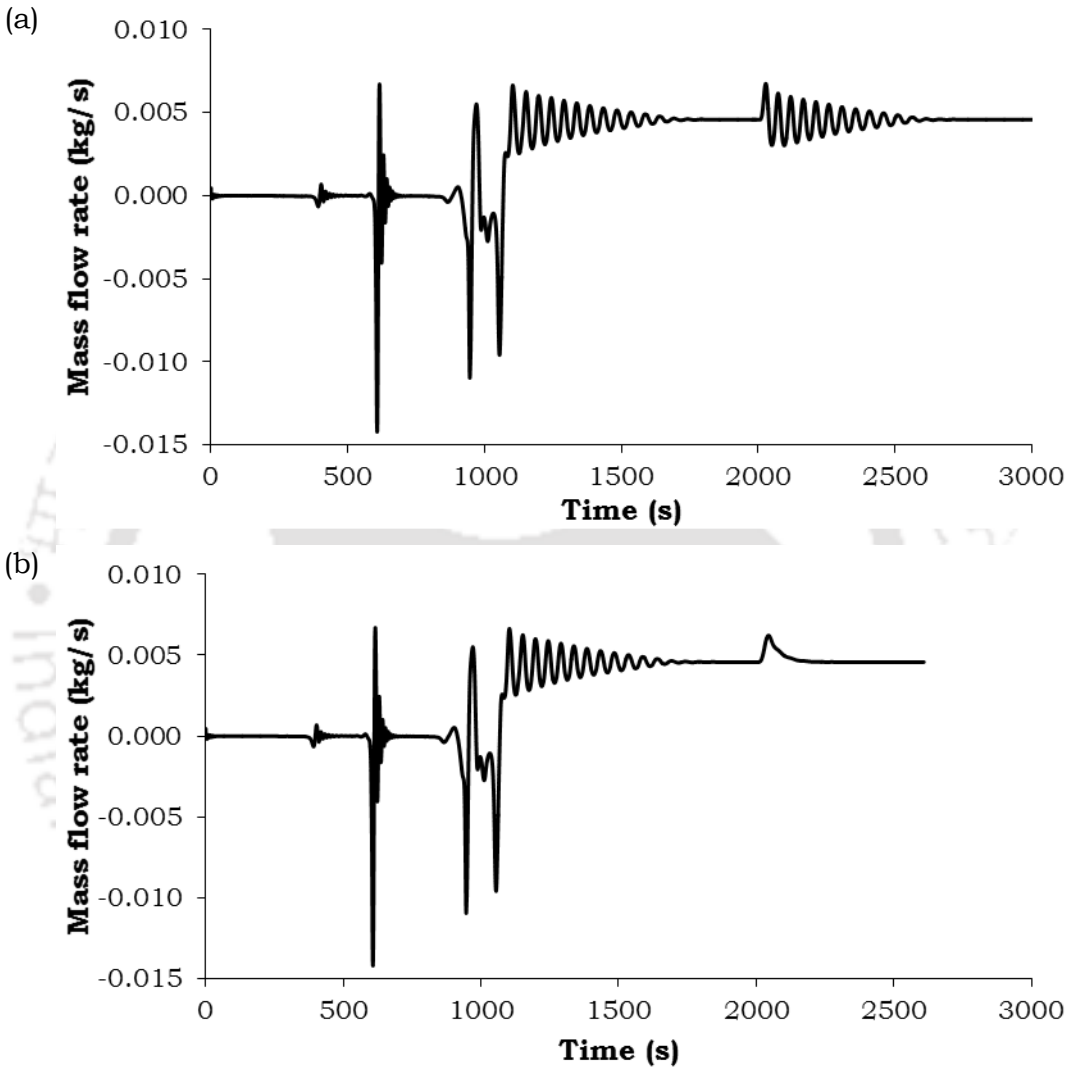

Figure 8-14. Gradually increase heat flux from stable base condition to 1500 W/m^2 in (a) 10 seconds and (b) 30 seconds, after that hold 10 seconds and then again decrease to 700 W/m^2 in (a) 10 seconds and (b) 30 seconds and continued for further simulation.

The last categories of the process of altering input heat fluxes are also two types. Here also the initial and final input heat fluxes are same. Figure 8-14 a and b show the corresponding results of the gradually and slowly changing input heat fluxes respectively. In this special cases, the systems are holding for 10 seconds at changed input power level (1500 W/m^2) and then

comes back to initial condition with identical rate and then continued with that condition. Similar to previous categories, here also after some periodic oscillations the system finally goes to stable condition.

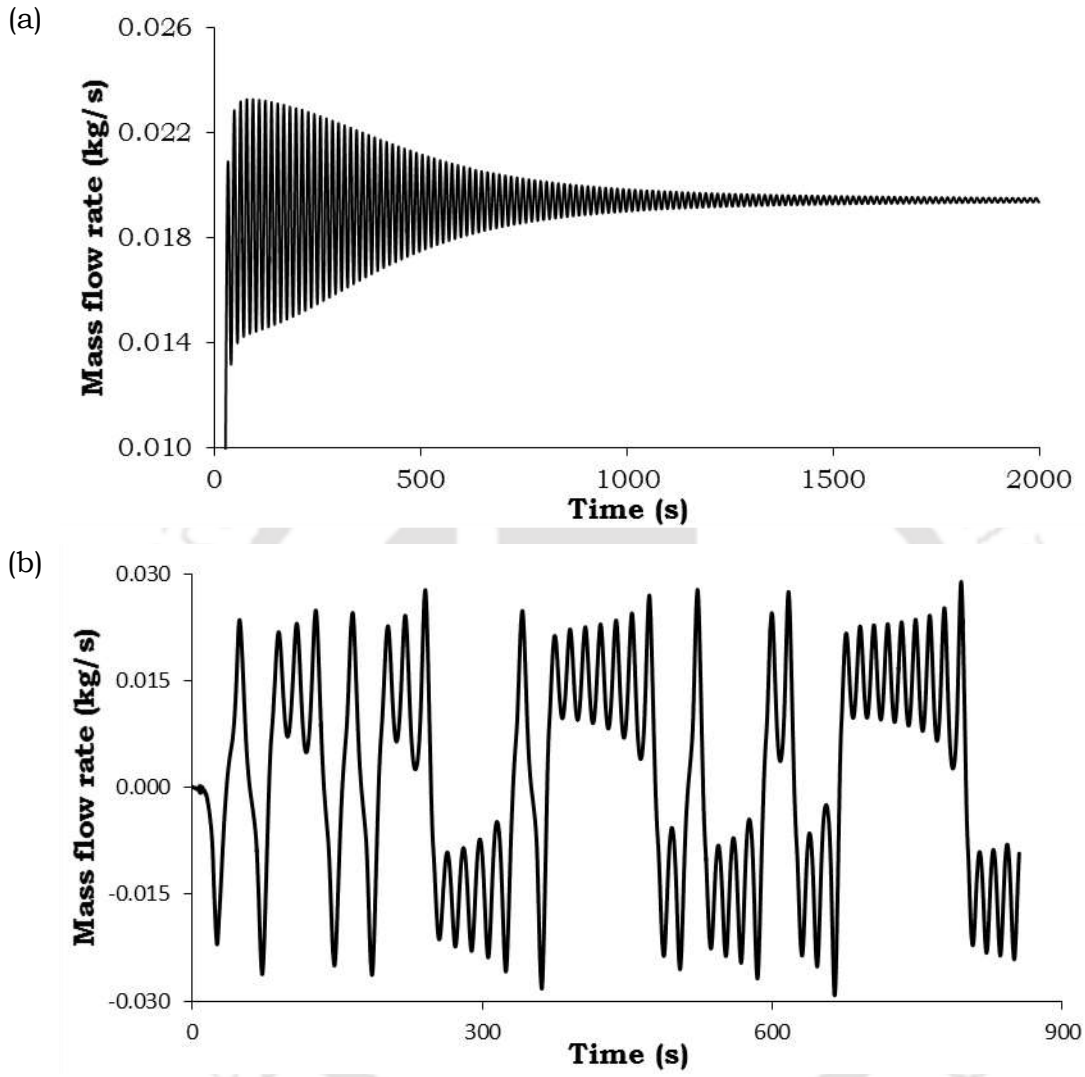

Figure 8-15. Mass flow rate distribution for (a) 17050 W/m^2 and (b) 15000 W/m^2 heat flux for 295 K sink temeperature

A thorough dynamic performance study suggested that, the maximum amplitude of oscillation is decreased with perturbation time. The main outcomes of this section of study is that for all the cases the systems are finally gone to stable condition. Whereas, the system (1500 W/m^2) is purely unstable (Figure 8-11b) when it directly operate from 'zero' initial condition. The amplitude of oscillations are extremely depended on the span of the perturbation. Although, the final state of the systems are stable, the process of changing input heat fluxes greatly affects the systems performance. A direct change of input heat flux produces a shock to the system and the result is

higher oscillation than slow changes. When the changes are gradually or slowly then the systems gets required time to self-change according to input condition. While, for direct change of input condition the system can't be able to get self-change and thus an uneven oscillations occurs. An additional reason is that, a stable system always tries to diminish the uneven occurrences, which are developed due to the changes of operating parameters and tries to remain in stable condition (Figure 8-12 to Figure 8-14).

As already mentioned that in this discussion two arbitrary stable points (700 W/m^2 and 17050 W/m^2) have been chosen for dynamic performance evaluation of sCO_2 based SCNCL. For the second case, 295 K sink temperature and 10 MPa pressure are considered as operating condition of the system. The real situation of 17050 W/m^2 and 15000 W/m^2 input heat flux condition are shown in Figure 8-15 a and b. In both the cases simulation starts directly from 'zero' initial condition. As similar to previous selection, the first case is clearly evident of the stable system, whereas second one is unstable system. For upper threshold, 17050 W/m^2 input heat flux condition is chosen as 'base case'. Essentially the location of 'base case' is on the upper stable zone or above the upper threshold of the stability map (Figure 8-8). To observe the dynamic response of the system, the input heat flux of the 'base case' is changed to 15000 W/m^2 by various ways. The Figure 8-16 shows the three different processes of changing input heat fluxes from 17050 W/m^2 to 15000 W/m^2, which are directly, gradually (10 sec) and slowly (30 sec) to final state. After reaching the final state the system is continued with that condition for all the cases. To make this unsteady heat flux input condition for gradually and slowly cases, two different types of UDF are used. Here also, the span of perturbation is greatly affects the amplitude of oscillations of the systems. The oscillations is maximum when the changing occurs instantly and the amplitude is reduced according to perturbation time. For all the cases considered here, the final state of the system is unstable. As we know that, a stable system always tries to weaken the uneven occurrences, which are developed due to the changes of operating parameters and tries to remain in stable condition. But, when the uneven occurrences are so high then the system can't hold its state and finally goes to the unstable zone (Figure 8-16). Here, the final condition is 15000 W/m^2, which is basically an unstable system shown in Figure 8-15, located at unstable zone of the stability map (Figure 8-8). So, when input heat flux is reduced from 17050 W/m^2 to 15000

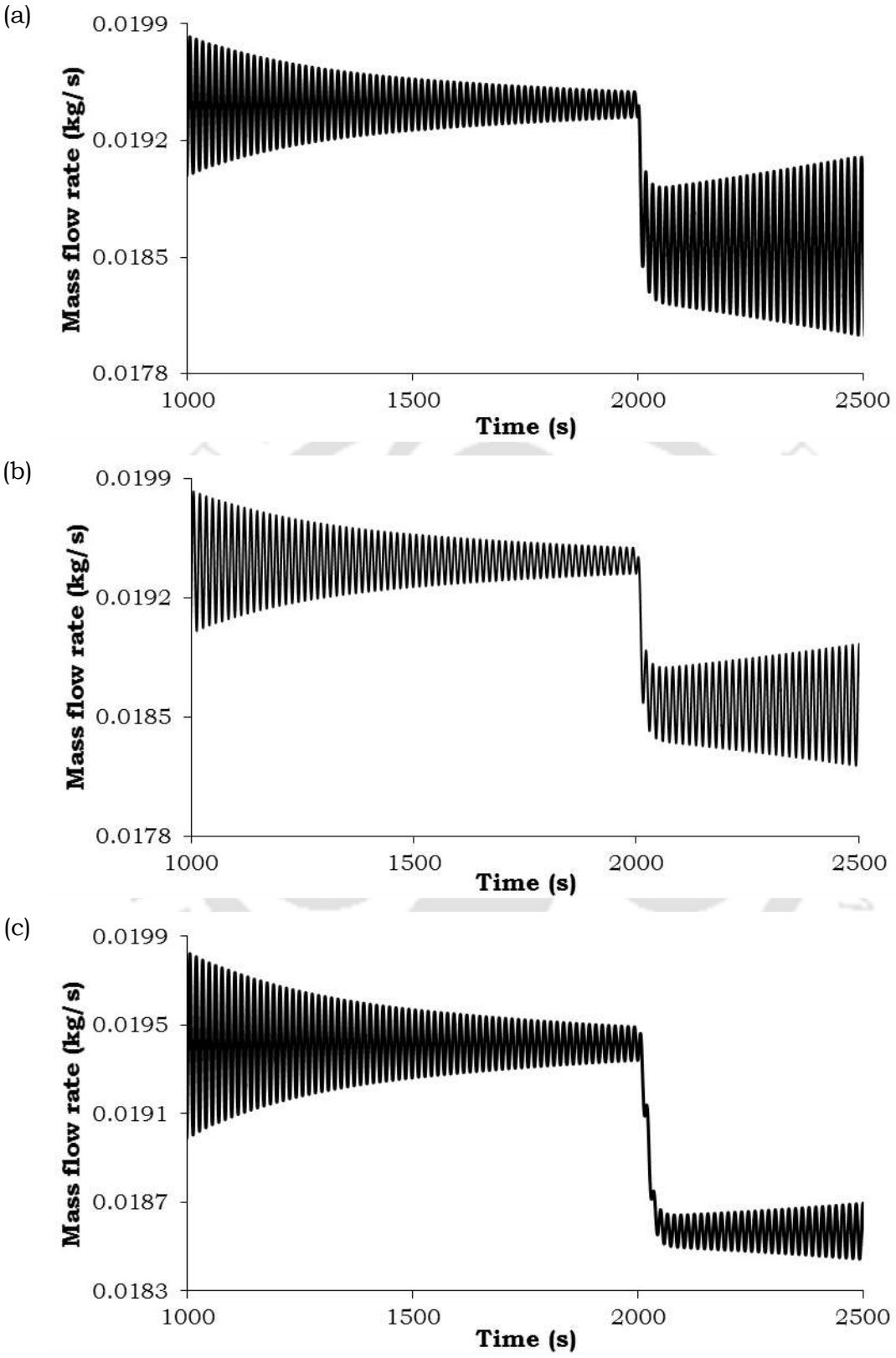

Figure 8-16. Heat flux decreases from 17050 W/m^2 to 15000 W/m^2 by (a) directly (b) gradually (in 10 seconds) and (c) slowly (in 30 seconds), then continued at that condition for further simulation

W/m^2 at low sink temperature (295 K) condition, the available buoyancy force is reduced, but at the same time, the frictional resistance markedly reduced with higher rate and thus the equilibrium condition is broken down and the system finally goes to unstable state.

8.9. Epilogue

To perform a complete study of SCNCL, transient analysis is also important as steady-state analysis. Transient analysis established a clear view over its stability behavior. Stability analysis should be performed for any engineering system to identify the condition for the stable zone of operation. Flow oscillation is sustained as well as is magnified for unstable system, which may cause mechanical vibration of the system and hamper the normal operation. Hence, in the present chapter a thorough investigations have been performed to observe the stability performance of the SCNCL. The system goes from stable to unstable region by crossing the lower and upper thresholds are due to the haphazardly changes of buoyancy and frictional forces. Basically, the buoyancy and the frictional forces interplay between each other and make a balance for the stable system. But, when any of the forces are unevenly growing or diminishing then the system is not capable to sustain in stable state. It has been found that the density changes across heater section for lower threshold power is large and hence generated buoyancy force is higher than optimum, as a result the system goes to the unstable zone. The input power for the upper threshold is directly related with the sink temperature of the system. While, the lower threshold powers hardly changes with the sink temperature.

A complete stability map has been developed with respect to sink temperature of the system. The generated buoyancy force is extremely high for low sink temperature condition and hence unstable zone is extra-large for this condition. The unstable zone is reduced with increase of sink temperature and after a certain condition, this zone is totally obliterated. Before changing the direction, mass flow rate oscillates with growing magnitude until it reaches an optimum amplitude. Once, the highest or critical amplitude occurs, then the flow changes its direction and a new sequence begins with a new sets of oscillations. After changing the direction of flow, oscillations grows gradually until the next change, but if the first peak in a given direction is huge, then

the flow direction reverses rapidly without additional increase in oscillation amplitude.

A Lorenz like chaotic flow is observed in unstable zone of operation of SCNCL. At the time of changing the flow direction, the vortex are formed in the elbow sections, while side by side growing opposite directional flow are observed in the horizontal and the vertical sections of the loop. Due to the presence of the local buoyancy, the fluid near the upper wall of the heater section and the lower wall of the cooler section are affected first and alter the flow direction. A comprehensive dynamic performance study suggests that, the span of perturbation greatly affects the amplitude of oscillations of the systems. The oscillations is maximum when the changing occurs instantly and the amplitude of the oscillations are reduced according to the perturbation time. A stable system always tries to diminish the uneven occurrences, which are developed due to the changes of operating parameters and tries to remain in stable state. But, when the uneven occurrences are tremendously high then the equilibrium condition breaks down and the system finally goes to unstable state. An instant change of input heat flux produces a shock to the system and the result is the generation of higher amplitude of oscillation than slow changes. In case of gradual or slow changes, the systems get required time to self-change according to input condition. Whereas, for instant change of input condition the systems are not able to get self-change and thus an uneven oscillations occurs.

Chapter 9: Conclusions

9.1. Conclusions of the Present Work

This dissertation comprehends, both numerical and experimental evaluation on thermalhydraulic and stability analysis of SCNCL. Several number of computation models have been developed to study the steady-state and transient analysis of SCNCL. Both Dirichlet and Neuman type heating modes are equally importance, according to the design of the system, and hence both are applied in the current study. To enlarge the field of working fluid for SCNCL, here several fluids are used at different operating conditions. To study the influence of various operating and geometric parameters on thermalhydraulics of SCNCL, several numerical investigations are performed successfully. A detailed experimental study has been performed for steady-state and transient analysis of SCNCL, using R134a as working fluid. The aim of present chapter is to provide a comprehensive overview of the outcomes, discussed in the dissertation. This chapter includes the outcomes of all the above investigations and very briefly summarized them in the following sections.

9.1.1. Numerical characterization of temperature coupled loop

✓ Significant amount of asymmetry can be observed in both velocity and temperature profiles at any cross-section in the horizontal arms due to local buoyancy effects. Extent of such asymmetry is more prominent for sCO_2-based loop due to substantial property variation around the pseudocritical point.

✓ Under identical operating condition, CO_2 exhibits the highest velocity magnitude at any particular cross section and also the lowest temperature value, with the radial location of largest velocity and lowest temperature conforming each other well. Largest velocity is achieved with the system pressure slightly above the critical.

✓ Mass flow rate increases with increase of temperature differential between heater and cooler for both water and R134a. Variation for CO_2 is

strongly dependent on both system pressure and imposed temperature range. CO_2 also exhibits the smallest mass inventory requirement among the three fluids considered here.

✓ Single-phase liquid nature of water yields the highest heat transfer coefficient, which remains nearly constant for the selected ranges of pressures and temperatures. When sink-side condition is below pseudocritical, CO_2 produces heat transfer coefficient comparable with water. However, a sharp deterioration is observed with change of state from trans-critical to supercritical.

✓ Rate of heat transfer for both R134a and water are directly proportional to the temperature difference between heater and cooler. CO_2 provides the largest heat transfer rate at higher pressures and also when the sink temperature is reasonably below the pseudocritical value.

✓ CO_2-based SCNCL can be identified as the preferred option from heat transfer point of view only for pressures reasonably above its critical value, and with source and sink temperatures lying on either side of the pseudocritical temperature corresponding to the system pressure. However, if the pressure approaches critical limit for CO_2 or the sink temperature is around or above the pseudocritical value, single-phase loop can be a better choice.

✓ Consistent thermalhydraulic performance and possibility of operating at reduced system pressure are added incentives for the water-based system. R134a, despite being a supercritical fluid, cannot be suggested as a feasible option for the ranges of parameters explored here, owing to lesser heat transfer rate and larger inventory requirement. Therefore the adoption of supercritical condition can be suggested only under favourable set of operating conditions.

9.1.2. Steady-state thermalhydraulic appraisal of heat flux supported loop

✓ Significant amount of asymmetry can be observed in both velocity and temperature profiles at any cross-section in the horizontal arms due to local buoyancy effects. Extent of such asymmetry is more prominent for sCO_2-based loop due to substantial property variation around the pseudocritical point.

✓ Mass flow rate for SCNCL increases with input power, till the lowest fluid temperature inside the loop remains lower than the pseudocritical temperature corresponding to the system pressure. Rapid rise in flow rate can be observed when the fluid crosses the pseudocritical point during its passage through the heater section, owing to the substantial density difference between the two vertical arms.

✓ Beyond a maxima, mass flow rate in SCNCL drops drastically, with corresponding jump in the maximum fluid temperature. The effect is more pronounced with higher sink temperatures and for system pressures close to the critical point. For pressure levels considerably away from the critical point, monotonic rise in flow rate can be observed, quite similar to the single-phase NCLs.

✓ The maxima in mass flow rate profile corresponds to a peak in sink-side heat transfer coefficient, followed by a rapid decline with further increase in power supply. That can be identified as the initiation of heat transfer deterioration in SCNCLs (FiHTD).

✓ Power level corresponding to the appearance of FiHTD can be increased by raising pressure and lowering sink temperature. A mechanism can also be devised to manoeuvre the sink temperature with heater power for delaying the appearance of such deterioration.

✓ Mass inventory requirement is the lowest for CO_2-based loop. At higher powers, inventory requirement for R134a is lesser than water, with similar order of maximum temperature and hence R134a can be a prospective fluid under such situations, provided the chemical stability limit is adhered with.

✓ A generalized non-dimensional number 'Γ' is coined for SCNCL, which directly signify the working zone of SCNCL. It has been found that FiHTD is occurred for several working fluids when Γ is higher than 10^{-4}. The condition for a healthy operation of SCNCL is $\rho^* > 1$ and $h^* < 0$ respectively.

✓ Under identical operating conditions, fluid temperature level for the CO_2-based loop is the lowest among the three fluids till the appearance of FiHTD and hence supercritical condition can be adopted. Beyond the power level corresponding to FiHTD, however, single-phase NCL is a safer option.

✓ Single-phase water-based loop presents monotonic profile of mass flow rate, magnitude of which is well-below the same of SCNCL upto the occurrence

of FiHTD, leading to elevated temperature level. Heat transfer coefficient for single-phase water-based NCL is consistently higher than SCNCL, owing to higher thermal conductivity of the working fluid.

9.1.3. Influences of geometric parameters on steady-state thermalhydraulics of SCNCL

✓ Loop diameter can be viewed as the most influencing parameter. Smaller-diameter loop imposes larger friction, reducing the flow rate and thereby enforcing an early initiation of FiHTD. Thermal asymmetry in any particular cross-section, as well as the local velocity magnitude, can be substantially larger for smaller-diameter loops. However, increased diameter results in larger material requirement, as well as greater space and cost consideration, and therefore some trade-off may become necessary.

✓ Change in loop height affect both buoyancy and frictional fields. Buoyancy being the dominant force initially, mass flow rate and power level corresponding to FiHTD keeps on increasing with height till some optimum level. Hardly any tangible benefit can be observed beyond that and hence it is important to locate such optimum, possibly through systematic simulations.

✓ Variation in heating length, while maintaining rest of the loop the same, hardly imposes any noticeable change. On the contrary, rise in cooler length delays the appearance of FiHTD quite significantly due to the lower level of heat transfer coefficient. Therefore it is better to fabricate both the source and sink covering the entire of respective horizontal sections.

✓ Change in horizontal length, without affecting the heat-exchanging sections, has similar effect of reducing the diameter. So the extent of the adiabatic horizontal sections should be smallest possible.

✓ Positioning of the source and sink in the horizontal arms does not influence the gross thermalhydraulic characteristics, apart from imposing a pre-defined flow direction. Effect of the corner bends is found to be restricted only in introducing minor asymmetry in profiles due to the centrifugal action.

✓ Despite reduction in driving buoyancy and hence the flow rate, providing inclination to the loop is found to have insignificant influence on the FiHTD. Therefore it can be treated as an effective option of stability control, without affecting the regime of operation under steady-state and that can be projected as the next step of research in the context of the present study.

9.1.4. Experimental assessment of steady-state and stability performance of SCNCL

✓ Qualitatively as well as quantitatively good agreement exhibits for experimental and simulated data. Both the results are significantly matches with each other, only few results are not matches quantitatively, but the deviation is limited to less than 15%.

✓ The most influencing parameter for any type of NCL is sink temperature. The rate of cooling is assessed according to sink temperature and hence the thermalhydraulics of NCL is highly dependent on it. Mass flow rate is increased according to the increase of power for a constant sink temperature loop.

✓ One of the most important influencing parameters for investigating the thermalhydraulics of any NCL is doubtlessly pressure. Due to change of operating pressure the state of the working fluid is changes sub-critical to supercritical state. Due to decrease of density, the available buoyancy force is decreased with further increase of pressure and the result is reduced mass flow rate.

✓ The buoyancy force dependent on both the density gradient between heater and cooler as well as the vertical distance between them. Center wise or average vertical distance between heater and cooler decreases with increase of tilt angle. Vertical distance is maximum in case of vertical loop and hence this type of loop generate the highest mass flow rate.

✓ The flow direction can be predefined by tilting the loop in x-y plane. Thus the flow rate is highly deflect in this case. Whereas, after tilting in y-z plane, the system remains in symmetric in nature and hence the influence of tilting in y-z plane is less pronouncing than x-y plane.

✓ Experimentally dynamic performance analyses have been performed by sudden increase and decrease of the input power for the source section. For the selected range of study, no unstable results are found in the experiments and for both the cases the system is remains in the stable condition.

✓ In case of step input load condition, the influencing parameter is heater power, thus heater responses quickly than cooler. Therefore, the temperature differences across the heater is significantly more than the cooler. A detailed

experimental analyses have been confirmed that the system is stable for all the selected operating conditions.

9.1.5. Transient analysis for stability appraisal of SCNCL

✓ The system goes from stable to unstable region by crossing the lower and upper thresholds are due to the haphazardly changes of buoyancy and frictional forces. Basically, the buoyancy and the frictional forces interplay between each other and make a balance for the stable system. But, when any of the forces are unevenly growing or diminishing then the system is not capable to sustain in stable state.

✓ It has been found that the density changes across heater section for lower threshold power is large and hence generated buoyancy force is higher than optimum, as a result the system goes to the unstable zone.

✓ The input power for the upper threshold is directly related with the sink temperature of the system. While, the lower threshold powers hardly changes with the sink temperature.

✓ A complete stability map has been developed with respect to sink temperature of the system. The generated buoyancy force is extremely high for low sink temperature condition and hence unstable zone is extra-large for this condition. The unstable zone is reduced with increase of sink temperature and after a certain condition, this zone is totally obliterated.

✓ Before changing the direction, mass flow rate oscillates with growing magnitude until it reaches an optimum amplitude. Once, the highest or critical amplitude occurs, then the flow changes its direction and a new sequence begins with a new sets of oscillations.

✓ After changing the direction of flow, oscillations grows gradually until the next change, but if the first peak in a given direction is huge, then the flow direction reverses rapidly without additional increase in oscillation amplitude.

✓ A Lorenz like chaotic flow is observed in unstable zone of operation of SCNCL. At the time of changing the flow direction, the vortex are formed in the elbow sections, while side by side growing opposite directional flow are observed in the horizontal and the vertical sections of the loop.

✓ Due to the presence of the local buoyancy, the fluid near the upper wall of the heater section and the lower wall of the cooler section are affected first and alter the flow direction.

✓ A comprehensive dynamic performance study suggests that, the span of perturbation greatly affects the amplitude of oscillations of the systems. The oscillations is maximum when the changing occurs instantly and the amplitude of the oscillations are reduced according to the perturbation time.

✓ A stable system always tries to diminish the uneven occurrences, which are developed due to the changes of operating parameters and tries to remain in stable state. But, when the uneven occurrences are tremendously high then the equilibrium condition breaks down and the system finally goes to unstable state.

✓ An instant change of input heat flux produces a shock to the system and the result is the generation of higher amplitude of oscillation than slow changes.

✓ In case of gradual or slow changes, the systems get required time to self-change according to input condition. Whereas, for instant change of input condition the systems are not able to get self-change and thus an uneven oscillations occurs.

9.2. Scopes for Future Work

The concept of SCNCL is relatively new, with lots of potential for application to several engineering fields in near future. Being a fresh idea, related knowledge base is relatively thin and involves several conflicting theories and controversies. Due to several advantageous features of SCNCL, it becomes a fascinating field of research for several researchers. Both numerical and experimental evaluation on thermalhydraulic and stability analysis of SCNCL have been carried out in the present study. Although, an enormous research efforts has been put for the development of study of SCNCL, there are still some scopes to improve the performance of study with more additional features. The current investigations have not only generated numerous stimulating results but have also pointed towards various possible direction of further research. This study can be extended by several ways, which are described in below.

✓A detailed study over the influence of geometric parameters have been carried out in the present dissertation. In future, this study can be extended by adding various sections with the base geometry. The number of heating and cooling sections can be added to observe the behaviour of the system. The adiabatic vertical arms also can added on either sides of the heating and cooling sections.

✓An extensive analysis is performed for different inclination angles by both numerical and experimental approach. This study can be extended by involving rolling motion into the system.

✓Apart from affecting flow rate, loop inclination also influences the loop transients. A thorough study can be performed for studying the effect of loop inclination on transients.

✓In the present numerical study, 2D model is used for transient analysis of SCNCL with sCO_2 as working fluid. In extension of this work a detailed transient analysis can be carried out by using 3D loop, with different working fluids.

✓The experimental analysis has been carried out with considering R134a as working fluid. The present experimental study can be prolonged for different fluids. The results can be obtained by using sophisticated measuring instrument.

✓By numerical study, it has been identified that thermalhydraulic of SCNCL utterly affected by several geometric parameters of the system. A detailed experimental analysis according to various geometric parameters of the loop can be carried out.

References

Adams, M.A., Otu, E.O., Kozliner, M., Szubra, J., Pawliszyn, J., 1995. Portable thermal pump for supercritical fluid delivery. Anal. Chem. 67, 212–219.

Ambrosini, W., 2016. On some relevant effects in the simulation of flow stability with fluids at supercritical pressure. J. Nucl. Eng. Radiat. Sci. 2, 031005-1–13.

Ambrosini, W., 2008. Lesson learned from the adoption of numerical techniques in the analysis of nuclear reactor thermal-hydraulic phenomena. Prog. Nucl. Energy 50, 866–876.

Ambrosini, W., Sharabi, M., 2008. Dimensionless parameters in stability analysis of heated channels with fluids at supercritical pressures. Nucl. Eng. Des. 238, 1917–1929.

ANSYS, 2015. Fluent Tutorial Guide Release 15.0, ANSYS Inc. Available online at http://www.ansys.com.

Archana, V., Vaidya, A.M., Vijayan, P.K., 2015. Numerical modeling of supercritical CO_2 natural circulation loop. Nucl. Eng. Des. 293, 330–345.

Atrens, A.D., Gurgenci, H., Rudolph, V., 2010. Electricity generation using a carbon-dioxide thermosiphon. Geothermics 39, 161–169.

Buongiorno, J., MacDonald, P., 2003. Supercritical water reactor (SCWR), Progress Report for the FY-03 Generation-IV R&D Activities for the Development of the SCWR in the U.S., 1-38.

Cammarata, L., Fichera, A., Guglielmino, I.D., Pagano, A., 2004. On the effect of gravity on the bifurcation of rectangular closed-loop thermosyphon. Heat Mass Transf. und Stoffuebertragung 40, 801–808.

Cao, Y., Zhang, X. rong, Zheng, M., Yamaguchi, H., Liu, Z.S., 2011. Investigation of convection-based energy systems using supercritical carbon dioxide as a working fluid. Int. J. ENERGY Res. 35, 346–357.

Cao, Y., Zhang, X.R., 2012. Flow and heat transfer characteristics of supercritical CO_2 in a natural circulation loop. Int. J. Therm. Sci. 58, 52–60.

Carbone, F., Ambrosini, W., 2016. Steady-state and stability analysis of natural circulation with fluids at supercritical pressure, in: Proceedings of the 2016 24th International Conference on Nuclear Engineering ICONE24 June 26-30, 2016, Charlotte, North Carolina. pp. 1–8.

Chang, H.M., Choi, Y.S., Van Sciver, S.W., Choi, K.D., 2003. Cryogenic cooling system of HTS transformers by natural convection of subcooled liquid nitrogen. Cryogenics (Guildf). 43, 589–596.

Chatoorgoon, V., 2001. Stability of supercritical fluid flow in a single-channel natural-convection loop. Int. J. Heat Mass Transf. 44, 1963–1972.

Chatoorgoon, V., 1986. SPORTS - A simple non-linear thermalhydraulic stability code. Nucl. Eng. Des. 93, 51–67.

Chatoorgoon, V., Voodi, A., Fraser, D., 2005a. The stability boundary for supercritical flow in natural convection loops: Part I: H_2O studies. Nucl. Eng. Des. 235, 2570–2580.

Chatoorgoon, V., Voodi, A., Upadhye, P., 2005b. The stability boundary for supercritical flow in natural-convection loops: Part II: CO_2 and H_2. Nucl. Eng. Des. 235, 2581–2593.

Chen, L., Deng, B.L., Jiang, B., Zhang, X.R., 2013a. Thermal and hydrodynamic characteristics of supercritical CO_2 natural circulation in closed loops. Nucl. Eng. Des. 257, 21–30.

Chen, L., Deng, B.L., Zhang, X.R., 2013b. Experimental study of trans-critical and supercritical CO_2 natural circulation flow in a closed loop. Appl. Therm. Eng. 59, 1–13.

Chen, L., Deng, B.L., Zhang, X.R., 2013c. Experimental investigation of CO_2 thermosyphon flow and heat transfer in the supercritical region. Int. J. Heat Mass Transf. 64, 202–211.

Chen, L., Zhang, X.R., 2014. Experimental analysis on a novel solar collector system achieved by supercritical CO_2 natural convection. Energy Convers. Manag. 77, 173–182.

Chen, L., Zhang, X.R., 2011. Simulation of heat transfer and system behavior in a supercritical CO_2 based thermosyphon: Effect of pipe diameter. J. Heat Transfer 133, 122505–122508.

Chen, L., Zhang, X.R., Cao, S., Bai, H., 2012a. Study of trans-critical CO_2 natural convective flow with unsteady heat input and its implications on system control. Int. J. Heat Mass Transf. 55, 7119–7132.

Chen, L., Zhang, X.R., Deng, B.L., 2016. Near-critical natural circulation flows inside an experimental loop: stability map and heat transfer. Heat Transf. Eng. 37, 302–313.

Chen, L., Zhang, X.R., Deng, B.L., Jiang, B., 2013d. Effects of inclination angle and operation parameters on supercritical CO_2 natural circulation loop. Nucl. Eng. Des. 265, 895–908.

Chen, L., Zhang, X.R., Jiang, B., 2014. Effects of heater orientations on the natural circulation and heat transfer in a supercritical CO_2 rectangular loop. J. Heat Transfer 136, 52501-1–12.

Chen, L., Zhang, X.R., Yamaguchi, H., Liu, Z.S., 2010. Effect of heat transfer on the instabilities and transitions of supercritical CO_2 flow in a natural circulation loop. Int. J. Heat Mass Transf. 53, 4101–4111.

Chen, Y., Zhao, M., Yang, C., Bi, K., Du, K., 2013e. Experiment of heat transfer of supercritical water in natural circulation with different diameters of heated tubes, in: The 6th International Symposium on Supercritical Water-Cooled Reactors ISSCWR-6 March 03-07, Shenzhen, Guangdong, China MNL.

Chen, Y., Zhao, M., Yang, C., Bi, K., Du, K., 2012b. An experiment on flow and heat transfer characteristics in natural circulation of supercritical water, in: The 3rd China-Canada Joint Workshop on Supercritical-Water-Cooled Reactors, CCSC-2012 Xi'an, China, April 18-20 MNL.

Chen, Y., Zhao, M., Yang, C., Bi, K., Du, K., 2012c. An experimental study of heat transfer in natural circulation of supercritical water, in: The 9th International Topical Meeting on Nuclear Thermal-Hydraulics, Operation and Safety (NUTHOS-9), September 9-13, Kaohsiung, Taiwan MNL. pp. 1–9.

Cheng, X., Yang, Y.H., 2008. A point-hydraulics model for flow stability analysis. Nucl. Eng. Des. 238, 188–199.

Choi, J.H., Cleveland, J., Aksan, N., 2011. Improvement in understanding of natural circulation phenomena in water cooled nuclear power plants. Nucl. Eng. Des. 241, 4504–4514.

Close, D.J., 1962. The performance of solar water heaters with natural circulation. Sol. Energy 6, 33–40.

Debrah, S.K., Ambrosini, W., Chen, Y., 2013a. Discussion on the stability of natural circulation loops with supercritical pressure fluids. Ann. Nucl. Energy 54, 47–57.

Debrah, S.K., Ambrosini, W., Chen, Y., 2013b. Assessment of a new model for the linear and nonlinear stability analysis of natural circulation loops with supercritical fluids. Ann. Nucl. Energy 58, 272–285.

Delmastro, D.F., 2000. Thermal-hydraulic aspects of CAREM reactor, in: Proc. IAEA Technical Committee Meeting on Natural Circulation Data and Innovative Nuclear Power Plant Design, July 18–21, Vienna, Austria.

Gharbi, N. El, Absi, R., Benzaoui, A., 2012. Effect of different near-wall treatments on indoor airflow simulations. J. Appl. Fluid Mech. 5, 63–70.

Greif, R., 1988. Natural circulation loops. J. Heat Transfer 110, 1243–1258.

Haider, S.I., Joshi, Y.K., Nakayama, W., 2002. A natural circulation model of the closed loop, two-phase thermosyphon for electronics cooling. J. Heat Transfer 124, 881–890.

IAEA, 2009. Passive safety systems and natural circulation in water cooled nuclear power plants. International Atomic Energy Agency, IAEA-TECDOC- 1624.

IAEA, 2005. Natural circulation systems: Advantages and challenges, International Atomic Energy Agency, IAEA-TECDOC-1474.

Jain, P.K., Rizwan-uddin, 2008. Numerical analysis of supercritical flow instabilities in a natural circulation loop. Nucl. Eng. Des. 238, 1947–1957.

Jain, P.K., Rizwan-uddin, 2006. Steady state and dynamic analyses of supercritical CO_2 natural circulation loop, in: Proceedings of ICONE14 International Conference on Nuclear Engineering, July 17-20, Miami, Florida, USA. pp. 1–10.

Jain, R., Corradini, M.L., 2006. A linear stability analysis for natural-circulation loops under supercritical conditions. Nucl. Technol. 155, 312–323.

Jiang, Y.Y., Shoji, M., 2003. Flow stability in a natural circulation loop: Influences of wall thermal conductivity. Nucl. Eng. Des. 222, 16–28.

Jo, D., Al-Yahia, O.S., Altamimi, R.M., Park, J., Chae, H., 2014. Experimental investigation of convective heat transfer in a narrow rectangular channel for upward and downward flows. Nucl. Eng. Technol. 46, 195–206.

Joen, C.T., Rohde, M., 2012. Experimental study of the coupled thermo-hydraulic – neutronic stability of a natural circulation HPLWR. Nucl. Eng. Des. 242, 221–232.

Kao, M.T., Lee, M., Ferng, Y.M., Chieng, C.C., 2010. Heat transfer deterioration in a supercritical water channel. Nucl. Eng. Des. 240, 3321–3328.

Keller, J.B., 1966. Periodic oscillations in a model of thermal convection. J. Fluid Mech. 26, 599–606.

Kim, D.E., Kim, M.H., Cha, J.E., Kim, S.O., 2008. Numerical investigation on thermal-hydraulic performance of new printed circuit heat exchanger model. Nucl. Eng. Des. 238, 3269–3276.

Kim, S.C., Won, J.P., Kim, M.S., 2009. Effects of operating parameters on the performance of a CO_2 air conditioning system for vehicles. Appl. Therm. Eng. 29, 2408–2416.

Kiss, A., Balaskó, M., Horváth, L., Kis, Z., Aszódi, A., 2017. Experimental investigation of the thermal hydraulics of supercritical water under natural circulation in a closed loop. Ann. Nucl. Energy 100, 178–203.

Koffi, P.M.E., Andoh, H.Y., Gbaha, P., Touré, S., Ado, G., 2008. Theoretical and experimental study of solar water heater with internal exchanger using thermosiphon system. Energy Convers. Manag. 49, 2279–2290.

Launder, B.E., Spalding, D.B., 1974. The numerical computation of turbulent flows. Comput. Methods Appl. Mech. Eng. 3, 269–289.

Liu, G., Huang, Y., Wang, J., Leung, L.H.K., 2016a. Heat transfer of supercritical carbon dioxide flowing in a rectangular circulation loop. Appl. Therm. Eng. 98, 39–48.

Liu, G., Huang, Y., Wang, J., Lv, F., 2015. Effect of buoyancy and flow acceleration on heat transfer of supercritical CO_2 in natural circulation loop. Int. J. Heat Mass Transf. 91, 640–646.

Liu, G., Huang, Y., Wang, J., Lv, F., Leung, L.K.H., 2016b. Experiments on the basic behavior of supercritical CO_2 natural circulation. Nucl. Eng. Des. 300, 376–383.

Liu, G., Huang, Y., Wang, J., Lv, F., Liu, S., 2017. Experimental research and theoretical analysis of flow instability in supercritical carbon dioxide natural circulation loop. Appl. Energy 205, 813–821.

Liu, L., Xiao, Z., Yan, X., Zeng, X., Huang, Y., 2013a. Numerical simulation of heat transfer deterioration phenomenon to supercritical water in annular channel. Ann. Nucl. Energy 53, 170–181.

Liu, L., Xiao, Z., Yan, X., Zeng, X., Huang, Y., 2013b. Heat transfer deterioration to supercritical water in circular tube and annular channel. Nucl. Eng. Des. 255, 97–104.

Lomperski, S., Cho, D., Jain, R., Corrandini, M.L., 2004. Stability of a natural circulation loop with a fluid heated through the thermodynamic pseudocritical point, in: Proceedings of ICAPP '04 Pittsburgh, PA USA, June 13-17, 2004 Paper ID 4268. pp. 1–6.

Marcel, C.P., Rohde, M., Masson, V.P., Van Der Hagen, T.H.J.J., 2009. Fluid-to-fluid modeling of supercritical water loops for stability analysis. Int. J. Heat Mass Transf. 52, 5046–5054.

Misale, M., Garibaldi, P., Tarozzi, L., Barozzi, G.S., 2011. Influence of thermal boundary conditions on the dynamic behaviour of a rectangular single-phase natural circulation loop. Int. J. Heat Fluid Flow 32, 413–423.

NIST, 2011. Standard Reference Database-REFPROP, Version 9.1.

Pearson, D.F., 2004. Development of carbon dioxide as a volatile secondary heat transfer fluid to replace glycols. In 6th IIR Gustav lorentzen Conference on natural Working Fluids, Aug.

Rai, S.K., Dutta, G., Sheorey, T., 2017. Stability analysis of supercritical water natural circulation loop with vertical heater and cooler, in: Proceedings of the 24th National and 2nd International ISHMT-ASTFE Heat

and Mass Transfer Conference (IHMTC-2017), December 27-30, 2017, BITS Pilani, Hyderabad, India.

Ridouane, E.H., Danforth, C.M., Hitt, D.L., 2010. A 2-D numerical study of chaotic flow in a natural convection loop. Int. J. Heat Mass Transf. 53, 76–84.

Rieberer, R., 2005. Naturally circulating probes and collectors for ground-coupled heat pumps. Int. J. Refrig. 28, 1308–1315.

Rohde, M., Marcel, C.P., Manera, A., Van der Hagen, T.H.J.J., Shiralkar, B., 2010. Investigating the ESBWR stability with experimental and numerical tools: A comparative study. Nucl. Eng. Des. 240, 375–384.

Rohde, M., Marcel, C.P., T'Joen, C., Class, A.G., Van Der Hagen, T.H.J.J., 2011. Downscaling a supercritical water loop for experimental studies on system stability. Int. J. Heat Mass Transf. 54, 65–74.

Sadhu, S., Ramgopal, M., Bhattacharyya, S., 2018a. Steady-state analysis of a high-temperature natural circulation loop based on water-cooled supercritical CO_2. J. Heat Transfer 140, 1–11.

Sadhu, S., Ramgopal, M., Bhattacharyya, S., 2018b. Experimental studies on an air-cooled natural circulation loop based on supercritical carbon dioxide – Part A: Steady state operation. Appl. Therm. Eng. 133, 809–818.

Sadhu, S., Ramgopal, M., Bhattacharyya, S., 2018c. Experimental studies on an air-cooled natural circulation loop based on supercritical carbon dioxide – Part B: Transient operation. Appl. Therm. Eng. 133, 819–827.

Sharma, M., Pilkhwal, D.S., Vijayan, P.K., Saha, D., Sinha, R.K., 2012. Steady-state behavior of natural circulation loops operating with supercritical fluids for open and closed loop boundary conditions. Heat Transf. Eng. 33, 809–820.

Sharma, M., Pilkhwal, D.S., Vijayan, P.K., Saha, D., Sinha, R.K., 2010a. Experimental and theoretical investigations on steady state behavior of natural circulation systems operating with supercritical carbon-dioxide, in: 20th National and 9th International ISHMT-ASME Heat and Mass Transfer Conference.

Sharma, M., Pilkhwal, D.S., Vijayan, P.K., Saha, D., Sinha, R.K., 2010b. Steady state and linear stability analysis of a supercritical water natural circulation loop. Nucl. Eng. Des. 240, 588–597.

Sharma, M., Vijayan, P.K., Pilkhwal, D.S., Asako, Y., 2014. Natural convective flow and heat transfer studies for supercritical water in a rectangular circulation loop. Nucl. Eng. Des. 273, 304–320.

Sharma, M., Vijayan, P.K., Pilkhwal, D.S., Asako, Y., 2013. Steady state and stability characteristics of natural circulation loops operating with carbon dioxide at supercritical pressures for open and closed loop boundary conditions. Nucl. Eng. Des. 265, 737–754.

Sharma, M., Vijayan, P.K., Pilkhwal, D.S., Saha, D., Sinha, R.K., 2010c. Linear and nonlinear stability analysis of a supercritical natural circulation loop. J. Eng. Gas Turbines Power 132, 102904-1–9.

Shitzer, A., Kalmanoviz, D., Zvirin, Y., Grossman, G., 1979. Experiments with a flat plate solar water heating system in thermosyphonic flow. Sol. Energy 22, 27–35.

Sinha, R.K., Kakodkar, A., 2006. Design and development of the AHWR-the Indian thorium fuelled innovative nuclear reactor. Nucl. Eng. Des. 236, 683–700.

Song, Y., Four, A., Baudouy, B., 2013. Nucleate boiling heat transfer in a helium natural circulation loop coupled with a cryocooler. Int. J. Heat Mass Transf. 66, 64–71.

Swapnalee, B.T., Vijayan, P.K., Sharma, M., Pilkhwal, D.S., 2012. Steady state flow and static instability of supercritical natural circulation loops. Nucl. Eng. Des. 245, 99–112.

Tilak, A.K., Basu, D.N., 2015. Computational investigation of the dynamic response of a supercritical natural circulation loop to aperiodic and periodic excitations. Nucl. Eng. Des. 284, 251–263.

Tokanai, H., Ohtomo, Y., Horiguchi, H., Harada, E., Kuriyama, M., 2010. Heat transfer of supercritical CO_2 flow in natural convection circulation system. Heat Transf. Eng. 31, 750–756.

Vijayan, P., Nayak, A., 2005. Natural circulation systems: Advantages and challenges, International Atomic Energy Agency, IAEA-TECDOC-1474.

Vijayan, P.K., 2002. Experimental observations on the general trends of the steady state and stability behaviour of single-phase natural circulation loops. Nucl. Eng. Des. 215, 139–152.

Vijayan, P.K., Sharma, M., Pilkhwal, D.S., Saha, D., Sinha, R.K., 2010. A comparative study of single-phase, two-phase, and supercritical natural circulation in a rectangular loop. J. Eng. Gas Turbines Power 132, 102913.

Welander, P., 1967. On the oscillatory instability of a differentially heated fluid loop. J. Fluid Mech. 29, 17–30.

Yadav, A.K., Bhattacharyya, S., Ram Gopal, M., 2016a. Optimum operating conditions for subcritical/supercritical fluid-based natural circulation loops. J. Heat Transfer 138, 112501.

Yadav, A.K., Ram Gopal, M., Bhattacharyya, S., 2016b. Effect of tilt angle on subcritical/supercritical carbon dioxide-based natural circulation loop with isothermal source and sink. J. Therm. Sci. Eng. Appl. 8, 011007.

Yadav, A.K., Ram Gopal, M., Bhattacharyya, S., 2014. Transient analysis of subcritical/supercritical carbon dioxide based natural circulation loops with end heat exchangers: Numerical studies. Int. J. Heat Mass Transf. 79, 24–33.

Yadav, A.K., Ram Gopal, M., Bhattacharyya, S., 2012a. Computational fluid dynamic analysis of a supercritical CO_2 based natural circulation loop with end heat exchangers. Int. J. Adv. Eng. Sci. Appl. Math. 4, 119–126.

Yadav, A.K., Ram Gopal, M., Bhattacharyya, S., 2012b. CO_2 based natural circulation loops: New correlations for friction and heat transfer. Int. J. Heat Mass Transf. 55, 4621–4630.

Yadav, A.K., Ram Gopal, M., Bhattacharyya, S., 2012c. CFD analysis of a CO_2 based natural circulation loop with end heat exchangers. Appl. Therm. Eng. 36, 288–295.

Yadav, A.K., Ramgopal, M., Bhattacharyya, S., 2017. Transient analysis of subcritical/supercritical carbon dioxide based natural circulation loop with end heat exchangers: experimental study. Heat Mass Transf. und Stoffuebertragung 53, 2951–2960.

Yamaji, A., Oka, Y., Koshizuka, S., 2005. Three-dimensional core design of high temperature supercritical-pressure light water reactor with neutronic and thermal-hydraulic coupling. J. Nucl. Sci. Technol. 42, 8–19.

Yu, J., Che, S., Li, R., Qi, B., 2011. Analysis of Ledinegg flow instability in natural circulation at supercritical pressure. Prog. Nucl. Energy 53, 775–779.

Zerrouki, A., Boumedien, A., Bouhadef, K., 2002. The natural circulation solar water heater model with linear temperature distribution. Renew. Energy 26, 549–559.

Zhang, X.R., Chen, L., Yamaguchi, H., 2010. Natural convective flow and heat transfer of supercritical CO_2 in a rectangular circulation loop. Int. J. Heat Mass Transf. 53, 4112–4122.

Zhang, X.R., Yamaguchi, H., Uneno, D., Fujima, K., Enomoto, M., Sawada, N., 2006. Analysis of a novel solar energy-powered Rankine cycle for combined power and heat generation using supercritical carbon dioxide. Renew. Energy 31, 1839–1854.

Zhao, C.R., Jiang, P.X., 2011. Experimental study of in-tube cooling heat transfer and pressure drop characteristics of R134a at supercritical pressures. Exp. Therm. Fluid Sci. 35, 1293–1303.

Zvirin, Y., 1981. A review of natural circulation loops in pressurized water reactors and other systems. Nucl. Eng. Des. 67, 203–225.

Appendix

Appendix A: Uncertainty Analysis

According to Kline and McClintock' method, consider a variable N (dependent) which is calculated from various measurements such as, u_1, u_2, u_3, ……., u_n and governed by the function

$$N = f(u_1, u_2, u_3, \ldots\ldots, u_n) \tag{1}$$

Then overall error is given by

$$\Delta N = \left[\left(\frac{\partial N}{\partial u_1}\Delta u_1\right)^2 + \left(\frac{\partial N}{\partial u_2}\Delta u_2\right)^2 + \left(\frac{\partial N}{\partial u_3}\Delta u_3\right)^2 + \cdots + \left(\frac{\partial N}{\partial u_n}\Delta u_n\right)^2\right]^{1/2} \tag{2}$$

And uncertainty in the parameter N is given as

$$\frac{\Delta N}{N} = \left[\left(\frac{\Delta u_1}{u_1}\right)^2 + \left(\frac{\Delta u_2}{u_2}\right)^2 + \left(\frac{\Delta u_3}{u_3}\right)^2 + \cdots + \left(\frac{\Delta u_n}{u_n}\right)^2\right]^{1/2} \tag{3}$$

In this study, energy balance equation ($\dot{Q}_{th} = \dot{m}c_p\Delta T$) is used for calculating the mass flow rate. Thus, mass flow rate is a function of heat transfer rate and temperature difference between heater inlet and outlet (specific heat of R134a is assumed to be constant), given as:

$$\dot{m} = f(\dot{Q}_{th}, \Delta T) \tag{4}$$

Hence, uncertainty in the mass flow rate is describe as follows,

$$\frac{\Delta\dot{m}}{\dot{m}} = \left[\left(\frac{\Delta\dot{Q}_{th}}{\dot{Q}_{th}}\right)^2 + \left(\frac{\Delta(\Delta T)}{\Delta T}\right)^2\right]^{1/2} \tag{5}$$

The uncertainties of rate heat transfer and temperature difference are calculated as 7.5% and 2.2% respectively. The overall uncertainty in mass flow rate is calculated from equation (5) is 7.8%.

Publications

Book Chapter

✓ Basu, D.N., Sarkar, M.K.S., 2017. Supercritical Natural Circulation Loop: A Technology for Future Reactors, in: L. Chen, Y. Iwamoto (eds.) Advanced Applications of Supercritical Fluids in Energy Systems, IGI Global, Hershey PA, USA, Ch. 6, pp. 188-214.

Journal

✓ Sarkar, M.K.S., Tilak, A.K., Basu, D.N., 2014. A state-of-the-art review of recent advances in supercritical natural circulation loops for nuclear applications, Annals of Nuclear Energy 73, 250–263.

✓ Sarkar, M.K.S. Basu, D.N., 2015. Working regime identification for natural circulation loops by comparative thermalhydraulic analyses with three fluids under identical operating conditions, Nuclear Engineering and Design 293, 187–195.

✓ Sarkar, M.K.S., Basu, D.N., 2017a. Numerical comparison of thermalhydraulic aspects of supercritical carbon dioxide and subcritical water-based natural circulation loop. Nuclear Engineering and Technology 49, 103-112.

✓ Sarkar, M.K.S., Basu, D.N., 2017b. Numerical appraisal on the suitability of supercritical condition in natural circulation loop with isothermal boundary conditions. International Journal of Thermal Sciences 111, 30-40.

✓ Sarkar, M.K.S., Basu, D.N., 2017c. Influence of geometric parameters on thermalhydraulic characteristics of supercritical CO_2 in natural circulation loop. Nuclear Engineering and Design. Nuclear Engineering and Design 324, 402-415.

✓ Sarkar, M.K.S., Basu, D.N., 2018. Stability appraisal and dynamic performance evaluation of CO_2 based supercritical natural circulation loop. (Under preparation).

✓ Sarkar, M.K.S., Basu, D.N., 2018. A study of experimental characterization of R134a based supercritical natural circulation loop. (Under preparation).

Conference

✓ Sarkar, M.K.S., Basu, D.N., 2013. CFD based performance analysis for a rectangular natural circulation loop with end heat exchanger. In: Proc. 22th National and 11th International ISHMT-ASME Heat and Mass Transfer Conference December 28–31, IIT Kharagpur, India.

✓ Sarkar, M.K.S., Basu, D.N., 2015. Numerical comparison of flow behavior and heat transfer aspects of supercritical CO_2 and subcritical water based natural circulation loop, Proceedings of ICONE-23, 23th International Conference on Nuclear Engineering, May 17-21, Chiba, Japan.

✓ Sarkar, M.K.S., Basu, D.N., 2015. Effect of inclination in thermalhydraulics of supercritical natural circulation loop, Proc. Indian Chemical Engineering Congress (CHEMCON 2015), Guwahati, India, December 27-30, Paper ID FM-105.

✓ Sarkar, M.K.S., Basu, D.N., 2016. Experimental and computational analysis of supercritical natural circulation loop, Proceedings of the 6th International and 43rd National Conference on Fluid Mechanics and Fluid Power December 15-17, MNNITA, Allahabad, U.P., India FMFP2016–PAPER NO. 440.

✓ Sarkar, M.K.S., Basu, D.N., 2016. Effect of geometrical parameters on thermalhydraulics of supercritical natural circulation loop, Proceedings of the 6th International and 43rd National Conference on Fluid Mechanics and Fluid Power December 15-17, MNNITA, Allahabad, U.P., India FMFP2016–PAPER NO. 551.

✓ Sarkar, M.K.S., Basu, D.N., 2017. Design and Numerical Performance Evaluation of a Scaled-Down Supercritical Natural Circulation Loop, Proc. 24th National and 2nd International ISHMT-ASTFE Heat and Mass Transfer Conference (IHMTC-2017), BITS Pilani, Hyderabad, India, December 27-30, Paper No. IHMTC2017-11-0617.